

Framework for combined control and design optimization of hybrid vehicle propulsion systems

Citation for published version (APA):

Hofman, T. (2007). *Framework for combined control and design optimization of hybrid vehicle propulsion systems*. [Phd Thesis 1 (Research TU/e / Graduation TU/e), Mechanical Engineering]. Technische Universiteit Eindhoven. <https://doi.org/10.6100/IR630265>

DOI:

[10.6100/IR630265](https://doi.org/10.6100/IR630265)

Document status and date:

Published: 01/01/2007

Document Version:

Publisher's PDF, also known as Version of Record (includes final page, issue and volume numbers)

Please check the document version of this publication:

- A submitted manuscript is the version of the article upon submission and before peer-review. There can be important differences between the submitted version and the official published version of record. People interested in the research are advised to contact the author for the final version of the publication, or visit the DOI to the publisher's website.
- The final author version and the galley proof are versions of the publication after peer review.
- The final published version features the final layout of the paper including the volume, issue and page numbers.

[Link to publication](#)

General rights

Copyright and moral rights for the publications made accessible in the public portal are retained by the authors and/or other copyright owners and it is a condition of accessing publications that users recognise and abide by the legal requirements associated with these rights.

- Users may download and print one copy of any publication from the public portal for the purpose of private study or research.
- You may not further distribute the material or use it for any profit-making activity or commercial gain
- You may freely distribute the URL identifying the publication in the public portal.

If the publication is distributed under the terms of Article 25fa of the Dutch Copyright Act, indicated by the "Taverne" license above, please follow below link for the End User Agreement:

www.tue.nl/taverne

Take down policy

If you believe that this document breaches copyright please contact us at:

openaccess@tue.nl

providing details and we will investigate your claim.

Framework for Combined Control and Design Optimization of Hybrid Vehicle Propulsion Systems

PROEFSCHRIFT

ter verkrijging van de graad van doctor aan de
Technische Universiteit Eindhoven, op gezag van de
Rector Magnificus, prof.dr.ir. C.J. van Duijn, voor een
commissie aangewezen door het College voor
Promoties in het openbaar te verdedigen
op dinsdag 6 november 2007 om 15.30 uur

door

Theo Hofman

geboren te Utrecht

Dit proefschrift is goedgekeurd door de promotor:

prof.dr.ir. M. Steinbuch

Copromotor:

dr.ir. R.M. van Druten

This research was financially supported by NWO – Nederlandse Organisatie voor Wetenschappelijk Onderzoek.

A catalogue record is available from the Eindhoven University of Technology Library

Hofman, Theo

Framework for combined control and design optimization of hybrid vehicle propulsion systems / by Theo Hofman. – Eindhoven : Technische Universiteit Eindhoven, 2007 – Proefschrift.

ISBN 978-90-386-1136-5

Trefwoorden: energiemangement / hybride aandrijfsystemen / brandstofverbruik / optimalisering

Subject headings: energy management systems / hybrid vehicle propulsion systems / fuel consumption / optimal control

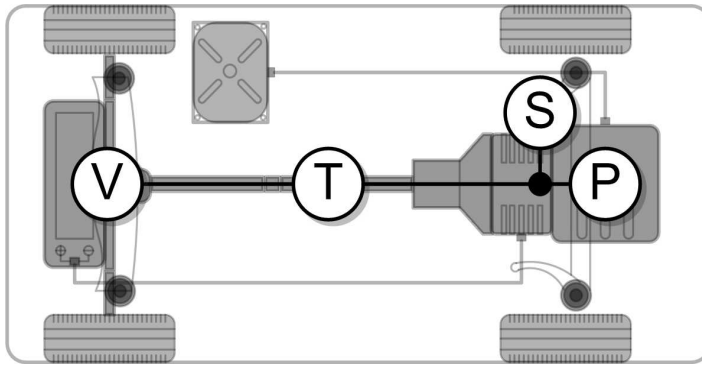
Cover design: Paul Verspaget / Theo Hofman

Copyright ©2007 by T. Hofman. All rights reserved.

This thesis was prepared with the \LaTeX 2_ε documentation system.

Reproduction: Universiteitsdrukkerij TU Eindhoven, Eindhoven, The Netherlands.

Framework for Combined Control and Design Optimization of Hybrid Vehicle Propulsion Systems



Samenstelling promotiecommissie:

prof.dr.ir. C.J. van Duijn (Voorzitter)
prof.dr.ir. M. Steinbuch
prof.dr.ir. P.P.J. van den Bosch
prof.dr. L. Guzzella, ETH Zürich, Zwitserland
prof.dr.ir. J. Hellendoorn, TU Delft
dr.ir. R.M. van Druten
prof.dr. L.P.H. de Goey
prof.dr. H. Nijmeijer

Contents

Contents	i
1 General Introduction	1
1.1 Background	2
1.1.1 Hybrid Vehicle Configurations and Classification	3
1.1.2 What makes the design of a hybrid vehicle challenging?	5
1.2 Problem Definition	10
1.2.1 Parametric Optimization	10
1.2.2 Modeling and Simulation Tools	13
1.3 Research Questions	13
1.4 Goals and Main Contributions of the Thesis	14
1.4.1 Control Strategy	15
1.4.2 Component Size and Technology	15
1.4.3 Reduced Hybrid Drive Train Modeling	17
1.5 Outline of the Thesis	17
2 Energy Management Strategies for Hybrid Vehicles	21
2.1 Introduction	21
2.1.1 Optimal Control Strategy – Dynamic Programming	22
2.1.2 Sub-Optimal Control Strategy – Heuristic Control Strategy	22
2.1.3 Sub-Optimal Control Strategy – Equivalent Consumption Minimization Strategy	22
2.1.4 Sub-Optimal Control Strategy – RB-ECMS	25
2.1.5 Outline of the Chapter	26
2.2 Problem Definition	26
2.3 Hybrid Driving Modes	27
2.4 The RB-ECMS	28
2.4.1 Power-Flow during the BER and the M Mode	31

2.4.2	Power-Flow during the MA, the CH, and the E Mode . . .	32
2.4.3	Optimization Routine (Offline) for calculating P_M^o	34
2.5	Simulation Results	35
2.5.1	Component Models	35
2.5.2	Control Models	36
2.5.3	Results	39
2.5.4	Evaluation of the Motor-Only Mode	42
2.6	Conclusion	43
3	Parametric Modeling for Specification of Components	45
3.1	Introduction	45
3.2	Objectives and Approach	46
3.3	Hybrid Drive Train Model	49
3.4	Control Model	50
3.4.1	Energy Management Optimization Problem	50
3.4.2	The Rule-Based Energy Management Strategy	50
3.4.3	Iterative Drive Train Loss Compensation Procedure	52
3.4.4	Reference Control Models: ADVISOR and DP	54
3.5	Results	54
3.5.1	Fuel Economy and Emissions	55
3.5.2	Control Models Parameters – ADVISOR	55
3.5.3	Parametric Efficiency Functions and Hybrid Drive Train Model	56
3.6	Conclusions	58
4	Design of CVT-Based Hybrid Passenger Cars	65
4.1	Introduction	65
4.1.1	Diversification of CVT Solutions	66
4.2	Problem Definition	67
4.3	Contribution and Outline of the Chapter	68
4.4	Modeling of the Drive Train Components	69
4.4.1	Base Line Vehicle Model	69
4.4.2	Hybrid Drive Train Models	71
4.4.3	Power-Split CVT	71
4.4.4	Battery Model	79
4.5	Simulation Method	82
4.5.1	Assumptions and Descriptions of the Design Parameters	85
4.6	Results	88
4.6.1	Effects of Parameter Variation (D. 1 – D. 8) on the Design Objective	88

4.6.2	Effects of the Electric-Only Vehicle Speed Threshold Value on the Design Objective for Different Brake Strategies (D. 7)	95
4.6.3	Effects of Changing the Hybrid Transmission Technology (D. 4) on the Design Objective and Component Efficiencies	95
4.7	Reduced Hybrid Drive Train Model	97
4.8	Conclusion	103
5	Design of Hybrid Medium-Duty Trucks	105
5.1	Introduction	105
5.1.1	Problem Description	106
5.1.2	Contribution and Outline of the Chapter	109
5.2	Modeling of the Drive Train Components	109
5.2.1	Power-Flow Description	110
5.2.2	Assumptions concerning Modeling and Sizing of the Components	110
5.2.3	Power-Based Component Efficiency Models	114
5.2.4	Sizing of Conversion and Storage Components	118
5.3	Control Model – RB-ECMS	119
5.3.1	Control Design Problem	120
5.4	Vehicle Dynamics Model	122
5.4.1	Acceleration Time 0–100 km/h (0–62 mph)	123
5.4.2	Gradeability at 89 km/h (55 mph)	125
5.5	Dual-Energy Storage Design Model	126
5.5.1	Battery Design Model	128
5.5.2	Ultra Capacitor Design Model	130
5.6	Simulation Results	130
5.6.1	Fuel Consumption, Acceleration Time, and Gradeability Results	130
5.6.2	Sizing Results of Dual-Energy Storage Systems	135
5.6.3	Cost Price of Sized Dual-Storage Systems	137
5.7	Conclusion	138
6	Conclusions and Recommendations	141
6.1	Conclusions	142
6.1.1	Control Design Methodology	142
6.1.2	Reduced Hybrid Drive Train Modeling and Design Methodology	143
6.2	Recommendations for Future Research	146
A	Model Components	149
A.1	Component Models of the Base Line Vehicle	149

A.1.1	Fuel Map Reconstruction	149
A.1.2	Torque Converter	151
A.1.3	Evaluation of the Component Models	153
Bibliography		157
Nomenclature		167
Summary		175
Samenvatting		179
Dankwoord		183
Curriculum Vitae		185

Chapter 1

General Introduction

Ongoing emission legislation and increasing fuel prices pursue many leading vehicle manufactures and their suppliers to put effort in developing and manufacturing new efficient, though cost-effective, drive train technologies. Hybrid drive train technologies are considered as short-term solutions in reducing the fuel consumption and emissions of automobiles, without comprising the vehicle's performance. In these new type of vehicle propulsion systems two power converters (usually an internal combustion engine and an electric machine) are combined. Due to the broad variety of the type of vehicles and the usage of these vehicles many solutions are provided for hybrid propulsion systems. Additionally, in recent years many researchers have devoted their attention to the development of sophisticated control systems in optimizing the power distribution between the two power sources. In literature (a broad overview is presented in [72]) this is also referred to as energy management.

Due to the large design space the question raises: how to design an hybrid propulsion system? In the last two decades different modeling and simulation tools for integral optimization, including the vehicle control system of hybrid vehicle propulsion systems, have been developed. However, these tools are characterized by large computation times due to the complexity (i.e., interdependency of the design parameters), the unknown sensitivity of the parameters to the design objective, and the multi-objective nature.

This study focusses on reduced modeling of the complexity of the following main design parameters: control strategy, component technologies, component sizes, and drive train topologies of hybrid vehicles. The effects of parameter variation on the main design objective, i.e., fuel consumption, can be investigated very quickly and with sufficient accuracy using the reduced models. This strongly alleviates the complex design problem, such that it can be used for optimization by effectively reducing the design space. The high-level modeling framework can be used for design analysis, which is decoupled from the choice of specific components, hybrid drive train configurations, and control strategy. Moreover, a different hybrid drive train configuration (i.e., series, parallel, series-parallel) implies a different transmission technology.

The method links the control design optimization with the component de-

sign optimization into a single framework. The development of a framework for combined control and design optimization of hybrid vehicle propulsion systems is the central theme of this thesis.

1.1 Background

The average carbon dioxide (CO₂)-emissions of gasoline and diesel passenger cars are strongly determined by their fuel consumption. In Figure 1.1 the average CO₂-emissions for passenger cars under test conditions in Europe and The Netherlands are shown [66]. In addition, the Euro95 gasoline prices [13] are depicted. The CO₂-emissions target set by the European (ACEA), Japanese (JAMA) and Korean (KAMA) umbrella organizations of car manufactures (representing 99% of the vehicle market in Europe) is to reduce the average CO₂-emissions to 140 g/km in 2008/2009 for the new European passenger fleet.

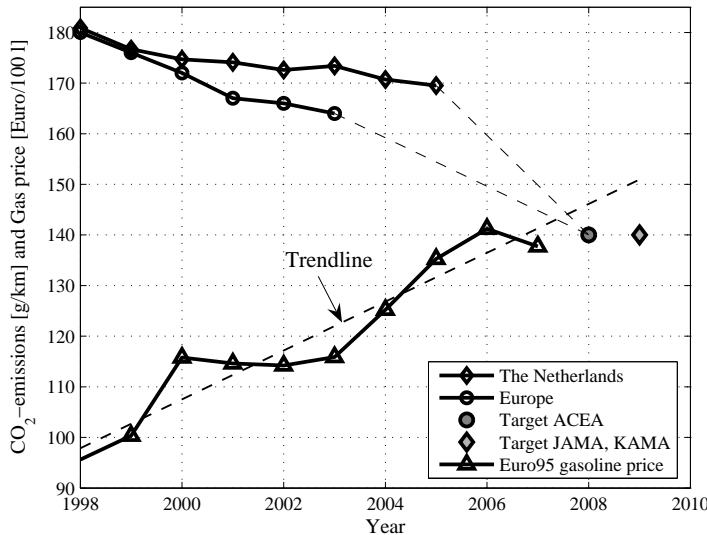


Figure 1.1 / CO₂-emissions in g/km of passenger cars in The Netherlands and Europe (EU-15) [66] and the Euro95 gasoline prices in The Netherlands [13].

In general, the average CO₂-emissions of passenger cars over the last seven years show a decreasing trend, while simultaneously the Euro95 gasoline prices show an increasing trend. Nevertheless, the fuel economy improvements of new conventional vehicles are relatively small and drastic measures are required to meet the near term emission targets. The disappointing decreasing trend in fuel

consumption and emissions reduction of new passenger cars is caused by the increasing trend in the average vehicle mass and the maximum engine power. The vehicles become heavier due to the increasing demand of vehicle safety and comfort while the performance of the vehicle is not allowed to be compromised. The average vehicle mass and the engine output power of new passenger cars in The Netherlands increased from 1998 to 2005 relatively by 11% and 20% respectively. The ‘costs’ of the increased average vehicle mass and engine size significantly diminish the ‘benefits’ obtained by the development of more fuel economic engines and more aerodynamic vehicles.

Advanced hybrid vehicle propulsion systems are very promising to achieve significant fuel consumption and emission reduction without compromising performance for vehicles. This is discussed in the following section.

1.1.1 Hybrid Vehicle Configurations and Classification

Hybrid vehicles are available, e.g., Citroën C3, Honda Civic IMA, Toyota Prius, Lexus RX400h. Some of these vehicles fulfill almost the same ‘hybrid functions’, e.g., engine off during vehicle standstill (Start-Stop function), Brake Energy Recuperation (BER), motor-assisting during driving, and pure electric driving. However, the drive train topology, engine size, electric machine size, transmission technology, and control system of these hybrid vehicles are completely different. Hybrid vehicles are categorized in the following three main types: series (e.g., TNO’s Hybrid Carlab [77]), parallel (e.g., Honda Civic IMA), or series-parallel hybrid configuration (e.g., Toyota Prius). Figure 1.2 visualizes schematically these different configurations and describes the main topological characteristics of how the power sources are connected to the drive train. Since the beginning of the twentieth century [38], ‘series hybrid configurations’ (Figure 1.2, top part) have been successfully applied besides in vehicles (1899) already in, e.g., diesel-electric powered ships (1903), and trains (1913). Engine operation at its maximum efficiency point(s), which is possible due to buffering of excess power, is an advantage of a series hybrid. However, a disadvantage of the series transmission is the relatively low transmission efficiency at relatively high vehicle loads compared to the other hybrid configurations. Unless the vehicle is mainly used for city driving (frequent and relatively low power demands), relatively large electric machines (kW) are required to transmit power from the battery and engine to the vehicle wheels at high vehicle speeds. The ‘parallel hybrid configuration’ (Figure 1.2, lowest part) has a higher transmission efficiency due to the mechanical connection between engine, electric machine, and the vehicle wheels. The propulsion power is supplied by the engine, electric machine, or by both sources very efficiently. The ‘series-parallel configuration’ (Figure 1.2, mid part) is a combination of the parallel and the series configuration, which merges the advantages of both

configurations. The engine propulsion power is divided into two power-flows transmitted to the wheels over a mechanical and an electrical branch.

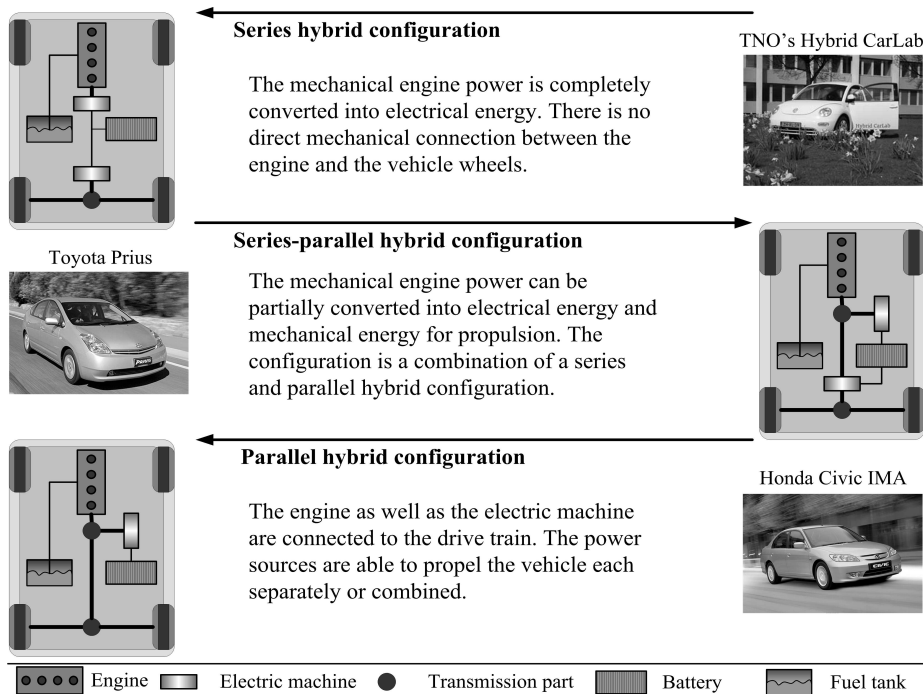





Figure 1.2 / Different hybrid drive train configurations.

The parallel and series-parallel configuration are further both classified from a micro-hybrid up to a full-hybrid vehicle. The transition from 'micro'- to 'full'-hybrid indicates an increase in the number of hybrid functions. Typically, the series configuration performs all hybrid functions and thus falls in the full-hybrid class. In Table 1.1 some typical hybrid system specifications for different hybrid vehicle classes are listed. In the table three hybrid vehicles, i.e., Citroën C3, Honda Civic IMA, and Toyota Prius, which fall inside each different hybrid vehicle class, are shown as an example. It is observed that an increase of hybridization, where the maximum engine and electric machine power respectively decreases and increases, causes reduced fuel consumption and CO₂-emissions.

Generally, it can be concluded, that there is a large variety in hybrid vehicles. However, fuel saving potential and additional cost of hybrid vehicles strongly depend on the drive train configuration and the degree-of-hybridization (sizes of the power sources). Selection of the right solution depends on both functional requirements and projected production volumes related to the manufacturing

Table 1.1 / Hybrid vehicle classification and specifications

Classification	Micro-hybrid	Mild-hybrid	Full-hybrid	
Hybrid Function	Start-Stop BER -	Start-Stop BER Motor-assisting -	Start-Stop BER Motor-assisting Electric driving	
Capacity, Size	1.5 – 3.5	10	> 30	kW
System voltage	14 (12) – 42 (36)	150 (144)	> 330 (288)	V
Add. cost [19]	200 – 900	900 – 2200	2500 – 5000	€
Fuel saving [†] [19]	3 – 10	15 – 25	20 – 30	%
	Citroën C3	Honda Civic IMA	Toyota Prius	
Hybrid vehicle				
Engine	1.4-l SI 67-kW	1.3-l SI 61-kW	1.5-l SI 57-kW	
EM size	3.5	10	50	kW
Fuel economy [†]	5.7	4.9	4.3	l/100km
CO ₂ -emission [†]	135	116	104	g/km

[†]NEDC = New European Drive Cycle; SI = Spark Ignition; EM = Electric Machine; BER = Brake Energy Recuperation.

investment. Hybrid systems that can be added on a conventional transmission may provide the most benefit for the least cost, which depends on the amount of changes required. The following section gives an overview of the design problem areas behind the hybridization of a vehicle propulsion system.

1.1.2 What makes the design of a hybrid vehicle challenging?

Let us denote the internal combustion engine as the Primary power source (P) and the battery system and the electric machine as the Secondary power source (S). Then hybridization implies adding S to P in order to improve the overall vehicle's performance. The Vehicle including the drive train, which is denoted as V, is defined as an energy source that stores kinetic energy during vehicle acceleration, and retrieves it during braking. The kinetic energy retrieved during braking is stored in the battery of S for later use. The brake energy storage is done at moments where the road load losses (e.g., air drag, roll resistance losses) are not sufficiently enough to decelerate the vehicle as desired.

Usually, for vehicle certification and comparison reasons the acceleration, braking, and steady-state driving periods of the vehicle are prescribed by a modal standardized drive cycle, e.g., the New European Drive Cycle (NEDC). A drive cycle is a series of data points representing the speed of a vehicle versus time.

A model at a high level of abstraction for the hybrid vehicle propulsion system

is schematically visualized in Figure 1.3. In the figure, S is parallel connected with P at the primary-, or engine-side of the transmission. In the example of Figure 1.3 the main mechanical transmission part is a push-belt Continuously Variable Transmission (CVT). The transmission technology between P, S, and V, which may also include, e.g., a wet-plate clutch, a torque converter, or a set of gear wheels, is denoted as T.

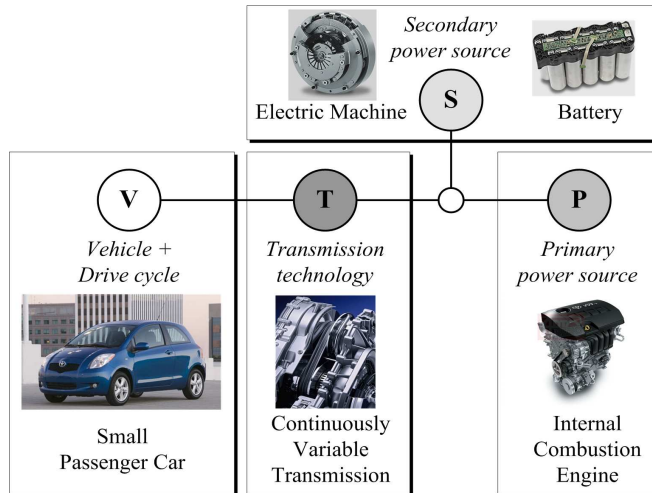


Figure 1.3 / A model at a high level of abstraction for the hybrid vehicle propulsion system. In this topology-example the secondary power source S is coupled at the engine-side of the transmission T. Example background pictures: Toyota Yaris and Toyota VVTi engine, push-belt CVT, electric machine/clutch and battery. Courtesy of Toyota; Daimler-Chrysler; ZF Friedrichshafen AG respectively.

One of the reasons that fuel consumption and emissions for a hybrid vehicle tested on a drive cycle are reduced is the fact that P is shut down during vehicle standstill (Start-Stop) and certain driving periods, which eliminate the idle and part load losses. Accordingly, S is used for restarting the engine quickly, or to propel the vehicle. The latter driving mode, where the vehicle is only propelled by the secondary power source S and the engine P is shut off, is defined as the (electro-)Motor-only (M) mode. Both hybrid functionalities, i.e., Start-Stop, and propulsion-only by S, depend on the power specification of S. The energy needed for this is mainly recovered during braking. This driving mode is defined as the Brake Energy Recovery (BER) mode.

In this thesis the balance of energy as depicted in Figure 1.4 is often used. In the figure, the ‘energy blocks’ on the energy balance represent the gross energy content at the input of S, where the discharged energy exactly counterbalances the charged energy. Due to storage, conversion, transmission losses, or by com-

ponent power specifications, the total (dis-)charged energy at the output of S may not be balanced.

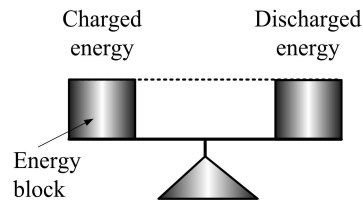


Figure 1.4 / Energy balance for the secondary power source S.

The energy-flow for each hybrid mode over a whole drive cycle in a parallel hybrid vehicle propulsion system is schematically visualized in Figure 1.5. Note that the (dis-)charge hybrid modes are not necessarily limited to the combinations shown in Figure 1.5. Nevertheless, the figure provides a schematic overview of a realistic energy management strategy. The propulsion-only mode by P (Figure 1.5(a), top) is also defined as the Engine-only (E) mode similar to a conventional vehicle. In this mode the secondary power source S is not used. The fuel savings and costs increase with each hybrid mode from Figure 1.5(b) to Figure 1.5(d). The BER and the M mode are depicted in Figure 1.5(b). Note that the energy needed for restarting P in the figure has been omitted, since the engine-restart energy is relatively small. The M mode results in ‘fuel saving’, as mentioned before, due to engine shut-off during certain driving periods.

Using charged energy, which has been retrieved from P during driving, for propulsion-only by S may further save fuel (even in the absence of stored kinetic energy, thus without utilizing the BER mode). This mode, as shown in Figure 1.5(c), is defined as the CHarging 1 (CH1) mode. The charged energy represents a certain ‘fuel cost’, since the charged energy is delivered by the engine.

Furthermore, the usage of S during vehicle operation in combination with P further optimizes the energy exchange between P, S, and V. The energy management strategy behind this is: to charge at moments where a large amount of accumulator energy costs only a relatively small amount of fuel (fuel cost), and use this energy at moments where it is beneficial to assist P with S, i.e., where a small amount of energy can save a relatively large amount of fuel (fuel savings). In literature [39] these (dis-)charging conversion ratios are also referred to as the ‘incremental fuel costs’ (or savings). The hybrid driving modes where the charged energy is used over a drive cycle for motor-assisting are defined as the CH2 and the MA2 mode respectively (Figure 1.5(d), bottom).

Summarizing, the ‘fuel saving potential’, which is defined as the difference between the ‘fuel savings’ and the ‘fuel costs’, are determined by the vehicle, the drive cycle, the component sizes (e.g., ability to propulsion-only by S), the component efficiencies, and the path efficiencies between the power sources. The ‘fuel savings’ are defined as the difference between the fuel consumption without and with utilizing S for propulsion (pure electric driving) or during driving (motor-assisting). Thereby, one of the design problems (also referred to as the energy management problem) is:

- How to determine the optimal power distribution between the power sources P and S among the different driving modes during vehicle operation?

The word ‘optimal’ refers to a yet undefined criterion. In literature (e.g., [39]) the minimization of the fuel consumption and/or emissions is used mostly. The boundary condition requires a balanced charged and discharged energy over a drive cycle. This condition is applied for vehicle comparison and certification reasons (similar to the use of standardized drive cycles).

The component efficiencies and the path efficiencies between the power sources are affected respectively by the component sizes, technologies, and the drive train topology. Therefore, in addition to the above mentioned control design problem the following design problems can be formulated:

- How to determine the optimal hybrid drive train topology?

Moreover, given the topology:

- How to find the optimal sizes of the hybrid components?
- How to select the optimal hybrid component technologies?

The drive train topology determines where and how the power sources are connected to the drive train. Hence, the topology also determines where the energy losses occur during energy exchange between the energy sources. This also holds for the selection of a Front- (FWD), a Rear- (RWD), or an All-Wheel Driven (AWD) vehicle, which implies a different topology choice. In Figure 1.6 an overview of some example topologies are shown.

The power sources are usually able to operate simultaneously. Therefore, adding a secondary power source S reduces the power specifications of the primary power source P for propulsion. Moreover, in case of an engine: it reduces the volumetric displacement and therefore inherently the pumping, compression, and friction losses. The optimal size of the power sources is a trade-off between maximizing the average efficiency of the primary power source P and

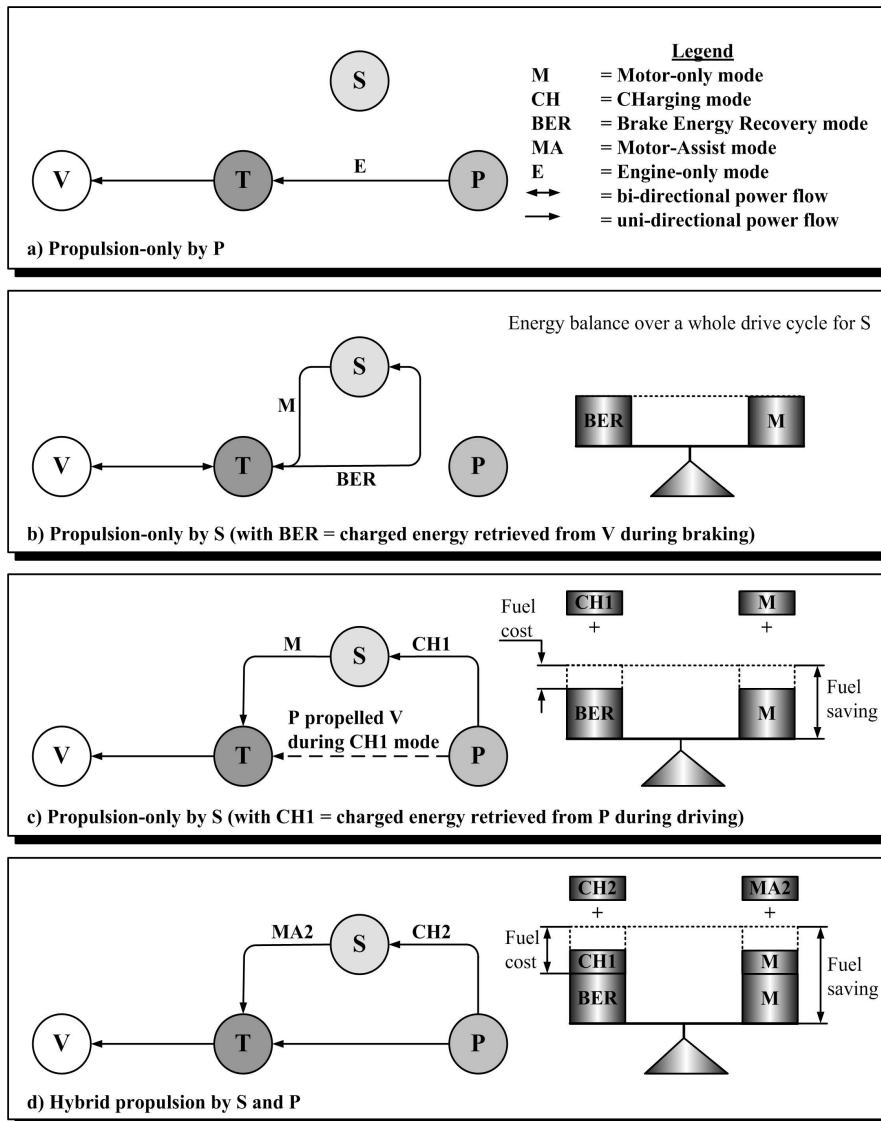


Figure 1.5 / Energy-flows over a whole drive cycle in a hybrid vehicle propulsion system.

the hybrid propulsion system. This is performed by down- and up-sizing of the primary P and secondary power source S respectively. However, the solutions are usually constrained by vehicle performance constraints (e.g., maximum vehicle acceleration, speed, or hill climbing specifications) and, thus, the total combined maximum (peak or continuous) output power of the power sources.

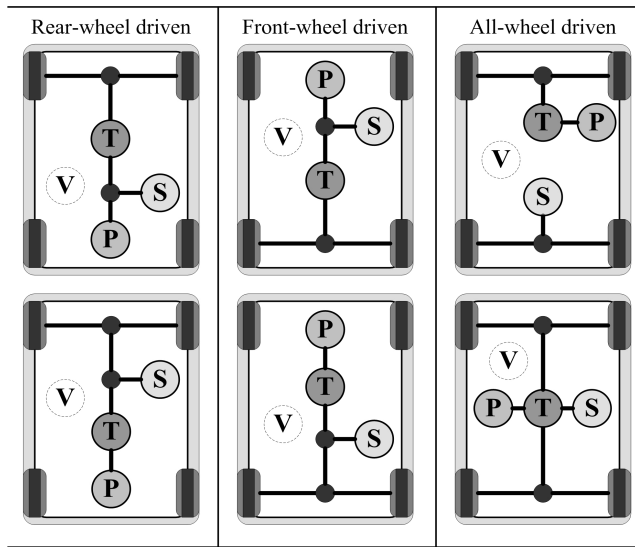


Figure 1.6 / Hybrid vehicle drive train topologies.

1.2 Problem Definition

The design of a hybrid propulsion system implies that choices are made regarding the topology, the technology of the power source, and sizing of the components. In combination with optimizing the vehicle control system, which determines the points of operation of the individual components at each time instant. This is a complex task due to the strong interdependency of these design parameters and the unknown sensitivity of the design parameters to the design objectives. The design complexity is schematically visualized in Figure 1.7. On the one hand, we have the design objectives: fuel economy, emissions and performance, and, on the other hand, we have the inherently interlinking design parameters: component technology, component size, topology, and control strategy. It should be noticed, that the design objectives may not be limited to the objectives shown (e.g., comfort, safety, or cost are not shown). Furthermore, performance is a broad understanding, which could be related to, e.g., acceleration, hill climbing, or towing requirements. A parametric optimization procedure is proposed, which allows investigation of parameter variation on the design objective.

1.2.1 Parametric Optimization

Parametric optimization implies finding the optimal set of design parameters, denoted as x^o , which are values of design parameters in x that result in an optimal value for an optimization objective function, denoted as $\Phi(x)$. In addition,

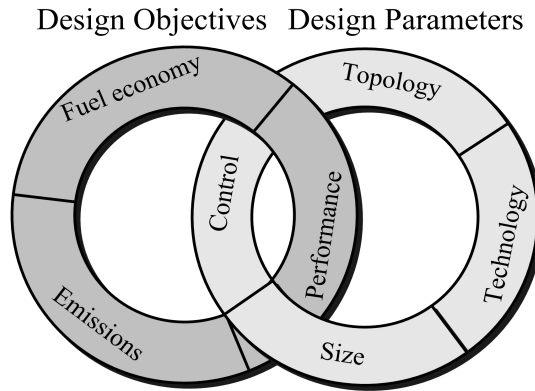


Figure 1.7 / Interlinking of the related design objectives and design parameters.

constraint functions $G(x)$ are defined to keep system properties and variables within certain bounds. Generally, the design optimization problem is formulated as [62]:

$$\min_x \Phi(x), \text{ subject to } G(x) \leq 0, x \in \mathcal{X} \subseteq \mathbb{R}^n, \quad (1.1)$$

where the feasible design space is assumed to be embedded in the set \mathcal{X} with dimension n . Solving this problem for hybrid vehicle propulsion systems is complex. The problem described by Equation (1.1) is possibly non-convex and therefore computational intensive using a conventional solving technique. In [48] a broad survey of nonlinear (multi-objective) optimization concepts and methods is given. The main conclusion of this study illustrates that no single method is superior, yet depends on the type of information that is provided in the problem, the designer's preferences, the solution requirements, and the availability of software.

The proposed design optimization procedure presented in this thesis is schematically shown in Figure 1.8. Initially, the optimization conditions are set: choices by the designer have to be made regarding the design parameters x , objective functions $\Phi(x)$, and constraints $G(x)$. This is done in the 'Optimization problem setup layer'. Any computable scalar quantity, e.g., acceleration time from 0 – 100 km/h, fuel consumption, or nitrogen oxide (NO_x)-emissions over a whole drive cycle, can be used as the system design objective function Φ .

Accordingly, in the 'Modeling and simulation layer' a response function $\Phi(x)$, which may be multi-dimensional, is created between the design parameters x , objective functions $\Phi(x)$, or constraint conditions $G(x)$. The design parameters represented by x , which include a topology choice, the component size, a component technology choice, and the control strategy for any given vehicle (including the vehicle parameters) and drive cycle, behave as a constant for a particular de-

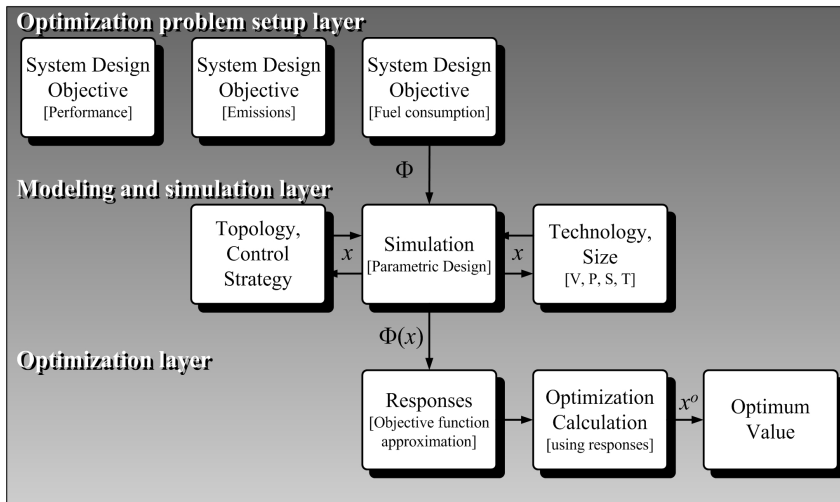


Figure 1.8 / Parametric design optimization for a hybrid vehicle propulsion system.

sign. However, the parameters can vary from one vehicle application to the next.

From a hybrid vehicle design point of view, the control design is considered as a subproblem. Therefore, the control design models use local design variables, such as the control power-flow of S . The following section discusses different optimization algorithms regarding the design of the control strategy. In order to find the optimal set of design parameters, the design optimization procedure operates by repeatedly evaluating the model at a certain design point x . In the modeling and simulation layer the numerical analysis is repeated as many times as set.

Finally, a relatively simple objective function approximation $\tilde{\Phi}(x)$ can be created using the responses $\Phi(x)$ in the 'Optimization layer'. In addition, an optimal solution can be found very quickly with a conventional optimization technique. The technique allows to capture the global trends in the design space. It should be noticed, that the accuracy of an optimal solution depends on the approximative accuracy of the objective function.

Multi-objective Optimization

In case of a multi-objective optimization, selection of a particular solution is done by giving more importance to some objectives. The simplest scalar substitute objective is obtained by assigning subjective weights to each objective and summing up all objectives multiplied by their corresponding weight [62]. The main weak-

ness of this approach is the difficulty to determine the appropriate weights when design information is not sufficiently available a priori. The approach requires multiple simulation runs to investigate the influence of weights on the substitute objective [25]. However, this is beyond the scope of the research presented in this thesis. Without loss of generality, a single-objective approach is employed where the main system design objective is minimization of the fuel consumption.

1.2.2 Modeling and Simulation Tools

In the last two decades, many different hybrid propulsion system modeling and simulation tools have been developed [11, 65, 88, 12, 67, 23, 4, 86, 53, 81]. Where from an optimization algorithm point of view, the modeling and simulation tool is a 'black box'. The simulation tools are based on pre-defined topologies, component technologies and control strategies. In [67, 23] a more flexible quasi-static modeling and simulation tool, i.e., 'QSS toolbox' is discussed, with which user-defined drive train topologies can be built quite easily. In [4, 53] the research is focused on developing optimization tools for optimizing component sizes and vehicle design parameters. The tools discussed in [4] and [53] are based on sequential quadratic programming and a clustering pareto evolutionary algorithm respectively. The tools use ADvanced VehIcle SimulatOR (ADVISOR) software [88] as a vehicle modeling and simulation platform. Another system design optimization approach as discussed in [74] uses globally optimal control strategy based on Dynamic Programming (DP) [8]. The disadvantages of the different heuristic control models used in ADVISOR are the numerous specific control rules, which depend strongly on the choice of hybrid propulsion system, need to be tuned on the optimal solution for a known drive cycle. DP eliminates the problem of tuning and is suitable for handling nonlinear non-convex problems. However, DP suffers from the 'curse of dimensionality' [9] and therefore requires (in contrary to ADVISOR) a relatively long computation time. These problems are addressed in this thesis.

1.3 Research Questions

The study presents a simulation-based optimization method, which is a step forward in developing a quick optimization and design analysis tool, where the overall fuel consumption of a hybrid propulsion system is predicted with reasonable accuracy for different vehicle classes and drive cycles. Within this context, a target is to find answers to the underlying research questions:

- (i) can a computationally efficient method be developed, which results in an optimized control strategy comparable to the strategy computed with DP?

- (ii) can reduced models be developed for topologies, component technologies and sizes, which can be employed for parametric design optimization with sufficient accuracy?

Calculation of the incremental fuel costs (savings) for all admissible control inputs during (dis-)charging, which are required as input for the control design model, can be a computational burden. Especially, if also the speed ratio of the transmission T is a design variable, or, in other words, if the static component efficiency models are used with freedom in engine speed and torque, on top of the power distribution problem in the control optimization process.

For a given vehicle speed and power demand at a certain time instant the speed ratio of the transmission T is selected, such that the efficiency of S , or P , or, the combined efficiency of S and P is maximum. If the losses of T are too large to be neglected (e.g., in case of the hydraulic actuated push-belt CVT [63]), then these losses play an important role in selecting the optimal speed ratio. The computation time further increases if this exercise is performed for, e.g., different component sizes, or transmission technologies. How these issues affect the hybrid propulsion system design are also discussed in this thesis.

Therefore, the second research question studies the possibility of reduced complexity modeling. Subsequently, the component efficiency models and the incremental fuel costs (savings) for all admissible control inputs required as input for the control design model are generated very quickly for different component sizes, technologies, and topologies.

1.4 Goals and Main Contributions of the Thesis

This thesis concentrates on methods for designing hybrid vehicle propulsion systems with significant reduction of fuel consumption and CO_2 -emissions on a representative drive cycle. Based on the two research questions posed in the previous section the main research objectives are:

- development of algorithms for calculating the control strategy and fuel consumption, and
- development of a reduced hybrid drive train model, which is decoupled from the choice of a specific hybrid drive train configuration, components, control, and can be used for hybrid drive train specification.

The idea of a high-level modeling framework decoupled from the choice of specific components as discussed in [67] is further elaborated by decoupling the design analysis from choice of a specific hybrid drive train configuration, and a

specific control strategy. Furthermore, it will be shown that, a different hybrid drive train configuration implies a different transmission technology T .

The used methods and the main expected contributions related to the different design parameters and the reduced hybrid drive train model are discussed below.

1.4.1 Control Strategy

In order to solve the control design problem several optimization methods have been studied and compared. Elaboration of global optimal optimization techniques (DP) and sub-optimal methods (Equivalent Consumption Minimization Strategies (ECMS), see, e.g., [59, 71]), and heuristic strategies have been investigated. This thesis presents a control design method based on the combination of Rule-Based (RB) strategies and ECMS. The developed method, called RB-ECMS, allows quick optimization, since the defined hybrid driving modes are independently of topology and tuning of many control rules on the optimal solution is not necessary. The control model uses one main design parameter, which affects the control design variable (power-flow of the secondary power source S). The main control design parameter is the maximum propulsion power of S during the M mode, denoted as P_M , which is not necessarily equal to the maximum available propulsion power. It will be shown, that the control design solution of the RB-ECMS is very close to the global optimal solution of DP. Furthermore, the method is used to explain the relationship between the fuel saving potential for each hybrid driving mode and the integral constraint of energy balance conservation.

1.4.2 Component Size and Technology

The component design problem is related to the component technology choice and sizing issues. In literature [67] scalable models for the main energy conversion components, i.e., the engine and the electric machine are discussed. The static efficiency map is scaled by changing, e.g., the engine's volumetric displacement, or the active rotor volume of the electric machine. Since the maximum power, denoted as P_{max} , is one of the main design parameters for the energy converters in this thesis, the static efficiency maps are linearly scaled up or down in order for their properties to match the desired values. The desired power of the component is obtained by linear altering of the torque curve. However, there is an uncertainty on the accuracy of the scaled models, thus scaling should be done with caution. Scaling of the energy storage components, e.g., batteries, or ultra capacitors, which are modeled as individual cells, can be done more easily by selecting the required number of cells in order to meet certain power or energy storage size specifications. The motivation for this approach is the lim-

Table 1.2 / Design parameters, parameter descriptions, and subparameters.

<i>Parameters</i>	<i>Description</i>	<i>Subparameters</i>
Topology	Determines the efficiency of power-flow paths, which indirectly influences the component efficiencies with changing the topology.	location of S and P in combination with a FWD, RWD, or AWD vehicle
Component size	Determines the maximum component output power (S and P), which indirectly affects the component efficiency with sizing.	component power limitation, P_{max}^\dagger
Component technology	Determines the component efficiency (P, S, and T).	fit coefficients, c_i^\dagger
Control strategy	Determines the power distribution between P, S and V, while minimization of the fuel consumption given certain component specifications and constraints.	control design parameter, P_M^\dagger

[†]These subparameters are in this thesis often also referred to as *characteristic component parameters*.

ited availability of nonproprietary component data for different technologies and sizes from third parties. Similar scaling approaches have been utilized by others [46, 2, 79, 3].

The possibility of describing the component efficiencies for T, P, and S as simplified power-based parametric fit functions is investigated in order to solve the component design problem. In this thesis, the coefficients of the power-based fit function, denoted as c_i (where subscript $i \in \mathbb{N}$), are also referred to as the ‘characteristic component parameters’ or ‘subparameters’. The characteristic component parameters are found by fitting linear or quadratic functions on the computed input and output powers for P, S, and T. The operation points, which are determined by the drive cycle, the vehicle load, and the control strategy, determine the values for the characteristic component parameters. Using the simplified power-based parametric functions in combination with the RB-ECMS, the effect of characteristic parameter variation of the components on the fuel consumption and control strategy can be investigated very quickly.

Table 1.2 gives an overview of the defined design parameters, their descriptions, and subparameters. For certain component technology choices (P, S, and T), a change in component size affects the maximum output power and indirectly the efficiency of the components. A change in topology influences the power-flow path efficiencies and therefore also indirectly affects the component efficiencies. In addition, the control strategy is influenced by these characteristics and therefore also the total fuel consumption over a drive cycle for a given vehicle is affected.

1.4.3 Reduced Hybrid Drive Train Modeling

The key idea behind a reduced hybrid drive train model is that a different topology, technology choice, or component size for P, S, and T simply implies a different set of subparameters. The same holds in principle for the design parameter of the control strategy, which is influenced by the component characteristic parameters.

This thesis contributes by showing that the characteristic component parameters describing the efficiency for P, S, and T can be determined with sufficient accuracy only dependent on the drive cycle and the vehicle parameters by assuming certain component operation preferences. This method allows the component efficiency models and the incremental fuel costs (savings) for all admissible control inputs, which are required as input for the RB-ECMS, to be generated very quickly for different component sizes, technologies, and topologies.

In this way a fast design analysis method is presented for the specification of a hybrid vehicle propulsion system by effectively narrowing down the initially large design space and reducing the complexity. Furthermore, the method links the control design optimization with the topology and the component design optimization into a single framework. The derived method has given insights in the basic principles that determine the fuel consumption and the direction of improvement with minimal system specifications.

The proposed hybrid drive train modeling approach with reduced complexity is studied and validated by means of simulation:

- for three different hybrid drive train configurations (or, transmission technologies) with fixed component sizes, vehicle and drive cycle, and
- for two different vehicles (i.e., a small passenger car, and a medium-duty truck) with different drive cycles and a fixed hybrid drive train configuration. The component sizes and technologies are optimized for the two vehicles as a design case study.

For this purpose, a detailed quantitative analysis is performed. The effects of the regenerative brake strategy, component sizing, technology selection, topology selection, and the speed ratio control strategy on the fuel consumption are investigated.

1.5 Outline of the Thesis

This thesis consist of 4 research chapters, Chapter 2 till Chapter 5. The Chapters 2 and 3 have been published respectively as journal articles in *International*

Journal of Electric and Hybrid Vehicles [31] and *World Electric Vehicle Association Journal* [30]. Chapter 4 has been submitted for publication to *IEEE Transactions on Vehicular Technology* [28] and Chapter 5 is accepted for publication in *International Journal of Heavy Vehicle Systems* [32]. The original text of each journal article is presented here and each chapter is self-containing. Finally, in Chapter 6 the main conclusions and recommendations for further research are given. Figure 1.9 shows schematically an overview of the chapters in relation to the reduced hybrid drive train model. A short description of the contents of each chapter is given next.

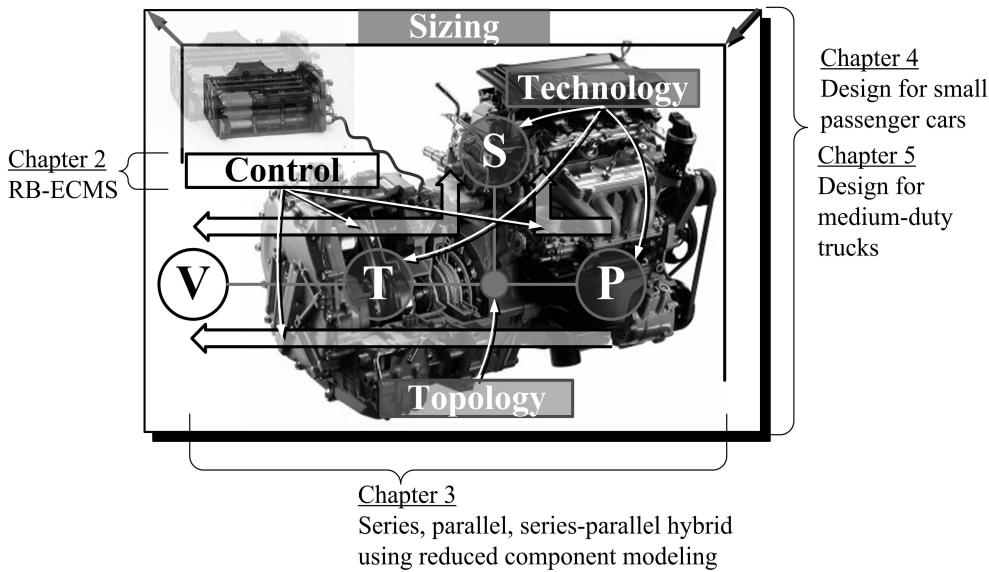


Figure 1.9 / An overview of the chapters of this thesis related to the high-level modeling and design framework, which can be employed for control design, topology selection, technology selection, and sizing of hybrid vehicle propulsion systems. Example background picture: drive train of a Honda Civic IMA [49]. Courtesy of Honda Motor Co.

In Chapter 2 [31] an overview of different control methods is given, and a new rule-based EMS is introduced based on the combination of Rule-Based and Equivalent Consumption Minimization Strategies (RB-ECMS). The RB-ECMS consists of a collection of driving modes selected through various states and conditions. In addition, a graphical representation of the influence of the hybrid driving modes on the energy balance and the fuel saving potential is discussed. Furthermore, the fuel consumption and the control strategy for the Toyota Prius (model 1998), cal-

culated with the RB-ECMS, are compared with results from Simulink/ADVISOR and DP.

Chapter 3 [30] investigates the possibility of overall model simplification for the hybrid vehicle propulsion system, including the control strategy using the RB-ECMS. This is performed by describing the component efficiencies and control rules with only a few characteristic model parameters that capture the fuel efficiency of the total system with sufficient accuracy. Using these parameters the modeling and simulation process is performed very quickly. The method is demonstrated on a series, a parallel, and a series-parallel hybrid drive train with specified component technologies, vehicle parameters, and drive cycle. The fuel consumption and control strategy results are compared with Simulink/ADVISOR and DP.

In Chapter 4 [28] the hybridization of a small passenger car equipped with a push-belt CVT and a gasoline engine is investigated as a design case study. The fuel consumption map is reconstructed based on measurements performed on a dynamo test bench and validated by simulation. The effects of changing the design parameters: component size (kW), topology, technology choice for conversion and transmission components, and CVT speed ratio control during braking and propulsion, on the fuel consumption are investigated. Moreover, Chapter 4 continues the concept of overall modeling simplification, where the effects of hybridization on the characteristic model parameters are investigated. Thereby, it seeks to investigate if a reduced hybrid vehicle model, under the same conditions as posed in Chapter 3, can be employed with sufficient accuracy for designing.

Chapter 5 [32] merges the ideas of overall model simplification for control and component efficiencies, and investigates again the effects of component sizing on the characteristic parameters, yet for different energy conversion and storage components. In this chapter the design problem is formulated for a medium-duty hybrid electric truck as a design case study. A method is proposed for determining the optimal degree-of-hybridization of the drive train and the energy storage system. The effects of hybridization on the vehicle acceleration performance, and the maximum gradeability are discussed. Moreover, the system storage mass and cost reduction benefits from hybridization of the energy storage system are discussed.

As stated, the final Chapter 6 will summarize the main results, and discusses possible future research.

Energy Management Strategies for Hybrid Vehicles

Abstract / The highest control layer of a (hybrid) vehicular drive train is termed the Energy Management Strategy (EMS). In this chapter an overview of different control methods is given and a new rule-based EMS is introduced based on the combination of Rule-Based and Equivalent Consumption Minimization Strategies (RB-ECMS). The RB-ECMS uses one main design parameter and requires no tuning of many threshold control values and parameters. This design parameter represents the maximum propulsion power of the secondary power source (i.e., electric machine/battery) during pure electric driving. The RB-ECMS is compared with the strategy based on Dynamic Programming (DP), which is inherently optimal for a given cycle. The RB-ECMS proposed in this chapter requires significantly less computation time with the similar result as DP (within $\pm 1\%$ accuracy).

2.1 Introduction

Hybridization in vehicles implies adding a Secondary power source with reversible energy buffer (S) (i.e., an electric machine/battery) to a Primary power source with irreversible energy buffer (P) (i.e., an engine/filled fuel tank) in order to improve vehicle performance. The major desirable improvements of the vehicle are regarding the fuel economy, emission reduction, comfort, safety, and driveability. The fuel consumption of a vehicle is reduced by down-sizing of the engine, which results in less idle-fuel consumption and a lower brake-specific fuel consumption. A second, though complementary method is recuperation of the brake energy and re-using this stored energy when momentary fuel costs are high avoiding idle-fuel consumption and engine operation points with high brake-specific fuel consump-

This chapter has been published in the form of a paper as / [31] Hofman, T., Van Druten, R., Serrarens, A., and M. Steinbuch, "Rule-based energy management strategies for hybrid vehicles", *Int. J. of Electric and Hybrid Vehicles*, vol. 1, no. 1, pp. 71-94, 2007.

tion. The Energy Management Strategy (EMS) plays an important role in an effective usage of the drive train components, see, e.g., [16, 59, 71, 68, 14, 39, 35]. Control strategies may be classified into non-causal and causal controllers respectively. Furthermore, a second classification is made among heuristic, optimal and sub-optimal controllers [24]. In the sections below some of these methods are discussed in more detail.

2.1.1 Optimal Control Strategy – Dynamic Programming

A commonly used technique for determining the globally optimal EMS is Dynamic Programming (DP), see, e.g., [73, 39, 74]. Using DP the finite horizon optimization problem is translated into a finite computation problem [8]. Note that although the DP solution may appear as an unstructured result, in principle the technique results in an optimal solution for the EMS. Using DP it is rather straightforward to handle non-linear constraints. However, a disadvantage of this technique is the relatively long computation time due to the relatively large required grid density. The grid density should be taken high, because it influences the accuracy of the result. Furthermore, it is inherently non-causal and therefore not real-time implementable.

2.1.2 Sub-Optimal Control Strategy – Heuristic Control Strategy

Most of the described Rule-Based (RB) control strategies in literature [88, 44, 89, 91] are based on ‘if-then’ type of control rules, which determine for example when to shut down the engine or the amount of electric (dis-)charging powers. The electric (machine) output power is usually prescribed by a nonlinear parametric function. Each driving mode uses different parametric functions, which are strongly dependent on the application (drive train topology, vehicle and drive cycle), and needs to be calibrated for different driving conditions. In [44, 89] and [91] the threshold values for mode switching and parameters are calibrated by using DP. Thereby, the power-split ratio between the secondary source S and the vehicle wheels for each driving mode is optimized. To overcome the difficulty of calibrating a large number of threshold values and parameters, control strategies are developed based on optimal control theory, which are discussed in the following section.

2.1.3 Sub-Optimal Control Strategy – Equivalent Consumption Minimization Strategy

In literature Equivalent Consumption Minimization Strategies (ECMS) are presented, see, e.g., [60, 59, 71, 54, 24], which are based on an equivalent fuel

mass-flow $\dot{m}_{f,eq}(t)$ (g/s). The equivalent fuel mass-flow uses an electric-energy-to-fuel-conversion-weight-factor, or equivalent (weight) factor $\lambda(t)$ (g/J) in order to weight the electrical power $P_s(t)$ (W) within the same domain at a certain time instant t (s). Basically, the $\lambda(t)$ is used to assign future fuel savings and costs to the actual use of electric power $P_s(t)$. Moreover, a well determined $\lambda(t)$ assures that discrepancy between the buffer energy at the beginning and at the end of the drive cycle with time length t_f is sufficiently small. The $\dot{m}_{f,eq}(t)$ is defined as,

$$\dot{m}_{f,eq}(t) = \dot{m}_f(P_s(t), t) - \lambda(t) \cdot P_s(t), \quad \lambda(t) > 0 \forall t \in \{0, t_f\}, \quad (2.1)$$

where $\dot{m}_f(P_s(t), t)$ is the instantaneous (actual) fuel mass-flow and can be expressed as a function of the electrical power $P_s(t)$. Although, for example, during discharging $P_s(t) < 0$ the actual fuel mass-flow $\dot{m}_f(P_s(t), t)$ is reduced, Equation (2.1) shows that the fuel equivalent of the electrical energy $-\lambda(t) \cdot P_s(t)$ is momentarily increased and vice-versa. The optimal momentary power set-point $P_s^o(t)$ for the secondary power source is the power, which minimizes Equation (2.1) given a certain $\lambda(t)$:

$$P_s^o(t) = \arg \min_{P_s(t)} (\dot{m}_{f,eq}(t) | \lambda(t)). \quad (2.2)$$

The $\lambda(t)$ depends on assumptions concerning the component efficiencies and chosen penalty functions on deviation from the target battery state-of-charge. Next, an overview on various approaches to this optimization problem seen in literature is given. Note that the first two methods require that the drive cycle is known.

Method 1

In [59] average efficiencies of the energy paths from fuel tank to battery, denoted as $\bar{\eta}_{tank \rightarrow bat}$, and vice-versa, denoted as $\bar{\eta}_{bat \rightarrow tank}$, are used to compute $\lambda(t)$:

$$\lambda(t) = \min \left(\lambda_{dis} \frac{P_s(t)}{|P_s(t)|}, \lambda_{chg} \frac{P_s(t)}{|P_s(t)|} \right) \cdot \frac{P_s(t)}{|P_s(t)|}, \quad (2.3)$$

with $\lambda_{dis} = 1/(\bar{\eta}_{tank \rightarrow bat} h_{lv})$, $\lambda_{chg} = \bar{\eta}_{bat \rightarrow tank} / h_{lv}$. The chemical content of fuel is represented by h_{lv} (J/g).

Method 2

In [71] the equivalent factors for (dis-)charging λ_{dis} , λ_{chg} are calculated using various constant values of the control variable by running different simulations for all admissible control inputs, given the drive cycle, the vehicle parameters and the upper and lower bounds for the state-of-charge. Accordingly, linear functions are fitted through the values of the total fuel energy use and the electrical energy

use during discharging and charging. The slopes of the straight lines that fit the data correspond with λ_{dis} and λ_{chg} respectively.

As mentioned by the authors [54], a disadvantage may be the strong sensitivity of $\lambda(t)$ and thus the equivalent factors on the relative state-of-charge $\xi(t)$ deviations. The main reason is lack of feedback or adaptation of $\lambda(t)$ according to the actual storage energy level. For online application the equivalent factor $\lambda(t)$ needs to be tuned, estimated, or adapted online, since, e.g., referring to method 1, the average component efficiencies are not known a priori and are different for each drive cycle. Next, some methods are discussed that do not require drive cycle information a priori.

Method 3

In [61] and [68] a non-linear penalty function is used to heuristically penalize the control power-flow of S using the discrepancy between the reference relative value of the state-of-charge of the battery $\xi_{ref} \triangleq \xi(t = 0)$ and the actual relative value $\xi(t)$. The shape of the penalty function

$$\lambda(t) = \phi_1 \left(1 - \left(\frac{\xi_{ref} - \xi(t)}{(\xi_{max} - \xi_{min})/2} \right)^{2\phi_2 + 1} \right) + \phi_3 \int_0^t (\xi_{ref} - \xi(\tau)) d\tau, \quad (2.4)$$

$$\phi_2 \in \mathbb{N}_0, \quad \{\phi_1, \phi_3\} \subseteq \mathbb{R}_0^+,$$

is adapted via certain parameters, *i.e.*, ϕ_1 , ϕ_2 , and ξ_{min} , ξ_{max} describing the desired relative state-of-charge ξ operation range. The integral term with the tune parameter ϕ_3 keeps track of the state-of-charge of the battery, which mainly influences the amplitude of the low-frequent oscillation of ξ . If ϕ_3 is chosen too large, then $\xi(t)$ may become unstable, *i.e.*, $\xi(t) \rightarrow \infty$.

Method 4

In [14] the instantaneous equivalent fuel rates are calculated a priori for all admissible control inputs, vehicle load torque, speed and equivalent factors. Then, the optimal engine torques (used as control input) and gear ratios are pre-calculated and are stored in look-up tables. Starting with an initial guess, $\lambda(t)$ is adjusted online with a pre-determined correction value $\Delta\lambda$ over the drive cycle:

$$\lambda(t) = \begin{cases} \lambda_u, & \text{if } \xi(t) > \xi_{max}, \\ \lambda_l, & \text{else if } \xi(t) < \xi_{min}, \\ \lambda' - \Delta\lambda, & \text{else if } \xi(t) = \xi_{ref} \wedge \lambda = \lambda_u, \\ \lambda' + \Delta\lambda, & \text{else if } \xi(t) = \xi_{ref} \wedge \lambda = \lambda_l. \end{cases} \quad (2.5)$$

If this correction number is chosen too large the equivalent factor $\lambda(t)$ may oscillate. The previous stored λ' is corrected for with $\Delta\lambda$ when ξ exceeds the upper or

lower boundary of ξ . The $\lambda(t)$ is ‘learned’ by using pre-determined fuel equivalent factors, i.e., λ_u , λ_l that are used to bring back the $\xi(t)$ to the reference value. Then, the $\lambda(t)$ is updated. The value of these parameters determine how fast the $\lambda(t)$ is learned. Practical experience is needed to tune or to optimize these parameters.

Method 5

In [39], [40] and [35] also the discrepancy between the actual value and reference value of ξ of the battery is used to calculate $\lambda(t)$ online, in this case by using a PI-controller:

$$\lambda(t) = \lambda_0 + K_p (\xi_{ref} - \xi(t)) + K_i \int_0^t (\xi_{ref} - \xi(\tau)) d\tau. \quad (2.6)$$

This solution seems rather straightforward and effective, however, the solution is sensitive to the initial value λ_0 and the choice of the control parameters K_p and K_i . If the K_p , K_i control parameters are chosen large, the power-flow of the accumulator is strongly penalized, such that the fuel saving will be smaller compared to mildly tuned control parameters. However, when a good estimation of λ_0 is obtained only a relatively mild PI-controller is required, because the relative change of $\lambda(t)$ over the drive cycle is usually very small.

2.1.4 Sub-Optimal Control Strategy – RB-ECMS

In order to tackle the drawbacks of DP, RB and ECMS, which is the aim of this chapter, a new and relatively simple solution for the EMS control problem is introduced having the following main features:

- the proposed method consists of a combination of methods, i.e., RB and ECMS (RB-ECMS),
- the maximum propulsion power of the secondary power source (i.e., electric machine / battery) during pure electric driving is used as the main design parameter, and
- the predefined hybrid modes and rules are independent on the type of drive train topology.

Since a drive train topology defines the paths and the efficiencies of the energy flow between P, S and the vehicle wheels. However, a topology choice influences the optimization of the design parameter. Summarized, an overview of the discussed methods is shown in Table 2.1.

2.1.5 Outline of the Chapter

The remainder of this chapter is structured as follows: first, the general control optimization problem of a hybrid drive train is discussed in Section 2.2. Then, the derived hybrid driving modes and the RB-ECMS are discussed in the Sections 2.3 and 2.4 respectively. Furthermore, a physical background for not using all potentially available motoring power during pure electric driving is given. The relationship between $\lambda(t)$ as used in ECMS and the design parameter as used in the proposed RB-ECMS is discussed. In Section 2.5, results of the proposed RB-ECMS are compared for a specific application (Toyota Prius, model 1998) with results from DP and the vehicle simulation platform ADVISOR [88]. Finally, the conclusions are given in Section 2.6.

Table 2.1 / Overview of discussed methods (-/+ : dis-/advantage).

DP	RB	ECMS	RB-ECMS (this chapter)
+ globally optimal	- sub-optimal	- sub-optimal	- sub-optimal
- apparently unstructured result	- tuning of many parameters, threshold values	+ few calibration parameters	+ few calibration parameters
- long computation time	+ relatively simple, engineering intuition	+ short computation time	+ short computation time
- offline strategy	+ on-/offline strategy	+ on-/offline strategy	+ on-/offline strategy
+ handling non-linear constraints	- specific rules depend strongly on the topology choice	- $\lambda(t)$ sensitive to $\xi(t)$ deviations	+ modes/rules independent on the topology choice

2.2 Problem Definition

The optimization problem is finding the control power-flow $P_s(t)$, given a certain power demand at the wheels $P_v(t)$ minimizing the cumulative fuel consumption, denoted by the variable Φ_f , over a certain drive cycle with time length t_f , subject to several constraints, i.e.,

$$\Phi_f = \min_{P_s(t)} \int_0^{t_f} \dot{m}_f(E_s(t), P_s(t), t | P_v(t)) dt, \quad (2.7)$$

subject to $\vec{h} = 0, \vec{g} \leq 0,$

where \dot{m}_f is the fuel mass-flow in g/s, which can be expressed as a function of the state variable E_s and the control input variable P_s . The state is equal to the stored

energy E_s in the secondary reversal energy buffer in J, and the control input is equal to the secondary power-flow P_s in W (see, also Figure 2.1). The energy level in the battery is a simple integration of the power and is calculated as follows,

$$E_s(t) = E_s(0) + \int_0^t P_s(\tau) d\tau. \quad (2.8)$$

The main constraints on the secondary power source S are energy balance conservation of E_s over the drive cycle, constraints on the power P_s , and the energy E_s :

$$\begin{aligned} h_1 &:= E_s(t_f) - E_s(0) = 0, \\ g_{1,2} &:= P_{s,min} \leq P_s(t) \leq P_{s,max}, \\ g_{3,4} &:= E_{s,min} \leq E_s(t) \leq E_{s,max}. \end{aligned} \quad (2.9)$$

The optimal solution is denoted $P_s^o(t)$. In this chapter the value for the energy

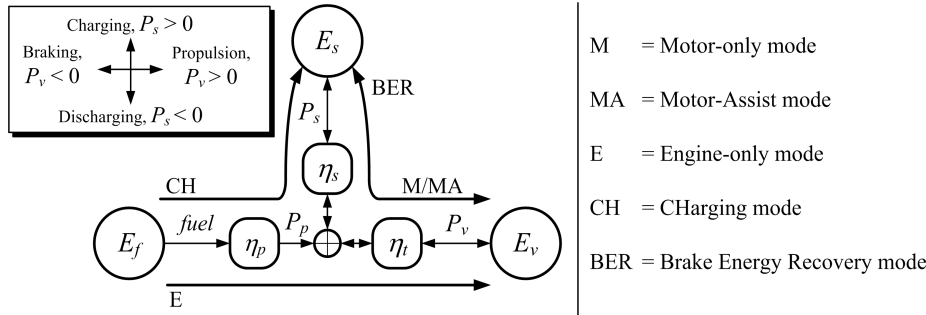


Figure 2.1 / Power-flows for the different hybrid driving modes. Secondary power source S is connected at the engine-side of the transmission.

level instead of the charge level in the battery has been used. Note that, if the open-circuit voltage of a battery is assumed constant, then the relative state-of-charge ξ is equal to the relative state-of-energy, i.e., $\xi(t) = E_s(t)/E_{cap}$. The energy capacity of the battery E_{cap} is assumed to be constant. However, for battery systems the open-circuit voltage typically changes slightly as a function of ξ . This is not considered in this chapter.

2.3 Hybrid Driving Modes

A hybrid drive train can be operated in certain distinct driving modes. In Figure 2.1, a block diagram is shown for the power distribution between the different energy sources, i.e., fuel tank with stored energy E_f , S with stored energy E_s , and the vehicle driving over a drive cycle represented by a required energy E_v .

The efficiencies of the fuel combustion in the engine, the storage and electric motor S, and the Transmission (T) are described by the variables η_p , η_s , and η_t respectively. The energy exchange between the fuel tank, source S and the vehicle can be performed by different driving modes (depicted by the thick lines). The engine power at the crank shaft is represented by P_p . The power demand at the wheels (P_v) and the power-flow to and from S (P_s) determine which driving mode is active. The following operation modes are defined:

- M: Motor-only mode, the vehicle is propelled only by the electric motor and the battery storage supply (S) up to a fixed propulsion power (design parameter) for the whole drive cycle, which is not necessarily equal to the maximum available propulsion power of the electric machine. The engine is off, has no drag and no idle losses.
- BER: Brake Energy Recovery mode, the brake energy is recuperated up to the maximum generative power limitation and stored into the accumulator of S. The engine is off, has no drag and no idle losses.
- CH: CHarging mode, the instantaneous engine power is higher than the power needed for driving. The redundant energy is stored into the accumulator of S.
- MA: Motor-Assisting mode, the engine power is lower than the power needed for driving. The engine power is augmented by power from S.
- E: Engine-only mode, only the engine power is used for propulsion of the vehicle. S is off and generates no losses.

The engine is off during the M and BER mode and uses no fuel. This is also referred to as the start-stop mode. Since the electrical loads in vehicles are expected to increase in the near future it may be important to define more hybrid (charging) modes. However, the auxiliary loads are not considered in this chapter. The reader is referred to [36] in which heating and airconditioner loads are discussed.

2.4 The RB-ECMS

The operation points for P and S given certain driving conditions (drive cycle and vehicle parameters) can be found in certain distinct driving states, or modes. For the ease of understanding, the modes are represented as operation areas in a static-efficiency engine map separated by two iso-power curves as are shown in Figure 2.2. The solid iso-power curve separates the M mode from the CH mode, and the E mode. The dotted iso-power curve separates the operation points of

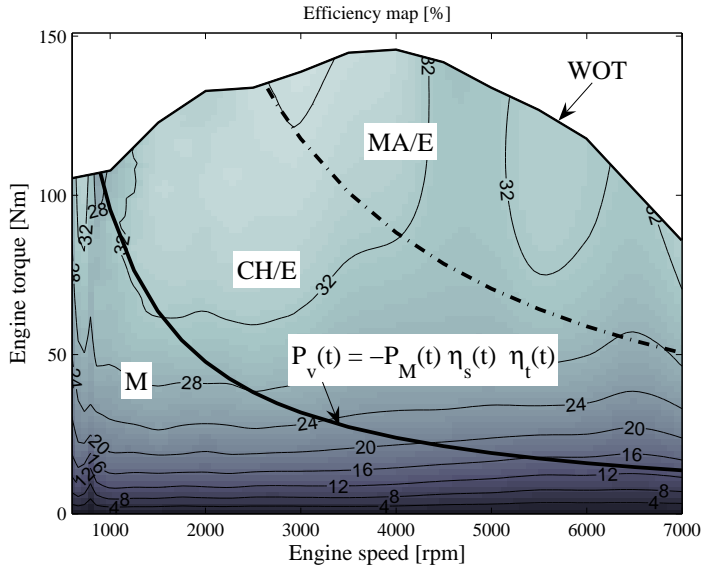


Figure 2.2 / Contour plot of the engine efficiency in % as a function of the engine torque and speed. WOT = Wide-Open Throttle torque.

the engine during the CH and the MA mode. The vehicle drive power values for which the secondary source during the M mode is sufficient (i.e., below the solid line in Figure 2.2) is given by,

$$P_v(t) \leq -\max(\min(0, P_s(t)), P_M(t)) \eta_s(t) \eta_t(t), \quad (2.10)$$

with $P_{s,min} \leq P_M(t) \leq 0$ the largest possible motor-only power. The minimum discharging power is denoted as $P_{s,min}$. So we also have that in M mode:

$$P_v(t) = -P_M(t) \eta_s(t) \eta_t(t), \quad (2.11)$$

which is shown as a solid line in Figure 2.2. Following from the EMS calculated with DP, the decision variable $P_M(t)$ determining when to switch between the M mode and the other modes, appeared to be approximately constant with the vehicle power demand $P_v(t)$, i.e., $P_M(t) \approx P_M \forall t \in \{0, t_f\}$. Whereas the (dis-)charging power and the mode switch between MA and CH mode varies with the vehicle power demand.

In order to fulfill the integral energy balance constraint over the drive cycle (see, Equation (2.9)), the energy required for the M and the MA mode needs to be regenerated during the BER mode or charged during the CH mode. To

explain the basic principles of the RB-ECMS, which is a trade-off between energy balance and fuel consumption, consider the following two arbitrary cases. Both cases are schematically shown in Figure 2.3. The energy of the CH₁ or the MA₁ mode is always balanced with the M or the BER mode respectively. Either case represents a different choice for P_M , where the recuperated brake energy (BER) is: (i) not sufficient, and (ii) more than sufficient for supplying the energy during the motor-only mode (M) over a given drive cycle.

- (i) The additional required energy for the M mode has to be charged during the CH₁ mode resulting in additional fuel cost.
- (ii) The redundant energy of the BER mode can be used for motor-assisting during the MA₁ mode resulting in additional fuel savings.

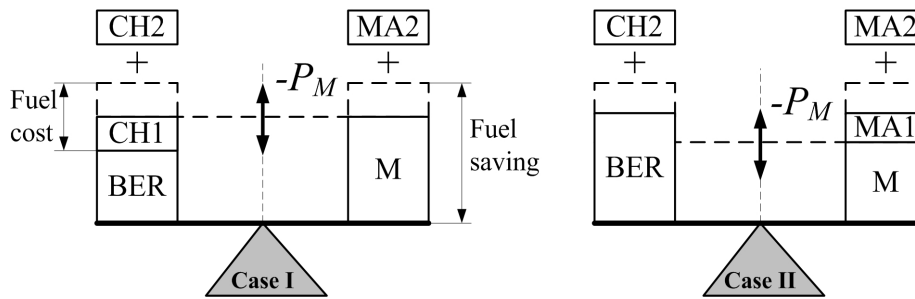


Figure 2.3 / Energy balance and fuel consumption, after completion of a whole drive cycle.

Referring to case (i), if $-P_M$ is lowered, then the additional fuel cost becomes lower due to decrease of the required charging energy. However, the fuel saving due to the M mode is also reduced, and vice-versa, if $-P_M$ is increased. The same holds for case (ii): the fuel saving during the MA₁ mode is increased if $-P_M$ is lowered, but the fuel saving due to the M mode is reduced.

For both cases, additional charging (CH₂ mode) during driving and using this buffered energy for motor-assisting (MA₂ mode) can be beneficial. The energy of the CH₂ mode is always balanced with the MA₂ mode. This is illustrated with an example as is shown in Figure 2.4. In this figure the fuel mass-flow \dot{m}_f as a function of the engine power P_p at a certain engine speed ω_p is shown. Typically, for engines the fuel mass-flow increases more than linear (convex curvature) with the output power at any given speed [40]. Therefore, if charging is done at a low engine power demands and used for assisting at a high engine power demands, then it can be seen that fuel is saved by subtracting the fuel saving minus the

fuel cost. This fuel saving potential increases, if the progressiveness of the fuel mass-flow as a function of the engine power increases.

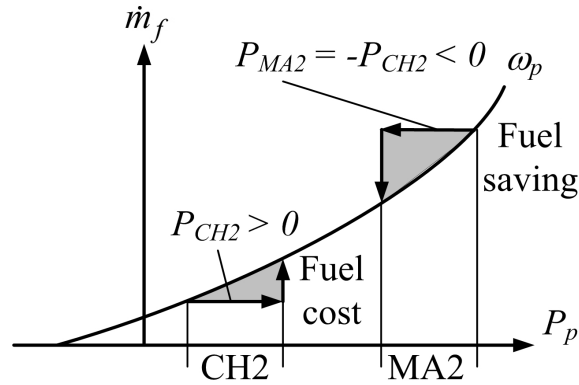


Figure 2.4 / The fuel mass-flow as a function of engine power at a certain engine speed.

However, it should be noticed, that the additional fuel saving potential is relatively small and limited, because:

- the fuel mass flow as a function of engine power is usually quite linear, resulting in smaller fuel mass-flow differences,
- the conversion losses between P and S, and the storage losses of S further decrease the fuel saving potential, and
- the energy of the high drive power demands dependent on the driving conditions (drive cycle, vehicle parameters) is usually relatively small.

The optimal value of P_M has to be a trade-off between the BER, M, CH (CH_1+CH_2), and the MA (MA_1+MA_2) mode. This requires some kind of optimization in which all modes are included and will be explained in the following three sections.

2.4.1 Power-Flow during the BER and the M Mode

Based on the EMS from DP, the optimal power set-point $P_s^o(t) = P_{s,I}^o(t)$ during the M and the BER mode is respectively,

$$P_{s,I}^o(t) = -\max(\underbrace{P_v(t)/(\eta_s(t) \eta_t(t))}_{\text{M mode}}, \underbrace{P_v(t) \eta_s(t) \eta_t(t)}_{\text{BER mode}}). \quad (2.12)$$

The subscript I indicates the power-flow during the BER and M mode. The minus sign in Equation (2.12) indicates that the source S is discharging during

propulsion and charging during braking. Notice that, if the source S is coupled at the wheel-side of the transmission, then $\eta_t(t)$ in Equation (2.12) is left out. The power set-point is limited between the following constraints,

$$P_{s,min} \leq P_M^o \leq 0 \leq P_{s,I}^o(t) \leq P_{s,max}. \quad (2.13)$$

Braking powers larger than the maximum charging power $P_{s,max}$ are assumed to be dissipated by the wheel brake discs. If only the M and/or the BER mode are utilized, then the energy difference $\Delta E_{s,I}$ at the end of the drive cycle becomes,

$$\Delta E_{s,I} = \int_0^{t_f} P_{s,I}^o(t) dt, \quad \Delta E_{s,I} \in \mathbb{R}. \quad (2.14)$$

In order to fulfill the equality constraint h_1 of Equation (2.9) this energy has to be counterbalanced with the relative energy $\Delta E_{s,II}$ at the end of the cycle during the MA and the CH mode as is shown in Figure 2.5, where,

$$-\Delta E_{s,I} = \Delta E_{s,II}. \quad (2.15)$$

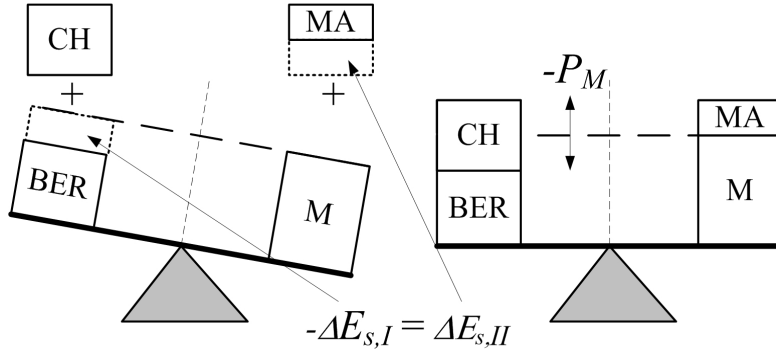


Figure 2.5 / Energy balance during the BER/M and the CH/MA modes.

2.4.2 Power-Flow during the MA, the CH, and the E Mode

The fuel mass-flow during the BER/M mode is $\dot{m}_f(P_{s,I}^o(t), t) = 0$. Therefore, the total fuel mass-flow $\dot{m}_f(t)$ can be written as the sum of the fuel mass-flow only depending on the drive power demand $P_v(t)$ (engine-only, E mode) and some additional fuel mass-flow $\Delta \dot{m}_f(t)$ depending on the (dis-)charging power $P_{s,II}(t)$ during the MA and the CH mode,

$$\dot{m}_f(t) = \begin{cases} 0, & \text{if } -P_v(t)/(\eta_s(t) \eta_t(t)) \geq P_M^o, \\ \underbrace{\dot{m}_f(P_v(t), t)}_{\text{E mode}} + \underbrace{\Delta \dot{m}_f(P_{s,II}(t), t)}_{\text{CH/MA mode}}, & \text{elsewhere.} \end{cases} \quad (2.16)$$

If $P_{s,II}(t) = 0$, then the vehicle is propelled by the engine-only (E mode). During the MA and the CH mode the engine is on and the optimal motor-assisting or charging power $P_{s,II}^o(t) \neq 0$ depends on the drive power demand $P_v(t)$, the component efficiencies and the amount of energy $\Delta E_{s,II}$ that needs to be counterbalanced with the energy used during the BER/M mode $\Delta E_{s,I}$. The optimization problem becomes finding the optimal power-flow $P_{s,II}^o(t)$ during the CH and the MA mode given a certain power demand $P_v(t)$ while the cumulative fuel consumption denoted by the variable Φ_f over a certain drive cycle with time length t_f is minimized subjected to the energy constraint of Equation (2.15):

$$\Phi_f = \min_{P_{s,II}(t)} \int_0^{t_f} \dot{m}_f(P_{s,II}(t), t | P_v(t)) dt, \text{ subject to} \quad (2.17)$$

$$\int_0^{t_f} P_{s,II}(t) dt = \Delta E_{s,II}.$$

Finding a solution to this problem is solved via an unconstrained minimization of the Lagrangian function Φ'_f using a Lagrange multiplier $\lambda(t)$.

$$\Phi'_f = \min_{P_{s,II}(t)} \int_0^{t_f} (\dot{m}_f(P_{s,II}(t), t | P_v(t)) - \lambda(t) P_{s,II}(t)) dt \quad (2.18)$$

$$+ \lambda(t) \Delta E_{s,II}.$$

The optimal solution is calculated by solving,

$$\frac{\partial \Phi'_f}{\partial P_{s,II}(t)} = 0, \text{ and } \frac{\partial \Phi'_f}{\partial \lambda(t)} = 0. \quad (2.19)$$

The solution is given by,

$$\frac{\partial(\dot{m}_f(P_{s,II}(t), t | P_v(t)))}{\partial P_{s,II}(t)} - \lambda(t) = 0, \text{ and } \int_0^{t_f} P_{s,II}(t) dt = \Delta E_{s,II}. \quad (2.20)$$

If $\dot{m}_f(P_{s,II})$ is approximated as a convex quadratic relation [39]:

$$\dot{m}_f(P_{s,II}) \approx c_2 P_{s,II}^2 + c_1 P_{s,II} + c_0, \quad c_2 > 0, \quad (2.21)$$

then there exists a unique solution for $\lambda(t)$, i.e., $\lambda(t) = \lambda_0$ and $P_{s,II}(t)$ imposed by the (in-)equality constraints (see, also for proof [80]). The parameters c_i are time varying, because the parameters are dependent on $P_v(t)$. Moreover, from classical optimal control theory, it follows that the solution for $\lambda(t)$ is a constant (see, e.g., [16], [24]). This under the assumption that the storage power-flow is not affected by the state-of-energy of the accumulator. This holds if the change in, e.g., the internal battery parameters (open circuit voltage, internal resistance) is neglected, which is assumed in this chapter. The constant λ_0 is also referred to the average equivalent weight factor. The optimizing solution λ_0 requires the

a priori information of the complete drive cycle. If λ_0 is known, then the optimal accumulator power $P_{s,II}^o(t)$ is calculated by solving at the current time instant t :

$$P_{s,II}^o(t) = \arg \min_{P_{s,II}(t)} (\dot{m}_f((P_{s,II}(t), t) | P_v(t)) - \lambda_0 P_{s,II}(t)), \quad (2.22)$$

where the power set-point is limited between the following constraints,

$$P_{s,min} \leq 0 \leq P_{s,II}^o(t) \leq P_{s,max}. \quad (2.23)$$

Then $\Delta E_{s,II}$ is discharged (charged) at vehicle power demands where the fuel savings (costs), i.e., $\Delta \dot{m}_f$ are maximum (minimum). In addition, the energy quantities during the MA and the CH mode are in balance with the BER and M mode over the whole drive cycle.

2.4.3 Optimization Routine (Offline) for calculating P_M^o

Summarized, the optimal power set-point for the secondary power source S as discussed in the previous two sections during the BER/M and the CH/MA mode becomes respectively:

$$P_s^o(t) = \begin{cases} P_{s,I}^o(t) \text{ (see, Equation (2.12)), if } -P_v(t)/(\eta_s(t) \eta_t(t)) \geq P_M^o, \\ P_{s,II}^o(t) \text{ (see, Equation (2.22)), elsewhere.} \end{cases} \quad (2.24)$$

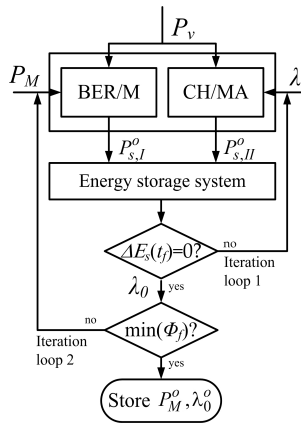
In the Figure 2.6(a), a block diagram is shown of the offline optimization routine suggested in this chapter. The routine consist of two iteration loops. In addition, some example results of the iteration loops are shown in the Figures 2.6(b), 2.6(c) and 2.6(d) respectively. The results are based on a hybrid vehicle, which will be discussed in more detail in the following section. In iteration loop 1, the value for λ using a chosen fixed mode switch value of $P_M = [P_{s,min}, 0]$ is determined, which assures that for the whole drive cycle the energy during the BER/M modes is in balance with the energy during the CH/MA modes (see, Figure 2.6(b)). The corresponding λ is denoted as λ_0 :

$$\lambda_0 \in \{\Delta E_s = \Delta E_s(\lambda) | \Delta E_s(\lambda_0) = 0 \wedge \Delta E_s = \Delta E_{s,I} + \Delta E_{s,II}\}. \quad (2.25)$$

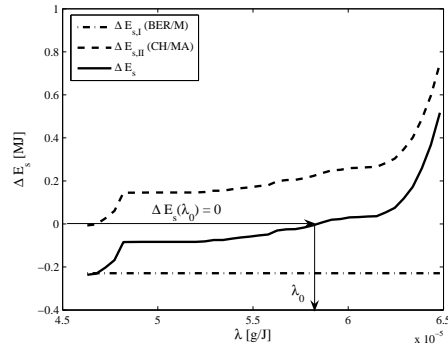
In Figure 2.6(c) the resulting Φ_f as a function of different chosen fixed values for P_M is shown. In iteration loop 2, the optimal value for P_M is determined, which minimizes the total fuel consumption Φ_f :

$$P_M^o = \arg \min_{P_M} \Phi_f(P_M). \quad (2.26)$$

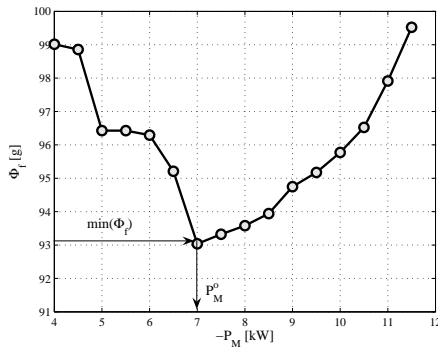
Then, simultaneously the corresponding value for λ_0 , denoted as λ_0^o , is stored as is shown in Figure 2.6(d). In the following section based on the results with DP and the RB-ECMS, the relationship between P_M^o and λ_0^o is discussed in more detail.



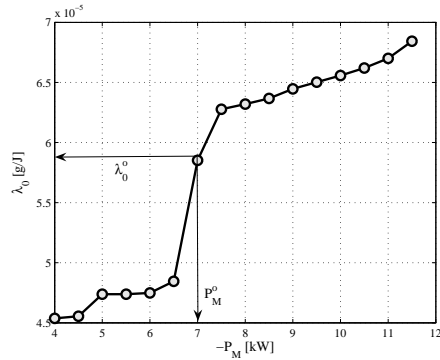
(a) Optimization routine.



(b) Iteration loop 1, an example of $\Delta E_s = \Delta E_s(\lambda)$.



(c) Iteration loop 2, an example of $\Phi_f = \Phi_f(P_M)$.



(d) Iteration loop 2, determination of the corresponding λ_0 with P_M^o .

Figure 2.6 / Numerical optimization scheme for calculation of P_M^o (offline), and example results of iteration loop 1 and 2.

2.5 Simulation Results

2.5.1 Component Models

Simulations were done for a series-parallel hybrid transmission type (Toyota Prius, 1998). In Figure 2.7 the control model, which is used to calculate the optimal control signal is shown. The arrows indicate the direction of power-flow and the components, which are schematically represented as blocks, are modeled as static efficiency functions. The control model is a backwards facing or differentiating model. The input is the vehicle speed, which is assumed to be tracked exactly. The transmission technology under investigation consists of one plan-

etary gear set and an electric variator (electric machine 1 and 2). The engine is connected to the carrier, electric machine 1 is connected to the sun gear, electric machine 2 and the propulsion shaft are both connected to the annulus of the planetary gear set. In this case S is part of T. However, if only the components, that are used during the BER and M mode, are defined to be functional part of S, then electric machine 2 (connected at the wheel-side of T) is part of S (see, Figure 2.7).

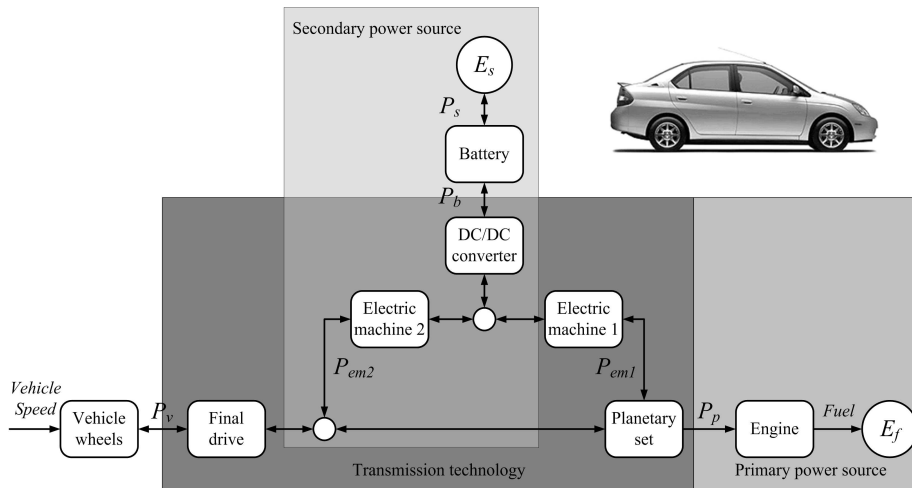


Figure 2.7 / Power-flow in the hybrid vehicle drive train (backwards facing control model).

In Table 2.2 an overview of the component data [57] is given. The inertias of the electric machines, engine and auxiliary loads are, for simplicity, assumed to be zero. All simulations performed presented in this chapter have been done for the JP10-15 mode cycle [34]. It is derived from the 10-mode cycle (maximum speed of 40 km/h) by adding another 15-mode segment of a maximum speed of 70 km/h. In Figure 2.8 the vehicle speed and the corresponding drive power demand at the wheels as a function of time is shown. Furthermore, the engine is assumed to be operated at its maximum efficiency operation points.

2.5.2 Control Models

For comparison the control strategy based on measurement data as is implemented in ADVISOR [88] is compared with the results from the RB-ECMS and DP. The control strategies, which are compared, are listed in Table 2.3.

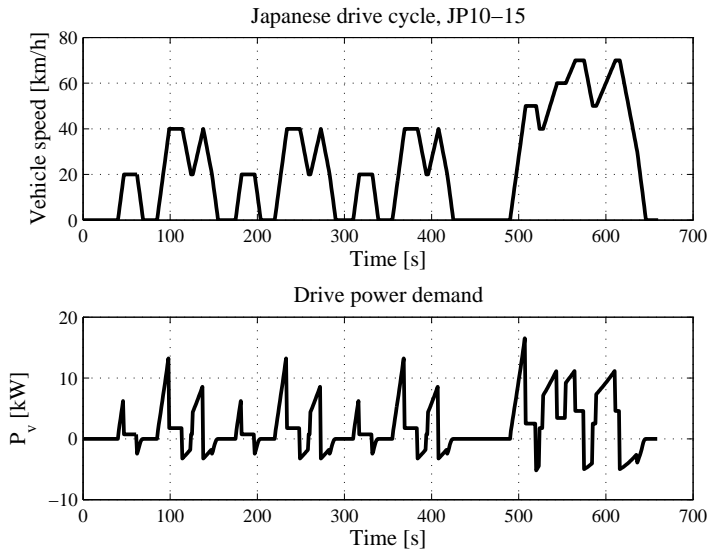


Figure 2.8 / Vehicle speed and mechanical drive power demand at vehicle wheels.

Table 2.2 / Relevant component data.

<i>Series-parallel hybrid configuration</i>	
Electric machine 1 (engine-side)	Manufacturer: Toyota; 15-kW (continuous) PM motor/inverter, Torque range: from 55 Nm to 26 Nm (corresponding speed from 0 rpm to 5500 rpm). The efficiency map includes the inverter/controller efficiencies.
Electric machine 2 (wheel-side)	Manufacturer: Toyota; 30-kW (continuous) PM motor/inverter, Torque range: from 305 Nm to 47.7 Nm (corresponding speed from 0 rpm to 6000 rpm). The efficiency map includes the inverter/controller efficiencies.
Planetary gear set/Final drive	The planetary gear set ratio and the final drive ratio are -2.6 and 0.2431 respectively. The efficiencies are both constant 0.98 assumed.
<i>Energy storage system</i>	
Battery pack	Manufacturer: Panasonic; Type: Ni-MH, Nominal voltage 288 Vdc, Capacity 6 Ah, $\xi_{min} = 45\%$, $\xi_{max} = 75\%$, $\xi_{ref} = 55\%$.
<i>Vehicle data</i>	
Mass: 1368 kg, Air drag coefficient: 0.29, Frontal area: 1.746 m ² , Roll resistance coefficient: 0.9%, Maximum regenerative brake fraction: 0.5.	
<i>Engine data</i>	
Manufacturer: Toyota; Displacement and type: 43-kW (at 4000 rpm) 1.5-l SI Atkinson internal combustion engine. Maximum torque: 102 Nm at 4000 rpm	

Reference Heuristic Control Model – ADVISOR

In the Table 2.4 the rule-based conditions that define which hybrid mode is active are given. If the wheel torque demand is negative, i.e., $T_v(t) < 0$, then the

Table 2.3 / Simulated strategies for comparison.

RB1	Default ADVISOR control strategy
RB2	Optimized ADVISOR control strategy
RB-ECMS	RB-ECMS control strategy
DP	The strategy based on the outcome of the DP algorithm.

BER mode is active. The control parameters $f_M = P_p(t)/P_{p,max}$ (engine-power-ratio threshold value) and v_M (vehicle-electric-launch-speed threshold value) determine if the M mode is active. The battery is allowed to operate within a certain defined state-of-charge window, i.e., $\xi(t) = [\xi_{min}, \xi_{max}]$. If the state-of-charge $\xi(t)$ gets too low, then the battery is charged during driving (CH mode) with a certain charging power, which is the output of a proportional controller of which the input is the difference between ξ_{ref} and $\xi(t)$. Motor-assisting (MA mode) is only performed if the engine torque demand is larger than the maximum available engine torque $T_{p,max}$, which is a function of the engine speed $\omega_p(t)$. The default control parameters f_M and v_M as implemented in ADVISOR (RB1) were optimized (RB2) to achieve the highest fuel economy, while the final $\xi(t_f)$ is maintained within a certain tolerance band $\pm 0.5\%$ from its reference value ξ_{ref} .

Table 2.4 / Rule-based control model as is implemented in ADVISOR.

Mode	Rule-based condition:
BER	$\xi(t) < \xi_{max} \wedge T_v(t) < 0$
M	$\xi(t) \geq \xi_{min} \wedge P_p(t) < f_M P_{p,max} \vee v(t) < v_M$
CH	$\xi(t) < \xi_{min} \vee \xi(t) < \xi_{ref} \wedge P_p(t) \geq f_M P_{p,max}$
E	$\xi(t) = \xi_{ref} \wedge P_p(t) \geq f_M P_{p,max}$
MA	$\xi(t) \geq \xi_{min} \wedge T_p(t) > T_{p,max}(\omega_p(t))$

Reference Optimal Control Model – Dynamic Programming

Using DP for solving the optimal control problem requires discretization of the Equation (2.7) with a time step Δt . First, the continuous variables are mapped onto a fixed grid. The DP strategy is used with an input grid of 250 W and a state grid of 250 J. The relevant state variable is the energy level in the battery, which becomes

$$E_s(k+1) = E_s(k) + P_s(k) \Delta t, \text{ for } k = [1, \dots, n-1] \in \mathbb{N}_0, \quad (2.27)$$

with the constraints put on $P_s(k)$,

$$P_{s,min} \leq P_s(k) \leq P_{s,max}, \quad (2.28)$$

and the bounds on $E_s(k)$ is written as constraints on $P_s(k)$ in the following way,

$$E_{s,min} - E_s(1) \leq \sum_{k=1}^{n-1} P_s(k) \Delta t \leq E_{s,max} - E_s(1). \quad (2.29)$$

Furthermore, the energy balance conservation requires,

$$E_s(n) = E_s(1) \Rightarrow \sum_{k=1}^{n-1} P_s(k) \Delta t = 0. \quad (2.30)$$

Then, a cost-to-go matrix Φ_f is calculated, where each element represents fuel costs for reaching the final end-state. The DP algorithm holds,

$$\Phi_f(E_s(k), k) = \begin{cases} 0, & \text{for } k = n, \\ \min_{P_s(k)} \left(\begin{aligned} &\Phi_f(E_s(k+1), P_s(k+1), k+1) \\ &+ \dot{m}_f(P_s(k), k) \Delta t \end{aligned} \right), & \text{for } k = [n-1, \dots, 1]. \end{cases} \quad (2.31)$$

Finally, at each time step k of the optimization search, the function $\Phi_f(E_s(k), k)$ is evaluated only at the grid points of the state variable. The recursive equation is solved backwards and the path with minimal costs represents the optimal trajectory (see, Figure 2.9).

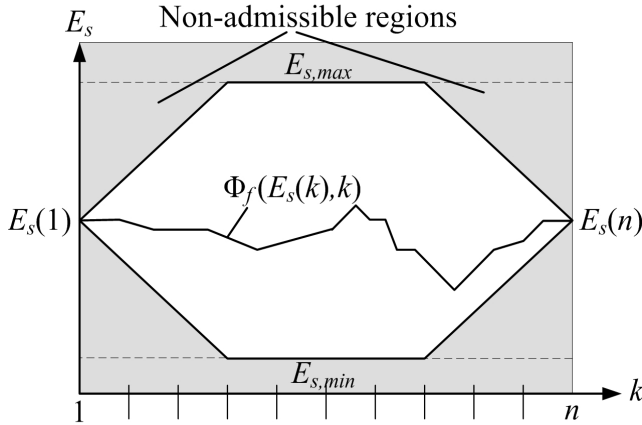


Figure 2.9 / Illustration of feasible domain for battery energy and optimal trajectory resulting from DP algorithm along the drive cycle.

2.5.3 Results

In Table 2.5 the fuel economy results for the different strategies are listed. Note that the measured fuel economy reported by Toyota is 3.57 l/100km (28 km/l).

In Figure 2.10 the energy distribution over the different hybrid driving modes for each strategy is shown. In the Figures 2.11(a) and (b) the energy difference over time $\Delta E_s(t)$ and the fuel consumption $\Phi_f(t)$ for the different strategies are shown respectively. With the default control parameters as implemented in RB1 ($f_M = 0.20$, which is equivalent to $P_M \eta_s(t) = -6$ kW, and $v_M = 12.5$ m/s), it was found, that during propulsion at relatively low $P_v(t)$ and braking the engine was not always allowed to shut off. This resulted in less idle stop and less effective regenerative braking power due to additional engine drag torque losses respectively. The optimized control parameters for the RB2 are $f_M = 0.116$, which is equivalent to $P_M^o \eta_s(t) = -5$ kW, and $v_M = 20$ m/s. The optimal value for f_M is lower than the default value, which decreases the energy used during the M mode and the required additional charging cost during the CH mode (see, Figure 2.10). Furthermore, if the threshold value v_M is set to a larger value than the maximum cycle speed, then effectively more energy is charged during the BER mode, which reduces the required additional charging cost during the CH mode further. Although, electric machine 2 is specified at

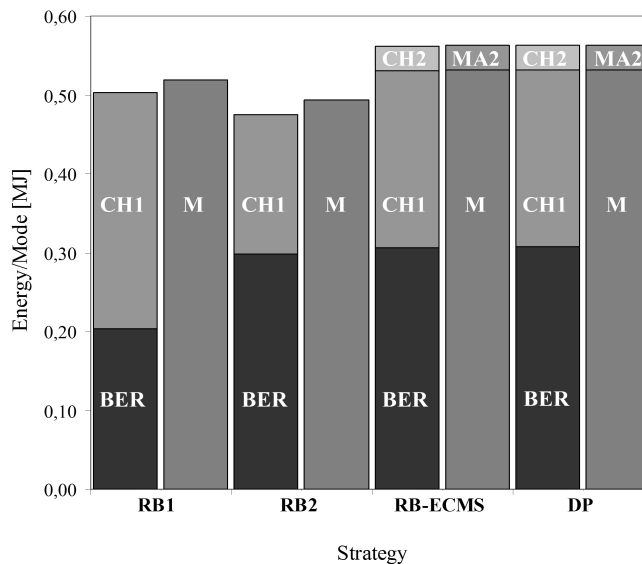
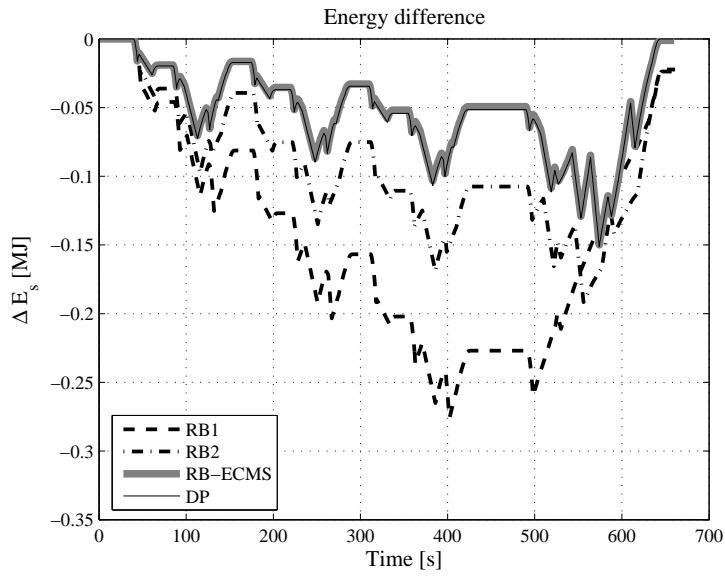
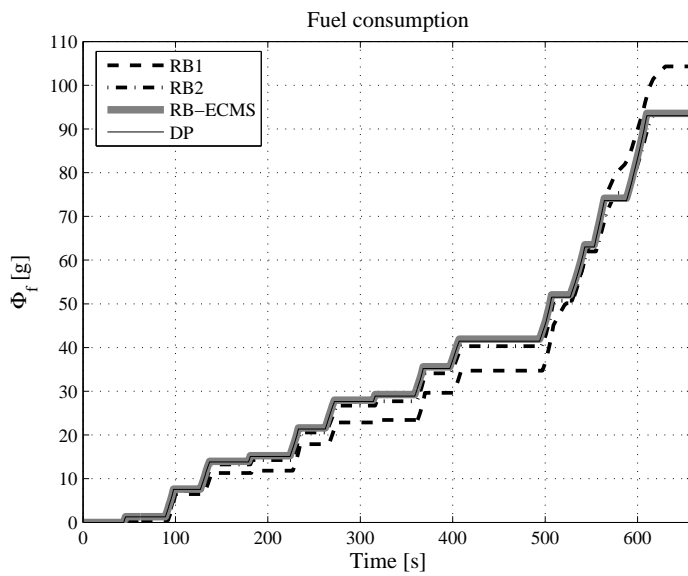


Figure 2.10 / Energy balances for the different strategies.

30-kW only approximately 4.9 kW is effectively used for propulsion during pure electric driving (see, RB-ECMS in Table 2.5). The redundant machine power is mainly used for vehicle performance requirements. The discrepancy between the fuel economy results and the energy difference over time calculated with the RB-ECMS and DP is small ($\pm 1\%$). It can be concluded, that the fuel economy



(a) Energy difference over time.



(b) Fuel consumption over time.

Figure 2.11 / The energy difference and fuel economy over time for the different strategies.

with the RB-ECMS is calculated very quickly and with sufficient accuracy.

Table 2.5 / Fuel economy results.

Strategy	$P_M^o \eta_s$ (kW)	f_M (-)	v_M (m/s)	Fuel economy (l/100km)			$\Delta E_s(t_f)$ (kJ)	Computation time(s)*
				City	Highway	Combined		
RB1	-6.0	0.20	12.5	2.33	4.27	3.34	-22.4	8.0
RB2	-5.0	0.12	20.0	2.70	3.25	2.99	-23.8	8.0
RB-ECMS	-4.9	-	-	2.78	3.17	2.98	0.9	7.8
DP	-4.9	-	-	2.78	3.17	2.96	0	462.0

* Pentium IV, 2.6-GHz, with 512-MB of RAM

In Table 2.6 the fuel saving for the different hybrid modes are shown. The reference fuel economy of 5.35 l/100km is calculated with the same vehicle simulation model under the condition that $P_s(t) = 0 \forall t \in \{0, t_f\}$. It is observed, that the largest fuel saving improvement 39.6% is realized with the BER and M mode. Additional charging (CH1 mode) and using this energy for the M mode increases the relative fuel saving with approximately $43.6\% - 39.6\% = 4\%$. The smallest fuel saving improvement $44.4\% - 43.6\% = 0.8\%$ is obtained by performing some additional charging (CH2 mode) and using this energy for motor-assisting (MA2 mode) during driving.

Table 2.6 / Fuel economy results and relative improvements (RB-ECMS).

Hybrid mode (active = x):					Fuel economy (l/100km)	Relative fuel consumption	Relative fuel saving
BER	M	CH1	CH2	MA2			
-	-	-	-	-	5.35	100.0%	-
x	x	-	-	-	3.23	60.4%	39.6%
x	x	x	-	-	3.04	56.4%	43.6%
x	x	x	x	x	2.98	55.6%	44.4%

2.5.4 Evaluation of the Motor-Only Mode

The fuel mass-flow of the engine can be approximated by the affine relationship [40],

$$\dot{m}_f(t) \approx \dot{m}_{f,0} + \lambda_1 P_p(t), \quad \dot{m}_{f,0} \triangleq \dot{m}_f(P_p(t) = 0) \text{ (idle fuel mass flow)}. \quad (2.32)$$

The idle fuel mass-flow at zero mechanical power is represented by $\dot{m}_{f,0}$. The slope of Equation (2.32) λ_1 is approximately constant and expresses the additional fuel mass-flow over demanded engine power. If the optimal threshold power for the engine to switch on corresponds to $P_p^o(t) = -P_M^o(t) \eta_s(t)/\eta_t(t)$, then the

maximum fuel saving in the M mode is given by,

$$\Delta \dot{m}_f(t) = \dot{m}_{f,0} + \lambda_1 \cdot -P_M^o(t) \eta_s(t)/\eta_t(t). \quad (2.33)$$

It is found with results from RB-ECMS and DP, that the engine switches on at the motoring power, where the equivalent fuel cost for charging described by λ_0^o is equal to the maximum fuel saving in the M mode:

$$\lambda_0^o \cdot -P_M^o(t) = \dot{m}_{f,0} + \lambda_1 \cdot -P_M^o(t) \eta_s(t)/\eta_t(t) \quad (2.34)$$

$$\Leftrightarrow P_M^o(t) = -\frac{\dot{m}_{f,0}}{\lambda_1 \cdot \eta_s(t)/\eta_t(t) - \lambda_0^o}, \quad (2.35)$$

describing the relationship between the optimal motoring threshold power $P_M^o(t)$ and λ_0^o . The optimal motoring threshold power is approximately constant given that the secondary source - and transmission efficiency are approximately constant for values around P_M^o , i.e.,

$$P_M^o(t) \approx (P_M^o | \eta_s(t) \approx \eta_s \wedge \eta_t(t) \approx \eta_t), \quad (2.36)$$

which is sufficiently accurate to be used with the RB-ECMS as shown in the previous section. For motoring threshold powers larger than $-P_M^o$ the fuel cost for recharging become larger than the fuel saving, which is schematically depicted in Figure 2.12.

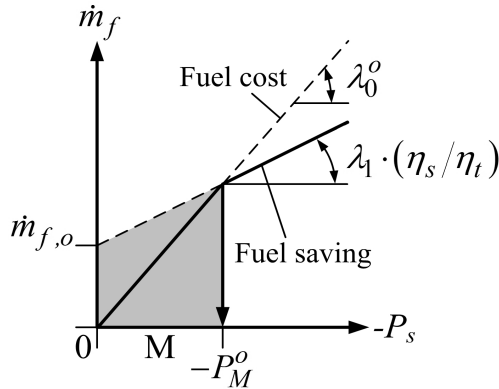


Figure 2.12 / Mode switch design parameter P_M^o .

2.6 Conclusion

In this chapter, an overview of different control methods is given and a new rule-based EMS is introduced based on the combination of Rule-Based and Equivalent

Consumption Minimization Strategies (RB-ECMS). The RB-ECMS consists of a collection of driving modes selected through various states and conditions. In addition, a graphical representation of the influence of the hybrid driving modes on the energy balance and the fuel saving potential is discussed. The RB-ECMS uses one main design parameter and requires no tuning of many threshold control values and parameters. The main decision control variable is the maximum propulsion power of the secondary power source (i.e., electric machine/battery) during pure electric driving. The optimal maximum propulsion power is trade-off between the fuel saving with pure electric driving (idle-stop), motor-assisting and the fuel charging cost for counterbalancing the electric energy use. The fuel economy and control strategy for the Toyota Prius (1998) calculated with the RB-ECMS was compared with results from the vehicle simulation platform ADVISOR and DP strategy. The results show, that the default strategy as is implemented in ADVISOR is significantly improved (12%) and that the results of the RB-ECMS are very close to the global optimal solution calculated with DP (accuracy $\pm 1\%$). The discussed RB-ECMS is optimized offline very quickly, which can be used as part of a hybrid drive train topology selection and component specification tool, which is currently under development by the authors. In future work the RB-ECMS implemented in an online control application will be investigated.

Parametric Modeling for Specification of Components

Abstract / Drive train hybridization implies adding a secondary power source (electric machine/battery) to a primary power source (engine/filled fuel tank) in order to improve: fuel economy, emissions, drivability (performance), comfort and safety. Designing a hybrid vehicle drive train fulfilling the required vehicle driving functions is therefore a complex task. Many researchers have put effort formulating and developing overall hybrid drive train analysis, design and optimization models including top-level vehicle control strategy for optimal fuel economy. This chapter seeks to investigate the possibility of overall model simplification for the hybrid drive train system including the control strategy. This is performed by describing the component efficiencies and control rules with only a few characteristic parameters that capture the total systems fuel efficiency with sufficient accuracy (error $\pm 1\%$). Using these parameters the modeling and simulation process can be done very quickly. The method is demonstrated on a series, a parallel and a series-parallel hybrid drive train with specified component technologies, vehicle parameters and drive cycle. The fuel economy and control strategy results are compared with Simulink/ADVISOR and Dynamic Programming.

3.1 Introduction

Ongoing emission legislation and increasing fuel prices pursue many leading vehicle manufactures, and their suppliers to put effort in developing and manufacturing new efficient, though cost-effective, drive train technologies. On nowadays passenger vehicle market, hybrid vehicles are available, e.g., the Honda Civic IMA, Toyota Prius, Ford Escape, Lexus RX400h, etc. All these vehicles fulfill al-

This chapter has been published in the form of a paper as / [30] Hofman, T., Van Druuten, R., Serrarens, A., and M. Steinbuch, "Parametric modeling of components for selection and specification of hybrid vehicle drive trains", *WEVA Journal*, vol. 1, no. 1, pp. 215-224, 2007.

most the same hybrid functions, e.g., energy recuperation during braking, motor-assisting, engine off during standstill. However, their drive train topology, transmission technology, and control are completely different. The objectives of a hybrid drive train are to some extent improving the driving functions of a vehicle: fuel economy, emissions, driveability (performance), comfort, and safety.

Due to the complexity of hybrid vehicle drive trains, the design of topologies, component technologies and the control strategy forms a considerable challenge for engineers. Therefore, many researchers have devoted their attention to develop different hybrid drive train modeling and simulation tools [65, 88, 12, 67, 23, 4]. The tools are usually based on predefined drive train topologies, specific component technologies, and control strategies. In [67, 23] a more flexible modeling and simulation tool ('QSS toolbox') is discussed, with which user-defined drive train topologies can be build quite easily. In [4, 53] the research is focused on developing system design tools for optimizing component sizes and vehicle design parameters, where ADVISOR [88] is used as vehicle modeling and simulation platform. Other system design optimization approaches use globally optimal control strategy based on Dynamic Programming (DP) [74]. However, an integral system design approach is usually characterized by large computational times, complex design problem (optimization) formulations, multiple subsystem simulations, non-smooth, or non-continuous models. In addition, insights into the design problem at hand are lost when a single final design proposal is presented as a result of a complex integral design process. Interactions between the different drive train components, topology, and control are then difficult to investigate.

3.2 Objectives and Approach

This chapter presents a 'modeling approach' in characterizing the component technologies in order to select topologies and for designing the control strategy of hybrid vehicle drive trains (see, Figure 3.1 for an overview). Thereby, a simplified or reduced 'hybrid drive train model' is introduced, where the main power sources, i.e., Primary power source (P) (fuel tank/engine), Secondary power source (S) (battery/electric machine) and Transmission technology (T) (depicted as 'black box models') are modeled by simplified parametric 'power-based efficiency fit functions'. If an affine relationship is assumed, then the input power P_{in} as a function of the output power P_{out} becomes $P_{in} = c_1 \cdot P_{out} + c_0$. The static power losses are represented by c_0 and the reciprocal of the inner efficiency by c_1 respectively. Furthermore, the parameter P_{max} represents the output power limitation of the component. In order to capture the high power-loss effects of the engine a second order approximation gives better-fit results [39].

The operation points of P, S, and T determine the characteristic parameters (c_1 , c_0) of the power-based efficiency functions. The operation points are determined the drive cycle, the vehicle load, and the control strategy. The main assumptions to accelerate the modeling/simulation process are discussed below.

- The operation points during regenerative braking and pure electric driving over a whole drive cycle are used to fit linear functions describing the S efficiency. If S is coupled at engine-side of the transmission, then S is operated at the highest efficiency points by selecting the optimal transmission ratios. If S is coupled at the wheel-side, then the transmission ratio is fixed.
- The operation points during the engine-only mode (with a battery power equal to zero) over a whole drive cycle are used to fit a linear function describing the T efficiency. During the engine-only mode P is operated at the highest efficiency points. This chapter shows that operating S during hybrid driving modes has effect on the transmission efficiency. However, the change in transmission efficiency has a negligible effect on the overall fuel economy.

The modeling approach discussed in this chapter is a step forward in developing a quick modeling and simulation tool for component sizing and topology selection where the fuel economy is calculated very quickly and with sufficient accuracy. Thereby, a target is to find answers to the underlying research questions.

- (i) Can the component efficiency models and the control model be described with sufficient accuracy by a limited set of characteristic parameters?
- (ii) What is the influence of the drive train component technology and the topology on the fuel economy and emissions?

The first research question studies the influence of the operation points on the component efficiency. Thereby, ADVISOR and DP are used as reference ‘control models/algorithms’ (see, Figure 3.1 bottom part). In addition, a novel ‘Rule-Based Energy Management Strategy’ (RB EMS) is used with which the fuel economy and control strategy are calculated very quickly and with the same accuracy as DP (error $\pm 1\%$) [27].

The second research question studies if a simplified hybrid drive train model can be used independently on the type of hybrid transmission technology. Therefore, the influence of three typical different hybrid drive train topologies, i.e., ‘series’, ‘parallel’ and a ‘series-parallel’ hybrid configuration with different component technologies on fuel economy and emissions is investigated. The maximum vehicle power specification consisting of the engine and the electric machine output power is kept constant, such that the (acceleration) performance of the vehicle

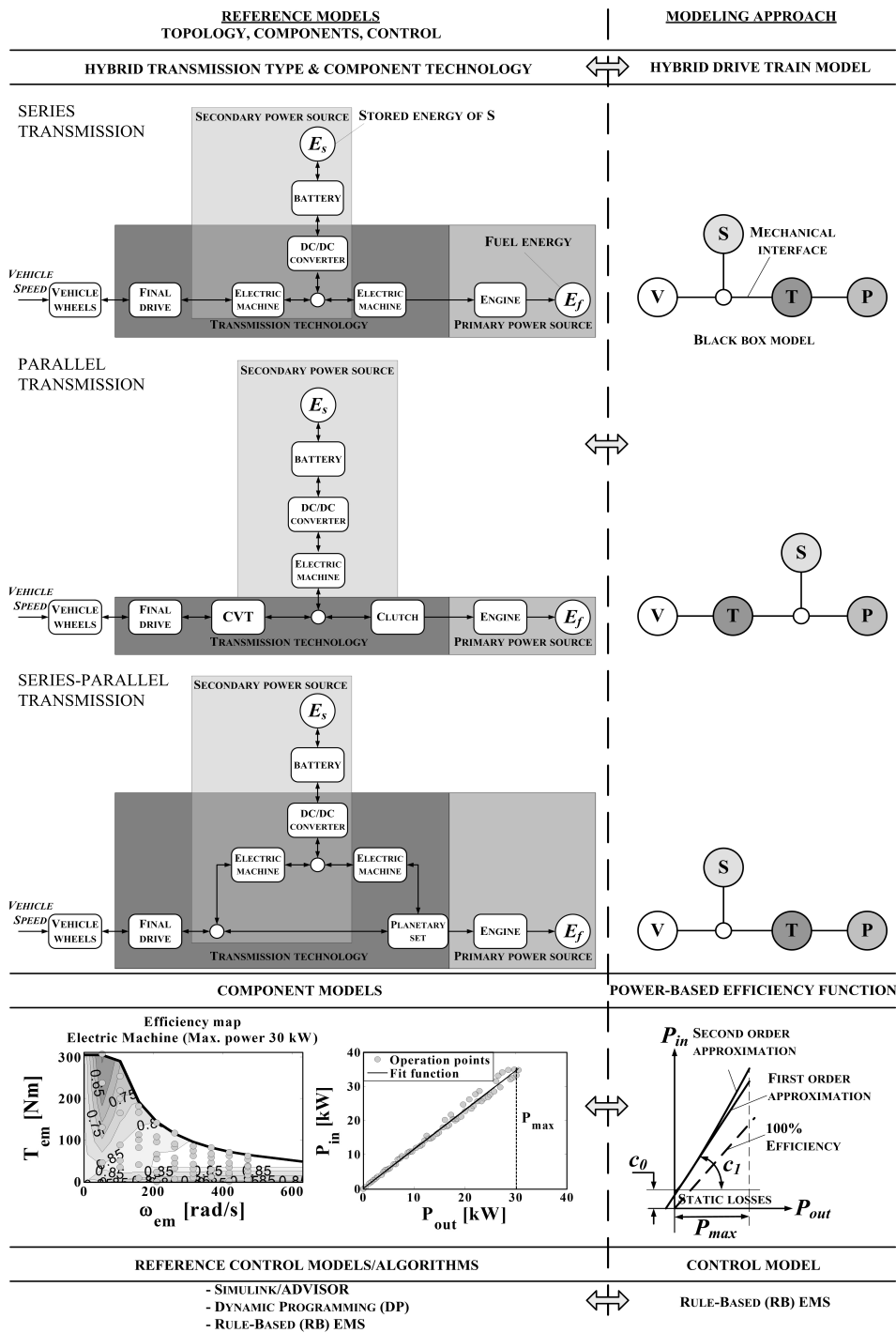


Figure 3.1 / Configuration overview of different hybrid drive trains and modeling approach.

is not compromised. Furthermore, for comparison the main vehicle parameters and the drive cycle describing the vehicle load are also kept constant.

The topology and the rule-based control model are discussed in the Sections 3.3 and 3.4 respectively. The simulation results of the topology and the parametric component modeling study are discussed in Section 3.5. Finally, the conclusions are described in Section 3.6.

3.3 Hybrid Drive Train Model

A drive train topology defines the possible connections and puts constraints on the transmission ratios between P, S, and the vehicle wheels V. For the series and the series-parallel configuration the advantage is that S is integrated with T. However, looking at a higher abstraction level for both transmission types, S is functionally coupled to the wheel-side of the transmission, as is shown in Figure 3.1 (top-right). Thereby, the intrinsic functions for S are defined as performing recuperation of brake energy (BER) and propulsion-only by S, while P is shut-off (eliminating the engine drag and friction losses). In addition, for the parallel and series-parallel configuration CHarging (CH) or Motor-Assisting (MA) during driving is possible with S. In case of the series or the series-parallel configuration respectively this will or can also be done with the electric machine connected at the engine-side respectively. However, some of the charged energy with the electric machine at the engine-side is directly transmitted to electric machine at the wheel side (avoiding additional battery losses). In Section 3.4, the hybrid modes are discussed in more detail. For the parallel configuration S is connected at the engine-side of T. The variator of the series and the parallel configuration consists respectively of two electric machines and a push-belt Continuously Variable Transmission (CVT). One of the major advantages of the series configuration is the infinitely variable transmission ratio. Thereby, it is possible to operate the engine and the generator intermediately, yet continuously at its highest efficiency point(s). However, at higher requested vehicle loads, the transmission losses of the electrical variator are typically larger than compared to a mechanical variator. The CVT losses in the parallel configuration are lower at higher vehicle loads. However, due to the overdrive constraint not all optimal operating points of the engine can be reached. The series-parallel configuration combines the electrical and mechanical paths, which consists of a planetary gear set combined with two electric machines. The two electric machines form the electrical variator part of T. The advantages of a series-parallel configuration, compared to a series configuration are:

- the transmission efficiency is higher, since most of the power is transmitted over the mechanical branch, and

- an electrical variator with a lower maximum power specification can be used.

However, a disadvantage is the possible occurrence of recirculation power thereby reducing the transmission efficiency. The operation of the variator and the influence of the battery power on the power-flows and the overall efficiency are discussed in more detail in [26].

3.4 Control Model

3.4.1 Energy Management Optimization Problem

The optimization problem is finding the optimal control power-flow $P_s(t)$ of the power source S given a certain power demand at the wheels $P_v(t)$, while the cumulative fuel energy, denoted as the variable E_f , over a certain drive cycle with time length t_f is minimized, i.e.,

$$E_f = \min_{P_s(t)} \int_0^{t_f} P_f(E_s(t), P_s(t), t) dt, \text{ subject to } \vec{h} = 0, \vec{g} \leq 0, \quad (3.1)$$

where the fuel power $P_f(t)$ is the product of the fuel rate (g/s) and the lower heating value h_{lv} (J/g) for fuel. The main constraints are energy conservation balance of $E_s(t)$ over the drive cycle, constraints on the power $P_s(t)$, and the energy $E_s(t)$:

$$h_1 := \Delta E_s = E_s(t_f) - E_s(0) = \int_0^{t_f} P_s(t) dt = 0, \quad (3.2)$$

$$g_{1,2} := P_{s,max} \leq P_s(t) \leq P_{s,max}, \quad (3.3)$$

$$g_{3,4} := E_{s,min} \leq E_s(t) \leq E_{s,max}. \quad (3.4)$$

3.4.2 The Rule-Based Energy Management Strategy

The control strategy used in this chapter is based on a Rule-Based (RB) Energy Management Strategy (EMS) as is described in [27]. Thereby, the hybrid drive train can be operated in certain distinct driving modes. In Figure 3.2, a block diagram is shown for the power distribution between the different energy sources, i.e., fuel tank with stored energy E_f , power source S with stored energy E_s and the vehicle driving over a drive cycle represented by a required energy E_v . The efficiencies of the fuel combustion in the engine (P), the storage and electric motor (S), and the transmission (T) are described by the variables η_p , η_s , and η_t respectively. The energy exchange between the fuel tank, S and the vehicle can be performed in different driving modes. The engine power at the crankshaft is

represented by P_p . The power demand at the wheels (P_v) and the power flow to and from the power source S (P_s) determine which driving mode is active.

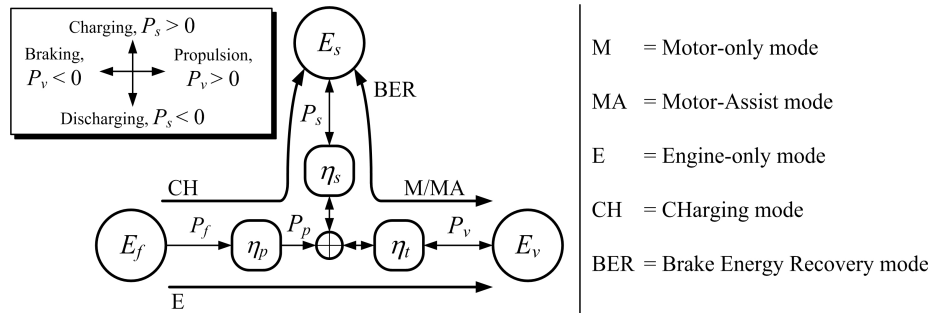


Figure 3.2 / Power-flows for the different hybrid driving modes. Secondary power source S is connected at the engine-side of the transmission.

The following operation modes are defined:

M: Motor-only mode, the vehicle is propelled only by the electric motor and the battery storage supply S up to a certain power level P_M , which is not necessarily equal to the maximum available propulsion power. The engine is off, has no drag, and no idle losses.

BER: Brake Energy Recovery mode, the brake energy is recuperated up to the maximum generative power limitation and stored into the accumulator of S. The engine is off, has no drag and no idle losses.

CH: CHarging mode, the instantaneous engine power is higher than the power needed for driving. The redundant energy is stored into the accumulator of S.

MA: Motor-Assisting mode, the engine power is lower than the power needed for driving. The engine power is augmented by power from S.

E: Engine-only mode, only the engine power is used for propulsion of the vehicle. S is off and generates no losses.

The engine is off during the M and the BER mode and uses no fuel. This is also referred to as the start-stop mode. In order to fulfill the integral energy balance constraint over the drive cycle, the energy required for the M and the MA mode needs to be regenerated during the BER mode, or charged during the CH mode. To explain the basic principles of the RB EMS, which is a trade-off between energy balance and fuel consumption, consider the following two cases. Either

case represents a different choice for P_M , where the recuperated brake energy (BER) is: (i) not sufficient, and (ii) more than sufficient for supplying the energy during the motor only mode (M) over a given drive cycle.

- (i) The additional required energy for the M mode has to be charged during the CH mode resulting in additional fuel cost.
- (ii) The redundant energy of the BER mode can be used for motor-assisting during the MA mode resulting in additional fuel savings.

Both cases are schematically shown in the Figure 3.3. Note that $P_M < 0$, since S is discharged during electric driving. Referring to case (i), if $-P_M$ is lowered, then the additional fuel cost becomes lower due to decrease of the required charging energy. However, the fuel saving due to the M mode is also reduced, and vice-versa, if $-P_M$ is increased. The same holds for case (ii): the fuel saving during the MA mode is increased if $-P_M$ is lowered, but the fuel saving due to the M mode is reduced. For both cases, additional charging during driving and using for motor-assisting can be beneficial, if the energy is charged at a lower driving power, and this energy is used for motor-assisting at a higher driving power. However, the additional fuel saving is relatively small, because the drive energy at higher powers is relatively small. For more details concerning calculation of the optimal value for P_M , denoted as P_M^o , is referred to [27].

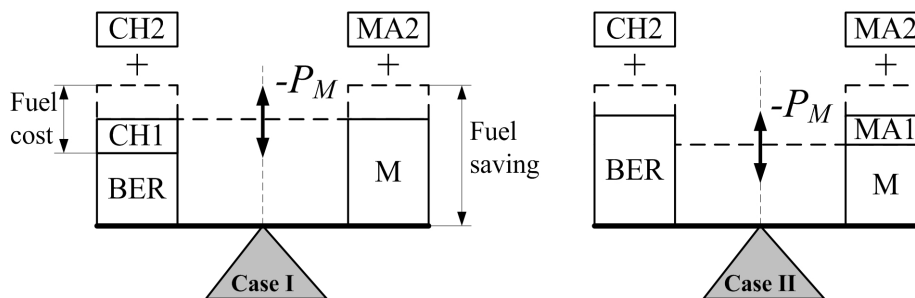


Figure 3.3 / Energy balance and fuel consumption, after completion of a whole drive cycle.

3.4.3 Iterative Drive Train Loss Compensation Procedure

The operation points over the engine output power range in the static-efficiency map of an engine, which maximizes the engine efficiency are collected by the Engine Optimal Operation Line (EOOL). The transmission efficiency, which is the ratio of the vehicle power demand and the optimal engine output power $\eta_t =$

P_v/P_p^o , is determined by the optimal engine torque T_p^o and speed ω_p^o (prescribed by the EOOL). However, the required T_p^o and ω_p^o are determined by η_t and the required P_v . Due to this causality conflict it is impossible to determine the T_p^o and ω_p^o exactly. In this study the losses in T and S are iteratively estimated and are compensated for the engine power P_p^o . The error or the drive train loss at a certain time instant t in each iteration step i is defined as,

$$\varepsilon(i, t) = |P_p^o(i+1, t) - P_p^o(i, t)|, \quad (3.5)$$

with iteration step $i \in \mathbb{N}_0$. The iteration is repeated until the error $\varepsilon(i)$ between the iteration steps at a certain time instant becomes sufficiently small. In Figure 3.4 the iterative procedure is schematically shown. A mathematical condition to prevent the iteration loop from instabilities, in terms of the estimation $P_p^o(i, t)$ is

$$|P_p^o(i+1, t) - P_p^o(i, t)| < \gamma \cdot |P_p^o(i, t) - P_p^o(i-1, t)|, \quad 0 < \gamma < 1. \quad (3.6)$$

This condition implies that error ε of each estimate decreases in each iteration step i . If the ratio of the error between the previous and the subsequent step becomes equal to 1 the estimates will not further improve. This corresponds with the transition between stable and unstable iteration loops.

At later time instants the required P_p^o can be calculated using the known value for the efficiency at the previous time instant. Thereto, the requested P_v is divided by the computed η_t . Using the modified T_p^o and ω_p^o prescribed by the EOOL, which are stored-in look-up tables, the optimal power-flow P_s is calculated using DP or the RB EMS given the drive cycle and the vehicle parameters.

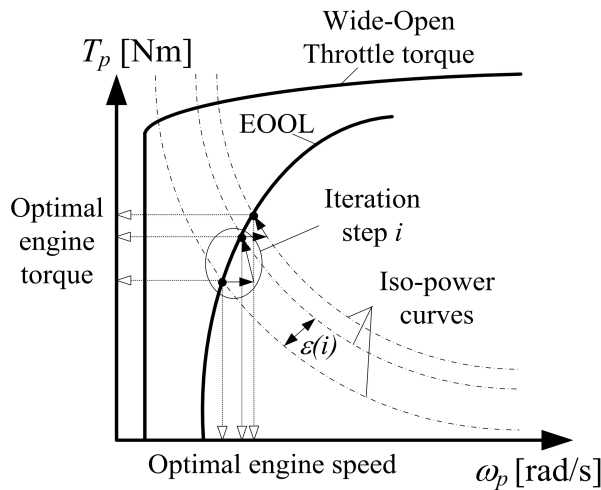


Figure 3.4 / Drive train loss compensation procedure.

3.4.4 Reference Control Models: ADVISOR and DP

For comparison the control strategies, which are implemented in ADVISOR, are compared with the results from DP and the RB EMS. In Table 3.1 the rule-based conditions that define which hybrid mode is active for the different hybrid transmission types are given. Thereby, the battery is allowed to operate within a certain defined state-of-charge ξ window, i.e., $\xi = [\xi_{min}, \xi_{max}]$. The control parameters as implemented in ADVISOR were optimized to achieve the highest fuel economy, while the final $\xi(t_f)$ is maintained within a certain zero change in $\xi(t_f) \pm 0.5\%$ tolerance band. The optimizing torque fraction parameter $f_{1,1}$, the power fraction parameters $f_{0,1}$, $f_{0,2}$, and the vehicle electric launch speed threshold value v_M are intrinsic parameters of the control strategy. The parameters are used to assure that the engine is operated in the relatively high efficiency areas. For details on these parameters and the functions for calculating the amount of charging/discharging power for the different topologies is referred to [88].

Table 3.1 / Rule-based control models as are implemented in ADVISOR.

Mode	Rule-based condition
BER	$\xi < \xi_{max} \wedge T_v < 0$
M	$\xi \geq \xi_{min} \wedge \{P_p < f_{0,1}P_{p,max} \vee T_p < f_{1,1}T_{p,max}(\omega_p) \vee v < v_M(\xi)^* \vee v < v_M^{**}\}$
CH	$\xi < \xi_{min} \vee \xi < \xi_{ref} \wedge \{f_{0,1}P_{p,max} \leq P_p \leq f_{0,2}P_{p,max}\}$
E	$\xi = \xi_{ref} \wedge \{f_{0,1}P_{p,max} \leq P_p \leq f_{0,2}P_{p,max}\}$
MA	$\xi \geq \xi_{min} \wedge \{P_p > f_{0,2}P_{p,max} \vee T_p > T_{p,max}(\omega_p)^{*,**}\}$

Additionally, in case of the *parallel configuration with CVT or the **series-parallel configuration

Using DP the finite horizon optimization problem is translated into a finite computation problem [27], [8]. Note that in principle the technique results in an optimal solution for the EMS. However, the grid step size also influences the accuracy of the result. Furthermore, the engine and the generator of the series configuration are operated at the System Optimal Operation Line (SOOL). For the parallel configuration the electric machine and the engine are operated separately at the maximum efficiency points during the BER, M and the E mode (EOOL). During the CH and the MA mode the engine and the electric machine are operated at the SOOL. For the series-parallel configuration the engine is operated at the EOOL alone.

3.5 Results

All simulations presented in this chapter were performed on the JP10-15 drive cycle. The inertias of the electric machines, engine and auxiliary loads are, for simplicity, assumed to be zero. During braking energy is partially recuperated up

to the maximum generative power limitation of the electric machine. In addition, some of the braking energy is dissipated between the front - and the rear-wheels in the wheel-brake discs. The braking energy distribution is prescribed by a non-linear function, which is dependent on the vehicle speed [88]. During braking the engine is assumed to be shut-off or disengaged eliminating the engine drag losses. The Base Line vehicle (BL) is equipped with a 74-kW 1.6-l SI engine and a push-belt CVT as is used in the parallel configuration. In Table 3.6 an overview of the component data is given. The total power specification for every hybrid drive train configuration is kept constant at approximately 74 kW. The battery pack is sized to meet the power specifications of the motor controller/electric machine.

3.5.1 Fuel Economy and Emissions

In Table 3.2 the fuel economy and emission results for the different hybrid topologies and control models are listed. In Table 3.4 the characteristic parameters describing the P, S, T efficiency, which are used with the Control model (C) (RB EMS) in order to calculate the fuel economy (tests 12-14), are listed. Although the cost function consists only of the fuel consumption, the HC-, CO-, and NO_x-emissions are reduced for all hybrid drive trains. However, except for the series configuration, the NO_x-emissions are increased. This can be solved by using a weighted cost function consisting of the sum of the fuel use and emissions and increasing the weight factor regarding the NO_x-emissions. However, this has not been investigated in this chapter. The relative influence of engine downsizing (without a battery), topology choice and hybridization (adding an S) on the fuel economy results is shown in Table 3.3. The lowest fuel economy is realized with the series-parallel configuration. Due to coupling of S at the wheel-side of T for the series-parallel configuration (maximizing the regenerative brake efficiency) the fuel economy is lower than for the parallel hybrid configuration. In Figure 3.5 and Figure 3.6 the energy distribution between different hybrid modes and the energy difference ΔE_s over time for the different topologies and strategies are shown respectively. Although, S is coupled at the wheel-side of the transmission for both the series-parallel and the series hybrid configuration, it is observed, that the energy recuperation during braking (BER) for the series-parallel is larger than for the series. Since, the S efficiency of the series-parallel is higher than the S efficiency of the series configuration. The series configuration has the highest fuel consumption mainly due to the lowest transmission efficiency.

3.5.2 Control Models Parameters – ADVISOR

The fuel economy is mainly determined by the control constraints or rules, which determine where the engine is allowed to be turned off (BER and M mode).

Therefore, the main control parameters within ADVISOR are $f_{0,1}$, $f_{1,1}$, or v_M (see, Table 3.1). The calibrated $f_{0,1}$ for each topology is also listed in Table 3.4. Thereby, $f_{1,1} \geq f_{0,1}$ and v_M is larger than the maximum cycle speed. The calibrated $f_{0,1}$ for the series configuration is 0.51 (equivalent to $P_M^o = -32.5$ kW). At this power fraction the engine and generator are operated at the ‘sweet spot’ of the engine (highest efficiency) and energy is charged with minimum fuel cost. However, with DP it is found that the fuel consumption is reduced if the electric machine at the wheel-side is partially supplied by the battery up to a drive power of approximately 6.1 kW. At higher power demands the battery power is augmented by power from the engine that is a function of the drive power P_v and the state-of-charge ξ . It appeared to be not straightforward to adapt the default rules within ADVISOR by changing the main control parameters to the preferred optimal control settings. This explains the relatively large discrepancy between the results of DP and ADVISOR for the series configuration. The optimized $f_{0,1}$, based on the results from DP, for the parallel and the series-parallel configuration are 0.10 (equivalent to $P_M^o = -6.1$ kW) and 0.12 (equivalent to $P_M^o = -7.5$ kW) respectively. The default control parameters as implemented in ADVISOR for series-parallel configuration (Toyota Prius 1998) cause that in the high-speed areas the engine is not allowed to shut off at relatively low P_v resulting in less idle stop. In addition, generative torque of the motor during braking is reduced due to additional engine drag torque. Since, the vehicle speed is then larger than v_M . If v_M is set to a larger value than the maximum cycle speed effectively more (free) energy is charged during the BER mode, which reduces the additional charging fuel cost. Furthermore, it is found that the optimal EMS is focused on charging during driving in the low-speed areas ($v < 40$ km/h) by the generator (15-kW) and in the high-speed areas by the motor (30-kW) respectively. This has influence on the optimal P_M^o as will be discussed in the following section.

3.5.3 Parametric Efficiency Functions and Hybrid Drive Train Model

Although the static-efficiency map of the engine is very nonlinear, the fuel power P_f as a function of the engine output power P_e calculated at the EOOL is well approximated by a quadratic fit function, i.e., $P_f = c_2 \cdot P_p^2 + c_1 \cdot P_p + c_0$ (see, also [26]). In Figure 3.7(a) and (b) the linear functions fitted through the operation points for S (BER and M mode) and T (only E mode) are shown. For sake of clarity, the S efficiency for the parallel configuration as shown in Figure 3.7 includes the T efficiency. The found component parameters including the calculated optimal control parameter P_M^o used in the RB EMS are shown in Table 3.4. In Figure 3.7(a) also P_M^o is shown of tests 9, 10, and 11. Due to uncertainty on the found fit coefficients, the relative small static losses c_0 for S can be larger than zero. The electric machines at the engine-side of the series and the series-parallel

Table 3.2 / Simulation results.

Test	Topology	Fuel economy (l/100km)	Emissions (g/km) [†]		
			HC	CO	NO _x
Simulink/ADVISOR (efficiency model: $\eta_* = \eta_*(T_*, \omega_*)$)					
1.	BL / 74 kW	8.24	-	-	-
2.	BL / 43 kW	6.13	1.53	2.99	0.63
3.	SE	4.99	0.65	2.44	1.10
4.	PA	3.33	0.54	1.62	0.61
5.	SP	2.99	0.49	1.46	0.54
Dynamic Programming (efficiency model: $\eta_* = \eta_*(T_*, \omega_*)$)					
6.	SE	3.88	0.48	1.64	0.68
7.	PA	3.02	0.48	1.47	0.55
8.	SP	2.84	0.45	1.39	0.53
Rule-Based EMS (efficiency model: $\eta_* = \eta_*(T_*, \omega_*)$)					
9.	SE	3.89	0.52	1.88	0.82
10.	PA	3.07	0.48	1.49	0.58
11.	SP	2.98	0.46	1.46	0.56
Rule-Based EMS (efficiency model: $\eta_* = \eta_*(P_*)$, see, Table 3.4)					
12.	SE	3.90	-	-	-
13.	PA	3.04	-	-	-
14.	SP	2.93	-	-	-

BL: Base Line vehicle; SE: Series; PA: Parallel; SP: Series-Parallel.

[†]at engine exhaust system; * = {p, s, t}.

Table 3.3 / Relative fuel economy improvement.

	Series (l/100km)	Parallel	Series-Parallel
A: Downsizing	20.9% (6.52)	25.6% (6.13)	26.5% (6.06)
B: Hybridization	36.7% (3.88)	49.8% (3.08)	52.7% (2.96)

A: Reference test 1: 8.24 l/100km / B: Reference test 2: 6.13 l/100km

configuration are assumed to be part of T. Furthermore, charging and motor-assisting during driving is only possible with the electric machines at the wheel side (S). For the parallel configuration charging and motor-assisting during driving is done at the SOOL, which causes that the S efficiency is not similar to the S efficiency during the BER and M mode. These assumptions cause that the optimal $-P_M^o$ with the fit functions used with the simplified hybrid drive train model is lower than $-P_M^o$ with the actual drive train topology and component technology (see, Table 3.4). Thereby, the energy charged and discharged during driving (CH and M mode) is reduced (compare tests 9-11 with tests 12-14 in Figure 3.5). However, the lower value for $-P_M^o$ for every hybrid drive train topology has a small influence ($\pm 1\%$) on the overall fuel economy (compare tests 9-11 with tests 12-14 in Table 3.2). The battery power influences the transmission efficiency. In Figure 3.8, for example, the engine power as function of the vehicle drive power for dif-

Table 3.4 / Model parameters (see, Table 3.2, test 12-14).

Component	Topology	Model parameter for P, S, T, and C		
		c_2 (1/W)	c_1 (-)	c_0 (W)
P (43 kW)	SE/PA/SP	1.16e-5	2.09	5194
S (BER mode)	SE	-	-0.75	-73
S (M mode)	SE	-	-1.48	-46
T (only E mode)	SE	-	1.40	954
S (BER mode)	PA	-	-0.77	-111
S (M mode)	PA	-	-1.49	75
T (only E mode)	PA	-	1.11	371
S (BER mode)	SP	-	-0.85	12
S (M mode)	SP	-	-1.43	43
T (only E mode)	SP	-	1.11	192
Control model	Topology:	SE	PA	SP
C (ADVISOR)	$f_{0,1}/P_M^o$ (-/W)	0.51/-32.5	0.10/-7.5	0.12/-6.1
C (RB EMS, test 9-11)	P_M^o (W)	-9.0	-7.0	-7.0
C (RB EMS, test 12-14)	P_M^o (W)	-6.0	-6.0	-6.0

Table 3.5 / Transmission efficiency parameters.

Case	Series		Parallel		Series-Parallel	
	c_1 (-)	c_0 (W)	c_1 (-)	c_0 (W)	c_1 (-)	c_0 (W)
No battery power	1.40	954	1.11	371	1.11	192
Corrected with battery power	1.35	916	1.11	209	1.09	115

ferent battery powers calculated with DP for the series-parallel configuration is shown. The assumption that the transmission is used in the engine-only E mode ('pure transmission efficiency') over a whole drive cycle for the determination of the transmission efficiency is acceptable. Since, if the transmission input power is 'corrected with the battery power' during the CH and the MA mode, then it is observed that the 'corrected hybrid transmission efficiency' is slightly better than the 'pure transmission efficiency' ('no battery power'). However, the discrepancy is very small. Therefore, the difference in fuel economy is very small. This holds for every investigated topology (see, Table 3.5). It can be concluded, that the implicit sensitivity of the fit coefficients to battery power for the transmission T is small.

3.6 Conclusions

The results show that overall model simplification for the hybrid drive train topology, component technology, and control strategy regarding fuel economy can be done with sufficient accuracy (error $\pm 1\%$). Thereby, the component efficiencies, and the control model are only described by $P + S + T + C = 3 + 4 + 2 + 1 = 10$ char-

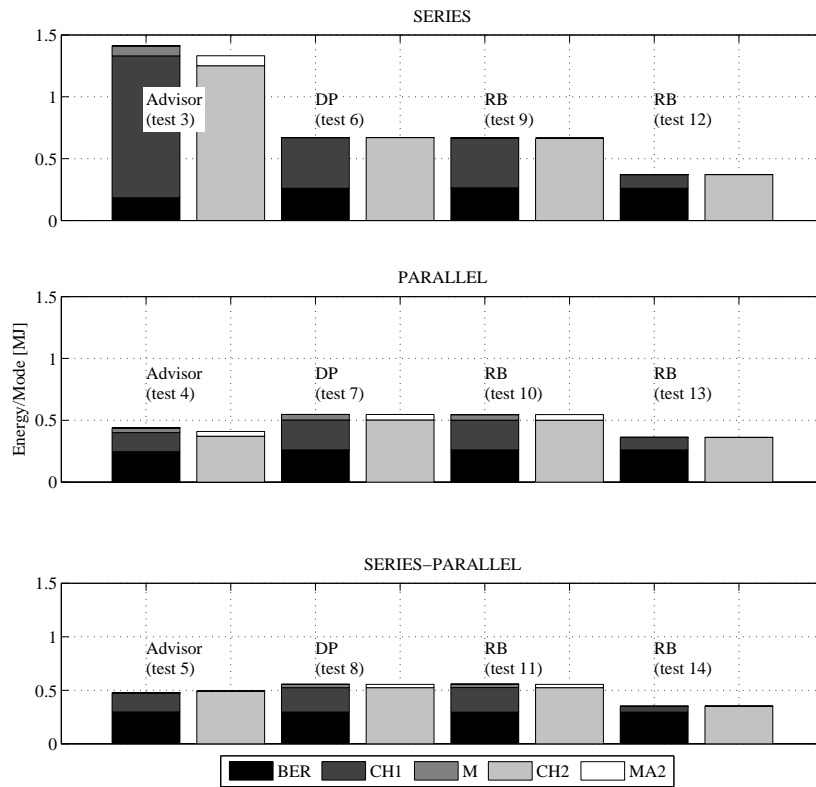


Figure 3.5 / Energy distribution over the hybrid modes.

acteristic parameters. This in contrary to the relatively large amount of required static component efficiency data, the different control rules used in ADVISOR, or the relatively long computation time with DP. Determination of the component parameters describing the component efficiencies, which depend on choice of engine -, or wheel-side coupling of S to the drive train (topology choice), the vehicle speed, and load, can be done with sufficient accuracy by using certain component operation preferences. Moreover, if for example realistic characteristic parameters for T in combination with a P and S are determined fulfilling a certain fuel economy improvement, then the component specifications for T (efficiency) can be derived, and consequently the transmission technology can be selected. Other components combinations are also possible. In this way, control design, optimization, component and topology selection, and specification are merged into a single methodology framework. In future work the design of

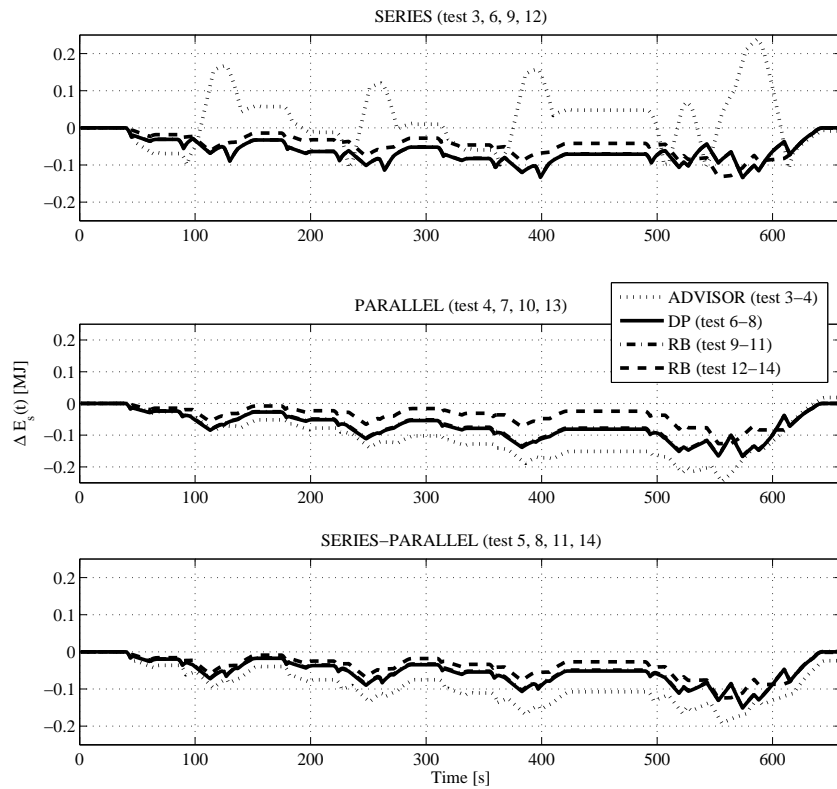
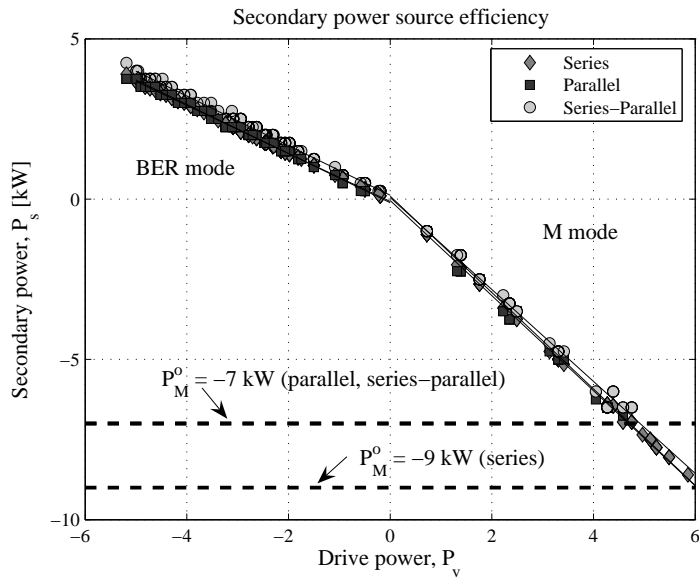
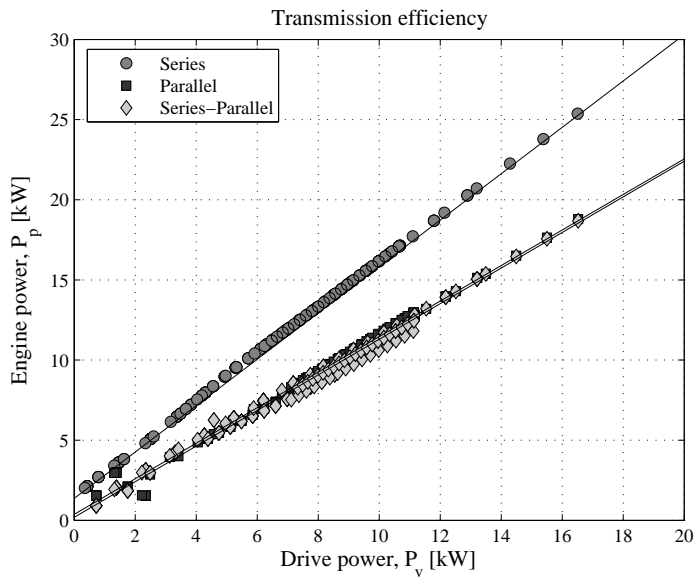


Figure 3.6 / Energy difference over time.

a hybrid vehicle drive train (a passenger car and a distribution truck case study) using the modeling approach as discussed in this chapter will be investigated.



(a) Output power as a function of the input power for S (during the BER/M mode).



(b) Output power as a function of the input power for T (pure transmission efficiency, only E mode).

Figure 3.7 / Secondary power source and Transmission efficiency.

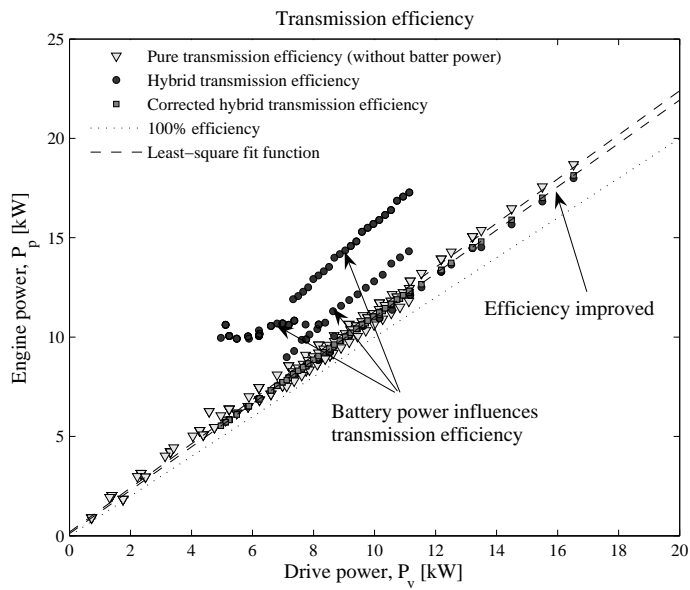


Figure 3.8 / Influence of battery power on transmission efficiency (all hybrid modes are active).

Table 3.6 / Component data for hybrid drive trains.

<i>Series configuration</i>	
Electric machine (wheel side)	Manufacturer: Westinghouse; 75-kW (continuous) AC induction motor/inverter, Torque range: from 271 Nm to 72 Nm (corresponding speed from 0 rpm to 10000 rpm). The efficiency map includes the inverter/controller efficiencies. (Data file ADVISOR: MC_AC76)
Electric machine (engine side)	Manufacturer: Mannesmann Sachs; 63-kW (continuous) PM motor/inverter, Torque range: from 157 Nm to 110 Nm (corresponding speed from 0 rpm to 5500 rpm). The efficiency map includes the inverter/controller efficiencies. (Data file ADVISOR: GC_PM63)
Final drive	The final drive ratio is 0.1472 with a constant efficiency of 0.98
<i>Parallel configuration</i>	
Electric machine (engine side)	Manufacturer: Toyota; 30-kW (continuous) PM motor/inverter, Torque range: from 305 Nm to 47.7 Nm (corresponding speed from 0 rpm to 6000 rpm). The efficiency map includes the inverter/controller efficiencies. (Data file ADVISOR: MC_PRIUS_JPN)
CVT/final drive	The push-belt CVT has an under-drive and over-drive ratio of 0.5 and 2.5 respectively. The final-drive ratio is 0.1715. The efficiency map includes the final drive efficiency. (Data file ADVISOR: TX_CVT50_SUBARU)
<i>Series-Parallel configuration</i>	
Electric machine (engine side)	Manufacturer: Toyota; 15-kW (continuous) PM motor/inverter, Torque range: from 55 Nm to 26 Nm (corresponding speed from 0 rpm to 5500 rpm). The efficiency map includes the inverter/controller efficiencies. (Data file ADVISOR: GC_PRIUS_JPN)
Electric machine (wheel side)	Manufacturer: Toyota; 30-kW (continuous) PM motor/inverter, Torque range: from 305 Nm to 47.7 Nm (corresponding speed from 0 rpm to 6000 rpm). The efficiency map includes the inverter/controller efficiencies. (Data file ADVISOR: MC_PRIUS_JPN)
Planetary gear set/Final drive	The planetary gear set ratio and the final drive ratio are -2.6 and 0.2431 respectively. The efficiencies are both constant 0.98 assumed.
<i>Energy storage system</i>	
Battery pack	Manufacturer: Panasonic; Type: Ni-MH, Nominal voltage 288 V, Capacity 6 Ah, $\xi_{min} = 0.30$, $\xi_{max} = 0.80$, $\xi_{ref} = 0.55$. (Data file ADVISOR: ESS_NIMH6)
<i>Vehicle data</i>	
Mass: 1368 kg, Air drag coefficient: 0.29, Frontal area: 1.746 m ² , Roll resistance coefficient: 0.9 %, Maximum regenerative brake fraction: 0.5. (Data file ADVISOR: VEH_PRIUS_JPN)	
<i>Engine data</i>	
Manufacturer: Toyota; Displacement and type: 43-kW (at 4000 rpm) 1.5-l SI Atkinson internal combustion engine. Maximum torque: 102 Nm at 4000 rpm. (Data file ADVISOR: FC_SI_15l_At_emis)	

Design of CVT-Based Hybrid Passenger Cars

Abstract / In this chapter the hybridization of a small passenger car equipped with a Continuously Variable Transmission (CVT) is investigated. Designing a hybrid drive train is a multi-objective design problem. The main design objectives are fuel consumption, emissions, and performance. However, it is difficult to find a global optimal integral design solution due to the interdependence of design choices (parameters) regarding the drive train topology, component sizes, component technologies, and the control strategy, and the unknown sensitivity of the design objectives to the design parameters. In this work a parametric optimization procedure is presented in solving the design problem, where the main design objective is fuel consumption. The effects of parameter variation on the fuel consumption have been investigated. Furthermore, a reduced hybrid drive train model is introduced with which the effects of design parameter variation is studied very quickly (approximately 50-100 times faster computation time than Dynamic Programming) and with an average error of less than 1.6%.

4.1 Introduction

Sales of hybrid vehicles are becoming more significant every year. The introduction of the Toyota Prius almost 10 years ago, changed the spectrum in the automotive power train market significantly. The Toyota Prius operates using an electric Continuously Variable Transmission (CVT) principle [55], whereas the Honda Civic IMA [49] uses a mechanical belt-driven CVT in parallel with an electric motor. The CVT principle in the Prius excels in driving agility and fuel consumption. However, the CVT is relatively costly, in particular, due to the dual electric machines, the power electronics, and the battery pack. This is one of the reasons why this hybrid system is now introduced in the higher class vehicles (e.g., large passenger cars, and large off-roaders). The Honda IMA system uses

This chapter has been submitted in the form of a paper as / [28] Hofman, T., Van Druten, R., Serrarens, A., and M. Steinbuch, "Design of CVT-Based Hybrid Passenger Cars", *IEEE Transactions on Vehicular Technology*, (submitted), 2007.

mature and low cost belt-driven CVT technology in combination with a much smaller electric machine. This saves cost though overall performance is penalized due to the limited electrical assist. Especially, if the relatively small electric machine is combined with a down-sized engine.

The main functional differences between a hybrid vehicle equipped with a CVT and a transmission with discrete set of gear ratios (e.g., an Automated Manual (AMT), or an Automatic Transmission (AT)) are:

- the engine, or the electric machine (i.e., only if the electric machine is pre-coupled to the CVT) can be operated at the optimal operation points,
- the electric machines are part of an electrical or an electro-mechanical CVT (i.e., in case of a series, or a series-parallel hybrid configuration respectively), and
- a CVT with infinite ratio coverage (e.g., Toyota Prius) allows smooth and quick engine re-start.

In this chapter, the hybridization of a small passenger car equipped with a CVT is analyzed and of which the component sizes (power specifications) are optimized. The base line vehicle is a Toyota Yaris equipped with a 4-cylinder 1.3 liter gasoline engine, a Torque Converter (TC), and a conventional push-belt CVT. For comparison the effects of changing the CVT technology on the fuel consumption are investigated. For this purpose, additionally two modern power-split CVTs, i.e., a one-mode [55] and a two-mode power-split CVT [83] are modeled. Within this context, a short overview is given below of different CVT solutions.

4.1.1 Diversification of CVT Solutions

An electrical CVT consists of two electric machines. Both electric machines can operate as motor or generator. If one electric machine is directly coupled to the engine and the other to the driven wheels, the size (maximum continuous power) of both machines has to be equal to the maximum power of the engine. The corresponding weight and cost would be too high for passenger car applications. Furthermore, the power conversion from the mechanical domain towards the electrical domain and vice-versa is not highly efficient. In order to reduce the size of the electric machines and to improve the efficiency of an electrical CVT, a power-split device (planetary gear set), that splits the engine-power into a mechanical and an electrical path, can be used. However, due to, e.g., the kinematics of the planetary gear, or the constraints on the ratio-coverage of the transmission, the reduction of the electric machine sizes is limited, yet still significantly compared to a pure electrical CVT.

Summarizing, the advantages of a power-split CVT compared to an electrical CVT are:

- the transmission efficiency is higher, since most of the power is transmitted over the mechanical branch consisting of planetary gears, and
- a lower maximum power-flow through the electrical branch is required, which results in smaller electric machines.

Developments in order to further reduce the size of the electric machines and to further increase the transmission efficiency is done by Renault [83], Bosch [70], and others [41]. However, these developments mostly lead to a design close to that of existing manuals, or automated manuals in which the clutches are replaced by electric machines in order to enable continuously variable shifts. This always leads to a transmission, that is much more complex than a conventional transmission. Moreover, the electronically controlled clutch to clutch shifts are so well performed nowadays that it is hard to feel that a shift took place.

The mechanical CVT, which is nowadays produced by Jatco, Aisin, ZF, Toyota, Subaru, Daimler Chrysler, Audi, etc., is considered a benchmark for all transmissions [47]. The mechanical CVT outperforms the manual transmission regarding fuel consumption. Moreover, a mechanical CVT outperforms the current automated manuals regarding cost and comfort [56]. In particular, due to the efforts of the Japanese transmission manufacturers, the mechanical CVT will have a high potential on a large scale. The potentials for further improvement of the CVT efficiency and the reduction of costs are high with new up-coming technologies, such as slip control [10], on-demand actuation systems [37], and involute chain technology [82].

4.2 Problem Definition

This chapter presents a modeling and design approach in order to find the optimal values for the following design parameters denoted as x : the drive train topology, the component technology, component size (kW), and the control strategy. This is performed for a parallel hybrid configuration equipped with a push-belt CVT for a small passenger car (Toyota Yaris). The topology determines where the power sources (engine, electric machine/battery) are connected to the drive train.

The main design criterium, which is used in order to find the optimal parametric values, is the minimization of the overall fuel consumption, denoted as Φ_f , on a defined drive cycle. In addition, constraint functions $G(x)$ can be defined in order to keep system properties and variables within certain bounds. The

design optimization problem is formulated as [62]:

$$\min_x \Phi_f(x), \text{ subject to } G(x) \leq 0, x \in \mathcal{X} \subseteq \mathbb{R}^n, \quad (4.1)$$

where the feasible design space is assumed to be embedded in the set \mathcal{X} with dimension n . From a hybrid vehicle propulsion design view point the control design is seen as a subproblem. Therefore, the control model uses a local design variable, such as the control power-flow of the energy storage system (battery/electric machine).

4.3 Contribution and Outline of the Chapter

Finding the optimal parametric values is a complex task due to the strong interdependency of the design parameters. Furthermore, calculation of the optimal control strategy can be a computational burden. In particular, if the control strategy is optimized with control freedom of component operation point on top of the power distribution problem between the main power sources. In this chapter, in order to alleviate the complex design problem, the effects of employing a high-level modeling framework in determining the optimal design parameters are investigated. Initially, detailed component models are used for analyzing the sensitivity of the design parameters to the design objective. Moreover, the effects of control freedom in operation point on the total fuel consumption are investigated. Within this context, one of the main questions of the underlying research is:

- can a reduced hybrid drive train model be employed with sufficient accuracy for designing?

This question is answered at the end of this chapter. The outline of this chapter is discussed next. In Section 4.4, the base line vehicle, the engine, and the push-belt CVT model used as a reference are discussed. Accordingly, the hybrid vehicle drive trains, the developed power-split CVT models, and the electrical storage model are discussed. The simulation methods and assumptions are discussed in Section 4.5. In Section 4.6, the effects of parameter variation on the main design objective fuel consumption for a parallel hybrid vehicle are discussed. A method for calculation of the component efficiencies used with the simplified hybrid drive train model is presented in Section 4.7. The component efficiencies are described by a few characteristic parameters. The fuel consumption using the reduced hybrid drive train model is calculated and compared with that of a detailed hybrid drive train model. Finally, the conclusions are described in Section 4.8.

4.4 Modeling of the Drive Train Components

In this section the used component models for the engine, transmission, and battery storage system are discussed. Some of the used models, i.e., electric machine and battery data are obtained from ADVISOR [88]. The static efficiency maps of the electric machines are (linearly) scaled up or down in order for their properties to match the desired values. Similar scaling approaches have been utilized by others [46, 2, 79, 3]. Nevertheless, some of the used static-efficiency models, i.e., for the engine, the push-belt CVT, and torque converter TC have been derived based on performed measurements. The control design method as described in [31] is used for determination of the optimal control strategy. The control method is based on the combination of rule-based and equivalent consumption minimization strategies with which the fuel consumption can be calculated quickly and with sufficient accuracy. Next the reference vehicle model and accordingly the hybrid vehicle drive trains including the drive train components are discussed.

4.4.1 Base Line Vehicle Model

The base line vehicle is a Toyota Yaris (2007) equipped with a 1.3-l SI 64-kW engine, a torque converter TC, and a hydraulic actuated push-belt CVT. The fuel consumption of this vehicle was measured on a dynamo test bench for the New European Drive Cycle (NEDC) (cold en hot engine starts), the Japanese J10-15 (only hot engine) cycles, additional different continuous driving speeds, and wide-open throttle measurement tests. Thereby, the injected fuel mass flow (g/s), engine crank shaft speed, the drive shaft speed, and torque were measured. Since the engine crank shaft torque and the efficiency of the actual TC and CVT were not measured, available experimental validated models [84] for the TC and the belt-driven CVT were used in order to calculate backwards the required engine crankshaft torque. The collected measurement data and the reconstructed engine torque assumed to mimic the actual engine torque were used to reconstruct the (hot) engine fuel map. A forwards-facing control model consisting of a driver model and a dynamic drive train model was used in order to validate the used component models with the measured data. The results are not discussed here and is beyond the scope of the research presented in this chapter (see, Appendix A for more details). Instead, only the fuel consumption results of the base line vehicle are given (see, Table 4.1). The simulation with a wet-plate clutch shows a relatively small fuel consumption improvement of 2%. The reconstructed fuel efficiency map as a function of the engine torque T_e and speed ω_e is shown in Figure 4.1. In the figure, the fitted or ‘smoothed’ Optimal Operation Line (OOL) is also shown. The OOL collects the set of engine operation points with maximum efficiency over the engine output power range.

Table 4.1 / Reference values: base line vehicle (forwards-facing control model).

Test	Fuel consumption on the JP10-15	
	l/100km	Relative values
Measured value (TC)	5.10	100.0%
Catalogue value (TC)	5.00	98.0%
Simulated value (TC)	5.00	98.0%
Simulated value (CL)	4.90	96.0%

TC = Torque Converter, CL = Wet-plate clutch

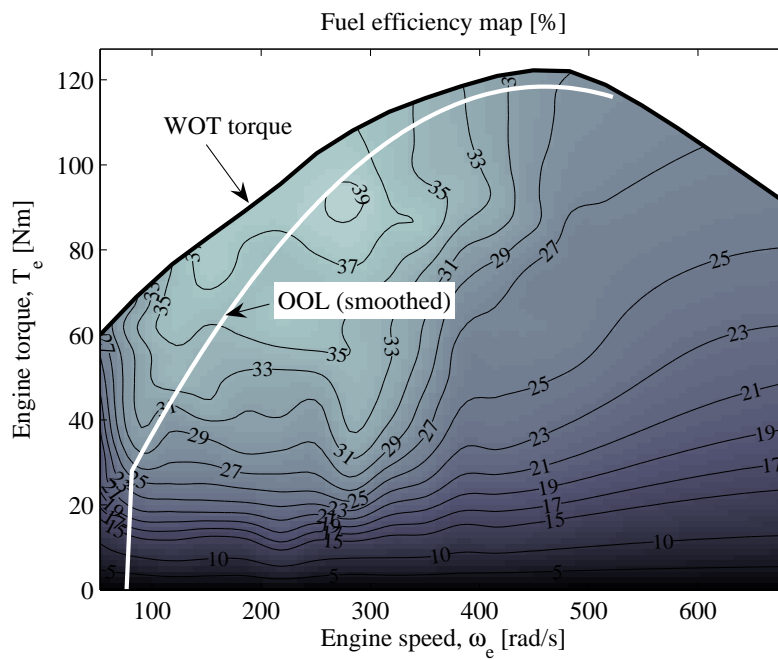


Figure 4.1 / Reconstructed 1.3-l VVTi 64-kW engine efficiency map and 'smoothed' Optimal Operation Line (OOL). WOT = Wide-Open Throttle torque.

4.4.2 Hybrid Drive Train Models

An overview of the hybrid vehicle models and the CVT technologies, which are investigated, is depicted in Figure 4.2. For the parallel hybrid configuration equipped with a push-belt CVT (Figure 4.2, top part), denoted as T_1 , the electric machine is coupled at the engine-side of the transmission between the clutch and the transmission. This allows turning the engine off during propulsion phases [39], since the vehicle can be propelled only by the electric machine. Smooth engine restart during stand-still with this configuration can not be done without an additional starter-alternator. This opposed to, e.g., for the Honda IMA, where the electric machine is directly connected to the engine crank shaft. The Honda IMA is able to restart the engine during stand-still with the same electric machine that is used, e.g., for brake energy recuperation or motor-assisting. However, the Honda IMA is not able to propel the vehicle solely by the electric machine efficiently due to the relatively large engine drag losses.

An electro-mechanical power-split CVT is used in the Toyota Prius (Figure 4.2, mid part), denoted as T_2 , which has only ‘one-mode’ implying that the CVT has no clutches nor brakes.

The second power-split CVT developed by Renault [83] (Figure 4.2, lowest part), denoted as T_3 , has two modes implying that the transmission can be operated in two modes depending on which brake (i.e., B_1 or B_2) is engaged. Furthermore, engine restart with T_2 and T_3 can be done at vehicle stand-still without using a starter-alternator.

The depicted power-split CVTs are characterized by the possible occurrence of recirculation power, which diminishes the overall transmission efficiency. The main power-flow cases are indicated by the arrow directions in the figure for T_2 and T_3 . In T_3 also ‘negative recirculation power’ at a certain speed ratio through the electrical variator occurs. However, this power-flow through the electrical branch is effectively reduced by applying a gear or a mode shift. In Section 4.4.3 more details on this subject are given. For an overview of the used model data for the main power sources and the specific electric machine data for T_1 - T_3 is referred to the Tables 4.2 and 4.3 respectively. Since, the electric machine data for T_3 is not available within ADVISOR (this in contrary to T_2), selected data is used and sized to meet the specifications close to the actual components of T_3 .

4.4.3 Power-Split CVT

In [50] a ‘black box model’ has been introduced for analyzing power-split CVTs with several modes, which is adopted in this chapter (see, Figure 4.3). In this black box model the transmission ‘subsystem’ consists of an arrangement of planetary gears. The clutches for mode switching and some gear stages (including the

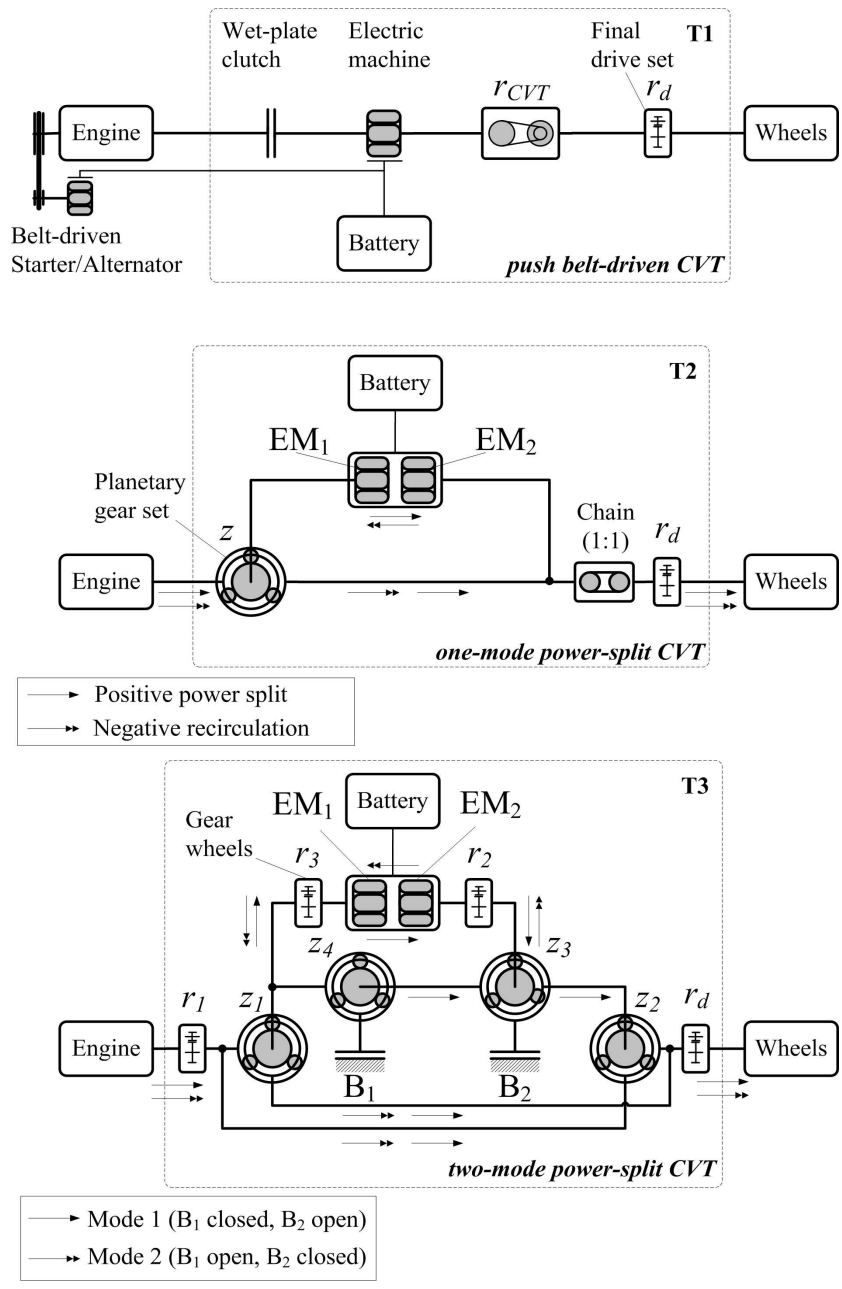


Figure 4.2 / Hybrid drive train models equipped with different hybrid transmission technologies: T1, T2, and T3.

Table 4.2 / Base component characteristics.

Engine	Toyota Vitz, 4-cylinder, 64-kW peak power (at 6000 rpm), 1.3-l VVTi, 124-Nm peak torque (at 4400 rpm), 40% peak efficiency
Electric Machine/Controller	PM brushless AC motor, 58-kW peak power (at 1250 rpm), 403-Nm peak torque, 92% peak efficiency, mass 70 kg (MC_PM58*)
Battery Pack	Panasonic, Ni-MH type, current capacity 6 Ah, nominal voltage 1.2 V/cell, storage mass 0.166 kg/cell (ESS_NIMH6*)

*model data file from ADVISOR

Table 4.3 / Electric machine characteristics for the hybrid vehicle models.

Hybrid topology	Power/torque range (\pm kW/Nm)	Base speed (rpm)	Speed range (rpm)	ADVISOR data file
T1	[1-15]/[7-104]	1250	4000	MC_PM58 [†]
T2	15/55	2500	\pm 5500	GC_PRIUS_JPN
T2	30/305	1000	6000	MC_PRIUS_JPN
T3	25/135	1800	\pm 11000	GC_PRIUS_JPN [†]

[†]linearly scaled as needed

final drive) are assumed to be part of this subsystem. Next, a loss-free analysis is performed. Accordingly, the power-losses and the efficiency model of the power-split CVT are discussed.

Loss-Free Analysis

Generally, the speed relations are written as,

$$\begin{bmatrix} \omega_{v,p} \\ \omega_{v,s} \end{bmatrix} = \begin{bmatrix} a & b \\ c & d \end{bmatrix} \cdot \begin{bmatrix} \omega_{t,p} \\ \omega_{t,s} \end{bmatrix} = \underline{M} \cdot \begin{bmatrix} \omega_{t,p} \\ \omega_{t,s} \end{bmatrix}, \quad (4.2)$$

and for the torque relation holds,

$$\begin{bmatrix} T_{t,p} \\ T_{t,s} \end{bmatrix} = -\underline{M}^T \cdot \begin{bmatrix} T_{v,p} \\ T_{v,s} \end{bmatrix}. \quad (4.3)$$

The variator speed ratio is defined as,

$$r_v = \frac{\omega_{v,s}}{\omega_{v,p}} = -\frac{T_{v,p}}{T_{v,s}}, \quad (4.4)$$

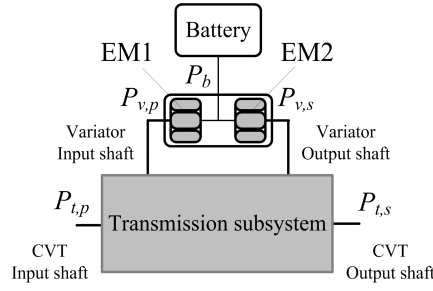


Figure 4.3 / Generic black box model for power-split CVTs [50].

and the overall CVT transmission speed ratio is similar defined as,

$$r_t = r_{CVT} \cdot r_d = \frac{\omega_{t,s}}{\omega_{t,p}} = -\frac{T_{t,p}}{T_{t,s}}, \quad (4.5)$$

resulting from the equilibrium of power at the input and output shafts of the variator and the transmission respectively. The loss-free case [64] shows, that the variator power ratio $P_{v,p}/P_{t,p}$ is written as,

$$\Psi = \frac{P_{v,p}}{P_{t,p}} = \frac{\omega_{v,p} \cdot T_{v,p}}{\omega_{t,p} \cdot T_{t,p}} = \frac{r_v}{r_t} \frac{dr}{dr_v}. \quad (4.6)$$

The variator power ratio Ψ after substitution of Equation (4.2), (4.4) and (4.5) into (4.6) becomes,

$$\Psi = \frac{-r_v (ad - bc)}{(ar_v - c)(br_v - d)}, \quad (4.7)$$

and the overall speed ratio after substitution of Equation (4.2) and (4.4) into (4.5) holds,

$$r_t = -\frac{ar_v - c}{br_v - d} \Leftrightarrow r_v = \frac{dr_t + c}{br_t + a}. \quad (4.8)$$

The coefficients of the matrix \underline{M} for the two different power-split CVTs are given in Table 4.4. In Table 4.5, the transmission model parameters for each transmission is shown.

The one-mode power-split CVT consists of one planetary gear set and an electrical variator. The engine is connected to the carrier, the generator EM1 is connected to the sun gear, and the annulus of the planetary gear set is connected to the output shaft of the transmission (see, Figure 4.2 mid-part). The generated power with EM1 is transmitted to the motor EM2. If the state-of-charge of the battery is too low, then this energy may be (partially) used for recharging during standstill or driving. The power-split situation depends on the variator power

Table 4.4 / Transmission coefficients.

Transmission topology	Matrix coefficient			
	a	b	c	d
T2	$1 - z$	$z r_d$	0	r_d
T3 (mode 1)	$r_2 z_2 / r_1$	$r_2 r_d (1 - z_2)$	$r_3 / r_1 (z_2 z_3 z_4 + (1 - z_3) (1 - z_1))$	$r_3 r_d (z_3 z_4 (1 - z_2) + z_1 (1 - z_3))$
T3 (mode 2)	$r_2 z_2 / r_1$	$r_2 r_d (1 - z_2)$	$(1 - z_1) (1 - z_3) r_3 / r_1$	$(1 - z_3) z_1 r_d r_3$

Table 4.5 / Transmission model parameters.

	T1	T2	T3
$r_{ud} =$	0.43	$z = -78/30$	$z_1 = -75/41$
$r_{od} =$	2.39	$r_d = 0.25$	$z_2 = -67/25$
$r_d =$	0.19		$z_3 = -63/29$
			$z_4 = -79/45$
			$r_1 = -55/31$
			$r_2 = 51/27$
			$r_3 = 26/30$
			$r_d = -67/41$

ratio Ψ and the typical situations are schematically depicted in Figure 4.4. The situations are depicted under ‘normal operation condition’ (as in a conventional drive train). The vehicle is defined to be propelled only by the engine and the generated power is directly transmitted to the motor. The battery is omitted in the figure. The electric machines EM1 and EM2 operate always mutual exclusive during the normal and the ‘hybrid operation condition’ (i.e., the engine and the battery are both used at the same time). During the electric-only modes (regenerative braking or propulsion) with the battery (the engine is shut-off): T2 uses only EM2 and T3 uses both electric machines EM1 and EM2 in the same operation (generative or motoring) mode respectively. During driving and braking in the electric-only modes there is small angular speed difference between the electric machines of T3.

One of the power-split situations, which is depicted in Figure 4.4(a), is defined as ‘power bifurcation’ or ‘positive’ power-split. The power-flow is regarded as positive going from left to right. If the power-flows through the variator and the mechanical subsystem have opposite directions, then recirculation power occurs. For the other power-split cases, as shown in the Figures 4.4(b), (c) and (d), holds that dependent on the direction of power-flow through the variator the recirculation power is regarded as positive or negative.

A special case, which is not shown in the figure, is $\Psi = 0$. In this situation, the transmission input power-flow is only transmitted through the mechanical

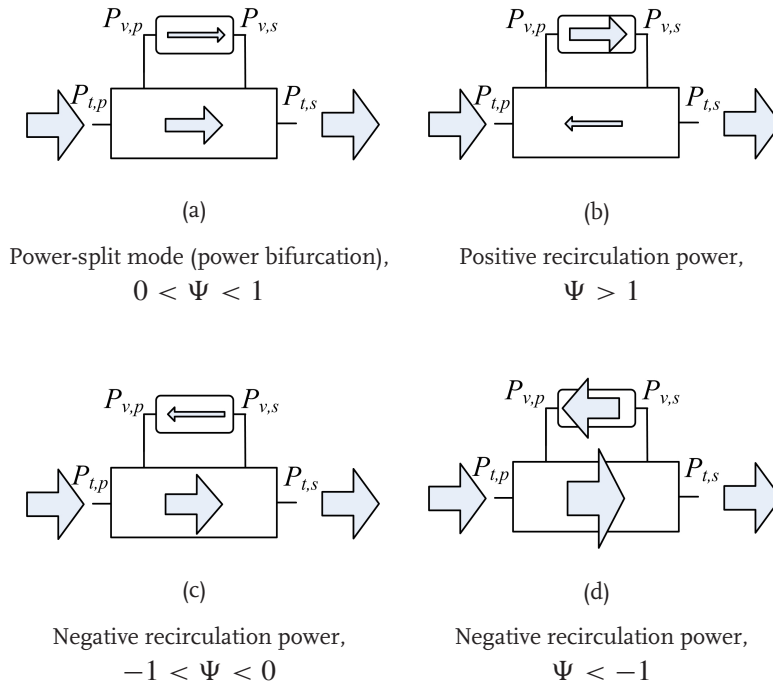


Figure 4.4 / Power-split cases dependent on the ratio $\Psi = P_{v,p}/P_{t,p}$ [50].

subsystem to the vehicle wheels and the power-flow through the variator is zero. Under this condition the transmission efficiency η_{CVT} is maximum, since the mechanical subsystem alone has a higher efficiency than the combined efficiency of the mechanical subsystem and the variator. If, for example, $\omega_{v,p} = 0 \wedge P_{t,p} > 0$, then the variator ratio becomes $r_v \rightarrow \infty$ with Equation (4.4). In addition, Equation (4.7) shows that the power-split ratio becomes,

$$\lim_{r_v \rightarrow \infty} \Psi(r_v) = 0, \quad (4.9)$$

and the overall speed ratio r_t with help of Equation (4.8) for the one-mode power split CVT (see, Table 4.4) becomes,

$$\lim_{r_v \rightarrow \infty} r_t(r_v) = -\frac{a}{b} = \frac{(z-1)}{z \cdot r_d} = r_t^*. \quad (4.10)$$

If $r_t > r_t^*$ for a certain transmission output torque, then too much transmission input torque $T_{t,p}$ is transmitted through the planetary gear set to the vehicle wheels. This causes that the motor torque $T_{v,s}$ changes sign, which results in a

mode switch between motor and generator function for EM2. Simultaneously, the generator speed $\omega_{v,p}$ changes sign causing a mode switch between generator and motor function for EM1 and the variator ratio becomes $r_v < 0$. The transmission efficiency η_{CVT} is reduced due to negative recirculation power. In the two-mode power-split CVT also negative recirculation power occurs. However, the power-flow transmitted through the electrical variator is reduced after mode switching at r_t^* . Thereby, the overall transmission efficiency is effectively increased over a larger speed ratio range.

Power Losses of the Power-Split CVT

The power losses P_{loss} of the power-split CVT under normal operation condition is calculated as the sum of:

- the losses of the electric machines (or the electric variator) $P_{v,loss}$ described by variator efficiency η_v on both generator and motor working modes,
- the losses of the planetary gears described by a constant efficiency $\eta_{ps} = 0.98$ for each planetary gear set, and
- the losses of the gearwheels, the chain for T2, and the final drive set including the differential described by constant efficiencies $\eta_i = 0.98$ (with $i \in \{1, 2, 3\}$) and $\eta_{fd} = 0.98$ respectively.

Note that the hydraulic power losses (and drag losses) of T3 for actuation of the brakes or dog clutches, which allow a mode change within less than 100 ms, are neglected. Hydraulic pressure is only required when a mode change occurs.

By utilizing the fact that the variator power ratios are known from the loss-free model (previous section), a simplified and computational relatively fast loss analysis of the two power-split CVTs can be made. The overall transmission efficiency η_{CVT} during positive and negative recirculation power is written as [50]:

$$\eta_{CVT} = \begin{cases} (\eta_{ps} \cdot (1 - \Psi) + \eta_v \cdot \Psi) \cdot \eta_{fd}, & \text{for } \Psi > 0, \\ (\eta_{ps} \cdot (1 + \eta_v \cdot \Psi) - \Psi) \cdot \eta_{fd}, & \text{for } \Psi < 0. \end{cases} \quad (4.11)$$

In [50] is shown that there is a good correspondence between a CVT efficiency model using free-body diagrams and the CVT efficiency model described by Equation (4.11) using a varying (electrical) variator efficiency model and constant efficiencies for the gearwheels and planetary gear sets. Therefore, in this chapter an electrical variator efficiency model dependent on the operation point ($T_{v,p}$, $\omega_{v,p}$) and variator ratio r_v is used. The variator efficiency η_v is determined by the electric machine efficiencies, the battery power P_b , and the variator input power $P_{v,p}$. The variator input power $P_{v,p}$ is determined by the direction of power flow or

the power-split ratio Ψ given $P_{t,p}$. The variator efficiency η_v is influenced by the battery power P_b as is explained in the following section. Note that for T3 the planetary gear set efficiencies are lumped into one planetary gear set efficiency.

Influence Battery Power on Variator Efficiency

The battery power P_b influences the desired operation points of the electric machines and therefore the variator losses $P_{v,loss}$ described by the electric machine efficiencies. The generated electrical power P_1 using the static-efficiency map of EM1 in generator mode η_{em1} and the variator output speed, given the variator input torque, speed, and ratio, is calculated respectively with:

$$P_1 = P_{v,p} \cdot \eta_{em1} \left(\begin{array}{l} \omega_{v,p}, T_{v,p} \mid \omega_{em1,min} \leq \omega_{v,p} \leq \omega_{em1,max} \\ \wedge T_{em1,min}(\omega_{v,p}) \leq T_{v,p} \leq T_{em1,max}(\omega_{v,p}) \end{array} \right), \quad (4.12)$$

and

$$\omega_{v,s} = r_v \cdot \omega_{v,p}. \quad (4.13)$$

Since the output variator torque is yet unknown, the vector of the required electric input powers of EM2 \vec{P}_2 is calculated using the given static-efficiency map of EM2 in motor mode η_{em2} , the variator output speed $\omega_{v,s}$ and a vector of available electric machine output torques \vec{T}_{em2} :

$$\vec{P}_2 = P_{v,s} / \eta_{em2} \left(\begin{array}{l} \omega_{v,s}, \vec{T}_{em2} \mid \omega_{em2,min} \leq \omega_{v,s} \leq \omega_{em2,max} \\ \wedge T_{em2,min}(\omega_{v,s}) \leq \vec{T}_{em2} \leq T_{em2,max}(\omega_{v,s}) \end{array} \right), \quad (4.14)$$

Given the battery power P_b and the calculated P_1 with Equation (4.12) the available electric machine input power for EM2 becomes:

$$P'_2 = -P_1 - P_b. \quad (4.15)$$

The resulting electric machine output torque $T'_{v,s}$ is calculated by interpolation. The available $T'_{v,s}$ is an element of the vector with available electric machine torques:

$$T'_{v,s} \in \{ \vec{T}_{em2} \mid \vec{P}_2(\omega_{v,s}, T'_{v,s}) - P'_2 = 0 \}. \quad (4.16)$$

Accordingly, the electrical variator efficiency is calculated with:

$$\eta_v = \frac{P_{v,s}}{P_{v,p}} = \frac{T'_{v,s} \cdot \omega_{v,s}}{T_{v,p} \cdot \omega_{v,p}} = \frac{T'_{v,s}}{T_{v,p}} \cdot r_v \wedge P_{v,loss} = (1 - \eta_v) \cdot P_{v,p}. \quad (4.17)$$

Initially, a loss-free analysis gives all speed and torques and thereby also the direction of the power-flow through the variator. The efficiency of the electric machine that acts as generator is calculated. Then, for a given battery power the resulting differential electric power between the electric machines is determined. The

desired output torque of the motor is calculated with Equation (4.16) (assuming positive power-split for example) and the variator efficiency is calculated with Equation (4.17). Accordingly, with help of Equation (4.11) the overall transmission efficiency is calculated. For a given output torque $T_{t,s}$, speed $\omega_{t,s}$, and speed ratio r_t a new set of transmission input torque and speed ($T_{t,p}$, $\omega_{t,p}$) can be calculated. The procedure is reiterated until desired accuracy is reached. The electrical variator (and transmission) efficiency as a function of the variator (and transmission) input speed, torque, speed ratio, and battery power for T2 and T3 are stored in look-up tables. The variator and the transmission efficiencies can therefore also be expressed as,

$$\eta_v = \eta_v(\omega_{v,p}, T_{v,p}, r_v, P_b) \text{ and } \eta_{CVT} = \eta_{CVT}(\omega_{t,p}, T_{t,p}, r_t, P_b). \quad (4.18)$$

In the Figures 4.5, 4.6, and 4.7, for example, the efficiency maps at a transmission input speed of $\omega_{t,p} = 209$ rad/s (2000 rpm) as a function of the overall speed ratio r_t and input torque $T_{t,p}$ given $P_b = 0$ for T1, T2, and T3 are shown respectively. The push-belt CVT efficiency is strongly influenced by the input torque for a fixed input speed. The efficiency increases with increase of input torque and with increase of speed ratio up to the ‘neutral’ speed ratio $r_{CVT} = 1$. The maximum efficiency for the push-belt CVT is at neutral speed ratio $r_{CVT} = 1$ (indicated with the dashed line in the figure). In contrary to the push-belt CVT the power-split CVTs are strongly affected by the speed ratio and a little affected by the input torque. For the power-split CVTs at gear ratios (also indicated by the dashed lines) where $r_t^* = -c/d \wedge r_v = 0$, or a mode switch occurs, i.e., $r_t^* = -a/b \wedge r_v = \pm\infty$, the transmission efficiency η_{CVT} is maximum. The variator power ratios Ψ as function of the overall speed ratio r_t for T2 and T3 are shown in Figure 4.8. The ratios at which $\Psi = 0$ are also indicated.

4.4.4 Battery Model

The maximum battery pack power is equally sized to the maximum possible output power specifications of the electric machine for the parallel hybrid drive train equipped with the push-belt CVT (T1), i.e., 15 kW. Thereby, the minimum number of 40 battery modules for the Ni-MH with a nominal battery system voltage of 288 V are needed in order to meet the estimated minimum voltage requirement of 120 V and the maximum current 125 A allowed by the motor controller/electric machine. These values are kept constant (see, Table 4.2). For comparison the same battery efficiency data is used with the other two power-split CVTs.

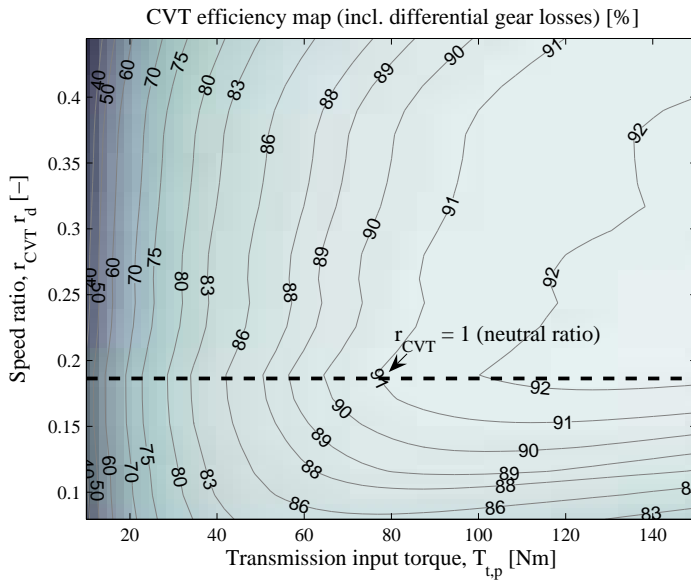


Figure 4.5 / Efficiency map for the belt-driven CVT (T1) at $\omega_{t,p} = 209$ rad/s (2000 rpm).

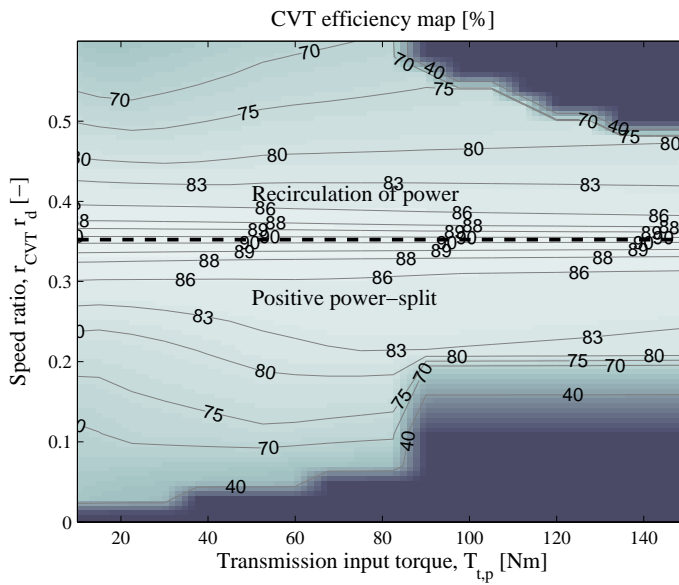


Figure 4.6 / Efficiency map for the one-mode power-split CVT (T2) at $\omega_{t,p} = 209$ rad/s (2000 rpm).

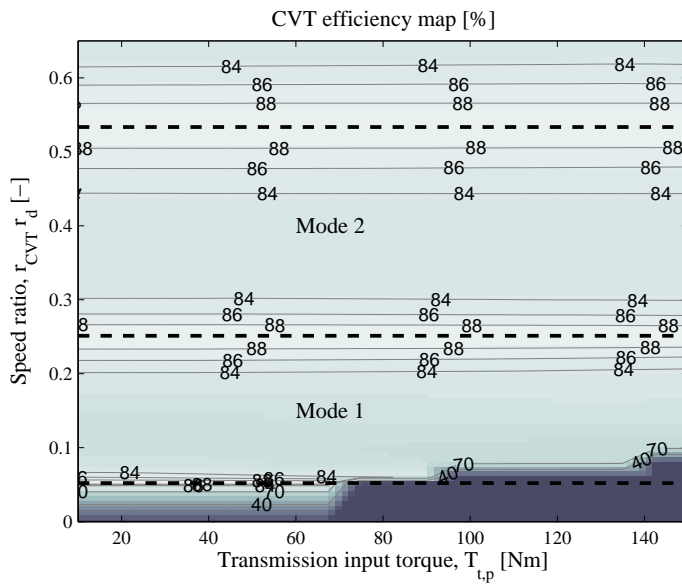


Figure 4.7 / Efficiency map for the two-mode power-split CVT (T3) at $\omega_{t,p} = 209$ rad/s (2000 rpm).

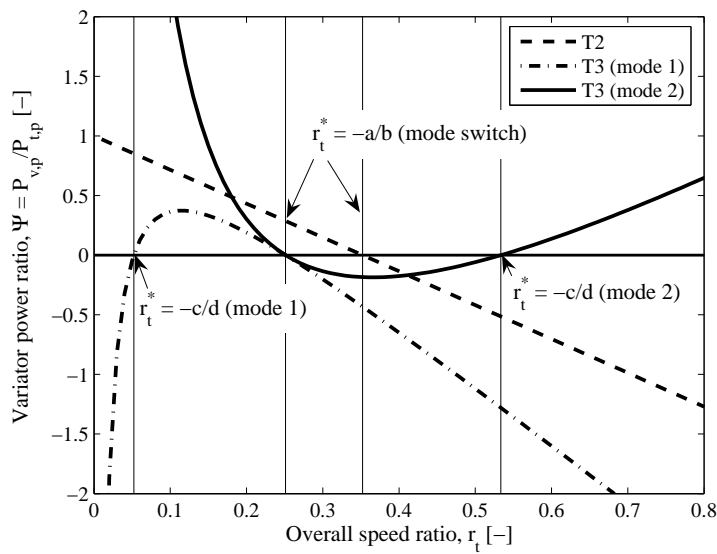


Figure 4.8 / The variator power ratio as a function of the overall speed ratio for T2 and T3.

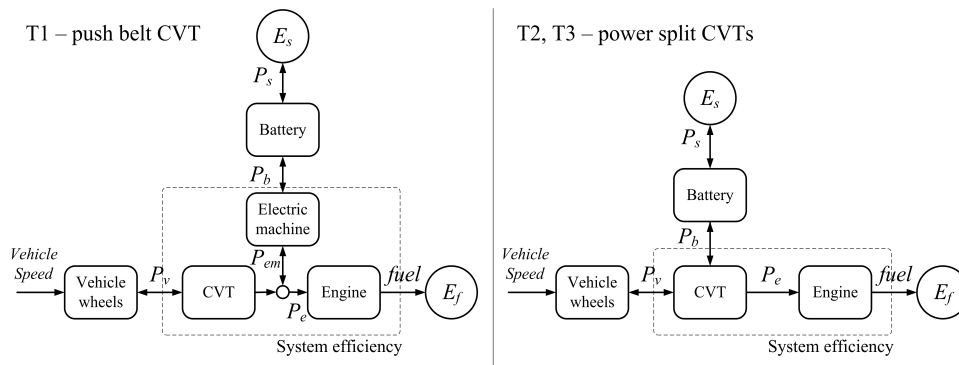


Figure 4.9 / Power-flow in the hybrid drive trains (backwards-facing control model) for T₁, T₂, and T₃.

Table 4.6 / Vehicle model parameters.

Description	Symbol	Value	Unit
Total mass	m_v	1134	kg
Wheel radius	r_w	0.277	m
Inertia of two wheels	J_w	1.5	kg m ²

4.5 Simulation Method

In Figure 4.9 the power-flows in the hybrid drive trains for T₁, T₂, and T₃ are schematically visualized, which is a backwards-facing model implying that the vehicle speed v_v prescribed by the drive cycle is assumed to be tracked exactly. This model is used to compute the optimal control signals that minimize the fuel consumption.

The inputs are the battery input power P_s , the velocity v_v described by the given drive cycle and the vehicle drive power demand P_v . The outputs are the engine speed ω_e and torque T_e , which are used to compute the fuel mass flow \dot{m}_f (g/s). The vehicle parameters of the Toyota Yaris determine the vehicle road load torque T_{rl} . The vehicle model parameters are listed in Table 4.6. Note that the battery power can be affected by additional electrical (auxiliary) loads, which is not shown in the figure. The vehicle road load depends on the vehicle speed v_v (m/s) (assuming no wheel slip) and is the sum of the roll resistance and the air drag torque:

$$T_{rl}(t) = 36.8 + 0.416 v_v(t) + 0.113 v_v(t)^2, \quad (4.19)$$

where the vehicle power demand as a function of time $P_v(t)$ becomes,

$$P_v(t) = T_{rl}(v_v(t))/r_w \cdot v_v(t) + (m_v + J_w/r_w^2) \cdot \dot{v}_v(t). \quad (4.20)$$

The vehicle mass, the inertia of the wheels, and the wheel radius are described by the parameters m_v , J_w , and r_w respectively. The energy level in the battery and in the fuel tank are represented by the variables E_s and E_f respectively.

The simulation procedure, which is described by sequential computation steps, in order to calculate the fuel mass flow rate \dot{m}_f as a function of the battery input power P_s given v_v and P_v , is discussed below.

Step 1. In the first step the transmission efficiencies η_{CVT} are computed for all admissible battery powers P_b , transmission input torques $T_{t,p}$, speeds $\omega_{t,p}$, and speed ratios r_t and are stored in multi-dimensional look-up tables. The transmission efficiency can be expressed as,

$$\eta_{CVT} = \eta_{CVT}(\omega_{t,p}, T_{t,p}, r_t, P_b). \quad (4.21)$$

This is performed for the hybrid vehicle configurations T1, T2, and T3.

Step 2. In the second step the fuel mass-flows \dot{m}_f (g/s) are computed for all admissible battery powers P_b given the drive power demand $P_v(t)$ and the angular vehicle wheel speed $\omega_v(t) = v_v(t)/r_w$. The fuel mass-flows are computed for two different control strategies focussing on maximizing the engine η_e or the system efficiency η_{sys} at each time instant. These two control strategies, which determine the engine operation point, are referred to as CS1 and CS2 respectively.

The system efficiency (see, Figure 4.9) is defined as the product of the engine and the transmission efficiency (without the battery) and is written as:

$$\eta_{sys} = \eta_e(\omega_e, T_e) \cdot \eta_{CVT}(\omega_e, T_e, r_t, P_b), \quad (4.22)$$

with $T_{t,p} = T_e$ and $\omega_{t,p} = \omega_e$. Since the input shaft of the CVT is directly connected to the output shaft of the engine. Accordingly, the optimal speed ratio and engine torque are selected:

$$(r_t^o(P_b, t), T_e^o(P_b, t)) = \arg \max_{(r_t, T_e) \in \mathcal{O}} (\eta_* | P_b, P_v(t), \omega_v(t)), \quad (4.23)$$

for $*$ \in $\{e, sys\}$ where the set \mathcal{O} covers the feasible solutions that satisfy the constraints:

$$\mathcal{O} = \left\{ \begin{array}{l} (r_t, T_e) | \omega_{**,min} \leq \omega_{**} \leq \omega_{**,max} \wedge \\ T_{**,min}(\omega_{**}) \leq T_{**} \leq T_{**,max}(\omega_{**}) \wedge \\ (r_{ud} \leq r_{CVT} \leq r_{od})|_{T1} \wedge \\ P_{b,min} \leq P_b \leq P_{b,max} \end{array} \right\}, \quad (4.24)$$

for $** \in \{e, em\}$ and r_{CVT} is limited by the (under-)over drive ratios r_{ud}, r_{od} for T1.

The optimal gear ratios and engine torques for all admissible battery powers for both control strategies (CS1, CS2) are stored in multi-dimensional look-up tables and are used to compute the fuel mass-flows using the engine fuel map. If the optimal gear ratios and engine torques at each time instant are known for different values of P_b given $P_v(t)$ and $\omega_v(t)$, then the fuel mass-flow can be expressed only as a function of the battery power,

$$\dot{m}_f = \dot{m}_f(P_b, t \mid P_v(t), \omega_v(t)), \quad (4.25)$$

for CS1 and CS2.

Note that in case of engine optimal operation (CS1) the transmission efficiency η_{CVT} is determined by the speed ratio $r_t^o(t, P_b)$ and engine torque $T_e^o(t, P_b)$ (pre-scribed by the OOL) given a certain vehicle speed $\omega_v(t)$. However, in a backwards-facing control model the required $r_t^o(t, P_b)$ and $T_e^o(t, P_b)$ given a certain speed $\omega_v(t)$ are determined by η_{CVT} and the given $P_v(t)$. Due to this causality conflict it is impossible to determine the $r_t^o(t, P_b)$ and $T_e^o(t, P_b)$ given a certain speed ω_v exactly. In this study for CS1 the transmission losses are iteratively estimated and are compensated for the engine power $P_e(t)$. The iteration error, denoted as ε , at time instant t in each iteration step i is defined as:

$$\varepsilon(i, t) = |P_e(i+1, t) - P_e(i, t)|. \quad (4.26)$$

The iteration is repeated until the error $\varepsilon(i, t)$ between the iteration steps at a certain time instant becomes sufficiently small (i.e., $\varepsilon(i, t) < 10$ W). A mathematical condition to prevent the iteration loop from instabilities, in terms of the estimation $P_e(i, t)$ is

$$|P_e(i+1, t) - P_e(i, t)| < \gamma |P_e(i, t) - P_e(i-1, t)|, \quad 0 < \gamma < 1. \quad (4.27)$$

This condition implies that the error ε of each estimate decreases in each iteration step i . If the ratio of the error between the previous and the subsequent step becomes equal to 1 the estimates will not further improve. This corresponds with the transition between stable and unstable iteration loops. At later time instants the required P_e is calculated using the known values for the efficiencies at the previous time instant. Therefo, the requested $P_v(t)$ is divided by the computed η_{CVT} .

Step 3. In the third step the optimal control strategy is determined using the control design model as described in [31], where the engine efficiency (CS1) or the system efficiency (CS2) at each time instant t is maximized and the total fuel consumption Φ_f is minimized. The optimization problem is finding the control power-flow $P_s(t)$ given a certain power demand at the wheels $P_v(t)$ and wheel

speed $\omega_v(t)$, while Φ_f over a drive cycle with time length t_f is minimized, i.e.,

$$\Phi_f = \min_{P_s(t)} \int_0^{t_f} \dot{m}_f(P_s(t), t | P_v(t), \omega_v(t)) dt, \quad (4.28)$$

subject to certain component constraints $\vec{h} = 0$, $\vec{g} \leq 0$, which are described below. The state is equal to the stored energy E_s in the battery in J, and the control input is equal to the battery input power P_s in W (see, Figure 4.9):

$$P_s = \min(P_b/\eta_b(P_b), P_b \eta_b(P_b)). \quad (4.29)$$

The battery efficiency η_b is only a function of the battery power P_b , since the influence of the relatively small variation in the battery energy level on the battery efficiency is small and therefore neglected. The energy level in the battery is a simple integration of the power and is calculated as follows,

$$E_s(t) = E_s(0) + \int_0^t P_s(\tau) d\tau. \quad (4.30)$$

The main constraints on the battery are energy balance conservation of E_s over the drive cycle and constraints on the power P_s :

$$\begin{aligned} h_1 &:= E_s(t_f) - E_s(0) = 0, \\ g_{1,2} &:= P_{s,min} \leq P_s(t) \leq P_{s,max}. \end{aligned} \quad (4.31)$$

The computation steps 1–3 are performed for different electric machine sizes (1–15 kW) in combination with other different design parameters. In the following section, the modeling assumptions, the descriptions, and the symbols of the investigated design parameters are discussed.

4.5.1 Assumptions and Descriptions of the Design Parameters

Initially, for the hybrid vehicle models the following Assumptions (A.) are made.

- A. 1 The drive train components (engine, transmission, electric machine, battery) are modeled as quasi-static efficiency models.
- A. 2 The electric machine characteristics (maximum torque curve and static-efficiency map) are linearly scaled as needed. The effect of the vehicle mass increase by up scaling of the electric machine is neglected.
- A. 3 For the whole drive cycle the electrical auxiliary loads are constant 200 W assumed. For the base line vehicle the electrical auxiliary loads increase the fuel consumption with 0.13 l/100km for the JP10-15.

- A. 4 The minimum engine speed during operation is 980 rpm equally to the reference vehicle with a conventional drive train.
- A. 5 The braking forces are evenly distributed between rear and front wheels. The brake force distribution ratio between front and rear wheels is denoted as f_{fb} . In order to maximize the vehicle stability an adaptive brake force distribution should be considered [21]. However, in this chapter ideally braking is not considered. Instead the influence of different constant values for f_{fb} , also referred to as regenerative brake fraction, is investigated.
- A. 6 The maximum electro-mechanical braking power is limited by the torque, speed and power constraints of the electric machine and battery respectively. Braking powers larger than the maximum electrical regenerative braking power are assumed to be dissipated in the front-wheel brake discs.
- A. 7 The engine has no drag or idle losses at vehicle stand still. This start-stop function decreases the fuel consumption with 0.66 l/100km for the JP10-15. Fuel saving with start-stop during propulsion depends on the degree-of-hybridization.
- A. 8 The fuel use for engine cranking is neglected, since the engine can be started with the electric machine in a very short time period (typically 100 ms - 300 ms). The required electrical energy for engine start (usually the engine is started when the vehicle is already driving) is therefore limited and very small. However, the power for engine start is relatively high.
- A. 9 During braking the CLutch is Open (CLO) and the Engine is assumed to be OFF (EOFF) (i.e., inducing no additional drag torques and no idle fuel consumption). This assumption decreases the fuel consumption with 0.45 l/100km.

If during braking in a real vehicle the engine is completely shut-off and disengaged, then quick engine restart during driving can be uncomfortable and therefore unacceptable. Unless, for example, the electric machine is sufficiently large in order to deliver the relatively large engine start-up torques, which are superposed on the drive torque demand. Therefore, two other braking strategies are investigated where the Engine remains ON (EON) during braking in combination with the electric-only vehicle speed threshold value, which is denoted as v_M . The engine is always on for vehicle speeds above this value, and vice-versa. This will be discussed by the descriptions of the design parameters in more detail.

- A. 10 The electric-only vehicle speed threshold value v_M is 20 km/h, which is equal to the measured value for the Toyota Prius on the JP10-15 cycle [17].

- A. 11 During the electric-only mode (propulsion and braking) the CVT speed ratio is assumed to be controlled, such that the electric machine is operated at the highest efficiency points. In [90] is shown, that this braking strategy provides increased recuperated energy.

Next the descriptions and the symbols of the Design (D.) parameters are given.

- D. 1 **Regenerative brake fraction:** determines the distribution fraction f_{fb} between the front- and the rear-wheels, where the regenerative braking power becomes $P_{BER}(t) = f_{fb} \cdot P_v(t \mid P_v(t) < 0)$ with $f_{fb} \in \{0\%, 50\%, 100\%\}$.
- D. 2 **Drive cycle:** the vehicle load is influence by using the New European Drive Cycle (NEDC) or the Japanese drive cycle (JP10-15) (see, Equation (4.19)).
- D. 3 **Component size:** the component efficiencies, the power-flow control strategy, and the fuel saving potential are affected by the size of the electric machine. The base electric machine size is linearly scaled as needed (see, Table 4.3).
- D. 4 **Transmission technology:** the efficiency of the power-flow paths between battery/electric machine, engine, and the vehicle wheels is determined by T_1 , T_2 , or T_3 .
- D. 5 **Topology:** determines where the electric machine is coupled to the transmission, i.e., at the PRImary (engine-side) (PRI), or at the SECondary side (wheel-side) (SEC) of the transmission. When it is coupled at the secondary side, a reduction set of gearwheels with a fixed speed ratio is selected, such that the electric machine is able to reach the maximum drive cycle speed (70 km/h for the JP10-15). The efficiency of the reduction set is constant 98% assumed. Note that start-stop is still possible with this configuration, since the engine is in principle restarted with the starter-alternator. Without a starter-alternator, engine restart with an electric machine coupled at the wheel-side requires a relatively large and more costly electric machine due to the transmission losses and relatively low torque multiplier factor [33].
- D. 6 **Actuation technology for the push-belt CVT:** one of the major power losses of the conventional push-belt CVT (which are in the order of 50% of the total power losses [1]) are caused by the hydraulic pump. Therefore, the influence of applying an Electro-Mechanical Actuation (EMA) system instead of a HyDraulic Actuation (HDA) system on the fuel consumption is investigated. The electro-mechanical actuation power, which is only required during operation of the push-belt CVT, is constant 90 W assumed. The

efficiency of the EMA system is constant 90% assumed, which results in a battery output power demand of 100 W.

- D. 7 **Regenerative brake strategy (combined with an electric-only vehicle speed threshold value):** the influence of the electric-only vehicle speed threshold value v_M on the fuel consumption is investigated in combination with the clutch state (i.e., closed, or open) during braking. Depending on the clutch state the engine applies ‘fuel cut-off’ (no fuel injection) and has engine drag losses, or idle fuel mass-flow during regenerative braking.
- a. **Clutch Open/Engine ON (CLO/EON):** the Engine is ON at idle speed 610 rpm and disengaged. The engine has idle-fuel mass-flow until $v_v(t) = v_M$. However, the engine has no drag losses. The electric machine is operated at the OOL during braking.
 - b. **Clutch Closed/Engine ON (CLC/EON):** the Engine is ON and engaged. The engine has no fuel mass-flow (i.e., fuel cut-off) until $v_v(t) = v_M$. However, the engine has drag losses. The drag losses cause reduction of the recuperative brake energy. Notice that the push-belt CVT is controlled, such that the engine output shaft is rotating at the minimum speed (610 rpm), while the engine drag losses are minimized.

For both cases the engine is switched off and disengaged during braking only if $v_v(t) < v_M$. The strategies are schematically visualized in the Figure 4.10.

- D. 8 **Speed ratio control strategy:** the CVT speed ratio is controlled based on engine optimal operation (CS1) or system optimal operation (CS2).

In the following section the effects of parameter variation (D. 1 – D. 8) on the fuel consumption are investigated.

4.6 Results

4.6.1 Effects of Parameter Variation (D. 1 – D. 8) on the Design Objective

The responses of the design objective (fuel consumption) Φ_f as a function of the electric machine size (D. 3) for the different design parameters (D. 1, D. 2, and D. 5 – D. 8) are shown in Figure 4.11. It should be noticed, that the transmission technologies T2 and T3 (D. 4) in combination with different electric machine sizes have not been varied. The electric machines of T2 and T3 are part of the transmission technology and are for these transmissions fixed. Although the response functions show small local oscillations (local minima), the global trend of

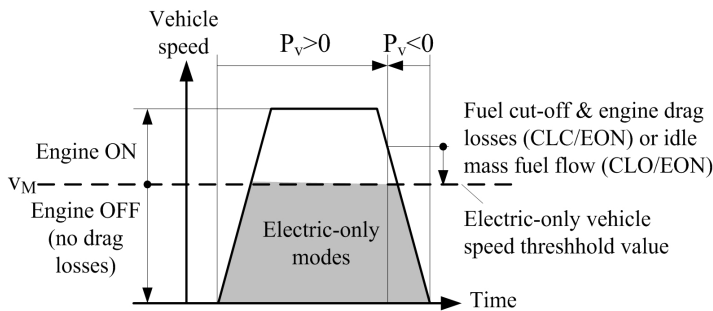


Figure 4.10 / Engine on/off strategy.

the response functions shows a convex curvature. The optimal electric machine sizes are easily determined and are depicted by the white-colored circular marks. The relatively fuel consumption values are shown in the figure at the right-side. A bar diagram with the fuel consumption at the optimal electric machine size (D. 3) as a function of the different design parameters is shown in Figure 4.12. In this figure the fuel consumption results for T₂ and T₃ (D. 4) with CS₁ are also shown. The Observations (O.), which are made following from the parameter variation study, are discussed next.

- O. 1 A 5-kW electric machine size is sufficiently for the EMA push-belt CVT (T₁) in order to minimize the fuel consumption on the JP₁₀₋₁₅. The optimal size is independent on the topology choice (D. 5), the regenerative braking strategy (D. 7), and the CVT speed ratio control strategy (D. 8).

In Figure 4.13 the static-efficiency maps of a small and a large electric machine is schematically visualized. The styled OOLs for both electric machines are also depicted. If the electric machine is operated during the electric-only modes at the OOL, then for a larger electric machine the desired optimal speed is lower than for a smaller electric machine given the same output power. However, the electric machine output torque is higher, which increases the push-belt CVT efficiency.

- O. 2 The optimal electric machine size is a trade-off between the average electric machine and CVT efficiency, which decrease and increase respectively with increase of electric machine size.

The optimal electric machine size for the HDA push-belt CVT is approximately 10 kW. The optimal electric machine size is larger than for the EMA push-belt CVT due to the higher static losses of the HDA push-belt CVT. For the NEDC

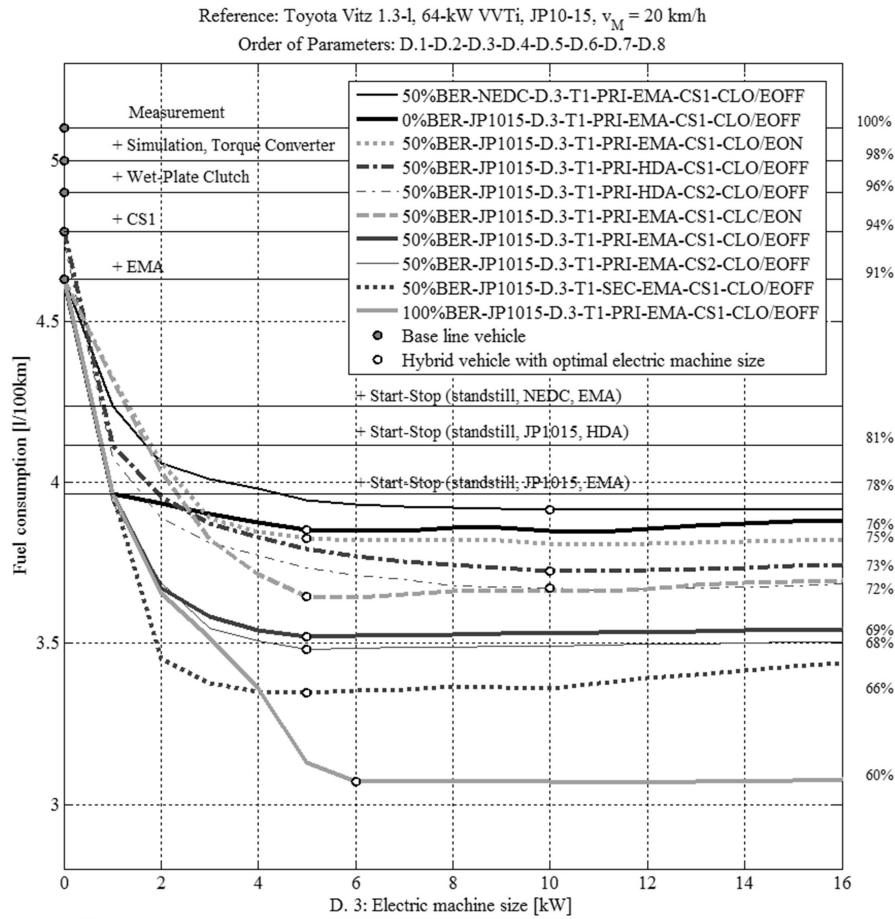


Figure 4.11 / Fuel consumption as a function of the electric machine size (D. 3) for different design parameters (D. 1, D. 2, and D.5 – D. 8).

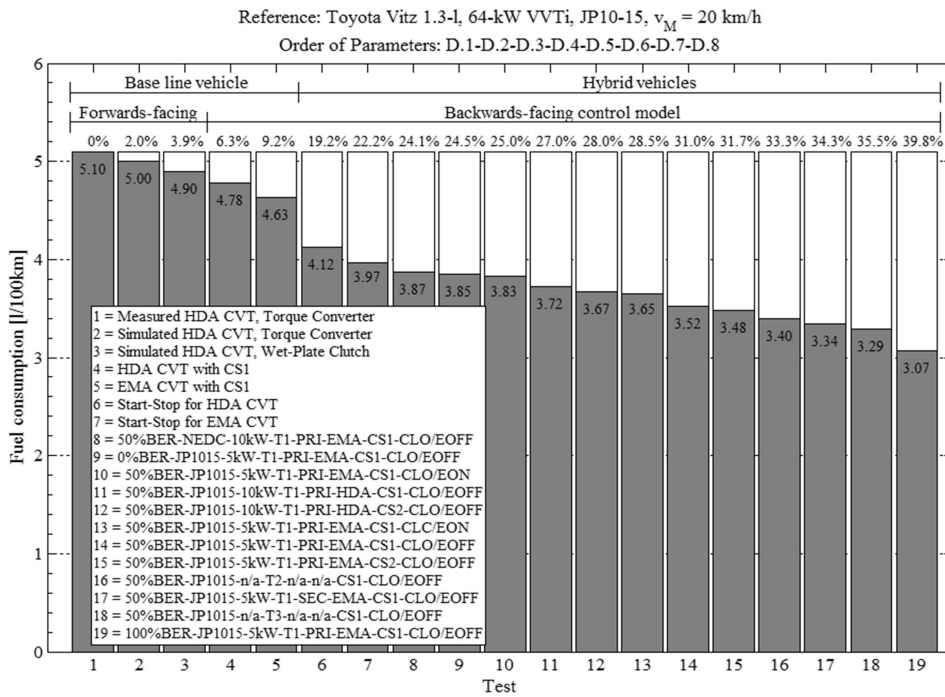


Figure 4.12 / Fuel consumption as a function of the technologies, control strategies, topologies, component sizes, and functions. n/a = not applicable.

the optimal electric machine size is also 10 kW due to the higher braking powers compared to the JP10-15. For the $f_{fb} = 100\%$ (100%BER) the optimal electric machine size is 6 kW due to increase of maximum braking power and regenerative brake energy on the JP10-15.

- O. 3 The start-stop function at vehicle standstill reduces the fuel consumption relatively by approximately 13.8% or 14.3%, which depends on the type of actuation technology (compare test 4 with 6 and test 5 with 7 of Figure 4.12).
- O. 4 The fuel saving increases with increase of the brake distribution fraction. It is observed, that if f_{br} is increased from 50% to 100% BER at the front wheels, that the fuel consumption is relatively decreased by 12.8% (compare test 14 with 19 of Figure 4.12).
- O. 5 The vehicle load prescribed by the NEDC increases the fuel consumption by 10% compared to the JP10-15 (compare test 8 with 14 of Figure 4.12).

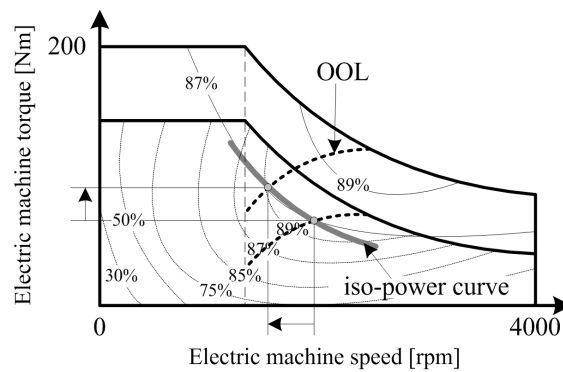


Figure 4.13 / Influence of the electric machine size on the efficiency.

- O. 6 Hybridization of the drive train with a 5-kW electric machine, which is connected at the engine-side of the EMA push-belt CVT with 50%BER, reduces the fuel consumption by approximately 3.5% or 11.3% depending on the regenerative brake strategy (excluding start-stop at vehicle standstill; compare test 7 with 10 and test 7 with 14 of Figure 4.12).
- O. 7 Changing the hybrid transmission technology reduces the fuel consumption by 3.4% for T₂ and 6.5% for T₃ (compare test 14 with 16 and test 14 with 18 of Figure 4.12).
- O. 8 Connecting the electric machine at the wheel-side of the push-belt CVT reduces the fuel consumption by 5.1% due to higher transmission efficiency during regenerative braking (compare test 14 with 17 of Figure 4.12).

However, due to the fixed gear ratio between electric machine and wheels, the electric machine operation points are prescribed by the drive cycle and the vehicle power demand. The operation points are therefore not optimally selected. In addition, the average electric machine efficiency decreases with increase of electric machine size, which causes a decrease in fuel saving again.

- O. 9 The EMA push-belt CVT compared to the HDA push-belt CVT reduces the fuel consumption by 3.1% and 5.4% for the base line and hybrid vehicle respectively (compare test 4 with 5 and test 11 with 14 of Figure 4.12).
- O. 10 Fuel cut-off (CLC/EON) during regenerative braking is more beneficial than idling of the engine (CLO/EON). The relative fuel consumption with CLC/EON compared to CLO/EON is 4.7% lower (compare test 10 with 13 of Figure 4.12).

O. 11 The influence of system optimal operation CS₂ compared to engine optimal operation CS₁ on the fuel saving for the hybrid vehicle is relatively small. The fuel consumption is reduced by 1.3% or 1.1%, which depends on the type of actuation technology (compare test 11 with 12 and test 14 with 15 of Figure 4.12).

In Figure 4.14 an overview is shown of the relative effects of the parameter variation on the fuel consumption change. Some of the bars, which are indicated with an (lower-)upper boundary value, represent the average values of the performed tests. The upper or lower boundary value represents the maximum or the minimum value respectively. Since the cross-correlation of parameters variation is not investigated, the relative effects that (de-)increase the fuel consumption can not be summed up. Nonetheless, it can be concluded, that the fuel saving potential is strongly affected by the following design parameters (D. 1 – D. 5): the regenerative brake fraction, the drive cycle (vehicle load), the component size (and start-stop), transmission technology, and the topology.

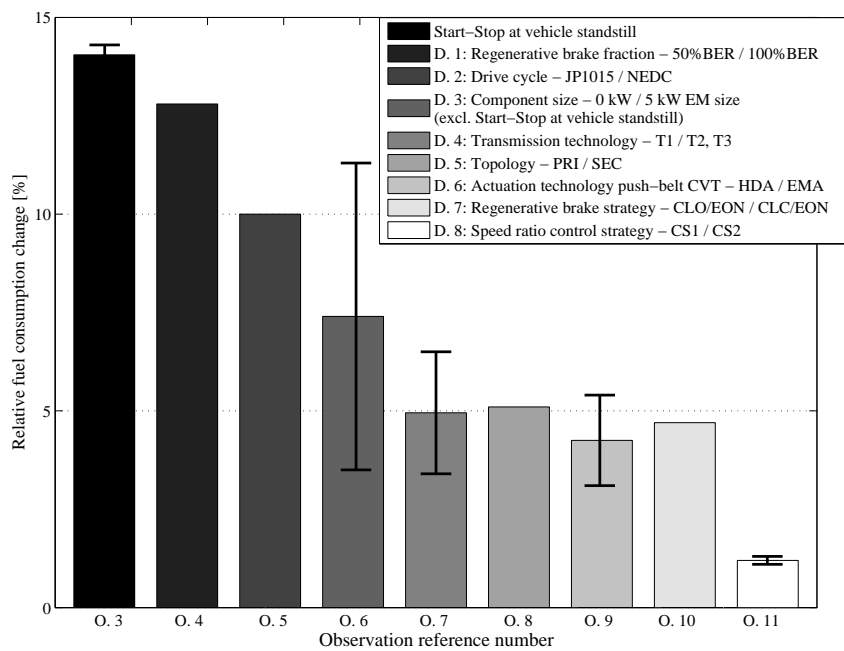


Figure 4.14 / Overview of the relative effects of parameter variation on the fuel consumption.

In Figure 4.15 the power-flow control strategies $P_s(t)$, including the battery energy level difference over time $\Delta E_s(t)$, are shown for comparison of the HDA-PRI push-belt CVT, EMA-PRI push-belt CVT, and the EMA-SEC push-belt CVT. The other design parameters, that are kept constant, are shown in the title of the figure. In the diagrams at the bottom of the figure, the strategies for the different regenerative brake fractions are shown. The transmission efficiencies during the electric-only modes are larger for the EMA-PRI CVT and the EMA-SEC CVT in comparison with the HDA push-belt CVT. This causes that effectively more brake energy can be used for electric driving. Furthermore, if the brake fraction f_{fb} increases, then the electric machine is more intensively used during the electric-only modes.

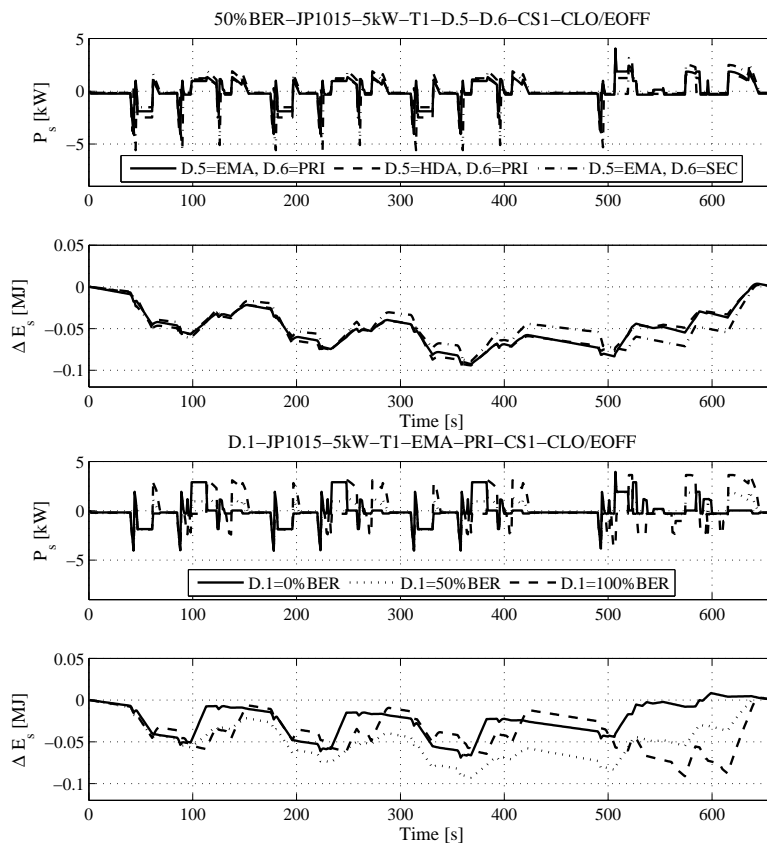


Figure 4.15 / Battery storage power and Battery energy level difference.

In this section the electric-only vehicle speed threshold value v_M was kept constant at 20 km/h for the different regenerative brake strategies. In the following section the effects of changing v_M on the fuel consumption for the different brake strategies are investigated.

4.6.2 Effects of the Electric-Only Vehicle Speed Threshold Value on the Design Objective for Different Brake Strategies (D. 7)

In the Figure 4.16 the contour plots of the fuel consumption for the CS1-EMA-50%BER-PRI-JP1015 as a function of the electric machine size (kW) and the electric-only vehicle speed threshold value v_M (km/h) for the CLO/EOFF, CLO/EON, and CLC/EOFF braking strategy are shown respectively. The following observations are made based on these results.

- O. 12 The CLO/EOFF strategy has by increasing of v_M larger than 20 km/h a negligible effect on the fuel consumption improvement. From the optimized control strategy it followed that propulsion-only by the electric machine during acceleration up to vehicle speeds higher than 20 km/h do not occur.
- O. 13 The CLC/EON strategy is preferable above CLO/EON strategy for electric-only vehicle speed threshold values lower than 40 km/h. The fuel savings by fuel cut-off and recuperation of brake energy are effectively larger, than the fuel costs of engine idling during braking although with the CLC/EON strategy the recuperative brake power is reduced.

4.6.3 Effects of Changing the Hybrid Transmission Technology (D. 4) on the Design Objective and Component Efficiencies

Table 4.7 shows the fuel consumption results for the base line vehicle and for the hybrid vehicle equipped with the different transmission technologies (T1-T3). For the base line vehicle the battery is not used, i.e., $P_s(t) = 0$. For the hybrid vehicle the fuel consumption results are similar to the results, which are shown in the Figure 4.12. The lowest fuel consumption is achieved with T1-EMA for the base line vehicle and with T3 for the hybrid vehicle. However, for the hybrid vehicle the relative differences between T1-EMA-SEC and T3, and, between T2 and T3 are very small, i.e., 1% and 2% respectively.

The higher fuel consumption of T2 compared to T3 for both the base line and the hybrid vehicle is caused by the lower average CVT efficiency of T2. For the base line vehicle this is explained with the Figure 4.17. In the figure, the CVT efficiency η_{CVT} as a function of the overall speed ratio r_t is shown for the base line vehicle equipped with T2 and T3 respectively. At low and high speed ratios the CVT efficiency of T3 is typically larger than the CVT efficiency of T2.

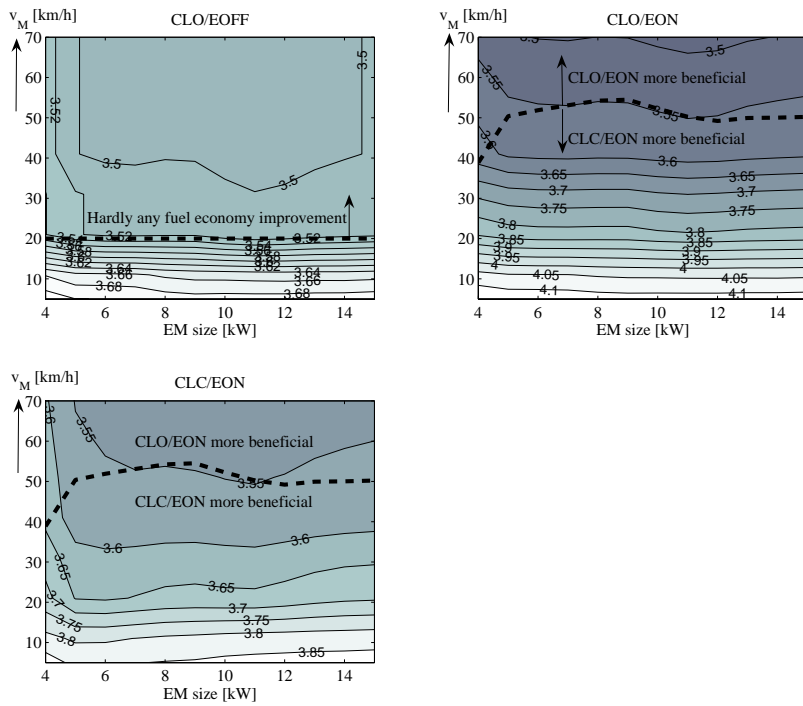


Figure 4.16 / Contour plots of the fuel consumption as a function of v_M and the electric machine size for different brake strategies.

Table 4.7 / Fuel consumption results with CSI, 50%BER, and $v_M = 20$ km/h.

CVT technology	Fuel consumption (l/100km) on the JP10-15	
	Base/Hybrid	Relative change %
T1 [†] -HDA-PRI	4.78/3.72	100%/79%
T1 [†] -EMA-PRI	4.63/3.52	97%/74%
T2	4.97/3.40	104%/71%
T1 [†] -EMA-SEC	4.63/3.34	97%/70%
T3	4.90/3.29	103%/69%

[†] 5 kW optimal electric machine size.

The figure shows that the difference between the CVT efficiency calculated with an average constant electrical variator efficiency (solid lines) and with a variable variator efficiency over a drive cycle is small. The average variator efficiency of T3 is lower than of T2 due to the larger electric machine EM_I of T3 compared to T2.

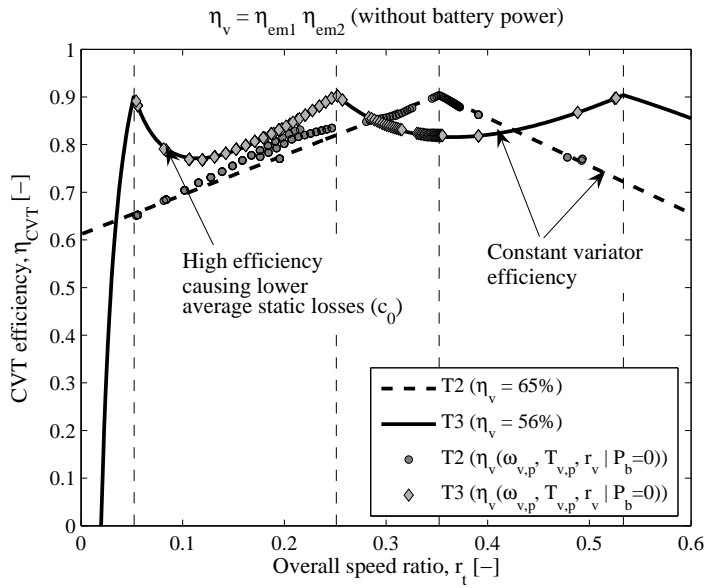


Figure 4.17 / Overall CVT efficiency η_{CVT} as a function of the overall speed ratio r_t for the base line vehicle equipped with T2 or T3 (without battery power $P_b = 0$) simulated on the JP10-15.

For the hybrid vehicle the average component efficiencies and the relative fuel savings as a function of the transmission technologies and topologies are shown in the Figure 4.18. The secondary power source efficiency, denoted as η_s , consists of the battery, the electric machine, and the transmission efficiency (e.g., the push-belt CVT, or the reduction set including the final drive set) from the battery to the wheels during the electric-only modes (regenerative braking, propulsion). The decrease in fuel consumption is in correspondence with the increase of the average component efficiencies. The fuel consumption is strongly correlated with the secondary power source η_s and the transmission efficiency η_t . Since the engine efficiency η_e remains approximately constant.

Due to the lower CVT efficiencies and the slightly higher secondary source efficiencies of T2 and T3 compared to T1-EMA-SEC the electric machines of T2 and T3 are more intensively used during the electric-only modes. This causes a larger battery energy depth of discharge as is shown in Figure 4.19.

4.7 Reduced Hybrid Drive Train Model

The computation steps as discussed in Section 4.5 are quite tedious to carry out. In this section, a reduced hybrid drive train model describing the main compo-

ment models and the topology is discussed, which can be used for design analysis decoupled from the choice of specific components, hybrid drive train configurations, and control strategy. The idea of a high-level modeling and design framework as presented in [30] is further investigated. First, the assumptions for simplified modeling of the components and topology are discussed.

- The component efficiencies are modeled as simplified parametric power-based fit functions, where, e.g., a linear relationship between input and output power is assumed: $P_{in} = c_1 \cdot \min(P_{max}, P_{out}) + c_0$.

The parameter P_{max} represents the output power limitation of the component. The parameters c_1 and c_0 represent the fit coefficients and correspond to the reciprocal of the internal efficiency and the static losses respectively. In Figure 4.20, for example, the input powers as a function of the calculated output powers on the JP10-15 for the base line vehicle equipped with different transmission technologies is shown. Clearly, there is an affine relationship between the input and output power for the transmissions, in contrary to the nonlinear relationship between the efficiency and the speed ratio (see, Figure 4.17). The engine (Primary power source = P) and the electric machine/battery (Secondary power source =

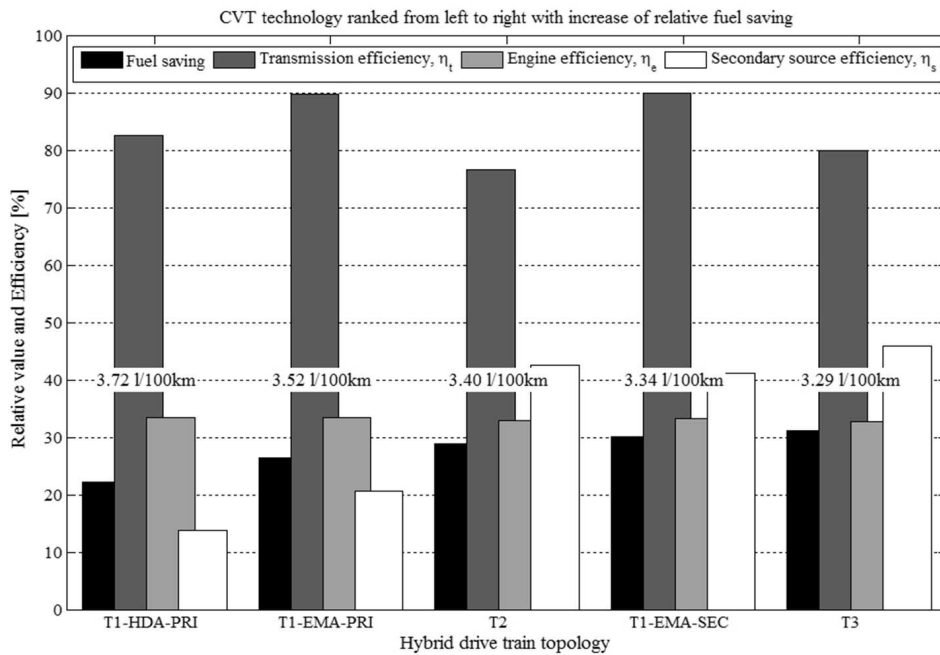


Figure 4.18 / Effects of the transmission technology and topology on the relative fuel saving, transmission, engine, and secondary source efficiency.

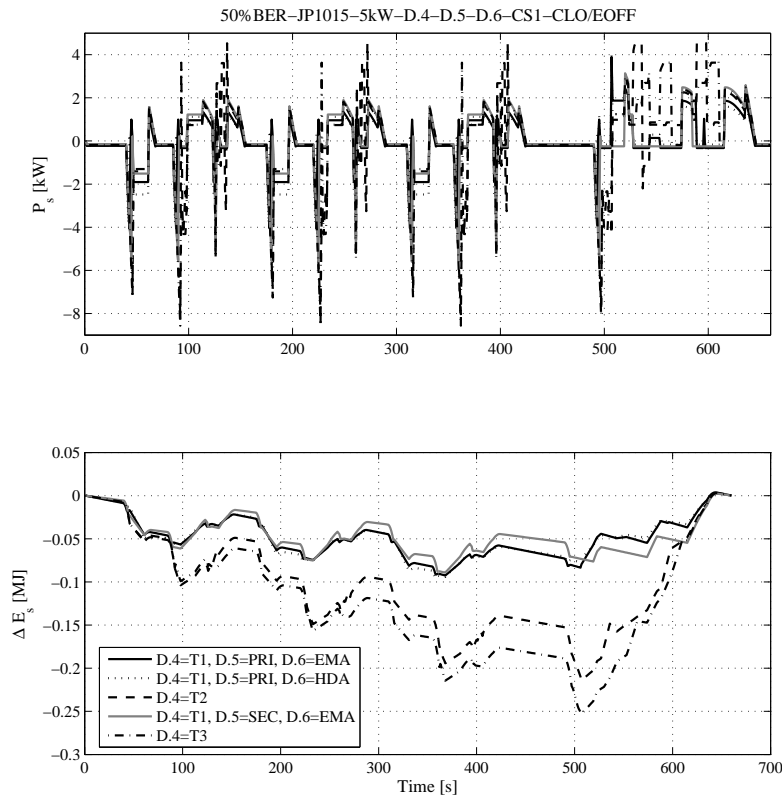


Figure 4.19 / Battery storage power and Battery energy level difference.

S) efficiency, similar to the CVT (Transmission technology = T) efficiency, are well described by an affine relationship.

The operation points determine the values for the fit coefficients (c_1 , c_0), which are also referred to as the characteristic component parameters. The operations points given a drive cycle and vehicle parameters are prescribed by assuming that,

- the engine is operated over a whole drive cycle at the maximum efficiency points (speed ratio control strategy CS1),
- the electric-only modes (regenerative braking, propulsion-only by secondary power source S) over a whole drive cycle are used for S, while S is operated at the OOL (i.e., only-if S is pre-coupled to T) and P is shut-off (CLO/EOFF), and

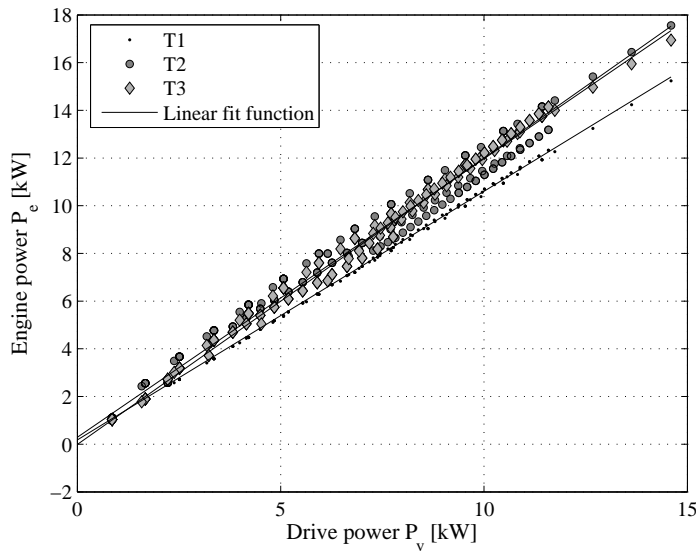


Figure 4.20 / Affine relationship between the input and output power for the different transmission technologies (base line vehicle, JP10-15, CS1).

- the engine-only mode over a whole drive cycle is used for transmission T, while the engine P is operated at the OOL and secondary power source S is shut-off (assuming no drag or idle losses).

These assumptions are sufficiently accurate for estimating the component efficiencies, since: (i) the influence of system optimal operation compared to engine optimal operation on the fuel consumption reduction for a hybrid vehicle is relatively small (1%-2%), and (ii) the influence of power exchange between S and P during driving (motor-assisting, charging) on the efficiency of S and T is relative small, as is discussed below.

The battery power influences the CVT efficiency. For the hybrid vehicle the CVT efficiency is decreased compared to the base line vehicle due to charging and motor-assisting during driving with S . If the transmission input power is corrected with the battery power during the hybrid driving modes (i.e., in this case for charging and motor-assisting during driving), then the CVT efficiency for the hybrid vehicle is slightly increased compared to the CVT efficiency for the base line vehicle. However, the difference is relatively small. This is observed by comparing the results for T as listed in Table 4.8. The lower value of c_0 (static losses) for T_3 compared to T_2 is due to the higher transmission efficiency at low powers (or at low speed ratios as is shown in Figure 4.17).

Table 4.8 / Transmission efficiency η_{CVT} (CSI, JP10-15)

CVT technology	Efficiency model parameters			
	Vehicle	c_1 [-]	c_0 [W]	$\bar{\eta}_{CVT}$ [%]
T1-EMA-PRI	Base	1.04	182	90.3
	Hybrid [†]	1.04	161	92.6
5-kW EM size	Hybrid	0.85	2040	79.4
T2	Base	1.17	291	80.2
	Hybrid [†]	1.14	341	83.0
	Hybrid	0.97	2110	76.5
T3	Base	1.20	-6	83.4
	Hybrid [†]	1.17	16	85.0
	Hybrid	1.18	543	79.9

[†] η_{CVT} corrected with battery power.

In Figure 4.21 the reduced hybrid drive train model for the different component technologies and the power-based fit function is schematically shown. For the power-split CVTs the electric machines coupled at the wheel-side of T, which perform the electric-only modes, are defined to be functionally part of S.

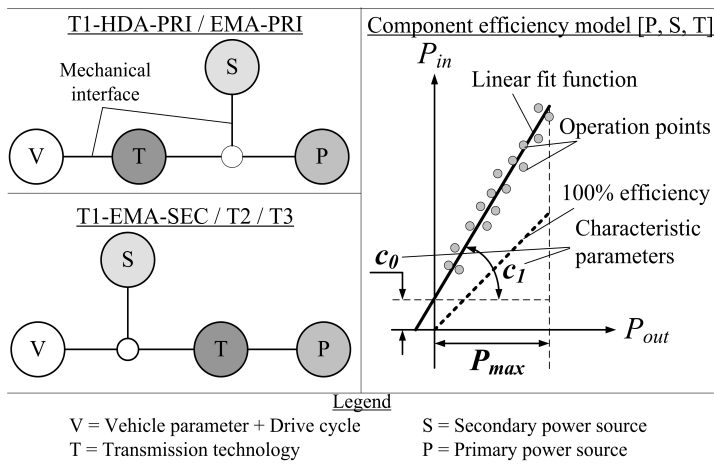


Figure 4.21 / Simplified hybrid drive train model: component technology (c_0 , c_1), size (P_{max}), and topology models (location of S and P).

The effects of parameter variation on the fuel economy and the optimal electric machine size (D. 3) using the reduced model are investigated next. This is performed in order to investigate if the assumptions, as posed in the beginning of this section, are sufficient accurate for design optimization. The varied design

parameters are: the regenerative brake fraction (D. 1), the drive cycle (D. 2), and the topology (D. 5). For different sizes of S (D. 3) the characteristic parameters (c_1, c_0) during the electric-only modes and for T during the engine-only mode are calculated for the EMA push-belt CVT.

The fuel consumption results for both cycles with the detailed hybrid drive train model, denoted as M1, and that of the reduced model, denoted as M2, are both shown in Figure 4.22.

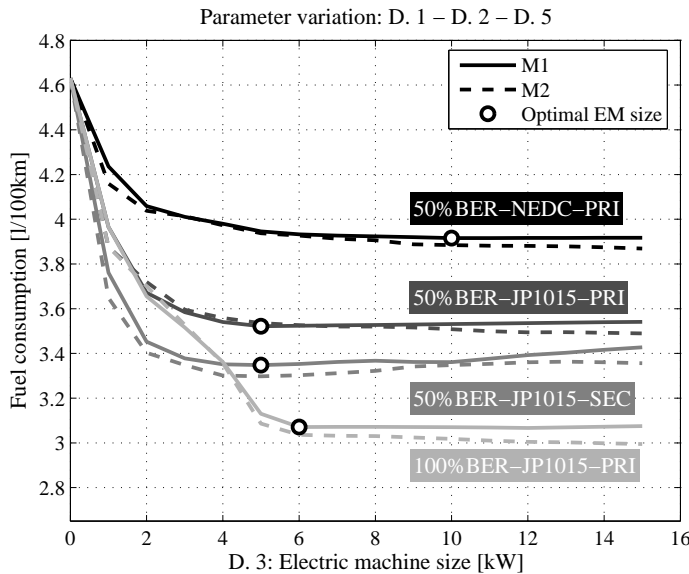


Figure 4.22 / The fuel consumption as a function of the electric machine size. The fuel consumption is calculated using a detailed hybrid drive train model M1 and a reduced hybrid drive train model M2.

The fuel consumption of the detailed model M1 is higher than calculated with the reduced hybrid drive train model M2. The differences tend to increase with increase of the electric machine size. The average relative errors, the maximum, and the minimum error values are shown in the Figure 4.23.

For the detailed model M1 the engine is assumed to be operated at the OOL and determines therefore the operation points of the electric machine during the hybrid driving modes (i.e., charging and motor-assisting during driving). This causes that the efficiency of S decreases with increase of the electric machine size. This relatively small effect is not been taken into account using the reduced hybrid drive train model M2, which causes that the objective function is sometimes not convex. Rather, a boundary optimum is determined at 15 kW. However, in this case an additional design constraint, that is put on the sensitivity of the

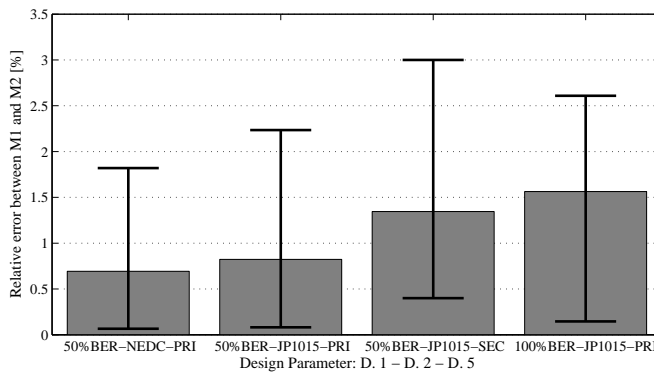


Figure 4.23 / The average relative error, the maximum -, and the minimum error values between the detailed model M1 and the reduced model M2 for the different design parameters.

objective function to the electric machine size, can be used in order to find the optimal electric machine size.

A different transmission technology (D. 4) or actuation technology (D. 6) simply implies a different set of characteristic parameters for T. The same holds for power-split CVTs. For example, if the electric machine size at the wheel-side of T is sufficiently large to maintain the transmission ratio coverage, yet it is too small in order to fulfill the required functions of S, then the electric machine size at the wheel-side of T needs to be increased. For the power-split CVTs changing the size of S affects indirectly the transmission efficiency. In this way, the characteristic parameters for T, which are determined by the engine-only mode, become also a function of the size of S. However, looking at the development of the transmission by Toyota, the increased size of S is mainly determined by performance and not by fuel consumption reduction or ratio coverage constraints.

Nevertheless, it can be concluded, that the effects of component sizing on the fuel consumption can be investigated using the reduced hybrid drive train model with the assumptions posed in the beginning of this section very quickly and with sufficient accuracy (maximum average error <1.6%).

4.8 Conclusion

The optimal electric machine size for a hybrid vehicle equipped with a CVT regarding the minimum fuel consumption was determined. Thereby, the effects of parameter variation, e.g., for the CVT technology and the topology on the fuel consumption was investigated. Other parameters that strongly influences the op-

timal electric machine size are related to the vehicle load (vehicle parameters and drive cycle) and the regenerative brake fraction. Finally, a reduced hybrid drive train model is introduced with which the influence of component technologies, sizes, and topology choice on the fuel consumption can be studied very quickly and with sufficient accuracy (maximum average error <1.6%).

Design of Hybrid Medium-Duty Trucks

Abstract / This chapter presents a modeling and simulation approach for determining the optimal degree-of-hybridization for the drive train (engine, electric machine size) and the energy storage system (battery, ultra capacitor) for a medium-duty truck. The influence of the gross-vehicle weight on optimal component sizing has been investigated. The results show that the degree-of-hybridization of known medium-duty hybrid electric trucks is close to the optimal degree-of-hybridization using the methods as described in this chapter. Furthermore, it is found, that the Li-ion battery (single storage) is from a energy and power density as well as cost point of view the most preferable energy storage system. However, if the cost of ultra capacitor cells is significantly decreased ($>50\%$), then hybridization of a Li-ion battery with an ultra capacitor module in combination with a boost converter may become an attractive technology package in the future.

5.1 Introduction

Medium-duty trucks are used in different transport activities ranged from urban and regional distribution to light-weight transport over long distances and special applications, such as those used at the municipal cleaning department and the fire department. The diesel engine efficiencies used in these types of vehicles are already relatively high compared to petrol engines. Moreover, the potential of weight and air drag reduction is constrained by the payload carrying requirements. Nevertheless, advanced hybrid propulsion systems are very promising to achieve the future fuel consumption and emission goals for trucks in this segment [89]. In Table 5.1 an overview of the component specifications of three different realized medium-duty hybrid electric trucks (parallel hybrid configuration) is shown. The Hybridization Factor, denoted as HF_{dt} , describing the degree-of-





This chapter has been accepted for publication in the form of a paper as / [32] Hofman, T., Van Druten, R., Serrarens, A., and M. Steinbuch, "Hybrid component specification optimization for a medium-duty hybrid electric truck", *Int. J. of Heavy Vehicle Systems*, (accepted), 2008.

hybridization of the different hybrid drive trains as shown in the table, is defined as [46],

$$\text{HF}_{\text{dt}} = \frac{P_{em,max}}{P_{em,max} + P_{e,max}} \cdot 100\%, \quad (5.1)$$

with $P_{em,max}$ and $P_{e,max}$ representing the maximum (continuous) electric machine power and engine power respectively. The vehicle mass, denoted as m_v , of the FedEx and the Nissan Condorr truck is approximately two times the mass of the Hino 4T Ranger truck, which probably resulted in an approximately two times larger hybridization factor for the FedEx and the Nissan Condorr compared to the Hino 4T Ranger. Furthermore, the hybrid trucks are equipped with three different electrical storage systems with different energy and power characteristics (Li-ion, Ni-MH, and Ultra Capacitor (UC)). The relationship between the vehicle mass and the degree-of-hybridization is investigated in this chapter. The influence of the storage technology on the fuel consumption is also addressed.

Table 5.1 / Reference medium-duty hybrid electric trucks.

		<i>Vehicle type</i>			
					
<i>Component</i>	<i>Unit</i>	FedEx W700	Nissan Condorr	Hino 4T Ranger	<i>This chapter</i>
Engine	kW/Nm	125/569	152/500	132/461	125/729-205/1192 [†]
Displacement	cil./l	4/4.3	6/6.93	4/4.73	6/5.2-8/8.5 [†]
Motor	kW/Nm	44/420	55/130	23/*	20/138-80/552 [†]
Transmission	spd/type	6/AMT	6/AMT	*	6/AMT
Storage	V/Ah	340/7.2	346/60-kW	274/6.5	130-600/6
Type	-	Li-ion	UC	Ni-MH	{Li-ion, UC Ni-MH}
Mass m_v	kg	7257	7756	3629	4000-12000
Cycle	-	FTP-75 [‡]	*	JP16 mode	FTP-75 [‡]
HF _{dt}	-	26%	27%	15%	10%-40%
Fuel economy	km/l	+45%	+50%	+20%	Section 5.6

* = no data available, AMT = Automated Manual Transmission, ‡ = modified cycle, † = assuming linear scaling engine displacement or maximum torque with peak power.

5.1.1 Problem Description

The control design of medium-duty hybrid electric or hydraulic trucks is extensively discussed in literature (see, [43], [5], [89]). However, not much work is found specifically related to the overall design of a medium-duty hybrid electric truck regarding fuel consumption and performance. The work presented in [20]

discusses the combined optimization of component design and power management of a hydraulic hybrid drive train for a 6x6 medium truck and comes close to the work presented in this chapter. One of the main differences is that in [20] Dynamic Programming (DP) is used for optimization of the pre-defined rule-based Energy Management Strategy (EMS). The EMS optimization presented in this chapter is performed using a novel Rule-based EMS [31] consisting of the combination of Rule-Based and Equivalent Consumption Minimization Strategies [54], [71] (RB-ECMS), the latter has not been shown in [20]. Moreover, employing RB-ECMS accelerates the control design process and therefore the overall design process significantly.

Therefore, in this chapter we would like to focus on determining the optimal degree-of-hybridization and suitability of electrical storage technology (Li-ion, Ni-MH, and UC) minimizing the fuel consumption for a medium-duty hybrid electric truck as a design case study. As an example of application study estimated vehicle parameters and a given drive cycle (modified FTP-75, see, [45]) for the FedEx truck are used. The iterative optimization design process is depicted in Figure 5.1.

For different component sizes (design parameter) for the engine and the electric machine, which are determined by the hybridization factor HF_{dt} , the fuel consumption on a drive cycle is determined. Initially, Li-ion is chosen as the energy storage system and is sized to meet the output power specifications of the electric machine. The influence of changing the vehicle mass m_v (vehicle parameter) on the fuel consumption is also investigated. Typically, m_v changes over time during picking up and delivering of goods. Since m_v plays an important role on the fuel consumption and driveability, the influence of different constant values for m_v over a whole drive cycle is investigated. The optimal degree-of-hybridization, described by the hybridization factor HF_{dt} , is defined where the fuel saving in comparison with the Base Line (BL) vehicle over a drive cycle is maximum. The other design parameters, i.e., topology choice, technology choice for the engine, electric machine, and the transmission technology, are kept constant. The efficiency of the components is varied by sizing of the components.

The vehicle performance (i.e., the acceleration time from 0-100 km/h and the maximum gradeability at 89 km/h) and the fuel consumption over a drive cycle are determined at the optimal hybridization factor HF_{dt} (see, Figure 5.1 bottom part) for different single energy storage systems. Maximum gradeability is defined as the maximum angle of slope on which a vehicle is able to drive continuously at the maximum combined output power (engine, electric machine). After determining the optimal degree-of-hybridization, the influence of hybridization of the energy storage system on the overall energy storage system mass (kg) and cost (\$) is investigated for a Li-ion and a Ni-MH battery in combination with an

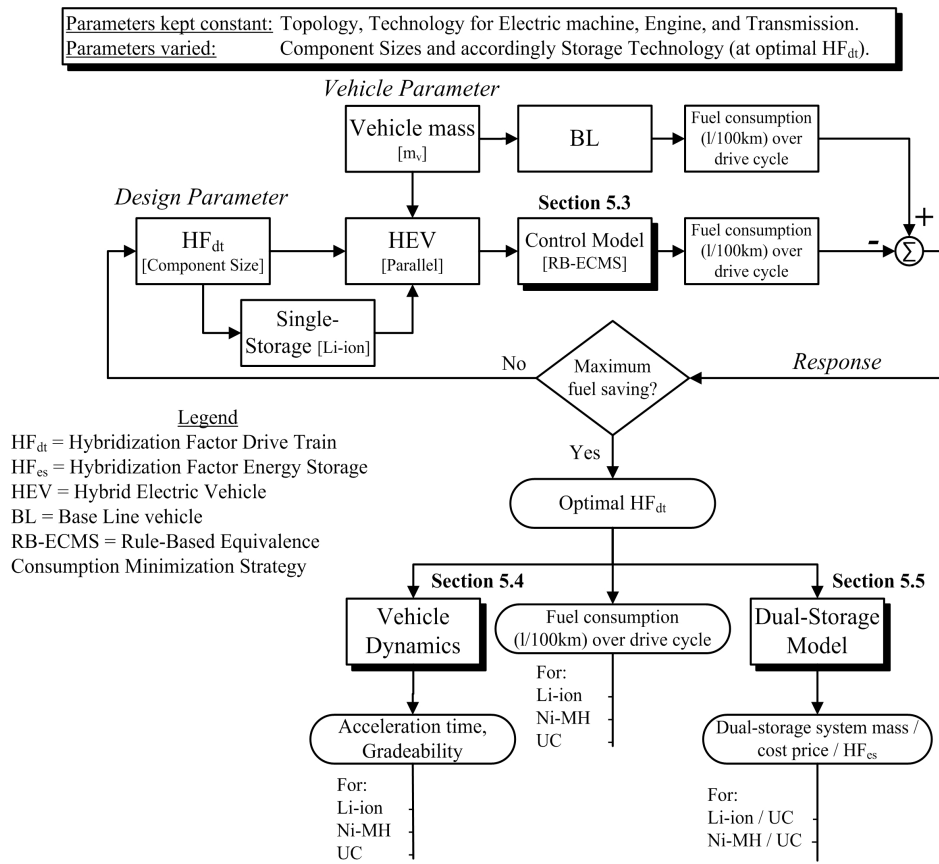


Figure 5.1 / Design optimization process.

ultra capacitor UC pack. In this chapter an additional hybridization factor for the energy storage system, denoted as HF_{es}, is defined:

$$HF_{es} = \frac{P_{b,max}}{P_{b,max} + P_{uc,max}} \cdot 100\%, \quad (5.2)$$

with $P_{b,max}$ and $P_{uc,max}$ representing the maximum battery power and ultra capacitor power respectively. The size of a battery pack is usually constrained by power and not by energy limitations, and vice-versa for the size of an ultra capacitor pack. The advantage of using a dual-storage system is the reduction of the power demands to the battery and therefore the aging of batteries, which should increase the lifetime significantly compared to the single-storage system [6]. Moreover, the cost would decrease and efficiency of the energy source would increase.

5.1.2 Contribution and Outline of the Chapter

The design of topologies, sizing of components, component technology selection, and the design of the control strategy form a considerable challenge for engineers due to the complexity of hybrid vehicle drive trains [12], [4], [23]. In order to alleviate the complex design problem at hand, in this chapter:

- simplified power-based fit functions describing the efficiency for each drive train component are discussed, and
- a novel EMS algorithm [31] based on the combination of Rule-Based and Equivalent Consumption Minimization Strategies (RB-ECMS) is used with which the fuel consumption is calculated very quickly (approximately 50-100 times faster than DP) and with sufficient accuracy (relative error $\pm 1\%$).

The efficiencies of the energy conversion components (engine, electric machine) are modeled as power-based fit functions, which can be described by a few fit coefficients. The fit coefficients are also referred to as the characteristic component parameters. The energy storage components for the different battery technologies (Li-ion, Ni-MH) and an ultra capacitor UC are also modeled using simplified power-based fit functions.

For the remainder of this chapter the outline is as follows. In Section 5.2, the component models and the modeling assumptions are discussed. The parametric efficiency modeling of the energy conversion, storage models, and the influence of component sizing on the characteristic parameters are also discussed. The ‘control model’ used for determining the EMS and the fuel consumption, the ‘vehicle dynamics model’ employed for calculation of the vehicle performances, and the ‘dual-storage system design model’ are discussed in the Sections 5.3, 5.4, and 5.5 respectively (see, also Figure 5.1). In Section 5.6, the simulation results are given regarding the optimal degree-of-hybridization, the influence of the storage technology on the fuel consumption and the vehicle performances, sizing results of the dual-storage systems, and the cost price of sized dual-storage systems. Finally, the conclusions are described in Section 5.7.

5.2 Modeling of the Drive Train Components

In this section, the used component models for the engine, electric machine, transmission, and energy storage systems (battery, ultra capacitor) are discussed. Since actual component data of the FedEx truck is not available, selected component data for the engine, the electric machine, and the battery from ADVISOR [57] are used with specifications close to the actual components of the FedEx hybrid truck.

5.2.1 Power-Flow Description

In Figure 5.2 the power-flow in the parallel hybrid drive train is shown. The drive train is a backwards facing or differentiating model. The vehicle speed, which is used as input, is tracked exactly. This model has been used to compute the optimal control signals that minimize the fuel consumption. The inputs are the battery input power P_s , the velocity v_v described by the given drive cycle, and the vehicle drive power demand P_v . The outputs are the engine speed ω_e and torque T_e , which are used to compute the fuel mass-flow \dot{m}_f (g/s) or the fuel power P_f . Note that the fuel power P_f equals the product of the fuel mass-flow \dot{m}_f (g/s) and the lower heating value for fuel h_{lv} (J/g).

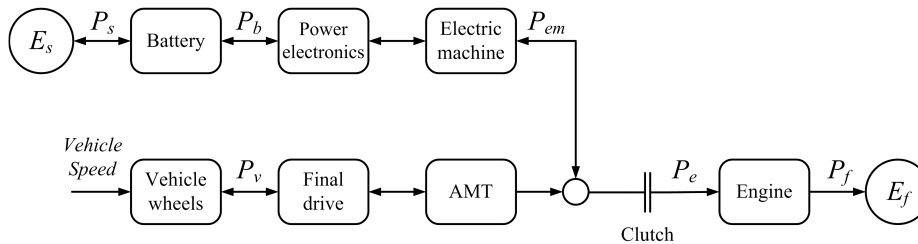


Figure 5.2 / Power-flow in the hybrid drive train (backwards facing control model).

5.2.2 Assumptions concerning Modeling and Sizing of the Components

The component characteristics (mass, maximum torque curve and static efficiency map) of the base engine and electric machine are linearly scaled as needed. The absolute mechanical (in-)output power during motoring and generating is assumed to be equal, whereas the electrical (in-)output power due to losses are differently. Furthermore, the maximum electric machine speed is assumed to be 2100 rpm, which is equal to the maximum engine speed. The base component characteristics, which are used for scaling, and the transmission technology are shown in Table 5.2. The main characteristics of the storage components (Li-ion, Ni-MH, and UC) are shown in Table 5.3. The other vehicle simulation input parameters, which determine the drive power demand P_v , are listed in Table 5.4.

Auxiliary loads (e.g., air condition, cooling systems, heating of seats) can be in the order of 6-10 kW [36] and play therefore an important role in the overall fuel consumption. However, only the minimum necessary engine auxiliary loads (dynamo, waterpump, power steering, airpump for the brakes) are taken into account by assuming an average constant auxiliary load torque of 10 Nm as a function of engine speed at the engine crank shaft. This results in an average auxiliary power of 505 W for the Base Line (BL) truck.

Furthermore, in this chapter, the required battery energy for engine cranking of the Hybrid Electric Vehicle (HEV) is neglected, since the engine can be started with the electric machine in a very short time period (typically < 500 ms). The required electrical energy for engine cranking (usually the engine is started when the vehicle is already driving) is therefore limited and very small. However, the power needed for engine cranking is relatively high.

Table 5.2 / Base engine, electric machine, and transmission characteristics.

Base Engine	Detroit diesel series 50, 8-cylinder, 205-kW peak power (at 2100 rpm), 8.5-l CI, 1192-Nm peak torque (at 1200 rpm), 44% peak efficiency, mass 860 kg (FC_CI205*)
Base Electric Machine/Controller	PM brushless AC motor, 58-kW peak power (at 1250 rpm), 400-Nm peak torque, 92% peak efficiency, mass 70 kg (MC_PM58*)
Base Transmission	Eaton, type FSO-8406A, 6 speed, Automated Manual, maximum transmission input torque 1166 Nm, mass 359 kg

*model data file from ADVISOR

Table 5.3 / Different energy (electrical) storage characteristics.

Manufacturer	Panasonic	Saft	Maxwell
Storage type	Ni-MH	Li-ion	UC
Nominal voltage (V/cell)	1.2	3.6	2.7
Current capacity (Ah)	6	6	-
Storage mass (kg/cell)	0.166	0.375	0.460
No. cells/module	6	6	1
Model data file (ADVISOR)	ESS_NIMH6	ESSLI7_temp	-

Assumptions concerning Regenerative Braking

Using the vehicle parameters as listed in Table 5.4 and the modified FTP-75 drive cycle (used for FedEx truck), the vehicle drive power demand as a function of time, denoted as $P_v(t)$, can be calculated. The amount of recoverable brake energy plays an important role in the achievable fuel saving potential [29]. The braking energy ratio to the total traction energy is defined as:

$$\beta_{br} = 100\% \cdot \frac{\int_0^{t_f} -P_v(t \mid P_v(t) < 0) dt}{\int_0^{t_f} P_v(t \mid P_v(t) > 0) dt}. \quad (5.3)$$

The fraction β_{br} reaches 48% for the modified FTP-75 cycle with time length t_f and the vehicle parameters as listed in Table 5.4. However, due to transmission losses (final drive, Automated Manual Transmission (AMT)) this ratio β_{br} is reduced to 38.4%. Evidently, the brake force distribution between the front and the

Table 5.4 / Vehicle model parameters.

Quantity	Symbol	Value	Unit
Total mass	m_v	7258(16000)	kg(lbs)
Frontal area	A_f	6.9	m ²
Air drag coefficient	c_d	0.73	-
Rolling resistance	c_r	0.8%	-
Air density	ρ	1.2	kg/m ³
Gravity	g	9.81	m/s ²
Wheel radius	r_w	0.3970	m
Traction coefficient rear-wheels	μ_r	0.9	-
Final drive ratio	r_d	0.30	-
Speed ratio set	\mathcal{R}	{0.14; 0.24; 0.40; 0.63; 1.00; 1.28}	-
Regenerative brake fraction	f_{rb}	0.4	-
Transmission efficiency	η_{AMT}	0.96	-
Final drive efficiency	η_{fd}^+, η_{fd}^-	0.90 (generating), 0.96 (propulsion)	-
Height center of mass	H	1.3	m
Distance between the rear wheel and the center of mass	L_r	2.5	m
Length of wheel base	L	4.8	m
Inertia of rotating parts	J_w	20	kg m ²

rear wheels plays a key role in the amount of recuperated brake energy. A significant part of the brake energy is dissipated in the front brakes, since we assume that only the rear brakes are used for brake energy recuperation. The brake force distribution ratio $f_{fb}(t)$ changes over time and is dependent on the amount of deceleration with $a_v(t) = -\min(0, a_v(t))$ [18]:

$$f_{fb}(t) = \frac{L_r}{L} + \frac{a_v(t) H}{g L}, \quad (5.4)$$

with the (vehicle) parameters L_r , L , H and g representing the distance between the rear wheels and the center of mass, the length of the wheel base, the height of the center of mass and the gravity constant respectively. This ratio varies for a 7.3 tons truck between 53%-60% assuming that the adhesive capability between the road and the tires could be fully utilized (ideally braking). The regenerative brake fraction defined as the ratio between brake force between the rear wheel and the front wheels becomes with help of Equation (5.4):

$$f_{rb}(t) = 1 - f_{fb}(t). \quad (5.5)$$

Note that the values for L_r and H as listed in Table 5.4 are estimated values, since these values are usually not given by the manufacturer and are difficult to obtain.

Figure 5.3 shows the vehicle speed $v_v(t)$, the power demand $P_v(t)$ and regenerative brake fraction $f_{rb}(t)$ for a 7.3 tons truck. In this chapter, without loss of

generality a constant regenerative brake fraction $f_{rb} = \min(f_{rb}(t)) = 40\%$ is assumed, since the actual brake strategy is not known. In addition, for safety reasons mechanical or hydraulic back-up braking systems are still required and fully ‘brake-by-wire’ systems are yet not applicable. This causes that β_{br} is significantly reduced from 38.4% to 15.4%. The remaining part of 60% of the total brake power is dissipated in the front wheel brake discs. The brake power in the rear wheels is regenerated up to the maximum generative power limitation of the battery/electric machine, larger brake powers are assumed to be dissipated in the rear wheel brake discs.

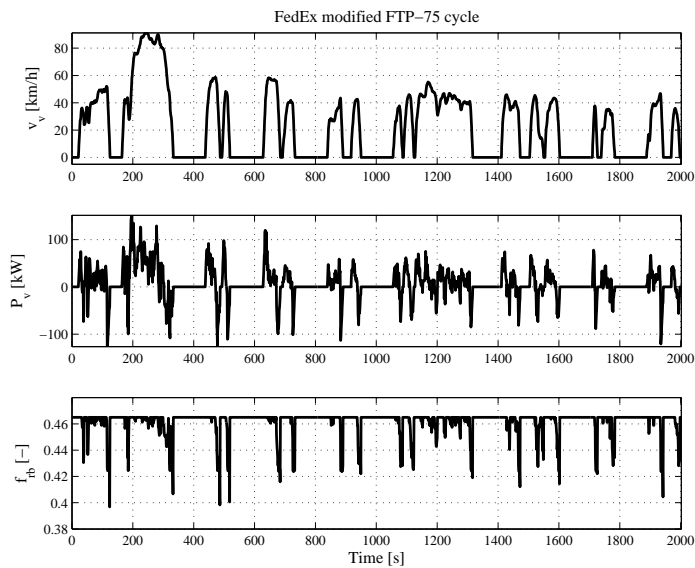


Figure 5.3 / Drive cycle, vehicle drive power demand, and regenerative brake fraction.

The power-based component efficiency model, the control model, the vehicle dynamics model, and the dual-storage design model, which are used to calculate the fuel consumption, the acceleration time from 0-100 km/h (0-62 mph), the gradeability at 89 km/h (55 mph), and the dual-storage system mass, are discussed next.

5.2.3 Power-Based Component Efficiency Models

In this chapter the energy conversion and storage devices are modeled as power-based efficiency functions [15],

$$P_{in} = P_{out} + P_{loss}(\cdot) = \phi(\cdot) \approx \sum_{j=0}^{j=n} c_j(\cdot) P_{out}^j, \quad c_j \in \mathbb{R}, \quad j \in \mathbb{N}, \quad (5.6)$$

with $\phi(\cdot)$ defined as the inverse efficiency $\eta^{-1}(\cdot)$ times the output power P_{out} , which are approximated by polynomial fit functions. For the engine and the electric machine, the losses $P_{loss}(\cdot)$ are a function of the output power P_{out} and the angular speed ω . In case of a battery, the losses are a function of the state-of-charge ξ , the battery storage power P_s , and the temperature T [39]. In this section, the derivation of the characteristic parameters $c_j(\cdot)$ describing the component efficiency for the engine, the electric machine, the battery technologies, and the ultra capacitor is discussed.

Engine and Electric Machine Efficiency

For the engine and the electric machine, the static power losses $P_{loss}(\cdot)$ at zero output torque are dependent on the angular speed ω_i . At zero output torque no measurement data is available. Since the static losses of an engine play an important role in calculating the fuel consumption improvement, the static losses are estimated by linear extrapolating the fuel mass-flow curves to zero output torque for the different given angular speeds.

In this chapter, the characteristic parameters c_j for the engine and the electric machine are determined by assuming that these components are operated at their maximum efficiency points determined by the optimal speed ω_i^o and torque T_i^o combinations. The Optimal Operation Line (OOL) connects the set Ω of optimal operation points,

$$\Omega = \left\{ (\omega_i^o, T_i^o) \mid P_i = T_i \omega_i \wedge \omega_{i,min} \leq \omega_i \leq \omega_{i,max} \wedge \right. \\ \left. T_{i,min}(\omega_i) \leq T_i \leq T_{i,max}(\omega_i) \right\}, \quad (5.7)$$

fulfilling the condition of minimum input power,

$$(\omega_i^o, T_i^o) = \arg \min_{(\omega_i, T_i) \in \Omega} \phi_i(\omega_i, P_i), \quad \text{with } i \in \{e, em\}. \quad (5.8)$$

It should be noticed, that not all desired optimal operation points can be reached during the engine-only and the electric-only driving modes (propulsion at low speeds and regenerative braking by the electric machine/battery) due to limited set \mathcal{R} of discrete speed ratios of the AMT (see, Table 5.4).

For example, if only the engine mode is utilized over a whole drive cycle where optimal gear ratios (close to maximum engine efficiency points, or in other words, close to the OOL) are selected, then the total fuel use is increased by approximately 4% compared to the situation where the engine is operated at the OOL (for a 205-kW engine and the vehicle parameters of Table 5.4). In order to explain the relatively small fuel consumption increase is referred to Figure 5.4. In this figure, the normalized component input power with the maximum component power for the electric machine (58 kW) and engine (205 kW) as a function of the normalized output power with the total available output power (electric machine + engine) for different electric machine and engine angular speeds are shown. The figure also depicts respectively: the required normalized engine input powers as a function of the normalized output powers for the AMT (circular marks), a quadratic function fitted through the normalized input powers as a function of the normalized output powers for the AMT (dashed line), and the required normalized input power as a function of the normalized output power for the engine operated at the Optimal Operation Line (OOL) (solid line). If a quadratic function is fitted through the operation points, then it is observed that the difference between the OOL and the fit function is relative small. This explains the relatively small influence of the AMT on the fuel consumption. The influence of the AMT on the average electric machine efficiency during the electric-only modes is smaller for the electric machine due to its higher efficiency compared to the engine.

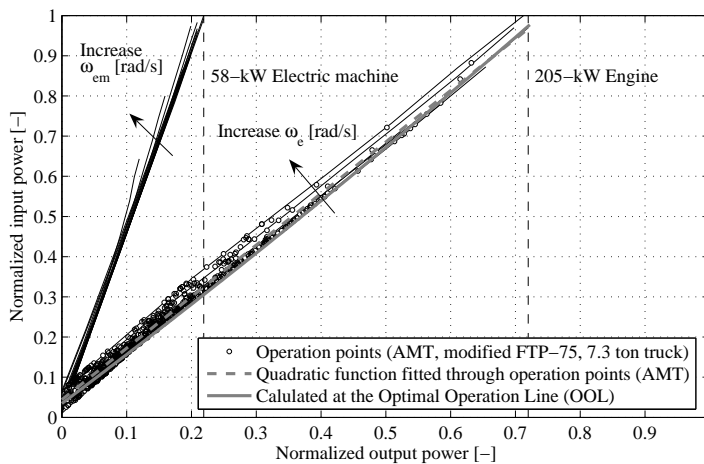


Figure 5.4 / Influence of the operation points on the input power for the electric machine and the engine.

Furthermore, coupling of the electric machine and the engine to the same

transmission input shaft requires selecting the optimal speed ratio, which maximizes the combined engine and electric machine/battery efficiency during a hybrid driving mode (charging or motor-assisting during driving). The effect of this on the total fuel consumption and the characteristic parameters c_j is left out of consideration in this chapter. The reader is referred to [42], which discusses more static optimization regarding the design of the shift logic for a hybrid vehicle, where shift quality and driving comfort aspects are also taken into account. The clutch losses and engine auxiliaries are taken into account. However, these powers are assumed to be supplied by the engine operated at the OOL.

If the input power values as a function of the output power values at the OOL for the engine and the electric machine are plotted, then the fuel power P_f (engine input power) during the engine-only mode is well approximated by a quadratic function with the engine power P_e at the crank shaft,

$$P_f = \phi_e(\omega_e^o, P_e) \approx c_0 + c_1 P_e + c_2 P_e^2, \text{ and } \{c_2, c_1, c_0\} \subseteq \mathbb{R}_0^+. \quad (5.9)$$

Furthermore, the battery output power P_b (electric machine input power) during the electric-only modes (regenerative braking, electric driving) is well approximated by a linear function for discharging (supscript: -) and charging (supscript: +) with the electric machine power P_{em} ,

$$P_b = \phi_{em}(\omega_{em}^o, P_{em}) \approx \max\left(c_0^- \frac{P_{em}}{|P_{em}|}, c_0^+ \frac{P_{em}}{|P_{em}|}\right) + \max(c_1^- P_{em}, c_1^+ P_{em}), \quad (5.10)$$

with the parameters $-1 < c_1^+ < 0$, $c_1^- > -1$, and $\{c_0^+, c_0^-\} \subseteq \mathbb{R}_0^-$.

Battery Efficiency

The battery losses P_{loss} are dependent on the state-of-charge $\xi(t)$, the storage power $P_s(t)$, and the temperature $T(t)$ [39],

$$P_b(t) = P_s(t) + P_{loss}(\xi(t), P_s(t), T(t)). \quad (5.11)$$

The charging (coulomb) losses due to irreversible parasitic reactions in the battery are taken into account by using an estimate of the average coulomb efficiency η_c (see, the data files ESS_NIMH6 and ESSLI7_temp of ADVISOR). Self-discharge, or parasitic current is not separately considered, yet these losses are assumed to be modeled by η_c . The state-of-charge of the battery, denoted as ξ , which is defined as the ratio between the electric charge $Q(t)$ and the maximum charge capacity Q_0 , is calculated as follows [72],

$$\xi(t) = \frac{Q(t)}{Q_0} \cdot 100\%, \text{ with } Q(t) = \eta_c \int_0^t I(\tau) d\tau. \quad (5.12)$$

The (dis-)charge currents $I(t)$ are assumed to be low enough, due to the relatively high battery pack voltage, so that the charge capacity Q_0 change (Peukert effects) is negligible small. Furthermore, the Li-ion and Ni-MH battery pack are both assumed to be operated within a state-of-charge window of $\xi_{min} = 40\% \leq \xi(t) \leq \xi_{max} = 80\%$. The open circuit voltage within this defined window of operation changes a little from 1.27 V/cell to 1.30 V/cell and 3.52 V/cell to 3.75 V/cell for the Ni-MH and the Li-ion battery respectively. Therefore, for simplicity, the state-of-charge and the state-of-energy of the battery are assumed to be approximately similar and only $\xi_{max} - \xi_{min} = 40\%$ of the energy storage capacity E_{cap} is effectively *available*:

$$\Delta E_{s,a} = 0.40 \cdot E_{cap} \approx 0.40 \cdot Q_0 \cdot U_{b,nom} \cdot n_b \cdot n_p, \quad (5.13)$$

with the nominal battery voltage per module, the number of battery modules, and the number of parallel strings of in series connected battery modules represented by the parameters $U_{b,nom}$, n_b and n_p respectively. If the variation in state-of-charge $\xi(t)$ (due to the high Q_0) and temperature is assumed to be small ($T(t) = 25^\circ\text{C}$), then the losses become only dependent on the (in-)output power and are approximated as quadratic with the stored power:

$$P_{loss}(P_s(t)) = \max\left(c_2^- \frac{P_s(t)}{|P_s(t)|}, c_2^+ \frac{P_s(t)}{|P_s(t)|}\right) P_s^2(t), \text{ and } \{c_2^+, c_2^-\} \subseteq \mathbb{R}_0^+. \quad (5.14)$$

The battery losses are therefore assumed to be different during charging and discharging, and only increase with the stored or retrieved power. In order to increase the efficiency at relatively high battery powers, a battery topology consisting of two parallel strings of in series connected battery modules is chosen ($n_p = 2$). In this way the internal resistance of the battery pack is reduced.

Ultra Capacitor Efficiency

In contrary to batteries, the state-of-charge of the ultra capacitor strongly depends on the voltage across the capacitor, denoted as $U_{uc}(t)$ [7]. The discharge voltage ratio σ represents the ratio between the minimum and the maximum allowed capacitor voltage $\sigma = U_{uc,min}/U_{uc,max}$ and is used in order to calculate the state-of-charge,

$$\xi(t) = \frac{Q(t)}{Q_0} \cdot 100\% = \frac{C_{uc} (U_{uc}(t) - U_{uc,min})}{C_{uc} (U_{uc,max} - U_{uc,min})} \approx \frac{1}{1 - \sigma} \left(\frac{U_{uc}(t)}{U_{uc,max}} - \sigma \right), \quad (5.15)$$

with the capacitance C_{uc} (F) assumed to be approximately constant. However, it is found, that the minimum and maximum relatively static losses, e.g., at 44 kW, vary a little between 1.1% and 6.4% for $\xi = 0$ and $\xi = 1$ respectively. Therefore, in this chapter, for simplicity, the fit coefficients of Equation (5.14), which are determined for the mean static power losses, are used.

5.2.4 Sizing of Conversion and Storage Components

The engine and electric machine static-efficiency maps are linearly scaled with the maximum output power. Some results of the determined fit coefficients are listed in Table 5.5. The internal efficiency of the electric machine during charging is approximately equal to the efficiency during discharging and corresponds to the slope of the linear curves, i.e., $c_1^+ \approx 1/c_1^- = 91\%$. The slope of the various engine curves is approximately constant at 2.1 corresponding to a typical combustion efficiency (without static losses) of approximately 47%. It is observed, that a smaller engine or electric machine size results in smaller static losses, i.e., a smaller c_0 .

Table 5.5 / Parameters for different engine and electric machine sizes.

Component	Parameter value				Unit
Engine	125	150	170	205	kW
c_2	1.10	0.92	0.87	0.72	$10^{-6} \cdot \text{W}^{-1}$
c_1	2.10	2.10	2.09	2.09	-
c_0	7.84	9.41	11.29	13.61	kW
Electric machine	22	44	60	80	kW
c_1^+/c_1^-	-0.92/-1.08	-0.92/-1.08	-0.91/-1.09	-0.91/-1.09	-
c_0^+/c_0^-	-102/-301	-227/-441	-302/-559	-362/-603	W

The maximum absolute battery pack power is sized to meet the maximum output power specifications of the electric machine. However, due to losses of the electric machine the net (in-)output power as described by Equation (5.10) is reduced. A minimum number of 40 and 13 in series connected battery modules for the Ni-MH and the Li-ion battery (as listed in Table 5.6) are needed to meet the minimum voltage requirement $U_{pe,min}$ and maximum current $I_{pe,max}$ allowed by the motor controller/electric machine, which are estimated to be 260 V and 170 A respectively. These values are kept constant and are based on the battery specification of the Eaton hybrid electric drive train with the 44-kW electric machine (see, Table 5.1). For both battery technologies each module consists of 6 battery cells.

Since the ultra capacitor pack is not limited by power, yet is limited by energy constraints, the number of required caps was iteratively optimized by performing different simulation runs, until the available energy content of the capacitor pack is sufficiently large enough.

The maximum allowable systems bus voltage is assumed to be 600 V. Due to this limitation, sizing of the Ni-MH battery pack or the ultra capacitor pack larger than 60 kW by selecting more than 78 modules or 222 caps respectively is not possible. In Table 5.6, it is observed, that the Li-ion battery pack has a

much higher energy (Wh/kg) and power density (kW/kg) specification compared to the Ni-MH battery pack. The maximum losses at 44 kW during discharging and charging correspond approximately to 9.8% and 12.3%, 13.6% and 16.3%, and 2.3% and 2.7% of the storage power for the Li-ion, Ni-MH and UC respectively. Note that for other component sizes, the characteristic parameters are determined by interpolating between the values as given in Table 5.5 and 5.6.

Table 5.6 / Parameters for different sized energy storage technologies.

Type	EM Size (kW)	22	44	60	80	Unit
Ni-MH	Nominal voltage	310	450	600	-	V
	No. modules [†]	40.2	58.2	78.2	-	-
	Mass	40	58	79	-	kg
	c_2^+/c_2^-	4.95/4.78	3.71/3.10	2.76/2.31	-	$10^{-6} \cdot \text{W}^{-1}$
	Power density	0.55	0.76	0.76	-	kW/kg
	Energy density	46.5	46.6	45.6	-	Wh/kg
Li-ion	Nominal voltage	283	294	316	338	V
	No. modules [†]	13.2	14.2	15.2	16.2	-
	Mass	30	32	34	36	kg
	c_2^+/c_2^-	2.64/2.31	2.80/2.24	2.43/1.81	2.28/1.63	$10^{-6} \cdot \text{W}^{-1}$
	Power density	0.73	1.38	1.76	2.22	kW/kg
	Energy density	56.6	55.1	55.8	56.3	Wh/kg
UC	Nominal voltage	450	580	600	-	V
	Voltage swing, σ	0.58	0.45	0.43	-	V/V
	No. caps	167	215	222	-	-
	Mass	78	101	104	-	kg
	c_2^+/c_2^-	0.59/0.52	0.61/0.53	0.63/0.52	-	$10^{-6} \cdot \text{W}^{-1}$
	Power density	1.9	1.8	1.8	-	kW/kg
Energy density	3.7	4.5	4.5	-	Wh/kg	

[†] Two parallel strings of in series connected battery modules.

5.3 Control Model – RB-ECMS

The used control strategy is based on the combination of Rule-Based and Equivalent Consumption Minimization Strategies (RB-ECMS). The main control design parameter, which determines when to switch between the different hybrid driving modes, is optimized [31]. The main control design parameter is the maximum propulsion power of the electric machine during pure electric driving. The RB-ECMS determines if it is beneficial: to propel the vehicle only by the electric machine (Motor-only: M mode), only by the engine (Engine-only: E mode), to assist the engine with the electric machine in motoring mode during driving (Motor-Assist: MA mode), or to charge using the electric machine in genera-

tive mode during driving (CHarging: CH mode). Recuperation of brake energy (Brake Energy Recovery: BER mode) is very beneficial and is always performed. During the BER, M mode, and vehicle standstill the engine is assumed to be off and has no drag or idle losses.

5.3.1 Control Design Problem

The optimization problem is finding the control power-flow $P_s(t)$ given a certain power demand at the wheels $P_v(t)$, while the cumulative fuel consumption, denoted as the variable Φ_f , over a certain drive cycle with time length t_f is minimized, i.e.,

$$\Phi_f = \min_{P_s(t)} \int_0^{t_f} \dot{m}_f(E_s(t), P_s(t), t | P_v(t)) dt, \quad \text{subject to } \vec{h} = 0, \vec{g} \leq 0, \quad (5.16)$$

where the variable $\dot{m}_f(t)$ is the fuel mass-flow in g/s, which can be expressed as a function of the state variable $E_s(t)$ and the control input variable $P_s(t)$. The state is equal to the stored energy $E_s(t)$ in the reversal energy buffer in J and the control input is equal to the power-flow $P_s(t)$ in W (see, Figure 5.2). The energy level in the battery (or ultra capacitor) is a simple integration of the power and is calculated as follows,

$$E_s(t) = E_s(0) + \int_0^t P_s(\tau) d\tau. \quad (5.17)$$

The main constraints on the battery (or ultra capacitor) are energy balance conservation of $E_s(t)$ over the drive cycle and constraints on the power $P_s(t)$:

$$h_1 := E_s(t_f) - E_s(0) = 0, \quad g_{1,2} := P_{s,min} \leq P_s(t) \leq P_{s,max}. \quad (5.18)$$

The optimal control power-flow from and to the secondary source during the M and the BER mode respectively is assumed to be,

$$P_{s,I}^o(t) = -\max \left(\begin{array}{c} \frac{P_v(t)}{\underbrace{\eta_b(P_v(t), t) \eta_{em}(P_v(t), t) \eta_{AMT} \eta_{fd}^-}_{\text{M mode}}}, \\ \underbrace{f_{rb} P_v(t) \eta_b(P_v(t), t) \eta_{em}(P_v(t), t) \eta_{AMT} \eta_{fd}^+}_{\text{BER mode}}} \end{array} \right), \quad (5.19)$$

where the power set-point is limited between the following constraints,

$$P_{s,min} \leq P_M^o \leq 0 \leq P_{s,I}^o(t) \leq P_{s,max}. \quad (5.20)$$

The minus sign in Equation (5.19) indicates discharging during propulsion and charging during braking. The component efficiencies η_b and η_{em} are described by the power-based functions of Equations (5.11), (5.14), and Equation (5.10) respectively. Whereas the AMT efficiency η_{AMT} , the final drive including the differential efficiency η_{fd} , are assumed to be constant. However, the latter efficiency η_{fd} is dependent on the direction of the power-flow $P_s(t)$ (see, Table 5.4). Powers larger than the maximum charging power, which are limited by the battery or electric machine power constraints, are assumed to be dissipated in the wheel-brake discs. During the motor-only mode (M) the vehicle is propelled up to the optimal value for the maximum propulsion power $-P_M^o$. If only the M and/or the BER mode are utilized, then the energy difference $\Delta E_{s,I}(t_f)$ at the end of the drive cycle becomes,

$$\Delta E_{s,I}(t_f) = \int_0^{t_f} P_{s,I}^o(t) dt, \quad \Delta E_{s,I}(t_f) \in \mathbb{R}. \quad (5.21)$$

In order to fulfill the equality constraint h_1 of Equation (5.18) this energy has to be counterbalanced with the energy difference $\Delta E_{s,II}(t_f)$ at the end of the cycle during the motor-assisting MA mode and the charging CH mode (see, Figure 5.5), or

$$-\Delta E_{s,I}(t_f) = \Delta E_{s,II}(t_f). \quad (5.22)$$

The optimal power-flow during the CH and the MA mode is calculated using the equivalent fuel mass-flow $\dot{m}_{f,eq}$. The equivalent fuel mass-flow uses an average electric-energy-to-fuel-conversion-weight-factor or an average equivalent (weight) factor λ_0 . The λ_0 is used to assign future fuel savings and costs to the actual use of electric power P_s . Moreover, a well determined λ_0 assures that discrepancy between the buffer energy $E_{s,I}$ used during the BER/M mode and the buffer energy used during the CH/MA mode $E_{s,II}$ is sufficiently small.

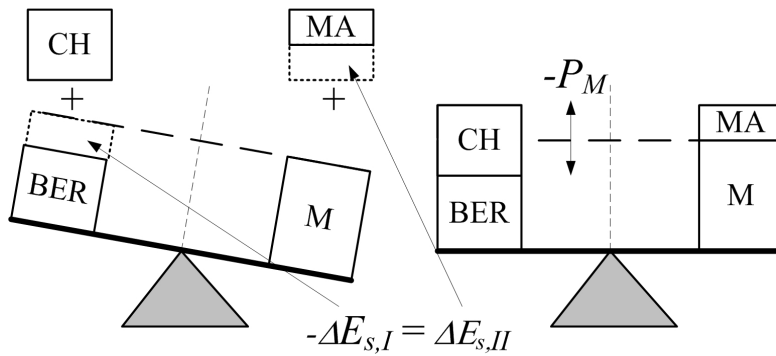


Figure 5.5 / Energy balance during the BER/M and the CH/MA modes.

The optimal power-flow during the CH and the MA mode, denoted as $P_{s,II}^o(t)$, is calculated by minimization of the equivalent fuel mass-flow $\dot{m}_{f,eq}$ at the current time t ,

$$P_{s,II}^o(t) = \arg \min_{P_{s,II}(t)} (\dot{m}_{f,eq}(t) | \lambda_0) = \arg \min_{P_{s,II}(t)} (\dot{m}_f(P_{s,II}(t), t) - \lambda_0 P_{s,II}(t)), \quad (5.23)$$

where the power set-point is limited between the following constraints,

$$P_{s,min} \leq 0 \leq P_{s,II}^o(t) \leq P_{s,max}. \quad (5.24)$$

Although, for example, during discharging $P_{s,II}(t) < 0$ the actual fuel mass-flow $\dot{m}_f(t)$ is reduced, Equation (5.23) shows that the fuel equivalent of the electrical energy $-\lambda_0 P_{s,II}(t)$ is momentarily increased and vice-versa. Then $\Delta E_{s,II}(t_f)$ is discharged (charged) at vehicle power demands where the fuel savings (costs) are maximum (minimum). Summarized, the optimal power set-point for the battery/electric machine as discussed in the previous two sections during the BER/M and the CH/MA mode becomes respectively:

$$P_s^o(t) = \begin{cases} P_{s,I}^o(t) \text{ (see, Equation (5.19))}, & \text{if } \frac{-P_v(t)}{\eta_b(P_v(t),t) \eta_{em}(P_v(t),t) \eta_{AMT} \eta_{fd}^-} \geq P_M^o, \\ P_{s,II}^o(t) \text{ (see, Equation (5.23))}, & \text{elsewhere.} \end{cases} \quad (5.25)$$

Finally, the EMS optimization scheme is shown in Figure 5.6. Starting with arbitrary values for P_M (limited by power constraints) and λ , the values for P_M and λ_0 are iteratively (loops 2 and 1 in Figure 5.6 respectively) updated until the cumulative fuel consumption Φ_f is minimized, while the integral energy balance constraint is satisfied. At the end of the loop, the optimal value for P_M minimizing the total fuel consumption, denoted as P_M^o , together with the optimal value for λ_0 , denoted as λ_0^o , are stored.

5.4 Vehicle Dynamics Model

In this section, the equations are derived in order to calculate the acceleration time, denoted as t_a , and the maximum gradeability, denoted as θ_{max} . The schematic layout of the hybrid drive train structure and the torques acting on the driven rear wheels are shown in Figure 5.7.

5.4.1 Acceleration Time 0–100 km/h (0–62 mph)

The dynamic torque balance at the propulsion shaft of the vehicle wheels gives for the vehicular acceleration (see, Figure 5.7):

$$a_v(t) = \dot{\omega}_v(t) \cdot r_w = \frac{1}{J_v} \cdot (T_v(t) - T_{rl}(t)) \cdot r_w, \quad (5.26)$$

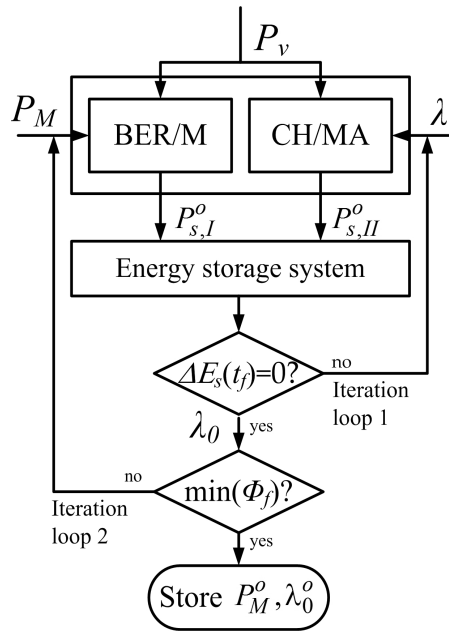


Figure 5.6 / Control strategy design optimization scheme (offline).

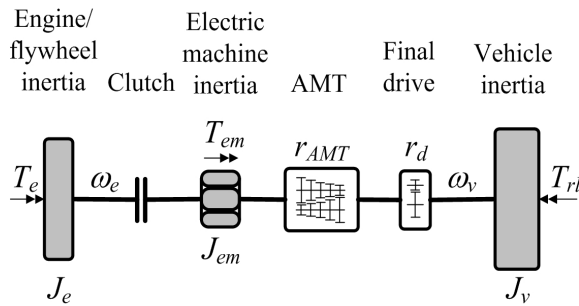


Figure 5.7 / Hybrid drive train structure.

with the total vehicle wheel torque $T_v(t)$ consisting of the sum of the engine $T_e(t)$ and electric machine torque $T_{em}(t)$ and an additional inertia torque term due to engine speed change during shifting,

$$T_v(t) = \left(\frac{T_e(t) + T_{em}(t)}{r_{AMT}(t) r_d} - \frac{J_e + J_{em}}{r_{AMT}(t) r_d} \cdot \dot{\omega}_e(t) \right) \eta_{AMT} \eta_{fd}^- \quad (5.27)$$

Since the vehicle wheel speed $\omega_v(t)$ is a function of the engine speed $\omega_e(t)$ and the gear ratio of the AMT r_{AMT} ,

$$\omega_v(t) = \omega_e(t) \cdot r_{AMT}(t) \cdot r_d, \quad r_{AMT}(t) \in \mathcal{R}, \quad (5.28)$$

the time derivative of the engine speed $\dot{\omega}_e(t)$ as is used in Equation (5.27) can be written as

$$\dot{\omega}_e(t) = \frac{\dot{\omega}_v(t)}{r_{AMT}(t) r_d} - \omega_e(t) \frac{\dot{r}_{AMT}(t)}{r_{AMT}(t)}. \quad (5.29)$$

The road load torque $T_{rl}(t)$ due to air drag, roll and road slope $\theta(t)$ resistance holds,

$$T_{rl}(t) = \frac{1}{2} \rho c_d A_f \omega_v(t)^2 r_w^3 + c_r m_v g \cos(\theta(t)) r_w + m_v g \sin(\theta(t)) r_w. \quad (5.30)$$

The engine inertia including the clutch and starter flywheel inertia, and the electric machine inertia are represented by the variables J_e and J_{em} respectively. The vehicle inertia J_v consists of the vehicle mass m_v , the inertia of the rotating parts J_w including the wheels and the final drive:

$$J_v = J_w + m_v r_w^2. \quad (5.31)$$

Initially, the vehicle acceleration is calculated with Equation (5.26) under the assumption that no wheel slip occurs. Then, using this acceleration value the torque required to initiate slip is calculated:

$$T_{slip}(t) = \mu_r m_v g \left(\frac{L_r}{L} + \frac{a_v(t)}{g} \frac{H}{L} \right) r_w, \quad (5.32)$$

for the rear wheel driven vehicle with the traction coefficient μ_r . The wheel base length and height of the center of gravity are represented, as stated before, by the parameters L and H respectively. The parameter H is assumed to increase linearly with increase of m_v . The wheel torque $T_v(t)$ during acceleration is compared with the wheel slip torque $T_{slip}(t)$. If $T_v(t) > T_{slip}(t)$, then slip occurs and the tractive torque becomes equal to the slip torque, i.e., $T_v(t) = T_{slip}(t)$. Using Equation (5.32) substituted into Equation (5.26) the vehicle acceleration under the slip condition is calculated. The gear ratio change rate $\dot{r}_{AMT}(t)$ is assumed to be sufficiently limited, such that a positive vehicle acceleration is guaranteed. A gear change time delay of 0.9 s at zero engine torque to the shifting sequence is assumed. During an upshift the net acceleration falls below zero during this shift period, due to road load forces that are acting on the vehicle. The vehicle speed is used to trigger upshifts. Therefore, in order to prevent downshifts during shift periods, upshifts are forced once the delay period is over. During acceleration the

engine and the electric machine are assumed to be operated (as much as possible) at their wide-open throttle and maximum torque curve respectively. Figure 5.8 shows an example result of the engine speed and vehicle speed over time during maximum acceleration. Note that the acceleration time t_a is limited by the minimum state-of-charge of the battery or the ultra capacitor, i.e., $\xi(t_a) \geq \xi_{min}$.

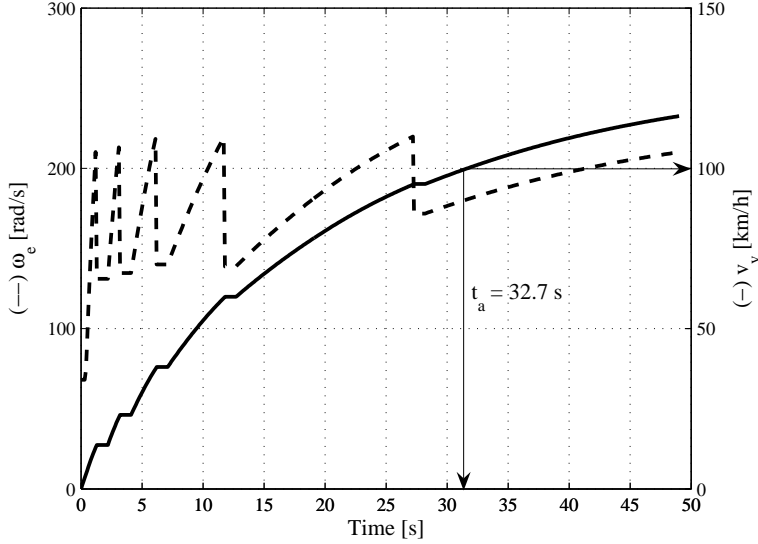


Figure 5.8 / An example result of the engine speed and the vehicle speed over time.

5.4.2 Gradeability at 89 km/h (55 mph)

The vehicle wheel torque T_v calculated with Equation (5.27) is a function of the speed ratio r_{AMT} and the vehicle speed v_v . Note that the vehicle speed is defined as $v_v = \omega_v r_w$. The engine and the electric machine are assumed to be operated at their wide-open throttle and maximum torque curve respectively. Moreover, the road load torque T_{rl} calculated with Equation (5.30) is a function of the road slope θ and the vehicle speed v_v . The set of feasible road slopes θ_0 at a given vehicle speed v_v , which is a function of the speed ratio r_{AMT} , are elements of the set of the stationary vehicle wheel torques T_v , which are in balance with the road load torques T_{rl} :

$$\theta_0(r_{AMT}) \subseteq \left\{ \begin{array}{l} T_v(r_{AMT}, v_v) - T_{rl}(\theta, v_v) = 0 \mid v_v = 89 \text{ km/h} \wedge \\ r_{AMT} \in \mathcal{R} \wedge 0^\circ \leq \theta \leq 45^\circ \end{array} \right\}. \quad (5.33)$$

The objective is to find the optimal gear ratio r_{AMT}^o , which maximizes the feasible road slopes:

$$r_{AMT}^o = \arg \max_{r_{AMT} \in \mathcal{R}} (\theta_0(r_{AMT})) \wedge \theta_{max} = \theta_0(r_{AMT}^o), \quad (5.34)$$

where no wheel slip occurs. Figure 5.9 shows an example result of the wheel torque as a function of the vehicle speed for different speed ratios.

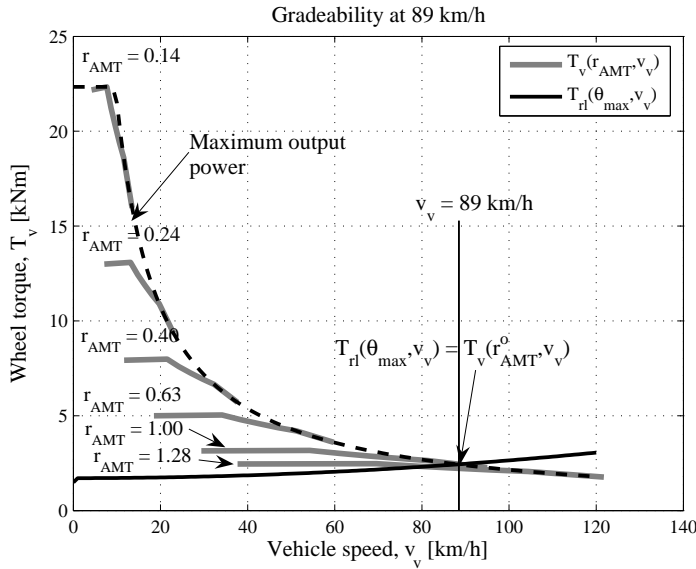


Figure 5.9 / An example result of the wheel torque as a function of the vehicle speed for different speed ratios.

5.5 Dual-Energy Storage Design Model

In this section the dual-energy storage design model is discussed, which is used in order to determine the optimal dual-storage size. The optimal dual-storage size is determined by minimizing the overall energy storage mass, denoted with the variable Φ_{es} , which is determined by the total number of battery modules n_b (6 cells/module) and ultra capacitor cells n_{uc} :

$$\Phi_{es} = K_b \cdot n_b(f_c) + K_{uc} \cdot n_{uc}(f_c). \quad (5.35)$$

The parameters K_b and K_{uc} represent the conversion factors (kg/cell) from number of cells to storage mass (see, Table 5.3). In order to determine the total number of required cells, power separation of the original optimized power signal

$P_s^o(t)$ (see, Equation (5.25)) is performed by using a digital filter H_f (Butterworth low-pass digital filter) given that the desired energy storage and peak power characteristics are achieved. In Figure 5.10 the power-flow in a dual-energy storage system is schematically shown.

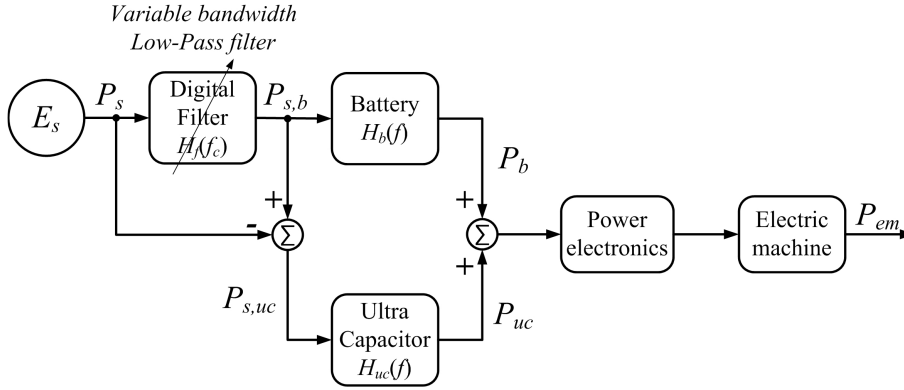


Figure 5.10 / Frequency-based power separation of battery and ultra capacitor usage.

The design variables (n_b, n_{uc}) are a function of the cut-off frequency f_c (Hz). Moreover, the frequency content of the battery usage $H_b(f)$ and capacitor usage $H_{uc}(f)$ is weighted at each frequency f :

$$H_b(f) + H_{uc}(f) = 1, \quad (5.36)$$

which is directly analogous to the Bode frequency criteria. The reader is referred to [58] and [69] where frequency-domain control structures are discussed to achieve frequency-based separation of the battery/ultra capacitor usage. Note that $P_s^o(t)$ used for the design of the dual-storage system is based on the EMS calculated for a single-storage system with a different storage efficiency. The influence of this effect on the overall desired size is assumed to be nihil. The battery input power $P_{s,b}(t)$ and the ultra capacitor storage energy $E_{s,uc}(t)$ as a function of time for a cut-off frequency f_c become respectively,

$$P_{s,b}(t) = H_f(f_c) * P_s^o(t), \quad (5.37)$$

$$E_{s,uc}(t) = \int_0^{t_f} (1 - H_f(f_c)) * P_s^o(t) dt. \quad (5.38)$$

Generally, an ultra capacitor is constrained by energy and not by power limitations, and a battery is constrained by power and not by energy limitations:

$$E_{s,uc,min}(n_{uc}) \leq E_{s,uc}(t) \leq E_{s,uc,max}(n_{uc}), \quad (5.39)$$

$$P_{s,b,min}(n_b) \leq P_{s,b}(t) \leq P_{s,b,max}(n_b), \quad (5.40)$$

which are a function of the design variables (n_b, n_{uc}) . Given $P_s^o(t)$, the optimal number of battery modules and ultra capacitor cells, denoted as n_b^o and n_{uc}^o respectively, are calculated from the following minimization,

$$(n_b^o, n_{uc}^o) = \arg \min_{(n_b, n_{uc}) \in \mathcal{N}} (\Phi_{es}(n_b, n_{uc}) | P_s^o(t)), \quad (5.41)$$

where the set \mathcal{N} covers the feasible solutions that satisfy the constraints in Equation (5.37)-Equation (5.40):

$$\mathcal{N} = \left\{ \begin{array}{l} (n_b, n_{uc}) | P_{s,b}(t) - H_f(f_c) * P_s^o(t) = 0 \\ \quad \wedge \\ E_{s,uc}(t) - \int_0^{t_f} (1 - H_f(f_c)) * P_s^o(t) dt = 0 \\ \quad \wedge \\ P_{s,b,min}(n_b) \leq P_{s,b}(t) \leq P_{s,b,max}(n_b) \\ \quad \wedge \\ E_{s,uc,min}(n_{uc}) \leq E_{s,uc}(t) \leq E_{s,uc,max}(n_{uc}) \end{array} \right\}. \quad (5.42)$$

Next the battery and ultra capacitor design models are derived for the determination of the available battery pack power and the storage energy of the ultra capacitors.

5.5.1 Battery Design Model

In Figure 5.11 the equivalent circuit of a battery is shown. The open-circuit voltage of the battery, the internal resistance causing a voltage drop, and the terminal voltage are represented by the variable U_{oc} , R_b , and U_b respectively. Kirchoff's law for the equivalent circuits yields the following equation,

$$U_b = U_{oc} - R_b I, \quad (5.43)$$

with the current defined as $I = P_b/U_b$. The battery pack consists of two parallel strings of in series connected battery modules in order to reduce the overall internal resistance. For (dis-)charging the maximum current is limited by the maximum allowed motor controller current $I_{pe,max} = 170$ A,

$$|I| \leq I_{pe,max}. \quad (5.44)$$

Although the open circuit voltage U_{oc} depends on the state-of-charge, an average value for U_{oc} is used for determining the number of battery modules fulfilling the maximum power requirements. The maximum (dis-)charging output power as a function the voltage and the number of battery modules n_b is calculated as,

$$P_{b,i}(n_b) = \frac{-2 U_{b,i}^2 + 2 U_{oc} U_{b,i}}{R_b} n_b, \quad i \in \{min, max\}, \quad (5.45)$$

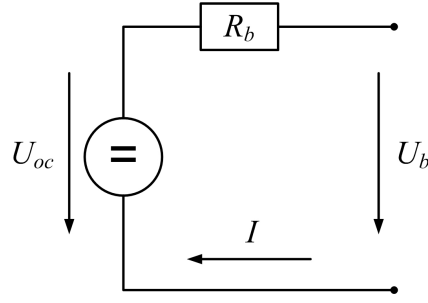


Figure 5.11 / Equivalent circuit of a battery.

with the maximum (dis-)charge input power as a function of the number of battery modules,

$$P_{s,b,i}(n_b) = P_{b,i}(n_b) - \left(\frac{R_b}{n_b U_{b,i}^2} \right) P_{b,i}^2(n_b). \quad (5.46)$$

The battery voltage corresponding with the minimum discharging output power by setting the derivative of $P_{b,min}$ with respect to U_b to zero becomes,

$$\frac{\partial P_{b,min}}{\partial U_{b,min}} = 0 \Rightarrow U_{b,min} = U_{oc}/2. \quad (5.47)$$

However, the minimum discharging output power $P_{b,min}$ is limited by three parameters, which are all related to the minimum *available* battery voltage at the terminal $U_{b,min,a}$. The three parameters are, the minimum input voltage of the motor controller $U_{pe,min} = 260$ V, the minimum battery voltage $U_{b,min}$, and the open circuit voltage divided by two $U_{oc}/2$ as calculated with Equation (5.47). The minimum available battery voltage at the terminal $U_{b,min,a}$ becomes,

$$U_{b,min,a} = \max(U_{pe,min}/n_b, U_{b,min}, U_{oc}/2). \quad (5.48)$$

Finally, the maximum charging input power $P_{b,max}$ and output power $P_{s,b,max}$ as a function of n_b is, besides the current limitation (see, Equation (5.44)), mainly limited by the maximum battery voltage $U_{b,max}$.

5.5.2 Ultra Capacitor Design Model

The maximum *available* usable storage energy, denoted as $\Delta E_{s,uc,a}$, that a capacitor can provide is defined by the equation [7]:

$$\Delta E_{s,uc,a}(n_{uc}) = E_{s,uc,max}(n_{uc}) - E_{s,uc,min}(n_{uc}) = \frac{1}{2} C_{uc} U_{uc,max}^2 n_{uc} (1 - \sigma^2), \quad (5.49)$$

with the discharge voltage ratio limited to the minimum available voltage (see, Equation (5.48)) to nominal voltage ratio of the battery,

$$\sigma \leq \frac{U_{b,min,a}}{U_{b,nom}}. \quad (5.50)$$

If an independent power processor interfaces the capacitor to the terminal voltage, then its voltage swing described by σ is only limited by the minimum input voltage of its power converter, which is typically 0.33 of the operating voltage [52]. Knowing the *needed* maximum usable energy for a given f_c with help of Equation (5.38),

$$\Delta E_{s,uc,n}(f_c) = \max(E_{s,uc}(t)) - \min(E_{s,uc}(t)), \quad (5.51)$$

the required number of ultra capacitor cells n_{uc} , which are coupled in series, is easy to be identified after substitution of Equation (5.51) into Equation (5.49),

$$n_{uc} = \frac{2 \Delta E_{s,uc,n}(f_c)}{C_{uc} U_{uc,max}^2} \frac{1}{(1 - \sigma^2)}, \quad (5.52)$$

with $\Delta E_{s,uc,a}(n_{uc}) = \Delta E_{s,uc,n}(f_c)$.

5.6 Simulation Results

In this section, the simulation results of the hybrid electric drive train are described for determining: the optimal degree-of-hybridization, the acceleration time from 0-100 km/h (0-62 mph), the maximum gradeability in percentage at 89 km/h (55 mph). The sizing results for the dual-energy storage systems and the cost price of sized dual-storage systems are also discussed (see, Figure 5.1 for an overview of the design optimization process).

5.6.1 Fuel Consumption, Acceleration Time, and Gradeability Results

The base line FedEx truck is equipped with a Cummins 175HP (131-kW) 6BT5.9 and an Allison AT542 NFE 4-speed automatic transmission [85]. Therefore, the 205-kW base engine is downscaled to produce 131 kW, which is used in the simulations for the Base Line (BL) vehicle. In Figure 5.12 the relative fuel savings (in Table 5.7 the reference values are listed) of the Hybrid Electric Vehicle (HEV) as a function of the hybridization factor $HF_{dt,125kW}$ for different vehicle masses are shown (kept constant: Li-ion battery and 125-kW engine). The observations, which are made following from the parameter variation study, for a constant engine size are discussed next.

1. If the vehicle mass increases, then the optimal HF_{dt} (or in this case the optimal electric machine size) increases due to increase of regenerative brake energy potential.
2. With a larger electric machine size (i.e., a higher HF_{dt}) effectively more brake energy is recuperated. However, the (static) losses of the electric machine increase progressively thereby reducing again the fuel saving potential. The (concave) curves show a certain maximum fuel saving potential.

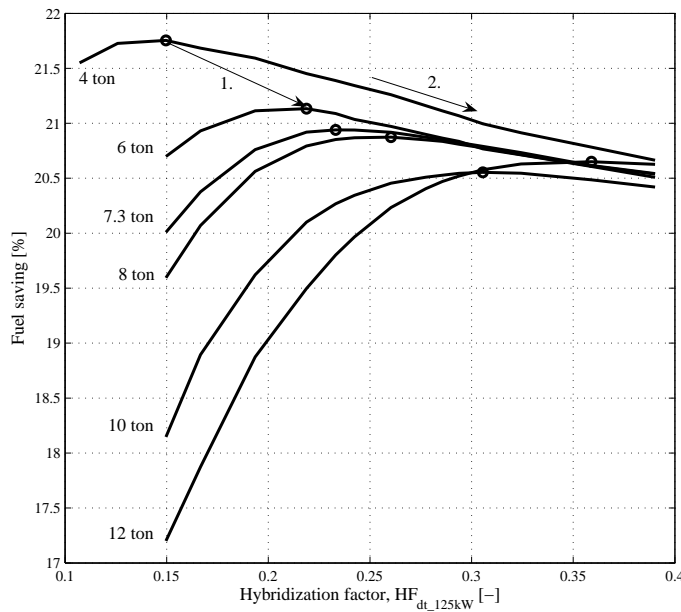


Figure 5.12 / Fuel saving as a function of $HF_{dt,125kW}$ for different vehicle masses (kept constant: Li-ion and 125-kW engine).

The optimal hybridization factor values $HF_{dt,125kW}$ for a truck mass of 7.3 ton and 4 ton are 23.3% and 15.0% respectively. These values are close to the hybridization factors of the FedEx ($HF_{dt,125kW} = 26\%$, $m_v = 7.3$ ton), the Nissan Condorr ($HF_{dt,152kW} = 27\%$, $m_v = 7.8$ ton), and the Hino 4T Ranger truck ($HF_{dt,132kW} = 15\%$, $m_v = 3.6$ ton).

In Figure 5.13 the optimal $HF_{dt,125kW}$ for a 7.3 tons truck as a function of the vehicle mass is shown. In the same figure the hybridization factor values are

shown in case the minimum braking power determines the electric machine size:

$$HF_{dt,125kW}(m_v) = \left(\frac{P_{em,min}}{P_{em,min}+125 \text{ kW}} \middle| m_v \wedge P_{em,min} = -\min(P_v(t) \eta_{AMT} \eta_{fd}^+) \right). \quad (5.53)$$

The results in Figure 5.13 show that the discrepancy between the hybridization factor $HF_{dt,125kW}$ determined by the maximum generative power and determined by the maximum fuel saving increases with vehicle mass. However, the maximum fuel consumption difference for the different vehicle masses for both cases is found to be negligible small. Nevertheless, in order to reduce the required power specifications for the electric machine the following observation is made.

3. For large vehicle masses (see, Figure 5.13 for $m_v \geq 6$ ton) the optimal degree-of-hybridization should be determined based on maximizing the fuel savings over a whole drive cycle and should not be determined based on the maximum braking power.

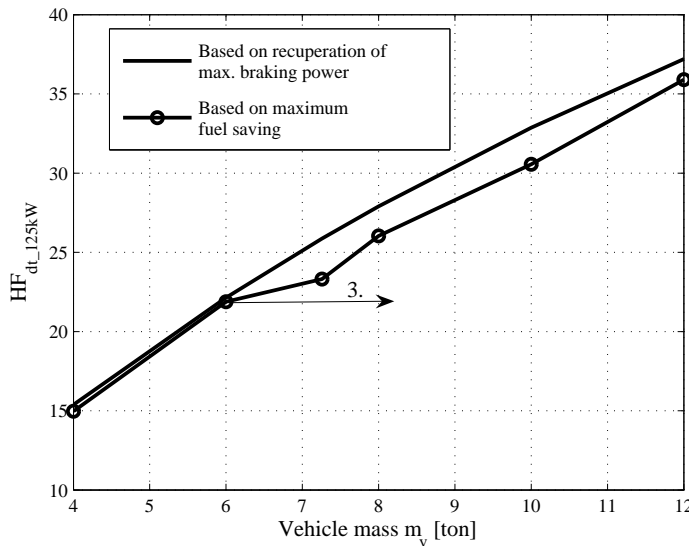


Figure 5.13 / Optimal $HF_{dt,125kW}$ as a function of the vehicle mass m_v (kept constant: Li-ion and 125-kW engine).

In Figure 5.14 the relative fuel savings (in Table 5.8 and 5.9 the reference values are listed) of the HEV as a function of $HF_{dt,P_{e,max}}$ for different engine sizes and two different vehicle masses are shown (kept constant: Li-ion). The following observations are made for a constant vehicle mass or a constant engine size respectively.

Table 5.7 / Fuel consumption results for different vehicle masses (kept constant: Li-ion and 125-kW engine).

Mass, m_v	Fuel consumption						10^3 kg
	4	6	7.3	8	10	12	
1 BL (131-kW engine)	11.9	14.5	16.0	17.0	19.5	21.9	l/100km
2 HEV (125-kW engine)	9.3	11.4	12.7	13.5	15.5	17.4	l/100km
Optimal $HF_{dt,125kW}$	15.0	21.9	23.3	26.0	29.4	30.6	%
$P_{em,max} / - P_M^o$	22/14	35/18	38/22	44/24	55/29	70/34	kW/kW
3 Fuel saving = $100\% \cdot (1-2)/1$	21.8	21.1	20.9	20.9	20.6	20.6	%

4. The relative fuel saving as a function of HF_{dt} for a smaller engine size is smaller than for a larger engine size due to increase of the engine static losses with increase of the engine size.
5. The maximum relative fuel saving at a certain engine size for a smaller vehicle mass is higher than at the same engine size (i.e., equal static losses) for a larger vehicle mass. The maximum relative fuel saving is decreased due to increase of the average vehicle power demands with vehicle mass.

In addition to observation 5, the following observation is made by comparing the results of Table 5.8 with Table 5.9.

6. The absolute maximum fuel saving at a certain engine size for a smaller vehicle mass is lower than at the same engine size for a larger vehicle mass.

Table 5.8 / Fuel consumption results for different engine sizes (kept constant: Li-ion and $m_v = 7.3$ ton).

Engine size, $P_{e,max}$	Fuel consumption				kW
	125	150	170	205	
1 BL	16.0	16.5	16.8	17.4	l/100km
2 HEV	12.7	12.9	13.1	13.3	l/100km
Optimal $HF_{dt,P_{e,max}}$	23.3	20.2	18.3	15.6	%
$P_{em,max} / - P_M^o$	38/22	38/22	38/22	38/22	kW/kW
3 Fuel saving = $100\% \cdot (1-2)/1$	20.9	21.6	21.9	23.4	%

In Table 5.10 the vehicle improvements regarding the fuel consumption and drivability for different storage systems are shown (kept constant: $HF_{dt,125kW} = 23.3\%$, $m_v = 7.3$ ton, $P_{e,max} = 125$ kW). The results in Table 5.10 show that the fuel consumption and the vehicle performances are improved in comparison with the BL vehicle. Note that there is only a small difference in fuel consumption for the HEV equipped with a Ni-MH battery compared to the HEV with a Li-ion battery and UC. For the HEV equipped with a Li-ion battery pack or an UC pack, the fuel consumption values are approximately similar.

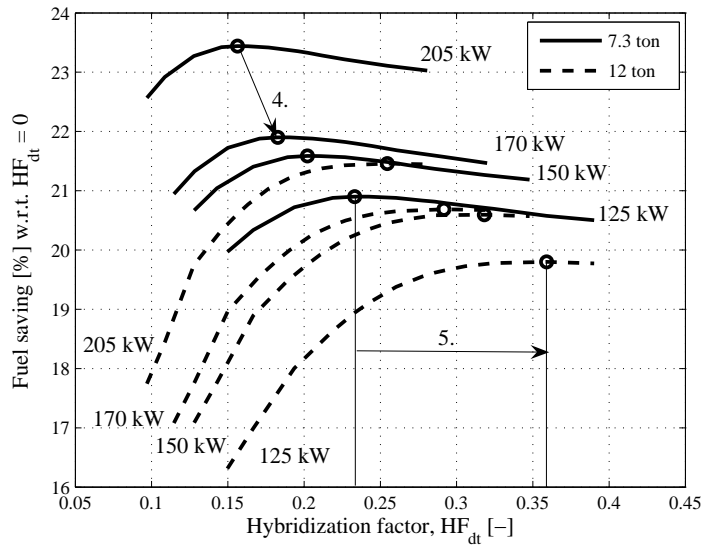


Figure 5.14 / Fuel saving as a function of $HF_{dt_{P_{e,max}}}$ for different engine sizes and two vehicle masses (kept constant: Li-ion).

Table 5.9 / Fuel consumption results for different engine sizes (kept constant: Li-ion and $m_v = 12$ ton).

	Engine size, $P_{e,max}$	Fuel consumption				kW
		125	150	170	205	
1	BL	21.7	22.5	23.0	23.7	l/100km
2	HEV	17.4	17.9	18.2	18.6	l/100km
	Optimal $HF_{dt_{P_{e,max}}}$	35.9	31.8	29.2	25.5	%
	$P_{em,max} / - P_M^0$	70/34	70/34	70/35	70/35	kW/kW
3	Fuel saving = $100\% \cdot (1-2)/1$	19.8	20.6	20.7	21.5	%

Table 5.10 / Fuel consumption and drivability improvements for Ni-MH, Li-ion, and UC (kept constant: $HF_{dt_{125kW}} = 23.3\%$, $m_v = 7.3$ ton, and 125-kW engine).

	BL	HEV	Change (%)
Engine size (kW)	131	125	-
Electric machine size (kW)	-	38	-
Fuel consumption (l/100km)	16.1	12.7 [†] /12.9 [‡]	+21%/+20%
Gradeability (θ_{max}) at 89 km/h (%)	4.5	6.7	+49%
Acceleration time (t_a) 0-100 km/h (s)	49.0	36	+27%
Maximum vehicle speed (v_{max}) (km/h)	116	129	+11%

-/+ = (de-)increased, [†] = Li-ion, UC, [‡] = Ni-MH

The time to sustain the maximum achievable vehicle speed v_{max} after an acceleration period, denoted as $t_{v,max}$, is limited by the minimum state-of-charge or available energy storage (see, Equation (5.13)) of the battery and the ultra capacitor pack. During the acceleration test, the initial state-of-charge for both the battery and ultra capacitor packs are 80% and 100% assumed respectively. Moreover, the battery and ultra capacitor pack are assumed to be discharged to $\xi_{min} = 40\%$ and $\xi_{min} = 0\%$ respectively. The results for the different storage systems, until $\xi(t_a + t_{v,max}) = \xi_{min}$ or in other words the minimum state-of-charge constraint is reached, are listed in Table 5.11.

Table 5.11 / Time to sustain the maximum speed after acceleration $t_{v,max}$ for different single-storage technologies (kept constant: $HF_{dt,125kW} = 23.3\%$, $m_v = 7.3$ ton, and 125-kW engine).

Storage type	No. modules [†] /No. caps	$t_{v,max}$ (s)
UC	202	8.3
Li-ion	13.2	12.2
Ni-MH	57.2	21.7

[†] Two parallel strings of in series connected battery modules.

Although the type of electrical storage system has a relatively small influence on the overall vehicle performance (total power is the same), $t_{v,max}$ is limited and significantly different for each type of storage system, mainly due to the different energy contents. Summarized, the Li-ion battery and UC pack have the highest storage efficiency, which results in a lower fuel consumption compared to the Ni-MH battery pack. In addition, the Ni-MH battery has the largest energy content and therefore the longest time to sustain the maximum vehicle speed $t_{v,max}$ until the minimum state-of-charge ξ_{min} is reached.

In the next section the sizing results of dual-storage systems at the optimal hybridization factor $HF_{dt,125kW} = 23.3\%$ for a 7.3 tons truck are presented. In addition, the cost prices of sized dual-storage systems are discussed.

5.6.2 Sizing Results of Dual-Energy Storage Systems

The UC cell (see, Table 5.3) has an equivalent series resistance value of 0.40 m Ω and a capacitance C_{uc} of 2600 F [51]. In Table 5.12 the average system voltage and the storage mass of the optimized (single-)dual-energy buffers are listed. The battery and ultra capacitor are assumed to be direct parallel coupled. The required battery pack size and output power specifications for both battery technologies are significantly reduced. However, the mass of the dual-storage system (without boost converter) is higher than the single-storage system mass, due to the relatively high specified minimum motor controller voltage value of 260 V.

A boost converter can solve this problem by increasing the storage output voltage and thereby reducing the number of required battery/capacitor cells [55]. For example the Toyota Prius contains an electric motor, which utilizes voltages of approximately 500 V. Without a boost converter 417 Ni-MH battery cells would be needed instead of the applied 168 cells. The converter boosts the voltage from 202 V up to 500 V. Therefore, a boost converter is assumed to be connected between the electric machine and the direct parallel coupled battery and ultra capacitor modules, which boosts the voltages from approximately 130 V up to 260 V. The results are also shown in Table 5.12. Only the total mass of the dual-storage system consisting of a Ni-MH/UC with boost converter is significantly reduced with 23% compared to the single-storage system mass. Although, adding an UC to a battery reduces the battery power demands and therefore the battery wear significantly, a boost converter is a critical element in reducing the dual-storage system mass. In particular, this holds for battery technologies with a relatively low power density (W/kg). In this case the Ni-MH battery has a lower power density than the Li-ion battery.

Table 5.12 / Optimal dual-storage size (kg) (kept constant: $HF_{dt,125kW} = 23.3\%$, $m_v = 7.3$ ton, and 125-kW engine).

Storage type	Nominal voltage (V)	Voltage swing, σ (-)	Mass (kg)			Relative mass (%)	HF_{es} (%)
			battery	capacitor	total		
UC	545	0.48	-	93	93	100	0
UC [†]	446	0.29	-	76	76	82	0
Li-ion	291	-	32	-	32	100	100.0
Li-ion/UC	261	0.65	27	44	71	222	6.2
Li-ion/UC [†]	132	0.51	14	22	36	113	9.5
Ni-MH	412	-	53	-	53	100	100.0
Ni-MH/UC	263	0.67	34	44	78	147	6.4
Ni-MH/UC [†]	138	0.67	18	23	41	77	12.0

[†] with boost converter

In Figure 5.15, for example, the power and energy distribution between the battery (Ni-MH) and UC with a boost converter as a function of time are shown respectively. The cut-off frequency is $f_c = 5.83$ mHz corresponding to a battery time constant of approximately 172 s.

5.6.3 Cost Price of Sized Dual-Storage Systems

The cost price of the batteries and an UC in \$/unit is shown in Table 5.13. In the same table the life expectancy is also given, which has been estimated by assuming that 1500 cycles correspond to approximately 5 years [22]. It is observed in Table 5.13 that an UC has approximately three times the life expectancy of a

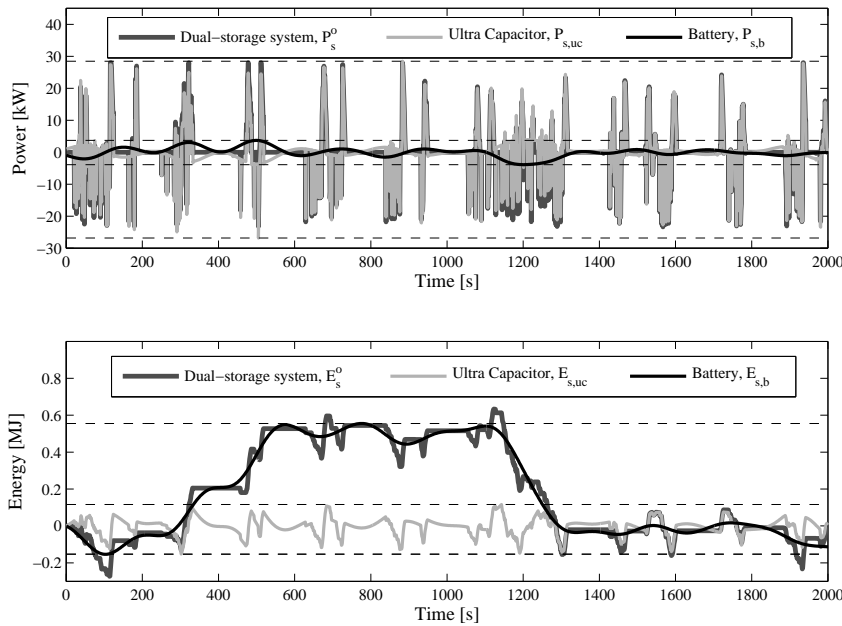


Figure 5.15 / Power and energy distribution over time between battery (Ni-MH) and ultra capacitor pack with boost converter.

battery (Li-ion, Ni-MH). In Table 5.14 the cost prices of the (single-)dual-storage systems are listed assuming an average cost price for the Li-ion and Ni-MH battery of 275 \$/kWh. The results in Table 5.14 show that only the total system cost for a dual-storage system consisting of a Ni-MH battery/UC with boost converter is reduced compared to the initial single-storage system. Note that the cost price for the boost converter is not considered. Moreover, the ability to increase the life expectancy of the battery with the use of the capacitor is not taken into account regarding the cost analysis. The life expectancy of the battery for the single- and the dual-storage system is kept constant, whereas in reality the life expectancy of the battery is potentially improved [6]. The relatively high cost price for the UC pack is caused by the relatively high required energy buffer size and the relatively high minimum controller input voltage specification. Although even with a boost converter the voltage swing is increased and σ is decreased from 0.48 to 0.29 (see, Table 5.12), the cost price of an UC system is still relatively high compared to the sized battery systems. Hybridization of the dual-storage system with a Li-ion battery has no cost benefits. This is explained further with help of Figure 5.16. In this figure the system cost price (for single- and dual-storage) as a func-

tion of the average battery cost price in \$/kWh for the Li-ion and Ni-MH battery is shown. The break-even cost price for the Ni-MH battery is 269 \$/kWh, whereas the break-even cost price for the Li-ion battery is much higher (> 300 \$/kWh). It is observed, that if the life expectancy of the battery, for example, would be increased from 3.3 years to 5 years, then the break-even cost price for a Ni-MH battery would decrease by 15% from 269 \$/kWh to 230 \$/kWh. Additionally, the figure shows that the cost of a dual-storage system with a Li-ion battery is close to a dual-storage system with a Ni-MH battery. Overall, it can be concluded, that the Li-ion battery is, from an energy, power density specification, and a cost price point of view, the most preferable energy storage system.

Furthermore, if the cost price of the UC decreases by 38% from 0.01 \$/Farad to approximately 0.0062 \$/Farad, then the cost price of a dual-storage system with a Li-ion and UC becomes equal to the initial single-storage battery system. This is shown in Figure 5.17. Note that the UC cost price reduction *target* for 2006 was 50% resulting in a decrease from 0.01 \$/Farad to 0.005 \$/Farad [51]. Obviously, energy storage hybridization of a Li-ion with an UC module may become in the future from a cost price point of view also an attractive option. However, this development strongly depends on the Li-ion battery specification developments and still requires drastic reduction of UC cost price.

Table 5.13 / Cost-price and cycle life of storage systems.

Storage type	Cost price	(\$/unit)	Cycle life	Life expectancy	Source
Li-ion	300	\$/kWh	1000+	3.3+ years	Saft
Ni-MH	250	\$/kWh	750 – 1200+	2.5 – 4+ years	Saft
UC	0.01	\$/Farad	$10^5 - 10^6$	10 years	Maxwell

Table 5.14 / System cost prices based on 10 years life expectancy (kept constant: $HF_{dt,125kW} = 23.3\%$, $m_v = 7.3$ ton, and 125-kW engine).

Storage type	Cost price (10 years)	Total cost price (excl. boost converter)
UC	\$ 5252	\$ 5252
UC [†]	\$ 4290	\$ 4290
Li-ion	\$ 1441	\$ 1441
Li-ion/UC	\$ 1293/\$ 2516	\$ 3809
Li-ion/UC [†]	\$ 654/\$ 1273	\$ 1928
Ni-MH	\$ 2039	\$ 2039
Ni-MH/UC	\$ 1304/\$ 2536	\$ 3840
Ni-MH/UC [†]	\$ 682/\$ 1327	\$ 2009

[†] with boost converter; battery cost price of 275 \$/kWh and life expectancy of 3.3 years assumed for Li-ion and Ni-MH battery cell.

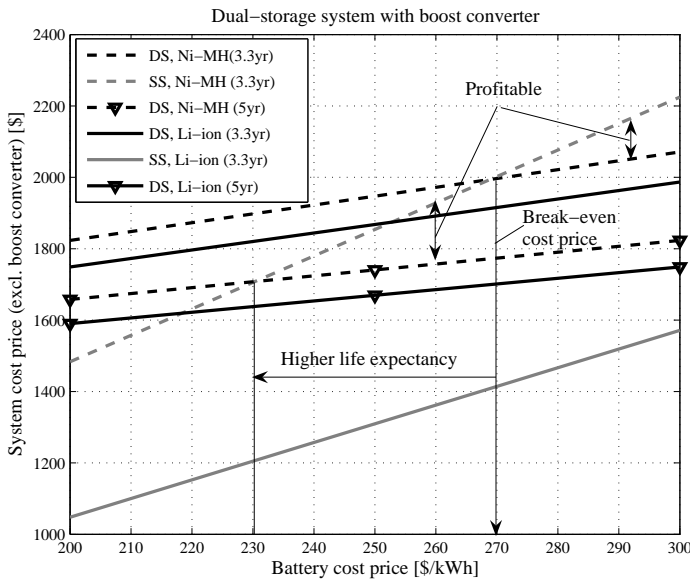


Figure 5.16 / System cost price as a function of the battery cost price in \$/kWh for different life expectancies (SS = Single-Storage; DS = Dual-Storage).

5.7 Conclusion

A modeling and simulation approach in characterizing the component technologies for a medium-duty hybrid electric truck was discussed. The optimal degree-of-hybridization for the drive train and energy storage system (dual-storage system) was determined. The influence of the gross-vehicle weight on optimal component sizing was investigated. The results show that the degree-of-hybridization of developed medium-duty hybrid electric trucks, where the fuel consumption is measured on different duty drive cycles, are close to the determined optimal degree-of-hybridization using the methods as described in this chapter. Only the total mass of the dual-storage system consisting of a Ni-MH/UC with boost converter is significantly reduced with 23% compared to the single-storage system mass. Although, adding an ultra capacitor to a battery reduces the battery power demands and therefore the battery wear significantly, a boost converter is a critical element in reducing the dual-storage system mass. In particular, this holds for battery technologies with a relatively low power density (W/kg). In this case the Ni-MH battery has a lower power density than the Li-ion battery. Finally, it can be concluded, that the Li-ion battery is from an energy, power density specification as well as cost point of view, the most preferable energy storage system. However, if the cost of ultra capacitor cells are significantly decreased (>50%),

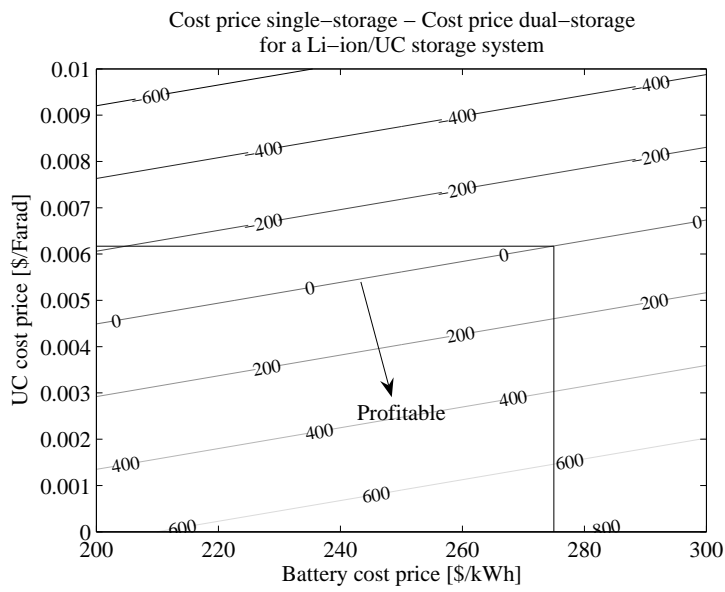


Figure 5.17 / Cost price benefits in \$ by comparing a single-storage battery system with a dual-storage system as a function of the UC cost price in \$/Farad and the battery cost price in \$/kWh.

then hybridization of a Li-ion battery with an ultra capacitor module in combination with a boost converter may become an attractive technology package in the future.

Conclusions and Recommendations

In the following two sections the main conclusions following from the previous chapters are drawn and the recommendations for future research are given.

Summarizing, this thesis contributes by proposing:

- a control design method, which is based on the combination of Rule-Based and Equivalent Consumption Minimization Strategies (RB-ECMS), for optimizing the control strategy, and
- a reduced hybrid drive train model described by a small set of subparameters, which can be employed with sufficient accuracy for hybrid drive train specification.

These two results followed from two research questions posed in the introduction:

- (i) can a computationally efficient method be developed, which results in an optimized control strategy comparable to the strategy computed with DP?
- (ii) can reduced models be developed for topologies, component technologies and sizes, which can be employed for parametric design optimization with sufficient accuracy?

The answer to the first research question is: yes, a control method called RB-ECMS is proposed, which is used for quick optimization and shows results comparable to the optimal solution of Dynamic Programming (DP). The answer to the second question is also affirmative. The effects of parameter variation on the fuel consumption can be investigated using the proposed high-level modeling and design approach, which is decoupled from the choice of specific components, drive train configuration, and control strategy. Furthermore, the control design and design parameter optimization are merged into a single framework. The proposed method is a step forward in the development of a quick optimization and design analysis tool where the overall fuel consumption of a hybrid propulsion system is predicted with reasonable accuracy for different vehicle classes and drive cycles.

6.1 Conclusions

The design problem for a hybrid vehicle drive train is formulated as an optimization problem, which is solved for various case studies. The control design problem is formulated as a subproblem using a local design variable (control power-flow of the secondary power source S). Several techniques for solving the control design problem were investigated. Firstly, the main conclusions regarding the investigated methods and the fuel saving strategies are discussed. Accordingly, the conclusions regarding the reduced hybrid drive train modeling approach for solving the hybrid drive train design problem are discussed.

6.1.1 Control Design Methodology

Dynamic Programming (DP) is used for solving the control design problem, which results in a global optimal solution. Therefore, the technique has the advantage, besides that it is suitable for solving nonlinear non-convex problems, that it can be used as a bench mark for other optimization methods. However, DP requires a relatively long computation time. Heuristic solvers are sub-optimal by their approximative solution. However, heuristic solvers are characterized by a relatively short computation. Heuristic control strategies based on engineering intuition usually require tuning of many specific control rules on the optimizing solution.

A control model (RB-ECMS) has been proposed in Chapter 2, where the hybrid drive train is operated in distinct hybrid driving modes. The optimization method is based on Rule-Based (RB) and Equivalent Consumption Minimization Strategies (ECMS). The developed method allows quick optimization (50-100 times shorter computation time compared to DP), since the defined hybrid driving modes are independently of topology and tuning of many control rules is unnecessary. The design variable is the control power-flow of the energy accumulator where the main design parameter is the maximum (electro-)motor-only power threshold value. The effects of the hybrid driving modes on the fuel saving potential and the energy balance have been investigated. The fuel consumption is reduced on a drive cycle with a hybrid drive train by:

- shutting-off the engine during vehicle standstill, pure electric driving, or braking, and
- reducing the engine power demand by motor-assisting during driving.

These fuel saving strategies, which are based on engine load leveling, employ generated energy during braking and driving with the engine. The fuel saving strategies can partially be enfolded by looking at the characteristics of the engine.

The idle losses or static engine losses are relatively large resulting in a relatively low engine part-load efficiency at low drive power demands. The second strategy is related to the fuel mass-flow as a function of engine output power. However, for most engines this function is approximately linear and limits therefore the amount of fuel saving with motor-assisting. In addition, the conversion losses between the engine and the battery and the battery storage losses further decrease the fuel saving. Due to the integral energy balance constraint the energy used by the secondary power source S for electric driving, motor-assisting, or engine restart needs to be generated. This energy is beneficially generated during braking or driving at moments where the incremental fuel cost are low.

The secondary power source is operated on a standardized drive cycle within a relatively small power range compared to the engine for both relatively low-frequent (regenerative braking, electric driving) and high-frequent drive power demands (charging, motor-assisting). This causes the engine to operate more stationary and closer to its optimum output.

The (electro-)Motor-only mode determined by the maximum motor-only power threshold value (control design parameter) has been evaluated. A relationship between the average incremental fuel cost or equivalent weight factor, which corresponds to the Lagrangian of the integral energy balance constraint [39], and the control design parameter has been found. In the global optimal solution the maximum motor-only power threshold value tends to vary a little over time on a drive cycle, due to small variations in the engine, the transmission, or the secondary source efficiency. The effect of this on the fuel consumption and the energy management strategy is found to be very small (within $\pm 1\%$ accuracy) by comparing the results of the RB-ECMS with DP.

6.1.2 Reduced Hybrid Drive Train Modeling and Design Methodology

A reduced hybrid drive train modeling approach has been proposed for solving the hybrid drive train design problem, and is validated for various case studies by simulation in the Chapters 3, 4, and 5. The overall hybrid vehicle model simplification holds for describing the drive train topology, the component sizes, component technologies, and control strategy by a limited set of subparameters. The component efficiencies described by the transmission technology T , the primary P , and the secondary power source S are modeled as simplified power-based parametric fit functions. The characteristic parameters are found by fitting linear or quadratic functions on the computed (in-)output powers for each component. The operation points, which are determined by the drive cycle, the vehicle load, and the control strategy, determine the values for the characteristic component parameters. The main conclusions are discussed below.

- A different hybrid drive train configuration (i.e., series, parallel, series-parallel) corresponds to a different transmission technology T.

A series-parallel configuration consists, for example, of a planetary gear set and two electric machines (Toyota Prius). The electric machine at the wheel-side, which performs the electric-only modes, is defined to be functionally part of the secondary power source S. Since, the electric machine of S is also part of T, sizing of S indirectly affects on the characteristic parameters that describe the transmission efficiency. If the electric machine size at the wheel-side of T is sufficiently large to maintain the ratio coverage of the transmission, yet it is too small in order to fulfill the required functions of S, then the electric machine size at the wheel-side of T needs to be increased. Basically, the same design strategy holds for a series configuration. However, looking at the development of the transmission by Toyota, the increased size of S is mainly determined by performance and not by fuel consumption reduction or ratio coverage constraints. The secondary power source S is gradually increased further, in order to become a plug-in hybrid vehicle [87], by reasons of fuel consumption and emissions reduction constraints in the future.

- A different topology, component size, technology, or control strategy is indirectly associated with a different set of characteristic parameters.

Employing the simplified component models in combination with the RB-ECMS, the effect of characteristic parameter variation of the components on the fuel consumption and control strategy can be investigated very quickly.

- The characteristic component parameters describing the efficiency for P, S, and T can be determined with sufficient accuracy only dependent on the drive cycle and the vehicle parameters by assuming certain component operation preferences. The component operation preferences related to each component are:
 - P: the engine is operated over a whole drive cycle at the maximum efficiency points;
 - S: the electric-only modes (BER mode, M mode) over a whole drive cycle are used, while S is operated at the maximum efficiency points (S is pre-coupled to T). P is shut-off. Moreover, P has no drag or idle losses;
 - T: the engine-only mode over a whole drive cycle is used, while P is operated at the maximum efficiency points. S is shut-off. In addition, S has no drag or idle losses.

The transmission technology T is assumed to be a Continuously Variable Transmission (CVT). Note that the topology and the transmission technology T determine if the secondary power source S and the primary power source P can be operated at (e.g., in case of a CVT), or close to (e.g., in case of T with a limited set of discrete gear ratios) its maximum efficiency points. Furthermore, if P or S has drag or idle losses, then these losses also influence the characteristic parameters for S and T .

The method with a priori articulation of component operation preferences allows that the component efficiency models and the incremental fuel costs (savings) for all admissible control design variables, which are required as input for the control design model, are computed efficiently and with sufficient accuracy for different component sizes, technologies, and topologies. The component operation preferences are originated from the following investigated observations (see, Chapter 4):

- the influence of system optimal operation compared to engine optimal operation on the fuel consumption reduction for a hybrid vehicle is relatively small (1%-2%), and
- the influence of power exchange between S and P during driving (motor-assisting, charging) on the efficiency of S and T is relatively small (2%-3%).

The effects of design parameter variation on the fuel consumption by comparing the results of a detailed and a reduced hybrid drive train model were investigated.

- Employing the reduced hybrid drive train modeling approach, the design of a hybrid passenger car is performed within an average error of less than 1.6%.

The influence of power exchange between S and P during driving (motor-assisting, charging) on the efficiency of S increases with increase of secondary power source S size. Since, the average efficiency of S during motor-assisting or charging tends to decrease with increase of size.

In Chapter 5, the reduced hybrid drive train modeling approach was used for the identification of the optimal hybridization of a medium-duty truck. The results show the application of the technique proposed and the potential usage of Li-ion batteries as the most preferable energy storage. Hybridization on the system level (hybrid drive train) towards subsystem level (energy storage system) was investigated by employing frequency-based power segmentation of the power signals. The approach is based on load leveling of the battery system, which finds a resemblance at system level for the battery/electric machine in combination with the engine. Ultra capacitors are suitable for supplying relatively high powers with

high frequencies (low energy content), whereas the battery is suitable for delivering the remaining relatively low powers with low frequencies. The dual-storage systems are expected to increase the overall storage system's life-time by reducing the battery wear. However, the overall system mass and cost reduction potential is found to be limited. Especially, for Li-ion batteries, which are characterized by relatively large energy and power density specifications.

6.2 Recommendations for Future Research

The described research focussed on the development of a high-level modeling and design framework, which can be employed for control design, topology, technology selection, and component sizing of hybrid vehicle propulsion systems regarding one of the main design objectives, i.e., fuel consumption reduction. The proposed method is recommended to be worked out in more detail by:

- experimental validation of the proposed design approach. Furthermore, measurements in acquiring experimental component data, initially on sub-system level and subsequently on system level, of real components is necessary. A start has been made in Chapter 4;
- incorporating other design objectives and/or constraints, which possible play an important role in the design of hybrid vehicle propulsion system. Some other design targets/constraints including, yet not limited to: the required acceleration performances, the required maximum power, the reduction of other pollutant emissions (during engine warm-up), the minimization of battery wear, or the minimum required traveled distance with zero emissions (electric-only driving as with a plug-in hybrid vehicle);
- solving other design cases including, yet not limited to: other vehicle classes and drive cycles, e.g., within the range from small passenger cars up to distribution trucks, the specification of new component technologies, or hybrid vehicle drive trains.

Within the context of solving other design cases, a software design tool with user-friendly interfaces for selecting the design objectives, constraints, and other component models, could be developed. Some design problem examples, which could be addressed using the framework proposed in this thesis, are discussed below.

The specification of hybrid vehicle drive trains in relationship with new upcoming engine - (e.g., Homogeneous Charge Compression Ignition (HCCI) engines) or exhaust-gas after-treatment technologies is recommended to include in

further research. The advantages of a HCCI engine are the relatively high thermal - and part-load efficiency (no throttling device), and the relatively low NO_x - and particle emissions [76]. The challenges with an HCCI engine are expanding the useful operation range, managing the transient behavior, and reducing the HC- and CO-emission.

Plug-in hybrid electric vehicles, which are equipped with a larger battery than a usual hybrid vehicle, allow range extension without any local polluting emissions are seen as promising future solutions for transport in cities and suburbs [78, 87]. After depleting the secondary power source, the control strategy switches to charge sustaining mode using the primary power source (e.g., an internal combustion engine, or a fuel cell). The required drive energy could be charged overnight when the demands are low resulting in a load leveling effect on the electric grid. The idle generating capacity during off-peak hours would be brought into productive use. Allowing plants to operate with less variability and closer to optimum output could enhance the overall efficiency of the electrical system. The introduction of these relatively new type of hybrid vehicles to the market depends on the progress in the development of new batteries, which tolerate frequent and fast load changes. Moreover, the additional production costs of the electrical components strongly dictate the market introduction time schedule of these types of hybrids.

Similar to the development of new engine technologies or other primary power sources (fuel cells), and the challenges with the usage of these technologies in hybrid vehicles, the usage of plug-in hybrid vehicles puts constraints on finding the optimal hybrid components (secondary power source S and transmission technology T), topology, and control strategy.

Model Components

A.1 Component Models of the Base Line Vehicle

In this appendix, the component models will be discussed that have been used in order to reconstruct the engine fuel map. The fuel map is validated by simulation using a forward-facing control model.

A.1.1 Fuel Map Reconstruction

In Figure A.1 the drive train structure for the Toyota Yaris is shown.

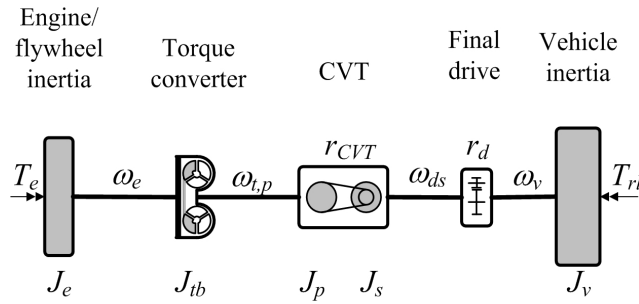


Figure A.1 / Drive train structure.

The engine fuel map is reconstructed based on the measured injected fuel mass-flow \dot{m}_f , the engine shaft speed ω_e , the drive shaft torque T_{ds} and - speed ω_{ds} . The engine torque T_e , as a result of the dynamic torque balance at the crankshaft (with a locked torque converter), is calculated with

$$T_e = J_v r_d^2 r_{CVT}^2 \dot{\omega}_{ds} + T_{loss} + r_{CVT} T_{ds} - (\dot{r}/r_{CVT}^2) \omega_{ds} (J_1 + J_e). \quad (A.1)$$

The total vehicle inertia moment, denoted as J_v , holds

$$J_v = (m_v r_w^2 + 2J_w) + J_1/(r_{CVT}^2 r_d^2) + J_s/r_d^2, \quad (A.2)$$

with the vehicle mass m_v , the wheel radius r_w , the final drive ratio r_d , the inertia parameters $J_1 = J_p + J_{tb}$ representing the sum of the primary pulley and turbine inertias respectively, and J_s the secondary pulley inertia.

The torque losses T_{loss} at the primary shaft of the CVT consist of mechanical torque losses (friction -, slip losses of the V-belt, bearing, final drive friction losses), denoted as T_{mech} , and hydraulic pumping torque losses, denoted as T_{pump} [84]:

$$T_{loss} = T_{mech}(T_{t,p}, \omega_{t,p}, R_p) + T_{pump}(p_l, \omega_{t,p}). \quad (\text{A.3})$$

The mechanical torque loss is represented by nonlinear static look-up map and is as a function of the transmission input torque $T_{t,p}$, speed $\omega_{t,p}$ and the primary running radius of the belt R_p . The primary running radius of the belt R_p is approximated with [84]:

$$R_p \approx \frac{r_{CVT}}{r_{CVT} + 1} \frac{L_b - 2x_c}{\pi}, \quad (\text{A.4})$$

and depends on the speed ratio r_{CVT} , the belt length $L_b = 650$ mm, and the pulley center distance $x_c = 156$ mm. The hydraulic pumping torque loss is also represented by a nonlinear static look-up map and is a function of the pump delivery pressure (line pressure) p_l and the transmission input speed $\omega_{t,p}$.

The transmission input torque $T_{t,p}$ is estimated with the measured drive shaft torque T_{ds} and the speed ratio r_{CVT} by assuming that,

$$T_{t,p} = T_{ds} \cdot r_{CVT}. \quad (\text{A.5})$$

Measurements on the test vehicle have shown that the pump delivery pressure p_l lies approximately 5 bar above the hydraulic clamping pressure, denoted as p_s , at the secondary pulley,

$$p_l \approx p_s + 5 \cdot 10^5 \wedge p_s = \frac{S_f T_{t,p} \cos \phi}{2 \mu R_p A_s} [\text{bar}]. \quad (\text{A.6})$$

The pressure increase due to centrifugal forces acting on the fluid and pulley cylinder surface has been neglected. The (minimum) clamping pressure is a function of the given safety factor $S_f = 1.3$, the pulley wedge angle $\phi = 11^\circ$, the traction coefficient between belt and pulley $\mu = 0.09$, and the secondary pulley cylinder surface $A_s = 0.0122$ m². Some improvement in predicting the line pressure is possible by investigation of the clamping pressure safety strategy used in the reference vehicle. In this appendix, a constant safety factor is modeled, whereas measurements on the reference vehicle show different values depending on the vehicle conditions during stand-still (idle mode) and coast-down.

The measured fuel mass-flow data is mapped onto a two dimensional grid of the measured engine speed ω_e and the engine torque T_e calculated with Equation (A.1):

$$\dot{m}_f = \dot{m}_f(\omega_e, T_e). \quad (\text{A.7})$$

The used vehicle model parameters are listed in Table A.1. Accordingly, the matrix containing all fuel mass-flow data is filtered using a median filtering technique in order to obtain a more smoothed fuel map. Each matrix output element contains the median value in a defined square neighborhood around the corresponding matrix input element. The reconstructed fuel efficiency map as a function of the engine torque T_e and engine speed ω_e is shown in Figure A.2. In the figure, the reconstructed engine Optimal Operation Line (OOL) and the fitted or ‘smoothed’ OOL are also shown. The depicted OOL collects over a certain engine power range the set of engine operation points with maximum efficiency. In the following section, the torque converter model is discussed, that has been used in the forwards-facing control model in order to evaluate the reconstructed engine fuel map.

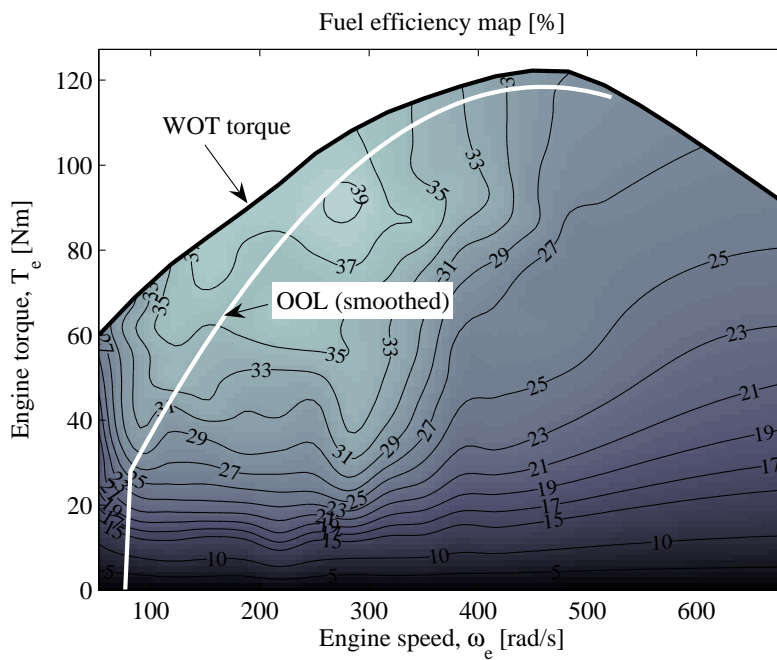


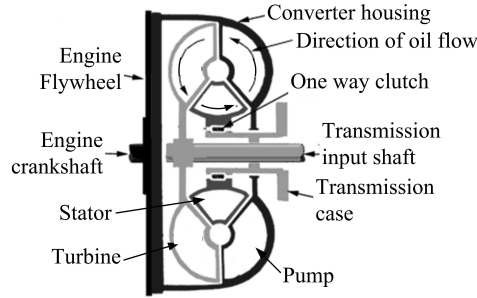
Figure A.2 / Reconstructed 1.3-l VVTi engine efficiency map and smoothed Optimal Operation Line (OOL). WOT = Wide-Open Throttle torque.

A.1.2 Torque Converter

The torque converter is basically a fluid coupling and consists of four important elements: the pump or impeller, stator, turbine and a one-way clutch for lockup. Figure A.3 shows that the engine output shaft and the transmission input shaft

Table A.1 / Vehicle model parameters.

Description	Symbol	Value	Unit
Total mass	m_v	1134	kg
Wheel radius	r_w	0.277	m
Engine inertia	J_e	0.12	kg m ²
Torque converter turbine inertia	J_{tb}	0.03	kg m ²
Secondary pulley inertia	J_s	0.033	kg m ²
Primary pulley inertia	J_p	0.04	kg m ²
Inertia of two wheels	J_w	1.5	kg m ²

**Figure A.3** / Cross-section of a torque converter.

are connected to the pump and the turbine rotor respectively. During launch the engine torque increases the pump speed, thereby increasing the present fluid velocity at the impeller. Initially, the fluid thrown into the turbine blades causing an impulse change that drives the turbine. When rotating the build-up pressure causes the fluid to flow toward the turbine of which the blades are curved in the reverse direction of the impeller. The speed ratio between the engine and the turbine shaft (connected to the CVT input shaft), denoted as r_{tc} , is defined as [75],

$$r_{tc} = \frac{\omega_{t,p}}{\omega_e}. \quad (\text{A.8})$$

The lockup condition is achieved when $r_{tc} = 1$. The slip ratio together with the impeller speed determines the reaction torque T_{im} at the impeller,

$$T_{im} = b_{tc} \omega_e^2, \quad (\text{A.9})$$

whereby b_{tc} is the torque converter capacitor factor. The torque amplification also depends on the torque converter slip and causes the hydraulic torque acting on the turbine,

$$T_{tb} = \alpha_{tc}(r_{tc}) T_{im}. \quad (\text{A.10})$$

For the torque converter used in the simulation, both b_{tc} and α_{tc} are plotted as a function of r_{tc} in Figure A.4.

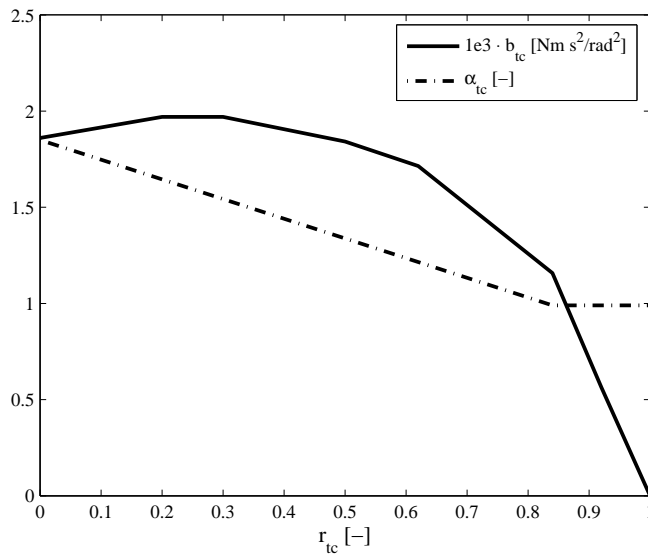


Figure A.4 / Torque capacity b_{tc} , and torque amplification α_{tc} characteristics as a function of the TC slip ratio r_{tc} .

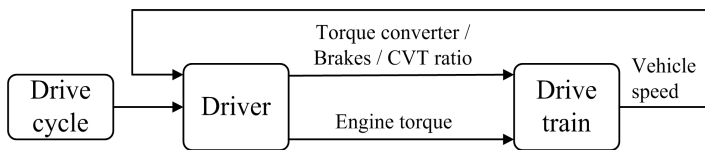


Figure A.5 / Forwards-facing control model used for conventional drive train analysis.

A.1.3 Evaluation of the Component Models

A forwards-facing (or integrating) control model consisting of a ‘driver model’ and a dynamic ‘drive train model’ for the vehicle is shown in Figure A.5. The control model is used in order to validate the calculated fuel mass-flow using the reconstructed engine map described by Equation (A.7) with the measured fuel mass-flow data on the JP10-15 drive cycle. The input of the drive train model is the engine torque $T_e(t)$, the wheel brake torque, the state of the torque converter (locked/unlocked), the speed ratio, and the output is the resulting vehicle speed $v_v(t)$.

To correctly simulate the engine operating points, it is important to have a sufficient accurate representation of CVT ratio control. For this purpose, a variogram has been constructed based on the measurement data. It was chosen to

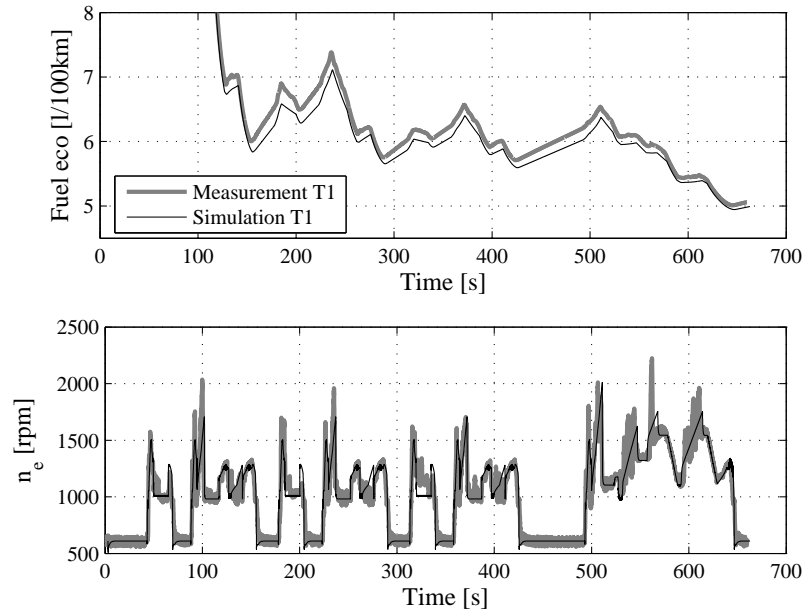


Figure A.6 / Results of the fuel consumption and the engine speed measurement test compared to a simulation test of the conventional drive train.

correlate the relationship between the CVT ratio $r_{CVT}(t)$, the vehicle speed $v_v(t)$, and the vehicle acceleration $a_v(t)$. The dependency on vehicle speed $v_v(t)$ and engine torque $T_e(t)$ was also considered, but the vehicle acceleration $a_v(t)$ gave better results. The driver model includes besides a variogram also a PI-controller in order to determine the desired engine torque or the wheel brake torque in order to track the desired vehicle speed $v_v(t)$ with sufficient accuracy. The vehicle parameters set at the dynamo test bench determine the vehicle road load $T_{rl}(t)$ of the Toyota Yaris. The vehicle road load depends on the vehicle speed $v_v(t)$ (m/s) (assuming no wheel slip) and is the sum of the roll resistance and the air drag torque:

$$T_{rl}(t) = 36.8 + 0.416 v_v(t) + 0.113 v_v(t)^2. \quad (\text{A.11})$$

The results of the measured and the calculated fuel consumption (l/100km) and the engine speed at the JP10-15 [34] cycle are shown in Figure A.6.

An average idle mass-flow of approximately 0.097 g/s has been measured at vehicle standstill. The fuel consumption for the vehicle equipped with a wet-plate clutch instead of a torque converter has also been calculated. The simulation with a wet-plate clutch shows a relative small fuel consumption improvement of 2%. The torque converter lock-up and unlock strategies have been investigated. Mea-

Table A.2 / Reference values: base line vehicle (forwards-facing control model).

<i>Test</i>	<i>Fuel consumption on the JP10-15</i>	
	<i>l/100km</i>	<i>Relative values</i>
Measured value (TC)	5.10	100.0%
Catalogue value (TC)	5.00	98.0%
Simulated value (TC)	5.00	98.0%
Simulated value (CL)	4.90	96.0%

TC = Torque Converter, CL = Wet-plate clutch

measurements show that Toyota incorporates an early lock-up strategy in the Yaris. The fuel consumption results are listed in Table A.2.

Bibliography

- [1] P. Albers and P. Veenhuizen, "Fuel economy benefits of advanced techniques for CVT actuation and control," in *Proc. of the 10th EAEC European Automotive Conference*, Belgrade, Yugoslavia, 2005.
- [2] I. Albert, E. Kahrmanovic, and A. Emadi, "Diesel sport utility vehicles with hybrid electric drive trains," *IEEE Transactions on Vehicular Technology*, vol. 53, no. 4, pp. 1247–1256, July 2004.
- [3] A. Antoniou, J. Komyathy, J. Bench, and A. Emadi, "Modeling and simulation of various hybrid-electric configurations of the high-mobility multipurpose wheeled vehicle (HMMWV)," *IEEE Transactions on Vehicular Technology*, vol. 56, no. 2, pp. 459–465, March 2007.
- [4] D. Assanis, G. Delagrammatikas, R. Fellini, Z. Fillipi, J. Liedtke, N. Michelena, P. Papalambros, D. Reyes, D. Rosenbaum, A. Sales, and M. Sasena, "Optimization approach to hybrid electric propulsion system design," *Int. J. of Mechanics of Structures & Machines*, vol. 27, no. 4, pp. 393–421, 1999.
- [5] D. Assanis, Z. Filipi, S. Gravante, D. Grohnke, X. Gui, L. Louca, G. Rideout, J. Stein, and Y. Wang, "Validation and use of simulink integrated, high fidelity, engine-in-vehicle simulation of the international class vi truck," in *SAE Paper 2000-01-0288*, Warrendale, PA, 2000.
- [6] A. Baisden and A. Emadi, "ADVISOR-based model of a battery and an ultracapacitor energy source for hybrid electric vehicles," *IEEE Transactions on Vehicular Technology*, vol. 53, no. 1, pp. 199–205, January 2004.
- [7] P. Barrade and A. Rufer, "The use of supercapacitors for energy storage in traction systems," in *Proc. of the IEEE Vehicle Propulsion & Power Conference*, Paris, France, 2004.

- [8] R. E. Bellman, *Dynamic programming*. Princeton University Press, 1962.
- [9] D. Bertsekas, *Nonlinear Programming*. Athena Scientific, Belmont, Massachusetts, 1995.
- [10] B. Bonsen, T. Klaassen, R. Pulles, S. Simons, M. Steinbuch, and P. Veenhuizen, "Performance optimization of the push-belt CVT by variator slip control," *Int. J. of Vehicle Design*, vol. 39, no. 3, pp. 232–256, 2005.
- [11] A. Burke and C. Somuah, "Computer-aided design of electric and hybrid vehicles," *Int. J. of Vehicle Design*, pp. 61–81, 1982.
- [12] K. Butler, M. Ehsani, and P. Kamath, "A matlab-based modeling and simulation package for electric and hybrid electric vehicle design," *IEEE Transactions on Vehicular Technology*, vol. 48, pp. 1770–1778, 1999.
- [13] Centraal Bureau voor de Statistiek (CBS), "Prijzen motorbrandstoffen," in <http://statline.cbs.nl>, 2007.
- [14] J. Chen and M. Salman, "Learning energy management strategy for hybrid electric vehicles," in *Proc. of the IEEE Vehicle Propulsion & Power Conference*, Chicago, USA, 2005, pp. 427–432.
- [15] B. de Jager, "Predictive storage control for a class of power conversion systems," in *Proc. of the European Control Conference*, Cambridge, UK, September 2003.
- [16] S. Delprat, J. Lauber, T. Guerra, and J. Rimaux, "Control of a parallel hybrid powertrain: optimal control," *IEEE Transactions on Vehicular Technology*, vol. 53, no. 3, pp. 872–881, 2004.
- [17] M. Duoba, H. Ng, and R. Larsen, "Characterization and comparison of two hybrid electric vehicles (HEVs) - Honda Insight and Toyota Prius," in *SAE Paper 2001-01-1335*, Costa Mesa, California, USA, 2001, SAE Paper 2001-01-1335.
- [18] J. Fenton, *Handbook of Automotive powertrains and chassis design*. Professional Engineering Publishing, 1998.
- [19] FEV Motorentechnik GmbH, "Cost/benefit considerations of hybrid systems," in <http://www.fev.com/>, Aachen, Germany, 2007.
- [20] Z. Filipi, L. Louca, B. Daran, C.-C. Lin, U. Yildir, B. Wu, M. Kokkolaras, D. Assanis, H. Peng, P. Papalambros, J. Stein, D. Szkubiel, and R. Chapp, "Combined optimisation of design and power management of the hydraulic

hybrid propulsion system for the 6x6 medium truck," *Int. J. of Heavy Vehicle Systems*, vol. 11, no. 3/4, pp. 372–402, 2004.

- [21] Y. Gao and M. Ehsani, "Electronic braking system of EV and HEV-integration of regenerative braking, automatic braking force control and ABS," *SAE 2001-01-2478*, pp. 1–9, 2001.
- [22] P. Griffith, "Don't give up on the battery-electric bus just yet.." in *Santa Barbara Electric Transportation Institute: Electric Bus Workshop*, Santa Barbara, CA, USA, www.electricdrive.org, 2002.
- [23] L. Guzzella and A. Amstutz, "CAE tools for quasi-static modelling and optimization of hybrid powertrains," *IEEE Transactions on Vehicular Technology*, vol. 48, no. 6, pp. 1762–1769, 1999.
- [24] L. Guzzella and A. Sciarretta, *Vehicle Propulsion Systems - Introduction to Modeling and Optimization*. Springer-Verlag, Berlin Heidelberg, 2005.
- [25] T. Hofman, D. Hoekstra, R. Van Druten, and M. Steinbuch, "Optimal design of energy accumulator systems for hybrid vehicle powertrains," in *Proc. of IEEE Vehicle Power and Propulsion Conference*, Illinois Institute of Technology, Chicago, USA, August 2005.
- [26] T. Hofman, M. Steinbuch, and R. Van Druten, "Modeling for simulation of hybrid drivetrain components," in *Proc. of IEEE Vehicle Power and Propulsion Conference*, Windsor, London, UK, 2006.
- [27] T. Hofman, R. Van Druten, A. Serrarens, and M. Steinbuch, "Rule-based energy management strategies for hybrid vehicle drivetrains: A fundamental approach in reducing computation time," in *Proc. of 4th IFAC Symposium on Mechatronic Systems*, Heidelberg, Germany, 2006.
- [28] T. Hofman, R. Van Druten, A. Serrarens, and M. Steinbuch, "Design of CVT-based hybrid passenger cars," *IEEE Transactions on Vehicular Technology*, (submitted), 2007.
- [29] T. Hofman, R. Van Druten, and A. Serrarens, "Design specifications for hybrid vehicles," in *Proc. of the 7th International Symposium on Advanced Vehicle Control*, Arnhem, The Netherlands, 2004, pp. 707–712.
- [30] T. Hofman, R. Van Druten, A. Serrarens, and M. Steinbuch, "Parameteric modeling of components for the selection and specification of hybrid vehicle drive trains," *WEVA Journal*, vol. 1, no. 1, pp. 215–224, 2007.

- [31] T. Hofman, R. Van Druten, A. Serrarens, and M. Steinbuch, "Rule-based energy management strategies for hybrid vehicles," *Int. J. of Electric and Hybrid Vehicles*, vol. 1, no. 1, pp. 71–94, 2007.
- [32] T. Hofman, R. Van Druten, A. Serrarens, and M. Steinbuch, "Hybrid component specification optimization for a medium-duty hybrid electric truck," *Int. J. of Heavy Vehicle Systems*, (accepted), 2008.
- [33] L. Hofmann, W. Steiger, P. Adamis, and R. Petersen, "Potential and technical limits of electric motors in powertrain-applications," in *VDI-Berichte, Nr. 1704, Innovative power train systems*, Dresden, 2002, pp. 249–269.
- [34] JISHA, "Japanese Industrial Safety and Health Association, Jisha Technical Standards 899," 1983.
- [35] J. Kessels, M. Koot, and P. van den Bosch, "Optimal adaptive solution to powersplit problem in vehicles with integrated starter/generator," in *Proc. of the IEEE Vehicle Propulsion & Power Conference*, London, UK, 2006, pp. 1–6.
- [36] J. Kessels, P. van den Bosch, M. Koot, and A. de Jager, "Energy management for vehicle power net with flexible electric load demand," in *Proc. of IEEE Conference on Control Applications*, Toronto, Canada, 2005, pp. 1504–1509.
- [37] T. Klaassen, B. Bonsen, K. van de Meerakker, B. Vroemen, P. Veenhuizen, F. Veldpauw, and M. Steinbuch, "The Empact CVT: Modeling, simulation and experiments," *Int. J. of Modelling, Identification and Control*, (accepted), 2007.
- [38] H. Köhler and W. Öhlers, "95 years of diesel-electric propulsion form a mekeshift solution to a modern propulsion system," in *2th International Diesel-Electric Propulsion*, Helsinki, Finland, April 1998, pp. 1–24.
- [39] M. Koot, J. Kessels, A. de Jager, W. Heemels, P. van den Bosch, and M. Steinbuch, "Energy management strategies for vehicular power systems," *IEEE Transactions on Vehicular Technology*, vol. 54, no. 3, pp. 771–782, 2005.
- [40] M. Koot, J. Kessels, A. de Jager, and P. van den Bosch, "Fuel reduction potential of energy management for vehicular electric power systems," *Int. J. of Alternative Propulsion*, vol. 1, no. 1, pp. 112–131, 2006.
- [41] W. Kriegler, B. Veenhuizen, and S. Friedmann, "Mechanical or electrical CVT's an outlook," in *VDI-Berichte, Nr. 1418, Innovative power train systems*, 1998.

- [42] H. Lee, S. Sul, H. Cho, and J. Lee, "Advanced gear shifting and clutch strategy for parallel hybrid vehicle with automated manual transmission," *IEEE Industry Applications Magazine*, pp. 26–32, 2000.
- [43] C.-C. Lin, Z. Filipi, L. Louca, H. Peng, D. Assanis, and J. Stein, "Modelling and control of a medium-duty hybrid electric truck," *Int. J. of Heavy Vehicle Systems*, vol. 11, no. 3/4, pp. 349–371, 2004.
- [44] C.-C. Lin, H. Peng, J. Grizzle, and J. Kang, "Power management strategy for a parallel hybrid electric truck," *IEEE Transactions on Control Systems Technology*, vol. 11, no. 6, pp. 839–849, 2003.
- [45] C.-C. Lin, H. Peng, J. Grizzle, J. Liu, and M. Busdiecker, "Control system development for an advanced-technology medium-duty hybrid electric truck," *SAE 03TB-45*, pp. 1–9, 2003.
- [46] S. Lukic and A. Emadi, "Effects of drivetrain hybridization on fuel economy and dynamic performance of parallel hybrid electric vehicles," *IEEE Transactions on Vehicular Technology*, vol. 53, no. 2, pp. 385–389, March 2004.
- [47] K. Mäder, "Continuously variable transmissions: Benchmark, status and potentials," in *4th International CTI symposium*, Berlin, 2005.
- [48] R. Marler and J. Aora, "Survey of multi-objective optimization methods for engineering," *Struc. Multidisc Optim.*, vol. 26, pp. 369–395, 2004.
- [49] M. Matsuki, Y. Hirano, and A. Matsubara, "Development of a power train for the hybrid automobile - the Civic IMA," in *Proc. of the 21st International Battery, Hybrid and Fuel Cell Electric Vehicle Symposium*, Monaco, France, 2005.
- [50] P. Mattsson, "Continuously variable split-power transmissions with several modes," Ph.D. dissertation, Chalmers University of Technology, 1996.
- [51] Maxwell, <http://www.maxwell.com>, 2007.
- [52] J. Miller, *Propulsion systems for hybrid vehicles*. IEE Power & Energy Series 45, 2004.
- [53] A. Molyneaux, G. Leyland, and D. Favrat, "Multi-objective optimisation of vehicle drivetrains," in *Proc. of Swiss Transport Research Conference*, Monte Verita, Ascona, March 2003.
- [54] C. Musardo, G. Rizzoni, and B. Staccia, "A-ECMS: An adaptive algorithm for hybrid electric vehicle energy management," in *Proc. of the 44th IEEE Conference on Decision & Control*, Seville, Spain, 12-15 December 2005, pp. 1816–1823.

- [55] K. Muta, M. Yamazaki, and J. Tokieda, "Development of a new generation hybrid system THS-II - drastic improvement of power performance and fuel economy," *SAE 2004-01-0064*, pp. 46–57, 2004.
- [56] K. Nowatschin, "Audi multitronic - the new generation of automatic transmissions," in *VDI-Berichte, Nr. 1565, Innovative power train systems*, 2000.
- [57] NREL, "National Renewable Energy Laboratory Center for Transportation Technologies and Systems, Advisor 2002," in <http://www.ctts.nrel.gov/analysis/>, 2002.
- [58] E. Ozatay, B. Zile, J. Anstrom, and S. Brennan, "Power distribution control coordinating ultracapacitors and batteries for electric vehicles," in *Proc. of the American Control Conference*, Boston, USA, June 2004.
- [59] G. Paganelli, S. Delprat, T. Guerra, J. Rimaux, and J. Santin, "Equivalent consumption minimization strategy for parallel hybrid powertrains," in *Proc. of the IEEE Vehicular Transportation Systems Conference*, Atlantic City, USA, 2002, pp. 2076–2081.
- [60] G. Paganelli, T. Guerra, S. Delprat, J. Santin, M. Delhom, and E. Combes, "Simulation and assessment of power control strategies for a parallel hybrid car," *Int. J. of Automobile Engineering*, vol. 214, no. 7, pp. 705–717, 2000.
- [61] G. Paganelli, M. Tateno, A. Brahma, G. Rizzoni, , and Y. Guezennec, "Control development for a hybrid-electric SUV: strategy, implementation and field test results," in *Proc. of the American Control Conference*, Arlington, USA, 2001, pp. 5064–5069.
- [62] P. Y. Papalambros, *Principles of optimal design*. Cambridge University Press, 2000.
- [63] R. Pfiffner, "Optimal operatin of CVT-based powertrains," Ph.D. dissertation, Swiss Federal Institute of Technology, 2001.
- [64] J. Polder, "A network theory for variable epicyclic gear trains," Ph.D. dissertation, Technische Universiteit Eindhoven, 1969.
- [65] B. Powell, K. Bailey, and S. Cikanek, "Dynamic modeling and control of hybrid electric vehicle powertrain systems," *IEEE Control Systems Magazine*, vol. 18, no. 5, pp. 17–33, 1998.
- [66] Rijksdienst voor het Wegverkeer (RDW) and European Committee, "CO₂-emissie per voertuigkilometer van personenauto's, 1998-2005," in <http://www.mnp.nl/mnc/i-nl-0134.html>, 2006.

- [67] G. Rizzoni, L. Guzzella, and B. Baumann, "Unified modeling of hybrid electric vehicle powertrains," *IEEE Transactions on Mechatronics*, vol. 4, no. 3, pp. 246–257, 1999.
- [68] G. Rizzoni, P. Pisu, and E. Calo, "Control strategies for parallel hybrid electric vehicles," in *Proc. of Symposium IFAC Advances in Automotive Control*, Salerno, Italy, 2004, pp. 508–513.
- [69] S. Schroeck and W. Messner, "On controller design for linear time-invariant dual-input single-output systems," in *Proc. of the American Control Conference*, San Diego, California, USA, June 1999.
- [70] M. Schulz, "Circulating mechanical power in a power-split hybrid electric vehicle transmission," *Int. J. of Automobile Engineering*, vol. 218, pp. 1419–1425, 2004.
- [71] A. Sciarretta, M. Back, and L. Guzzella, "Energy management strategies for vehicular electric power systems," *IEEE Transactions on Control Systems Technology*, vol. 12, no. 3, pp. 352–363, 2004.
- [72] A. Sciarretta and L. Guzzella, "Control of hybrid electric vehicles," *IEEE Control Systems Magazine*, pp. 60–70, 2007.
- [73] A. Sciarretta, L. Guzzella, and C. Onder, "On the power split control of parallel hybrid vehicles: from global optimization towards real-time control," *Int. J. of Automatisierungstechnik*, vol. 51, no. 5, pp. 195–205, 2003.
- [74] J. Scordia, M. Desbois-Renaudin, R. Trigui, B. Jeanneret, F. Badin, and C. Plasse, "Global optimisation of energy management laws in hybrid vehicles using dynamic programming," *Int. J. of Vehicle Design*, vol. 39, no. 4, pp. 349–367, 2005.
- [75] A. Serrarens, "Coordinated control of the zero inertia powertrain," Ph.D. dissertation, Technische Universiteit Eindhoven, 2001.
- [76] R. Sun, R. Thomas, and C. Gray, "An HCCI engine: Power plant for a hybrid vehicle," *SAE 2004-01-0933*, 2004.
- [77] TNO Automotive, "Advance Powertrains Hybrid CarLab," in <http://www.automotive.tno.nl/>, Delft, The Netherlands, 2003.
- [78] F. Toledo, C. Bleijs, T. Calliacoudas, and G. Beauzumont, "Charging systems for tomorrow's plug-in hybrids and electric vehicles," in *Proc. of the 22nd International Battery, Hybrid and Fuel Cell Electric Vehicle Symposium*, Yokohama, Japan, 2006, pp. 2236–2245.

- [79] J. Tyrus, R. Long, M. Kramskaya, Y. Fertmand, and A. Emadi, "Hybrid electric sport utility vehicles," *IEEE Transactions on Vehicular Technology*, vol. 53, no. 5, pp. 1607–1622, September 2004.
- [80] P. van den Bosch and F. Lootsma, "Scheduling of power generation via large-scale nonlinear optimization," *Int. J. of Optimiz. Theory Appl.*, vol. 55, pp. 313–326, 1987.
- [81] J. van Mierlo and G. Maggetto, "Innovative iteration algorithm for a vehicle simulation program," *IEEE Transactions on Vehicular Systems*, vol. 53, no. 2, pp. 401–412, 2004.
- [82] J. van Rooij et.al., "The GCI high torque CVT chain for torques up to 2500 nm," in *Proc. of the Int. CVT and hybrid transmission congress*, Yokohama, Japan, (submitted) 2007.
- [83] A. Villeneuve, "Dual mode electric infinitely variable transmission," in *Proc. of the Int. CVT and hybrid transmission congress*, 2005.
- [84] B. Vroemen, "Component control for the zero inertia powertrain," Ph.D. dissertation, Technische Universiteit Eindhoven, 2001.
- [85] D. Werts and J. Steffen, "Future w-series pick up/delivery vehicle," in *Request For Information document*, FedEx Express, Memphis, USA, February 2001, pp. 1–10.
- [86] S. Wilkins and M. Lamperth, "An object-orientated modelling tool of hybrid powertrains for vehicle performance simulation," in *Proc. of 19th Hybrid and Fuel Cell Electric Vehicle Symposium*, 2002.
- [87] R. Winkel and R. van Mieghem, "Global prospects of plug-in hybrids," in *Proc. of the 22nd International Battery, Hybrid and Fuel Cell Electric Vehicle Symposium*, Yokohama, Japan, 2006, pp. 1321–1337.
- [88] K. Wipke, M. Cuddy, and S. Burch, "ADVISOR 2.1: user-friendly advanced powertrain simulation using a combined backward/forward approach," *IEEE Transactions on Vehicular Systems*, vol. 48, no. 6, pp. 1751–1761, 1999.
- [89] B. Wu, C.-C. Lin, Z. Filipi, H. Peng, and D. Assanis, "Optimization of power management strategies for a hydraulic hybrid medium truck," *J. of Vehicle System Dynamics*, vol. 42, pp. 23–40, 2004.

- [90] H. Yeo, S. Hwang, and H. Kim, "Regenerative braking algorithm for a hybrid electric vehicle with CVT ratio control," *Journal of Automobile Engineering, Proc. of the Inst. of Mech. Eng., Part D*, vol. 220, no. 11, pp. 1589–1600, 2006.
- [91] Y. Zhu, Y. Chen, Z. Wu, and A. Wang, "Optimisation design of an energy management strategy for hybrid vehicles," *Int. J. of Alternative Propulsion*, vol. 1, no. 1, pp. 47–62, 2006.

Nomenclature

List of Acronyms

<i>Symbol</i>	<i>Description</i>
ADVISOR	Advanced Vehicle Simulator
AMT	Automated Manual Transmission
AT	Automatic Transmission
AWD	All-Wheel Driven
BER	Brake-Energy Recovery mode
BL	Baseline Vehicle
C	Control model
CL	Wet-plate clutch
CO	Carbon monoxide
CO ₂	Carbon dioxide
CH	Charging mode
CLC	Clutch Closed
CLO	Clutch Open
CVT	Continuously Variable Transmission
CS ₁ ,CS ₂	Control Strategy 1, 2
DS	Dual-Storage
DP	Dynamic Programming
E	Engine-only mode
EM	Electric Machine
EMA	Electro-Mechanical Actuation
EMS	Energy Management Strategy
EOOL	Engine Optimal Operation Line
ECMS	Equivalent Consumption Minimization Strategy
EON	Engine On
EOFF	Engine Off

List of Acronyms (continued)

<i>Symbol</i>	<i>Description</i>
IMA	Integrated Motor Assist
FWD	Front-Wheel Driven
FTP75	Federal Test Procedure-75 (United States drive cycle)
HC	Hydrocarbon
HEV	Hybrid Electric Vehicle
HDA	Hydraulic Actuation
JP10-15	Japanese 10-15 mode (drive cycle)
JP16	Japanese 16 mode (drive cycle)
Li-ion	Lithium ion
NEDC	New European Drive Cycle
Ni-MH	Nickel Metal Hydride
M	Motor-only mode
MA	Motor-Assist mode
NO _x	Nitrogen oxides
OOL	Optimal Operation Line
P	Primary power source (engine)
PA	Parallel hybrid configuration
PRI	Primary
RB	Rule-Based
RWD	Rear-Wheel Driven
S	Secondary power source
SE	Series hybrid configuration
SEC	Secondary
SP	Series-Parallel hybrid configuration
SOOL	System Optimal Operation Line
SS	Single-Storage
T	Transmission technology
TC	Torque Converter
UC	Ultra Capacitor
WOT	Wide-Open Throttle
V	Vehicle / Drive cycle
QSS	Quasi-Static Simulation

List of Symbols

<i>Symbol</i>	<i>Description</i>	<i>Unit</i>
a	Transmission matrix coefficient	-
a_v	Vehicle acceleration	m/s ²
b	Transmission matrix coefficient	-
b_{tc}	Torque capacity	Nms ² /rad ²
c	Transmission matrix coefficient	-
c_d	Air drag coefficient	-
d	Transmission matrix coefficient	-
c_i	Fit coefficient, characteristic parameter, $i \in \mathbb{N}$	-
c_0	Fit coefficient, characteristic parameter	W
c_1	Fit coefficient, characteristic parameter	-
c_2	Fit coefficient, characteristic parameter	1/W
c_r	Rolling resistance	-
$f_{0,1}, f_M$	Power ratio control parameter	-
$f_{0,2}$	Power ratio control parameter	-
$f_{1,1}$	Torque ratio control parameter	-
f_c	Cut-off frequency	Hz
f_{rb}	Brake force ratio between rear wheels and front wheels	-
f_{fb}	Brake force ratio between front wheels and rear wheels	-
g	Gravity	m/s ²
\vec{g}	Inequality constraints	W
\vec{h}	Equality constraints	J
h_{lv}	Lower heating value for fuel	J/g
i	Iteration step	-
\dot{m}_f	Fuel mass-flow	g/s
$\dot{m}_{f,eq}$	Equivalent fuel mass-flow	g/s
$\dot{m}_{f,0}$	Idle fuel mass-flow	g/s
$\Delta\dot{m}_f$	Difference in fuel mass-flow	g/s
m_v	Total vehicle mass	kg
n_b	Number of battery modules	-
n_p	Number of parallel strings of battery modules	-
n_{uc}	Number of ultra capacitor cells	-
p_l	Line pressure	bar
p_s	Hydraulic clamping pressure	bar
r_{AMT}	AMT speed ratio	-
r_{CVT}	CVT speed ratio	-
r_d	Final drive ratio	-

List of Symbols (continued)

<i>Symbol</i>	<i>Description</i>	<i>Unit</i>
r_t	Overall transmission speed ratio	-
r_{tc}	Speed ratio between the engine and the turbine shaft	-
r_{ud}, r_{od}	Under-, overdrive speed ratio	-
r_w	Wheel radius	m
\dot{r}	Time derivative of r	1/s
t	Time	s
t_a	Acceleration time	s
t_f	Final time	s
$t_{v,max}$	Time to sustain maximum vehicle speed	s
Δt	Time step	s
v_M	Vehicle speed electric-only threshold value	m/s
v_v	Vehicle speed	m/s
x	Design parameter	-
x_c	Pulley center distance	m
z	Epicyclic gear ratio of planetary gear	-
A_f	Frontal area	m ²
A_s	Secondary pulley cylinder surface	m ²
C_{uc}	Capacitance ultra capacitor	F
E_b	Energy storage level at output of battery	J
E_{cap}	Energy capacity of battery	J
E_f	Energy content of used fuel	J
E_s	Energy storage level of S	J
$E_{s,uc}$	Energy storage level at input of ultra capacitor	J
$E_{s,b}$	Energy storage level at input of battery	J
E_{uc}	Energy storage level at output of ultra capacitor	J
E_v	Energy vehicle demand for driving over a drive cycle	J
ΔE_s	Energy storage difference of S at the end of drive cycle	J
$\Delta E_{s,a}$	Available energy storage capacity	J
$\Delta E_{s,I}$	ΔE_s with BER/M mode	J
$\Delta E_{s,II}$	ΔE_s with CH/MA mode	J
$\Delta E_{s,uc,a}$	Available usable storage energy for ultra capacitor	J
$\Delta E_{s,uc,n}$	Needed usable storage energy for ultra capacitor	J
G	Design constraints	-
H	Height center of mass	m
H_b	Transfer function battery	-
H_f	Low-pass bandwidth filter	-

List of Symbols (continued)

<i>Symbol</i>	<i>Description</i>	<i>Unit</i>
H_{uc}	Transfer function ultra capacitor	-
HF_{dt}	Hybridization factor drive train	-
HF_{es}	Hybridization factor energy storage	-
I	Current	A
$I_{pe,max}$	Maximum current power electronics	A
J_e	Engine inertia	kg m ²
J_{em}	Electric Machine inertia	kg m ²
J_p, J_s	Primary -, secondary pulley inertia	kg m ²
J_{tb}	Turbine inertia	kg m ²
J_v	Total vehicle inertia	kg m ²
J_w	Inertia of rotating parts including wheels	kg m ²
K_b, K_{uc}	Battery -, ultra capacitor conversion factor	kg/cell
K_p, K_i	Proportional -, integrator control parameter	g/J
L	Length of wheel base	m
L_b	Belt length evaluated a neutral line	m
L_r	Distance between rear wheel and center of mass	m
\mathbb{N}	Set of natural numbers	-
\underline{M}	Matrix with transmission coefficients	-
P_e	Engine power	W
P_{em}	Electric machine power	W
P_f	Fuel power	W
P_{loss}	Power losses	W
P_{in}, P_{out}	Input -, output power	W
P_{max}	Maximum output power, characteristic parameter	W
P_M	Motor power threshold value, characteristic parameter	W
P_{BER}	Regenerative brake power	W
P_p	Primary source power	W
P_s	Secondary source (or storage) power	W
$P_{s,I}$	P_s during BER/M mode	W
$P_{s,II}$	P_s during CH/MA mode	W
$P_{s,b}, P_b$	Battery input -, output power	W
$P_{s,uc}, P_{uc}$	Ultra capacitor input-, output power	W
$P_{t,p}, P_{t,s}$	Primary -, secondary transmission (in-)output power	W
P_v	Vehicle drive power demand	W
$P_{v,loss}$	Power losses of variator	W
$P_{v,p}, P_{v,s}$	Primary -, secondary variator (in-)output power	W

List of Symbols (continued)

<i>Symbol</i>	<i>Description</i>	<i>Unit</i>
Q	Charge capacity	C
Q_0	Charge bulk capacity	C
R_b	Internal battery resistance	Ohm
R_p	Primary running radius	m
\mathbb{R}	Set of rational numbers	-
S_f	Safety factor	-
T	Battery temperature	$^{\circ}\text{C}$
T_e	Engine crank shaft torque	Nm
T_{em}	Electric machine torque	Nm
T_{im}	Impeller torque	Nm
T_{mech}	Mechanical torque loss	Nm
T_{pump}	Pump torque	Nm
T_{rl}	Road load torque	Nm
T_p	Output torque primary power source	Nm
T_s	Output torque secondary power source	Nm
T_t	Input torque transmission technology	Nm
T_{tb}	Turbine torque	Nm
T_{slip}	Wheel slip torque	Nm
$T_{t,p}, T_{t,s}$	Primary -, secondary transmission (in-)output torque	Nm
T_v	Vehicle wheel torque demand	Nm
$T_{v,p}, T_{v,s}$	Primary -, secondary variator (in-)output torque	Nm
U_b	Battery voltage	V
$U_{b,min,a}$	Minimum available battery voltage	V
$U_{b,nom}$	Nominal battery voltage	V
U_{oc}	Open-circuit voltage	V
$U_{pe,min}$	Minimum input voltage of the motor controller	V
U_{uc}	Ultra capacitor voltage	V
α_{tc}	Torque amplification	-
β_{br}	Braking energy ratio to the total traction energy	-
ε	Error iteration step	W
ϕ	Half the pulley wedge angle	II°
ϕ_i	Inverse component efficiency, $i \in \{e, f, em, b\}$	-
ϕ_j	Control parameters, $j \in \{1, 2, 3\}$	-
γ	Convergence ratio	-
$\bar{\eta}_{tank \rightarrow bat}$	Average path efficiencies (fuel tank to battery)	-

List of Symbols (continued)

<i>Symbol</i>	<i>Description</i>	<i>Unit</i>
η_{AMT}	AMT efficiency	-
η_c	Coulomb efficiency	-
η_{CVT}	CVT efficiency	-
$\bar{\eta}_{CVT}$	Average CVT efficiency	-
η_{em}	Electric machine efficiency	-
η_{fd}	Final drive set efficiency	-
η_p	Primary power source efficiency	-
η_{ps}	Planetary gear set efficiency	-
η_s	Secondary power source efficiency	-
η_{sys}	System efficiency	-
η_t	Transmission efficiency	-
η_v	Variator efficiency	-
λ	Lagrange multiplier, equivalent weight factor	g/J
λ'	Previous stored value for λ	g/J
$\lambda_{dis}, \lambda_{chg}$	Average incremental fuel cost discharging, charging	g/J
λ_u, λ_l	λ when crossing upper, lower boundary state-of-charge	g/J
λ_0	Average incremental fuel cost	g/J
λ_1	Incremental fuel cost	g/s
$\Delta\lambda$	Correction value for λ	g/J
μ_r	Traction coefficient between rear-wheels / road surface	-
μ	Traction coefficient between belt / pulley	-
θ	Road slope	$^\circ$
ρ	Air density	kg/m ³
σ	Discharge voltage ratio	-
ω_e	Angular engine speed	rad/s
ω_{em}	Angular electric machine speed	rad/s
ω_{ds}	Angular drive shaft speed	rad/s
ω_p	Angular speed of output shaft P	rad/s
ω_s	Angular speed of output shaft S	rad/s
ω_t	Angular speed of input shaft T	rad/s
ω_v	Angular vehicle wheel speed	rad/s
$\omega_{v,p}, \omega_{v,s}$	Primary -, secondary variator (in-)output speed	rad/s
$\omega_{t,p}, \omega_{t,s}$	Primary -, secondary transmission (in-)output speed	rad/s
$\dot{\omega}$	Time derivative of ω	rad/s ²
ξ	State-of-Charge value	-
ξ_{ref}	State-of-Charge Reference value	-

List of Symbols (continued)

<i>Symbol</i>	<i>Description</i>	<i>Unit</i>
ξ_{min}, ξ_{max}	Minimum -, maximum state-of-charge value	-
Φ	Objective function	-
Φ_f	Total fuel consumption	g
Φ_{es}	Total energy storage mass	kg
Ψ	Variator power ratio	-

Summary

Framework for Combined Control and Design Optimization of Hybrid Vehicle Propulsion Systems

The improvements of conventional drive train technologies of new passenger cars regarding fuel consumption and emissions reduction are diminished by the increasing trend in the average vehicle mass and the maximum engine power. The vehicles become heavier due to the increasing demand of vehicle safety and comfort, while the performance of the vehicle is not allowed to be compromised. Hybridization of the drive train allows to significantly reduce the fuel consumption and emissions without compromising the performance of the vehicle. Due to the broad variety of the type of vehicles, the usage of these vehicles, and the choice of component technologies and topologies, many solutions are provided for hybrid propulsion systems. A design analysis method is required to manage the complex and challenging design process regarding the specification of hybrid vehicle drive trains.

In the last two decades different modeling and simulation tools for integral optimization, including the hybrid vehicle control strategy, have been developed. However, these tools are characterized by large computation times due to the complexity (i.e., interdependency of the design parameters), the unknown sensitivity of the parameters to the design objective, and the multi-objective nature. Insights into the design problem at hand are lost when a single final design solution is presented as a result of a complex integral design process. Interactions between the different design parameters are then difficult to investigate. This thesis contributes by introducing a high-level modeling framework for combined control and design optimization regarding one of the main design objectives: minimization of the fuel consumption and CO₂-emissions.

In this thesis the design problem for a hybrid vehicle drive train is formulated as an optimization problem, which is solved for various case studies. The

control design problem is formulated as a subproblem using a local design variable (control power-flow). Several techniques for solving the control optimization problem are investigated. The control optimization problem is solved by using Dynamic Programming (DP). A Rule-Based (RB) control strategy is derived, which is based on the observed results with DP, where a hybrid drive train is operated in distinct hybrid driving modes. The optimality of the heuristic control strategy is significantly improved by combining the method with Equivalent Consumption Minimization Strategy (ECMS). The new combined method, called the RB-ECMS, requires significantly less computation time compared to DP and less tuning of rules compared to other heuristic methods. Moreover, it gives a physical understanding of the relationship between the defined hybrid modes, the fuel saving potential, and the energy balance conservation. Furthermore, the control method is decoupled from a specific hybrid component technology, size, or topology choice.

The component design problem is related to the component technology choice and sizing issues. In order to solve the component design problem, the possibility of describing the component efficiencies as simplified power-based parametric fit functions is investigated. The fit coefficients or characteristic parameters are found by fitting linear or quadratic functions on the computed (in-)output powers for each component. The operation points, which are determined by the drive cycle, the vehicle load, and the control strategy, determine the values for the characteristic component parameters.

A reduced hybrid drive train model describing the main components and the topology is introduced, which is used for design analysis of hybrid drive trains decoupled from the choice of specific components, hybrid drive train configurations, and control strategy. In this model, a different hybrid drive train configuration (i.e., series, parallel, or series-parallel) implies a different transmission technology. The key idea behind hybrid drive train modeling with reduced complexity is that a different topology, component technology, or size simply implies a different set of characteristic parameters. Employing simplified power-based parametric functions in combination with the RB-ECMS, the effect of characteristic parameter variation of the components on the fuel consumption can be investigated very quickly.

The thesis contributes by showing that the characteristic component parameters describing the efficiency are determined with sufficient accuracy only dependent on the drive cycle and vehicle load by assuming certain component operation preferences. The component efficiency models and the incremental fuel costs (savings) for all admissible control inputs, which are required as input for the RB-ECMS, are generated very quickly for different component sizes, technologies, and topologies. This alternative method in combination with the

RB-ECMS results in a fast design analysis method. The method can be used for the specification of a hybrid vehicle propulsion system by effectively narrowing down the initially large design space and reducing the complexity. Furthermore, the method links the control design optimization with the topology and the component design optimization into a single framework. The derived method gives insights in the basic principles that determine the fuel consumption and the direction of effective improvement with minimal system specifications.

Samenvatting

De verbeteringen van conventionele aandrijflijnen in nieuwe personenvoertuigen, met als doelstelling vermindering van het brandstofverbruik en schadelijke emissies, worden teniet gedaan door de toenemende trend in het gemiddelde voertuiggewicht en het maximum vermogen van verbrandingsmotoren. Voertuigen worden zwaarder door de toenemende eisen met betrekking tot veiligheid en comfort, terwijl de prestaties van het voertuig (bijvoorbeeld acceleratietijd) niet mogen worden gecompromitteerd. Hybridiseren van de aandrijflijn staat toe het brandstofverbruik en schadelijke emissies significant te reduceren zonder de voertuigprestaties te verminderen. Door de grote diversiteit van verschillende type voertuigen, het gebruik van deze voertuigen en de keuze van topologieën en component technologieën zijn er vele ontwerp oplossingen mogelijk voor hybride aandrijfsystemen. Om dit complexe en uitdagende ontwerpproces in goede banen te kunnen leiden is er een ontwerpanalyse methode nodig met betrekking tot het specificeren van hybride aandrijfsystemen.

De afgelopen twee decennia zijn er verscheidene modelleer- en simulatiesoftware programma's ontwikkeld voor het integraal optimaliseren van hybride aandrijfsystemen, inclusief de regelstrategie. Deze programma's worden over het algemeen gekarakteriseerd door lange rekestijden ten gevolge van de complexiteit (onderlinge afhankelijkheid van de ontwerpparameters), de onbekende gevoeligheid van de ontwerpparameters ten opzichte van de ontwerpdoelstelling en het multi-objectieve karakter van het ontwerpprobleem. Daarbij is de interactie tussen de verschillende ontwerpparameters moeilijk te onderzoeken, wanneer een uiteindelijke oplossing wordt gepresenteerd op basis van een complex integraal ontwerpproces. In dit proefschrift wordt een modelleermethode geïntroduceerd voor het gecombineerd optimaliseren van de regelstrategie en het hybride aandrijflijnontwerp met betrekking tot een van de belangrijkste doelstellingen: minimalisatie van het brandstofverbruik en CO₂-emissies.

In dit proefschrift wordt het ontwerpprobleem van een hybride aandrijflijn

geformuleerd als een optimalisatieprobleem, dat wordt opgelost voor verschillende ontwerpstudies. Het ontwerpprobleem van de regelstrategie wordt geformuleerd als een subprobleem met gebruikmaking van lokale ontwerpvariabelen, bijvoorbeeld de vermogensstroom uit de batterij. Verschillende technieken voor het oplossen van het ontwerpprobleem van de regelstrategie zijn onderzocht. Het probleem wordt oplost door gebruik te maken van Dynamisch Programmeren (DP). Gebaseerd op de resultaten van DP, is er een op heuristische regels gebaseerde (Engels: 'Rule-Based' = RB) strategie afgeleid, waarbij een aandrijflijn kan worden bedreven in verschillende hybride rijtoestanden. De optimaliteit van de heuristische regelstrategie wordt significant verbeterd door dit te combineren met Equivalente Consumptie Minimalisatie Strategie (ECMS). Deze nieuwe gecombineerde methode, afgekort RB-ECMS, heeft een significant kortere rekentijd in vergelijking met DP en vereist optimalisatie van minder regels in vergelijking tot andere heuristische methoden. Verder geeft de methode een fysische interpretatie van de relatie tussen de gedefinieerde hybride rijtoestanden, het brandstofbesparingspotentieel en het in stand houden van de energiebalans. Daaraan toegevoegd is de regelstrategie ontkoppeld van specifieke hybride componenttechnologieën, keuze van componentgrootte of de topologie.

Het ontwerpprobleem van componenten is gerelateerd aan de keuze van componenttechnologie en -grootte. Om het ontwerpprobleem van componenten op te lossen is de mogelijkheid onderzocht of de rendementen als vereenvoudigde parametrische fitfuncties kunnen worden beschreven. De fit coëfficiënten of karakteristieke parameters worden bepaald door het fitten van lineaire of kwadratische functies op de berekende in- en uitgaande vermogens voor elk component. De werkpunten, die worden voorgeschreven door de rijcyclus, de voertuiglast en de regelstrategie bepalen de waarden van de karakteristieke parameters.

Een vereenvoudigd hybride aandrijflijnmodel, dat de belangrijkste componenten en de topologie beschrijft, wordt geïntroduceerd. Dit model wordt gebruikt voor ontwerpanalyse van hybride aandrijflijnen, welke is ontkoppeld van de keuze van specifieke componenten, hybride aandrijflijnconfiguraties en regelstrategie. Een andere hybride aandrijflijnconfiguratie (series, parallel en series-parallel) impliceert een andere transmissietechnologie. Het essentiële idee achter het vereenvoudigd modelleren van de hybride aandrijflijn is, dat een andere topologie, componenttechnologie of -grootte, slechts een andere set van karakteristieke parameters impliceert. Door gebruik te maken van vereenvoudigde parametrische functies, in combinatie met de RB-ECMS, kan het effect van variatie in karakteristieke parameters van de componenten op het brandstofverbruik snel worden onderzocht.

In dit proefschrift wordt aangetoond dat de karakteristieke parameters, die het rendement beschrijven, kunnen worden bepaald met voldoende nauwkeurigheid

alleen afhankelijk van de rijcyclus en voertuiglast door het aannemen van bepaalde voorkeuren in het kiezen van componentwerkpunten. De rendementsmodellen en de incrementele brandstofkosten (c.q. besparingen), die nodig zijn als input voor de RB-ECMS, kunnen snel worden gegeneerd voor verschillende component groottes, technologieën en topologieën. Deze alternatieve methode, in combinatie met de RB-ECMS, resulteert in een snelle ontwerpanalysemethode voor het specificeren van een hybride aandrijfsysteem. Hierdoor wordt de initieel grootte ontwerpruimte effectief verkleind en de complexiteit verminderd. De methode brengt het ontwerpprobleem van de regelstrategie met het ontwerpprobleem van de topologie en de componenten samen in een enkel raamwerk. De afgeleide methode geeft inzichten in de basisprincipes, die het brandstofverbruik bepalen en de richting van hoe het brandstofverbruik effectief kan worden gereduceerd met minimale systeemspecificaties.

Dankwoord

Graag wil ik van deze plaats gebruik maken om enkele dankbetuigingen te uiten. Hierbij denk ik aan mensen zonder wie dit proefschrift, zoals het hier nu ligt, nooit tot stand had kunnen komen. Een aantal van hen wil ik graag speciaal hieronder noemen.

Allereerst wil ik mijn begeleider Roëll van Druten bedanken voor zijn inhoudelijke bijdragen. Roëll, dankzij jouw rol als initiator, die je uitstekend past, is er een mooi onderzoeksproject ontstaan. De overgang van vier jaar industrie naar vier jaar universiteit heb ik dan ook als zeer verfrissend ervaren. Daarnaast bedank ik Maarten Steinbuch voor zijn rol als begeleider en promotor. Maarten, jouw heldere kijk op zaken heb ik als zeer stimulerend en waardevol ervaren. Zonder voorkeur in volgorde wil ik tevens Alex Serrarens en Bas Vroemen bedanken voor hun belangrijke rol als discussiepartners en voor het fijne gezelschap tijdens de buitenlandse reizen. Bedankt voor jullie kritische blik en verhelderende reflectie bij het schrijven van artikelen, maar ook op zaken buiten het onderzoek om. Verder waardeer ik de inhoudelijke discussies en goede samenwerking met mijn collega's binnen het vakgebied, met name Michiel Koot en John Kessels. Mijn stagiaires Bastiaan Zuurendonk, Thijs Purnot en afstudeerders Douwe Hoekstra, Janneke van Baalen en Pablo Noben ben ik dankbaar voor hun inzet en bijdragen aan het onderzoek. De kerncommissieleden Lino Guzzella, Paul van den Bosch en Hans Hellendoorn wil ik graag bedanken voor het doorlezen en becommentariëren van het proefschrift. Uiteraard wil ik ook woord van dank uiten aan al mijn collega's van binnen en buiten de vakgroep met name van Drivetrain Innovations, voor de prettige samenwerking en het plezier, dat ik met hen heb beleefd tijdens diverse activiteiten en congresbezoeken. Tenslotte wil ik graag mijn familie, vrienden en vooral Christine, bedanken voor hun steun bij het afronden van dit proefschrift.

Eindhoven, 23 september 2007

Curriculum Vitae

- 1976 Born in Utrecht, The Netherlands
- 1988-1994 Secondary school: Atheneum at Openbare Scholengemeen-
schap Zeist
- 1994-1999 M.Sc. study: Mechanical Engineering at Technische Univer-
siteit Eindhoven
Internal traineeship on the EcoDrive project
External master's project at Thales-Cryogenics B.V.: "The de-
sign of a miniaturised cryogenic cooler"
- 1999-2003 Development Engineer at the Research & Development de-
partment at Thales-Cryogenics B.V.
- 2003-2007 Ph.D. candidate with the Section Control Systems Techno-
logy at the Department of Mechanical Engineering at the
Technische Universiteit Eindhoven
- 2006 Winner 'Youth Paper Award' at the 22nd International Bat-
tery, Hybrid and Fuel Cell Electric Vehicle Symposium & Ex-
position in Japan for the contribution "Parametric modeling
of components for selection and specification of hybrid vehi-
cle drive trains" (with M. Steinbuch, R. van Druten, and A.
Serrarens)

